frontiers | Research Topics

# Molecular predictive pathology in gynecologic malignancies

**Edited by**
Umberto Malapelle, Pierluigi Giampaolino, Stefano Uccella, Sabrina Chiara Cecere and Carmine De Angelis

**Published in**
Frontiers in Oncology

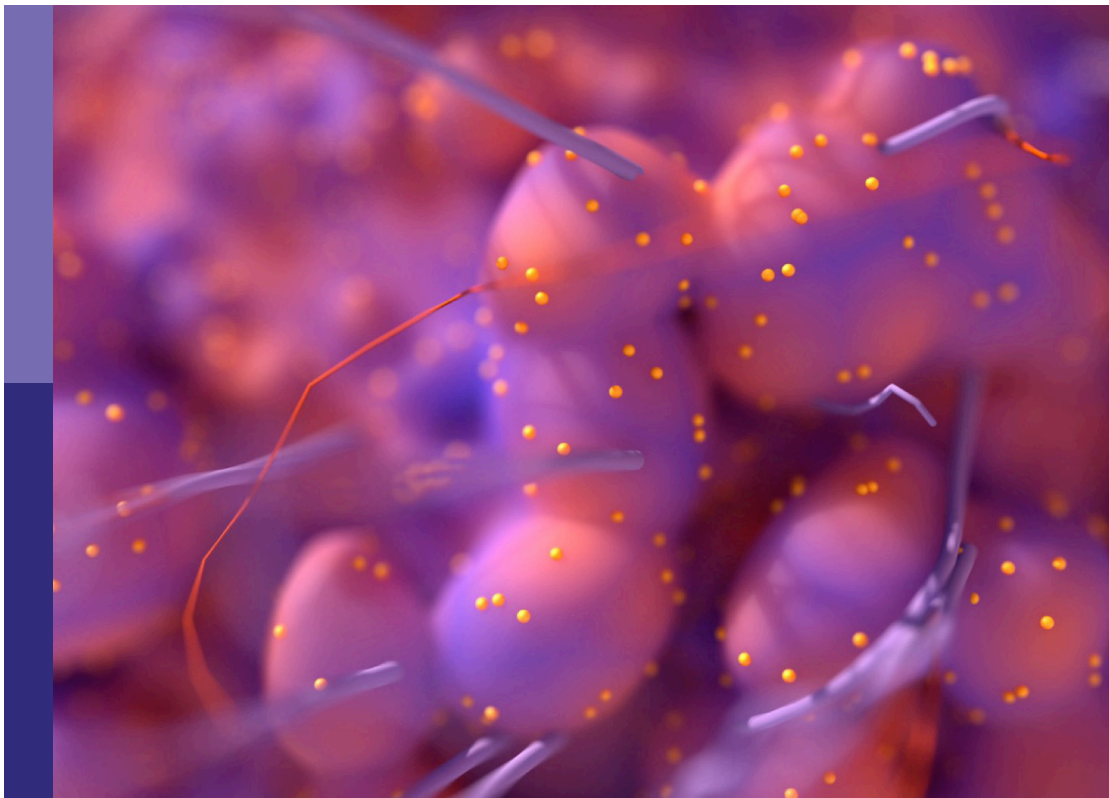

ISSN 1664-8714
ISBN 978-2-8325-3892-0
DOI 10.3389/978-2-8325-3892-0

## About Frontiers

Frontiers is more than just an open access publisher of scholarly articles: it is a pioneering approach to the world of academia, radically improving the way scholarly research is managed. The grand vision of Frontiers is a world where all people have an equal opportunity to seek, share and generate knowledge. Frontiers provides immediate and permanent online open access to all its publications, but this alone is not enough to realize our grand goals.

## Frontiers journal series

The Frontiers journal series is a multi-tier and interdisciplinary set of open-access, online journals, promising a paradigm shift from the current review, selection and dissemination processes in academic publishing. All Frontiers journals are driven by researchers for researchers; therefore, they constitute a service to the scholarly community. At the same time, the *Frontiers journal series* operates on a revolutionary invention, the tiered publishing system, initially addressing specific communities of scholars, and gradually climbing up to broader public understanding, thus serving the interests of the lay society, too.

## Dedication to quality

Each Frontiers article is a landmark of the highest quality, thanks to genuinely collaborative interactions between authors and review editors, who include some of the world's best academicians. Research must be certified by peers before entering a stream of knowledge that may eventually reach the public - and shape society; therefore, Frontiers only applies the most rigorous and unbiased reviews. Frontiers revolutionizes research publishing by freely delivering the most outstanding research, evaluated with no bias from both the academic and social point of view. By applying the most advanced information technologies, Frontiers is catapulting scholarly publishing into a new generation.

## What are Frontiers Research Topics?

Frontiers Research Topics are very popular trademarks of the *Frontiers journals series*: they are collections of at least ten articles, all centered on a particular subject. With their unique mix of varied contributions from Original Research to Review Articles, Frontiers Research Topics unify the most influential researchers, the latest key findings and historical advances in a hot research area.

Find out more on how to host your own Frontiers Research Topic or contribute to one as an author by contacting the Frontiers editorial office: frontiersin.org/about/contact

# Molecular predictive pathology in gynecologic malignancies

**Topic editors**

Umberto Malapelle — University of Naples Federico II, Italy
Pierluigi Giampaolino — University of Naples Federico II, Italy
Stefano Uccella — University of Verona, Italy
Sabrina Chiara Cecere — G. Pascale National Cancer Institute Foundation (IRCCS), Italy
Carmine De Angelis — University of Naples Federico II, Italy

**Citation**

Malapelle, U., Giampaolino, P., Uccella, S., Cecere, S. C., De Angelis, C., eds. (2023). *Molecular predictive pathology in gynecologic malignancies*. Lausanne: Frontiers Media SA. doi: 10.3389/978-2-8325-3892-0

*Umberto Malapelle has received personal fees (as consultant and/or speaker bureau) from Boehringer Ingelheim, Roche, MSD, Amgen, Thermo Fisher Scientifics, Eli Lilly, Diaceutics, GSK, Merck and AstraZeneca.*

# Table of contents

frontiers | Frontiers in Oncology

TYPE Editorial
PUBLISHED 04 October 2023
DOI 10.3389/fonc.2023.1301768



OPEN ACCESS

EDITED AND REVIEWED BY
Sophia George,
University of Miami, United States

*CORRESPONDENCE
Umberto Malapelle
umberto.malapelle@unina.it

RECEIVED 25 September 2023
ACCEPTED 27 September 2023
PUBLISHED 04 October 2023

CITATION
Malapelle U, Uccella S, Cecere SC, De Angelis C and Giampaolino P (2023) Editorial: Molecular predictive pathology in gynecologic malignancies. *Front. Oncol.* 13:1301768. doi: 10.3389/fonc.2023.1301768



# Editorial: Molecular predictive pathology in gynecologic malignancies

Umberto Malapelle[1]*, Stefano Uccella[2], Sabrina Chiara Cecere[3], Carmine De Angelis[4] and Pierluigi Giampaolino[1]

[1]Department of Public Health, University of Naples Federico II, Naples, Italy, [2]Department of Obstetrics and Gynecology, University Hospital of Verona, University of Verona, Verona, Italy, [3]Department of Urology and Gynecology, Istituto Nazionale Tumori IRCCS Fondazione G. Pascale, Napoli, Italy, [4]Department of Clinical Medicine and Surgery, University Federico II, Naples, Italy

KEYWORDS

**gynecological tumors, molecular biomarkers, liquid biopsy, genomic instability, target drug**

Editorial on the Research Topic
Molecular predictive pathology in gynecologic malignancies

Gynecologic malignancies (including endometrial, ovarian, cervical, etc.) represent one of the most common causes of mortality in women (1). The main cause of this phenomenon is related to the absence, except for cervical cancer (2), of valid screening approaches. As a matter of facts, current treatment strategies for advanced stage patients include chemotherapy and radiotherapy. Remarkably, as for other malignancies, giant strides have been made in the field of targeted therapies. Therefore, the identification and correct assessment of predictive biomarkers is pivotal to elect patients for targeted therapies. In this complex scenario, molecular predictive pathology has acquired a key role in the management of these patients (3). The efficacy of Poly (ADP-ribose) Polymerase (PARP) inhibitors (PARPi) in patients harboring genomic alterations in breast cancer (*BRCA*) 1 and 2 genes has been widely demonstrated in high grade serous ovarian carcinoma (HGSOC) (4), and a careful attention has been paid to the role of immune-checkpoint inhibitors (ICIs) in patients harboring a high microsatellite instability (MSI-H) status (5).

In this Special Topic of Frontiers in Oncology, we would like to discuss the methods, findings and prospects of evidence from molecular pathology that will help in the early diagnosis, treatment decision-making, and drug resistance prediction in gynecological malignancies.

Overall, the role of molecular pathology in the management of advanced stage gynecological malignancies has rapidly evolved during the last years. In particular, a number of different genomic alterations have been reported, and may be potential target

for personalized therapies (Jiang et al, Tang and Hu) In particular, Jiang et al reported that almost all analyzed patients (94.57%) harbored at least one mutation within *TP53*, *PIK3CA*, *PTEN*, *KRAS*, *BRCA1*, *BRCA2*, *ARID1A*, *KMT2C*, *FGFR2*, and *FGFR3* genes. Interestingly, patients with ovarian cancer showed a high rate of *BRCA1/2* mutations. Of note, patients harboring *TP53*, *PIK3CA*, *PTEN*, and *FGFR3* mutations showed a high tumor mutational burden.

As far as ovarian cancer is concerned, beyond *BRCA1/2* genomic alterations, other potential biomarkers are currently under investigation. Among these, STAT1, STAT4, and STAT6 may be potential targets as proposed by Gong et al. Beyond the predictive role, other biomarkers showed promising results for prognostic purposes. In this setting, Ryu et al. highlighted that the simultaneous expression of β-arrestin and glucorticoid receptor is associated with poor prognosis in ovarian cancer patients. Similarly, Song et al. demonstrated that NCOA5 high expression is associated with disease progression and can be considered as an independent factor affecting the prognosis of ovarian cancer patients. In another experience, Haque et al. showed that VGLL3 mRNA expression was significantly correlated with both advanced tumor stage and poor overall survival. From a diagnostic point of view, Galan et al. demonstrated the role of gangliosides GD2 and GD3 in the diagnosis of ovarian carcinoma in all stages with a high rate of selectivity and specificity.

Considering endometrial carcinoma, Passarelli et al. highlighted the positive predictive role of *PIK3CA* mutations for alpelisib administration. They reported, for the first time, an exceptional response and a good tolerance to alpelisib in a patient with advanced endometrial carcinoma harboring *PIK3CA* mutation.

Molecular pathology may play a crucial role in the diagnostic process, in particular in those morphological trouble cases. In the experience by Lu et al., the Authors highlighted the crucial role of the *COL1A1–PDGFB* fusion to refine the diagnosis of rare uterine sarcoma at cervix. Considering cervical cancer, significant advances have been made in the field of treatment. In particular, Li et al. showed that the expression of N-glycopeptide of MASP1, LUM, ATRN, CO8A, CO8B and CO6 may be potential biomarkers for predicting the efficacy of chemotherapy for these patients. In addition, a comprehensive genomic profiling associated with PD-L1 expression may help to select patients for ICIs administration.(Kim et al.) From a prognostic point of view, it has been highlighted the role of RPL24 as a potential biomarker to predict the prognosis of cervical cancer patients and assess chemotherapy efficacy.(Ming et al.)

Finally, an emerging tool for molecular purposes is represented by extracellular vesicles, that have demonstrated their utility as a novel biomarker and therapeutic target. (Wang et al.; Kong et al.)

Overall, this Research Topic has highlighted the recent evidences from molecular pathology that will help in the early diagnosis, treatment decision-making and drug resistance prediction in gynecological malignancies.

Ongoing research is warranted to improve the clinical outcome of these patients.

## Author contributions

UM: Conceptualization, Data curation, Formal Analysis, Funding acquisition, Investigation, Methodology, Project administration, Resources, Software, Supervision, Validation, Visualization, Writing – original draft, Writing – review & editing. SU: Conceptualization, Data curation, Formal Analysis, Funding acquisition, Investigation, Methodology, Project administration, Resources, Software, Supervision, Validation, Visualization, Writing – original draft, Writing – review & editing. SC: Conceptualization, Data curation, Formal Analysis, Funding acquisition, Investigation, Methodology, Project administration, Resources, Software, Supervision, Validation, Visualization, Writing – original draft, Writing – review & editing. CA: Conceptualization, Data curation, Formal Analysis, Funding acquisition, Investigation, Methodology, Project administration, Resources, Software, Supervision, Validation, Visualization, Writing – original draft, Writing – review & editing. PG: Conceptualization, Data curation, Formal Analysis, Funding acquisition, Investigation, Methodology, Project administration, Resources, Software, Supervision, Validation, Visualization, Writing – original draft, Writing – review & editing.

## Funding

The authors declare that no financial support was received for the research, authorship, and/or publication of this article.

## Conflict of interest

UM reports personal fees as consultant and/or from a speakers' bureau from Boehringer Ingelheim, Roche, Merck Sharpe & Dohme, Amgen, Thermo-Fisher Scientific, Eli Lilly & Company,

Diaceutics, GlaxoSmithKline, Merck, AstraZeneca, Janssen, Diatech, Novartis, and Hedera outside the submitted work.

The remaining authors declare that the research was conducted in the absence of any commercial or financial relationships that could be construed as a potential conflict of interest.

The author(s) declared that they were an editorial board member of Frontiers, at the time of submission. This had no impact on the peer review process and the final decision.

## Publisher's note



## References

1. Siegel RL, Miller KD, Wagle NS, Jemal A. Cancer statistics, 2023. *CA Cancer J Clin* (2023) 73:17–48. doi: 10.3322/caac.21763

2. Wang J, Bai Z, Wang Z, Yu C. Comparison of secular trends in cervical cancer mortality in China and the United States: an age-period-cohort analysis. *Int J Environ Res Public Health* (2016) 13:1148. doi: 10.3390/ijerph13111148

3. Bejar FG, Oaknin A, Williamson C, Mayadev J, Peters PN, Secord AA, et al. Novel therapies in gynecologic cancer. *Am Soc Clin Oncol Educ Book.* (2022) 42:1–17. doi: 10.1200/EDBK_351294

4. Fong PC, Boss DS, Yap TA, Tutt A, Wu P, Mergui-Roelvink M, et al. Inhibition of poly(ADP-ribose) polymerase in tumors from BRCA mutation carriers. *N Engl J Med* (2009) 361:123–34. doi: 10.1056/NEJMoa0900212

5. Mirza MR, Chase DM, Slomovitz BM, dePont Christensen R, Novák Z, Black D, et al. Dostarlimab for primary advanced or recurrent endometrial cancer. *N Engl J Med* (2023) 388:2145–58. doi: 10.1056/NEJMoa2216334

frontiers | Frontiers in Oncology

TYPE Original Research
PUBLISHED 29 November 2022
DOI 10.3389/fonc.2022.1054647



OPEN ACCESS

EDITED BY
Umberto Malapelle,
University of Naples Federico II, Italy

REVIEWED BY
J. Omar Muñoz-Bello,
National Institute of Cancerology (INCAN), Mexico
Isabel Soto-Cruz,
Universidad Nacional Autónoma de México, Mexico
Ming Jun Zheng,
Ludwig Maximilian University of Munich, Germany

*CORRESPONDENCE
Xiaodi Gong
gong_xdi@sina.com
Xiaojun Liu
liuxiaojun@smmu.edu.cn

SPECIALTY SECTION
This article was submitted to Gynecological Oncology, a section of the journal Frontiers in Oncology

RECEIVED 27 September 2022
ACCEPTED 14 November 2022
PUBLISHED 29 November 2022

CITATION
Gong X and Liu X (2022) In-depth analysis of the expression and functions of signal transducers and activators of transcription in human ovarian cancer.
*Front. Oncol.* 12:1054647.
doi: 10.3389/fonc.2022.1054647



# In-depth analysis of the expression and functions of signal transducers and activators of transcription in human ovarian cancer

Xiaodi Gong* and Xiaojun Liu*

Department of Gynaecology and Obstetrics, Changzheng Hospital, Naval Medical University, Shanghai, China

**Background:** Signal transducers and activators of transcription (STAT) transcription factors, a family of genes encoding transcription factors, have been linked to the development of numerous types of tumors. However, there is a relative paucity of a comprehensive investigation of the expression and functional analysis of STATs in ovarian cancer (OV).

**Method:** Gene expression profile interaction analysis (GEPI2A), Metascape, The Cancer Genome Atlas (TCGA), Kaplan-Meier Plotter, Linkedomics, and CancerSEA databases were used for expression analysis and functional enrichment of STATs in ovarian cancer patients. We screened potential predictive genes and evaluated their prognostic value by constructing the minor absolute shrinkage and selection operator (LASSO) Cox proportional risk regression model. We explored STAT5A expression and its effects on cell invasion using ovarian cancer cells and a tissue microarray.

**Results:** The expression level of STAT1 was higher, but that of STAT2-6 was lower in cancerous ovarian tissues compared to normal tissues, which were closely associated with the clinicopathological features. Low STAT1, high STAT4, and 6 mRNA levels indicated high overall survival. STAT1, 3, 4, and 5A were collectively constructed as prognostic risk models. STAT3, and 5A, up-regulating in the high-risk group, were regarded as risk genes. In subsequent validation, OV patients with a low level of P-STAT5A but not low STAT5A had a longer survival time ($P$=0.0042). Besides, a negative correlation was found between the expression of STAT5A and invasion of ovarian cancer cells (R= -0.38, $p < 0.01$), as well as DNA repair function (R= -0.36, $p < 0.01$). Furthermore, transient overexpression of STAT5A inhibited wound healing (21.8%, $P$<0.0001) and cell migration to the lower chamber of the Transwell system (29.3%, $P$<0.0001), which may be achieved by regulating the expression of MMP2.

**Conclusion:** It is suggested that STAT1, STAT4, and STAT6 may be potential targets for the proper treatment of ovarian cancer. STAT5A and P-STAT5A, biomarkers identified in ovarian cancer, may offer new perspectives for predicting prognosis and assessing therapeutic effects.

KEYWORDS

**bioinformatics, LASSO, STAT5A, cell invasion, ovarian cancer**

## Introduction

Among gynecological tumors, ovarian cancer is the leading cause of death. About 19,880 new cases of ovarian cancer will be diagnosed in the United States in 2022, the equivalent of about 54 new cases each day, and 12,810 deaths from ovarian cancer are projected to occur, approximately 35 deaths per day (1). Because ovarian cancer can be divided into at least five histological subtypes, accompanied by unique risk factors, origin cells, and genomic characteristics, it cannot be detected early in population-based screening and is usually diagnosed late (2). Upfront treatment mainly depends on cytoreductive surgery without residual disease and platinum-based chemotherapy, and anti-angiogenic agents are added in patients with stage IV and recurrence (3). However, recurrent cancer is often resistant to platinum chemotherapy, which leads to a lack of effective treatment. Fortunately, adding poly (ADP- ribose) polymerase (PARP) molecular inhibitors to recurrent patients with BRCA1/BRCA2 mutations has made significant progress in maintenance therapy (4). The combined treatment of multiple methods can slowly increase the 5-year survival rate of ovarian cancer, but the prognosis is still not significantly improved.

STAT transcription factors (STATs) were discovered in 1994 (5). Seven STATs family members are found in mammals with similar structural and functional characteristics, all encoded by their genes: STAT1 (chromosome position: 2q32.2), STAT2 (12q13.3), STAT3 (17q21.2), STAT4 (2q32.2), STAT5A (17q21.2), STAT5B (17q21.2) and STAT6 (12q13.3) (6). Each of them played unique roles in signal transduction. The Janus kinase (JAK) and STAT pathways are involved in the biological effects of more than 50 cytokines and growth factors (7). Activated JAK phosphorylates the conserved c-terminal tyrosine residue in STATs, facilitating them to form dimerization, which leads to the activation of STATs and then translocation into the nucleus through Ran-GTP-dependent mechanisms. Subsequently, STATs bind to specific target DNA promoter sequences to control corresponding gene transcription (5). In this way, the translocation of STATs from the cytoplasm to the nucleus realizes the transmission of extracellular signals. It then affects the expression of target genes to regulate cell proliferation, differentiation, apoptosis, and angiogenesis (8).

The activation of STATs in normal signal transduction is rapid and transient, and the sustained activation of STATs is closely related to the process of malignant transformation. Tumors of various types exhibit abnormal activation of STAT family members, including ovarian cancer (9), breast cancer (10), prostate cancer, and (11) hematological and head and neck cancer (12), of which have been confirmed to be involved in angiogenesis, invasion, and metastasis of tumor cells, as well as their escape from the immune system.

STAT1 played a dual role in ovarian cancer. For instance, a positive effect of STAT1 in ovarian cancer was that it upregulated the expression of inducible nitric oxide synthase (iNOS) (13), resulting in the release of cytotoxic nitric oxide (NO) (14) and accelerating the progression of the disease (15); however, NO could also promote ovarian cell apoptosis by increasing the expression of p53 (16). The contradictory role of STAT1 in promoting and inhibiting cancer also existed in invasion and metastasis (17, 18), angiogenesis (19), immunologic responsiveness (20), and chemotherapeutic drug reactivity of ovarian cancer (21).

The Fibrillin-1/VEGFR2/STAT2 signal axis modulated the process of glycolysis and angiogenesis by activating STAT2, which induced cisplatin resistance in ovarian cancer cells (22). Activated STAT3 facilitated migration and invasion of ovarian cancer by inducing the expression of MMP2 and MMP9 (23, 24), and assisting in the epithelial-to-mesenchymal transition (EMT) process of ovarian cancer (25). STAT3 regulated the expression of HIF-1α (26), contributing to ovarian cancer angiogenesis. In addition, ovarian cancer cells expressing STAT3 showed increased resistance to chemotherapy (27) and with cancer stem cells (CSCs) or CSC-like phenotypes (28). Likewise, STAT4 could induce activation of tumor-associated fibroblasts (CAF) through tumor-derived Wnt7a, which promoted peritoneal metastasis of ovarian cancer through the EMT process (29). Overexpression of human epidermal growth factor receptor 4 (HER4) in ovarian CSCs mediated STAT5 activation to enhance the survival and growth of ovarian CSCs (30). Upon oncoproteomic analysis, STAT5B was overexpressed in ovarian cancer that recurred after chemotherapy. Further research confirmed that STAT5B and RELA (NF-kappaB p65) were responsible for carboplatin resistance in ovarian

carcinoma (31). Moreover, the decreased STAT5B led to $CD8^+$ effector memory T ($T_{EM}$) cell dysfunction in ascites of high-grade serous ovarian cancer patients, thus causing shortened relapse-free survival (RFS) (32). Collagen triple helix repeat containing 1 (CTHRC1), secreted by epithelial ovarian Cancer (EOC) cells, promoted M2-like polarization of tumor-associated macrophages (TAMs) by activating STAT6. As a result, this facilitated EOC cell invasion and migration (33). Additionally, STAT6 was also involved in the stemness maintenance and function of ovarian CSCs (34).

Although there are partial reports on the role of individual STAT in the development and progression of ovarian cancer, the role of the entire STATs family in ovarian cancer has not been explored through bioinformatics. Here, a detailed analysis of STAT transcription factor expression in ovarian cancer was performed, and potential biomarkers were identified. We sought to ascertain the pattern of expression, potential biological function, and unique prognostic significance of STATs in ovarian cancer (Scheme 1).

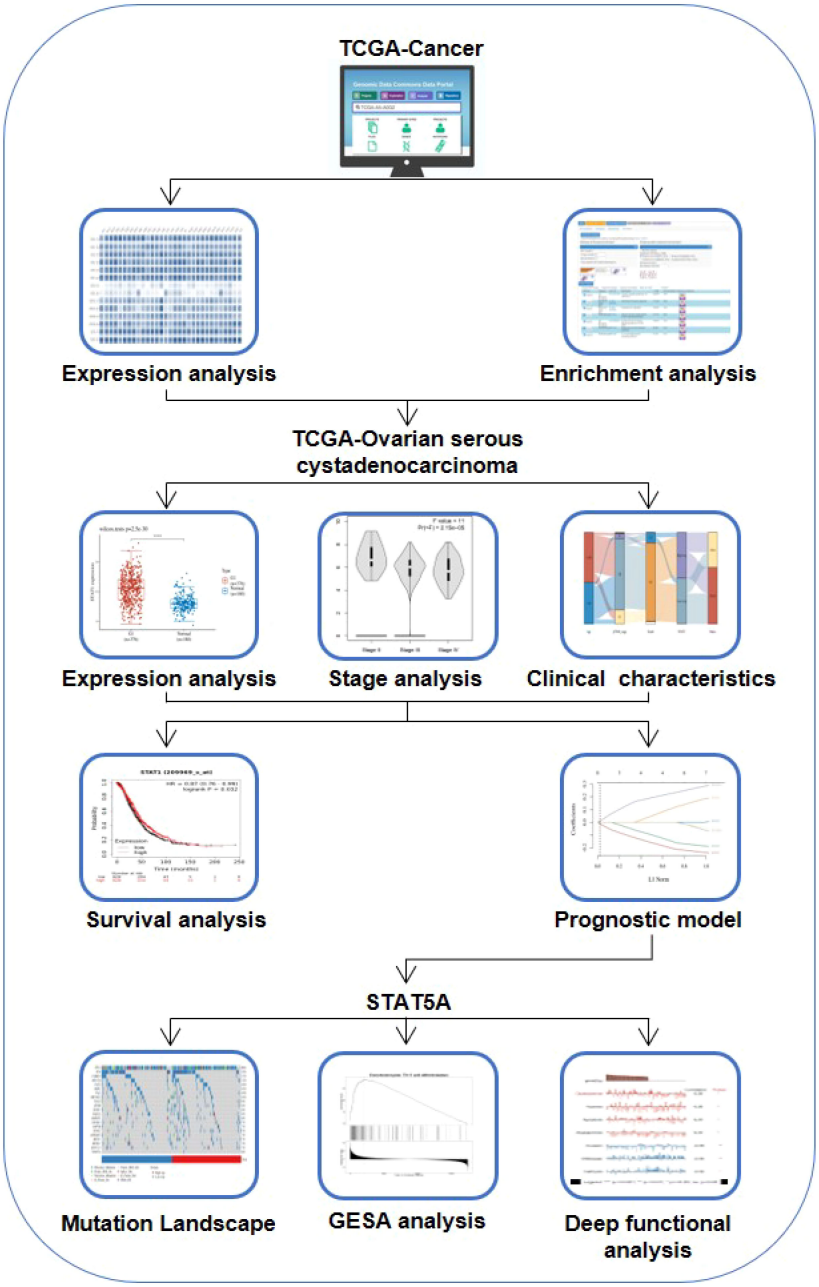


SCHEME 1
Protocol for investigating the role of STATs in ovarian cancer.

# Results

## The main functions of the STAT family

At present, researchers have identified seven STAT transcription factors in mammalian cells. A comparison was made between STAT transcription in cancers and normal tissues based on the gene expression profiling interactive analysis (GEPIA2) database (http://gepia2.cancer-pku.cn/#analysis). Selecting "TCGA normal+ GTEx normal" as the matched normal tissue data, Figure 1 shows the expression of STAT family members in 31 different tumors (T) and paired normal tissue (N), plotted using log2(TPM + 1) transformed expression data. Subsequently, the Metascape database was used for enrichment analysis of significant functions of 7 STAT family genes including STAT1, STAT2, STAT3, STAT4, STAT5A, STAT5B, and STAT6 (http://metascape.org/gp/index.html#/main/step1). Enrichment standards were as follows: an enrichment factor of >1.5, a minimum count of 3, and a *p*-value of 0.01. We found that the STAT transcription factors family played crucial roles in biological processes such as signaling, response to stimulus, immune system process, growth, developmental process, regulation of biological processes, positive regulation of biological processes, and cellular processes (Figure 2A). Moreover, Figure 2B **and** Supplementary Material Table 1 showed the top-level significantly enriched signal pathways, including receptor signaling pathway *via* JAK-STAT, Interleukin-20 family, Interleukin-21 signaling, Thymic stromal lymphopoietin (TSLP) signaling pathway growth hormone receptor signaling pathway *via* JAK-STAT, inflammatory bowel disease signaling, and IL-10 anti-inflammatory signaling pathway. The above-enriched signal pathways were shown in the form of a network in Figure 2C to understand the relationship between these GO terms. Edges were formed between terms with a similarity > 0.3. Each node represents an enriched term and is colored by its cluster ID, where nodes sharing the same cluster-ID are usually close to each other. For clarity, only one term tag was displayed per cluster in the lower right corner, and all node tags can be checked by visualizing the network using Cytoscape or a browser. Therefore, the ligand-dependent activated STAT transcription factors family acted as a signaling hub *via* modulating downstream target genes' expression and participating in the tumor occurrence and development.

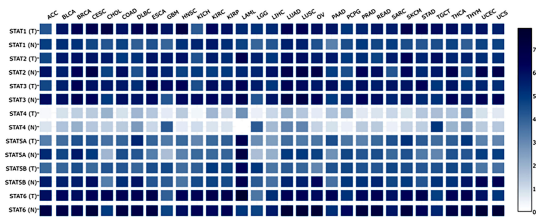


FIGURE 1
Expression matrix plots of STAT family members in various cancers. Abbreviations for tumor names are annotated above the plot. Their specific tumor names have been annotated one by one as follows. STAT family members from tumor tissues (T) and the normal counterpart (N) were enumerated on the left. The color bar at right is presented in $log_2$-scale and began at zero, which is indicated the expression level of the STATs genes. ACC: Adrenocortical carcinoma; BLCA: Bladder Urothelial Carcinoma; BRCA: Breast invasive carcinoma; CESC: Cervical squamous cell carcinoma and endocervical adenocarcinoma; CHOL: Cholangio carcinoma; COAD: Colon adenocarcinoma; DLBC: Lymphoid Neoplasm Diffuse Large B-cell Lymphoma; ESCA: Esophageal carcinoma; GBM: Glioblastoma multiforme; HNSC: Head and Neck squamous cell carcinoma; KICH: Kidney Chromophobe; KIRC: Kidney renal clear cell carcinoma; KIRP: Kidney renal papillary cell carcinoma: LAML: Acute Myeloid Leukemia; LGG: Brain Lower Grade Glioma; LIHC: Liver hepatocellular carcinoma; LUAD: Lung adenocarcinoma; LUSC: Lung squamous cell carcinoma; MESO: Mesothelioma; OV: Ovarian serous cystadenocarcinoma; PAAD: Pancreatic adenocarcinoma; PCPG: Pheochromocytoma and Paraganglioma; PRAD: Prostate adenocarcinoma; READ: Rectum adenocarcinoma; SARC: Sarcoma; SKCM: Skin Cutaneous Melanoma; STAD: Stomach adenocarcinoma; TGCT: Testicular Germ Cell Tumors; THCA: Thyroid carcinoma; THYM: Thymoma; UCEC: Uterine Corpus Endometrial Carcinoma; UCS: Uterine Carcinosarcoma; UVM: Uveal Melanoma.

## STAT transcription in ovarian cancer patients

Our analysis included 374 OV patients and 32 normal tissues filtered from the available data; an overview of their baseline data is provided in Supplementary Material Table 2. First, we assessed the expression of the STAT transcription factor by comparing ovarian cancer with normal ovarian tissues. According to research, ovarian cancer tissues exhibited higher STAT1 but lowered STAT2-6 expression than normal tissues (Figure 3A). Moreover, there was a positive correlation between the gene expression of different STAT family members in OV (Figure S1). Using the GEPIA2 database (http://gepia2.cancer-pku.cn/#analysis), an analysis was also performed of the association between the expression of STATs in ovarian cancer and major tumor stages. The results indicated that, in contrast to STAT6, the expression of other STATs family members varied significantly (Figure 3B). Based on the above results, STAT members exhibited different expression patterns in ovarian cancer and seemed involved in various phases of ovarian development.

## Expression distribution trend of STATs for different clinical characteristics of ovarian cancer patients

To further study the relationship between STAT family and tumor stage and grade, a Sankey diagram was drawn (Figure 4), which showed the distribution trend between different clinical

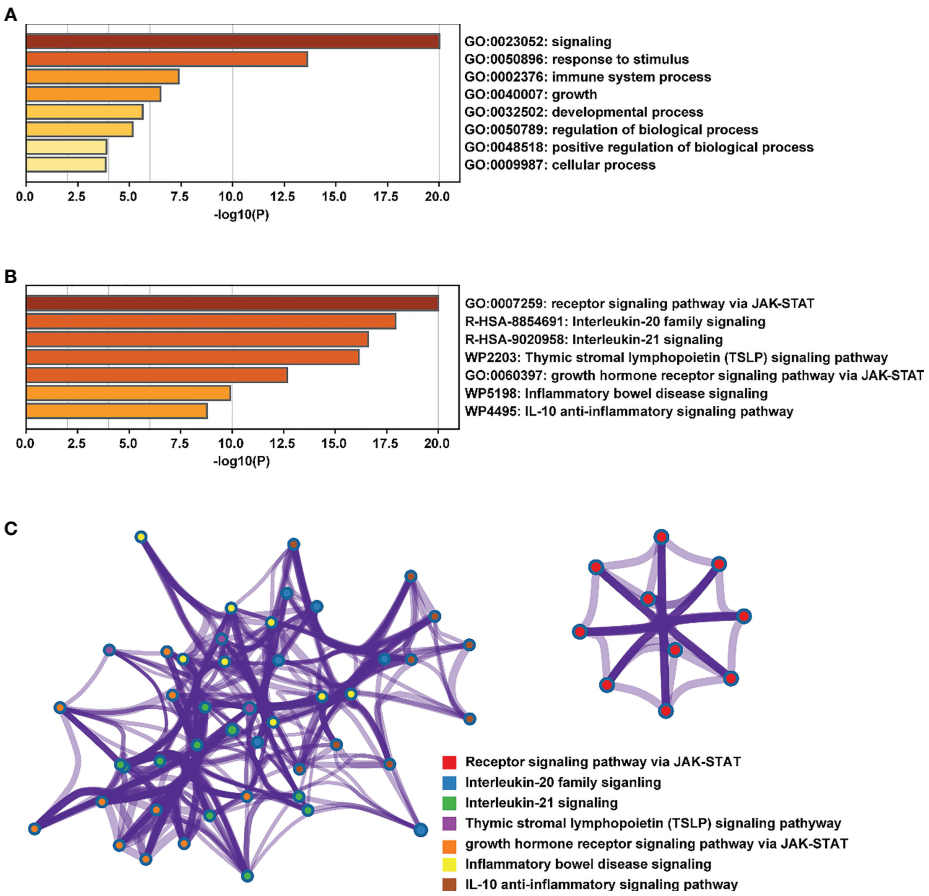


FIGURE 2
Enrichment analysis of the main functions of the STAT family. **(A, B)** biological processes and pathways related to STATs genes as enriched in Gene Ontology, colored by *p*-values. **(C)** An enrichment network: each node in a cluster is colored accordingly, with cluster IDs that are close together being grouped.

characteristics, including age, tumor stage, grade, and the expression of STAT gene family member, and the survival status of ovarian cancer patients. There were five columns representing age, pTNM_stage, Grade, STAT1-6 expression, and survival Status in each figure, respectively. Different colors represented different ages (<= 60 years and > 60 years), pTNM_stages (I, II, III, IV), Grades (G1, G2, G3), expression levels of STAT1-6 (High exp, Low exp), Status (Alive, Dead). The above variables are connected by connecting lines to obtain the distribution of the same ovarian cancer sample across various characteristics. Through the plotting of these diagrams, we can see that patients with advanced (III, IV) ovarian cancer were more likely to have low expression of STAT family members. Differentially, in high-grade (G3, G4) ovarian cancer, STAT1, 2, 4, and 5A were highly expressed, while STAT3 and STAT5B were mostly lowly expressed. In addition, the low expression group of other STAT members except STAT5B had more deaths. This reflected the complexity of the role of different STAT members in the occurrence and development of ovarian cancer.

## Association of the expression of STATs with the prognosis of ovarian cancer patients

Next, an assessment was made of the influence of STATs on ovarian cancer survival. According to openly accessible data (2021 version: http://kmplot.com/analysis/index. Php?p=service&cancer=ovar), using Kaplan-Meier Plotting tools, we investigated whether mRNA levels of STATs correlated with the survival time of ovarian cancer patients by "mean expression of selected genes" in multiple genes option. The desired Affy ID is valid: 200887_s_at (ISGF-3, STAT91, STAT1), 225636_at (STAT2), 225289_at (STAT3), 206118_at (STAT4), 203010_at (STAT5, MGF, STAT5A), 212549_at (STAT5B), 201331_s_at (STAT6, IL-

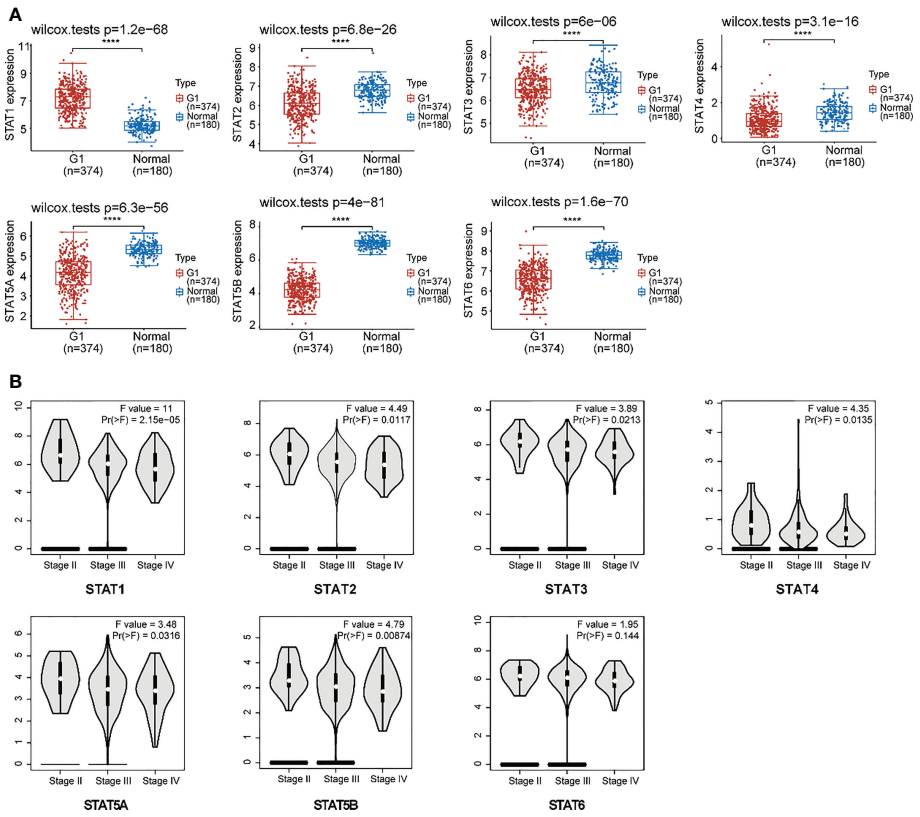


FIGURE 3
Expression of STAT family members in ovarian cancer. **(A)** The expression distribution of STAT family genes in ovarian cancer tissues (G) and normal tissues. Top-left represented the significance *P*-value, ****$P < 0.0001$. **(B)** An association between STATs expression and major tumor stages in patients with ovarian cancer.

4-STAT, D12S1644). Compared with the high-expression group of the STATs family, the overall survival (OS) and progression-free survival (PFS) of ovarian cancer patients in the low-expression group were higher in Figure 5. The median survival time (MST) for OS and PFS was 41.87 months *versus* 50.03 months (HR=1.42, $P$=0.0058), and 16 months *versus* 22.24 months (HR=1.61, $P=1.5\times10^{-5}$) in the high expression/low expression cohort, respectively. While the effect on post-progression survival (PPS) was not significant (HR=0.87, $P$=0.24, MST: 41 months *versus* 35 months). The whole high expression level of STATs transcription factors increased the risk of ovarian cancer death by 1.42 times. Therefore, the mean low expression of STATs members is beneficial to the survival of ovarian cancer patients.

Besides, the effect of each STAT member on the survival time of ovarian cancer patients was also analyzed using the same Probe Id as above (Table 1). Based on Kaplan-Meier curves and log-rank tests, the results in Figure 5 showed that a significant correlation was observed between increased STAT4 and 6 mRNA levels, decreased STAT1 mRNA levels, and overall survival (OS) in ovarian cancer patients. ($P < 0.05$). Ovarian cancer patients with a high level of STAT4 and 6 gene expression or a low level of STAT1 gene expression had high OS.

Moreover, in ovarian cancer patients with different pathological types, STAT expression was tested for potential correlation with OS, progression-free survival (PFS) as well as post-progression survival (PPS), respectively (Supplementary Material Tables 3–5 ). Patients with serous ovarian cancer expressed lower levels of STAT1 mRNA, while higher levels of STAT 2, 5A, and 5B mRNA had longer PFS but had no effect on patients with endometrioid carcinoma. Based on these above results, most members of the STAT family, except STAT3, may be promising prognostic indicators for ovarian cancer.

## Developing and evaluating a STATs prognosis prediction model

Four STAT members with potential prognostic significance were identified by LASSO (lambda.min=0.0234). A stepwise multivariate Cox regression model was constructed using

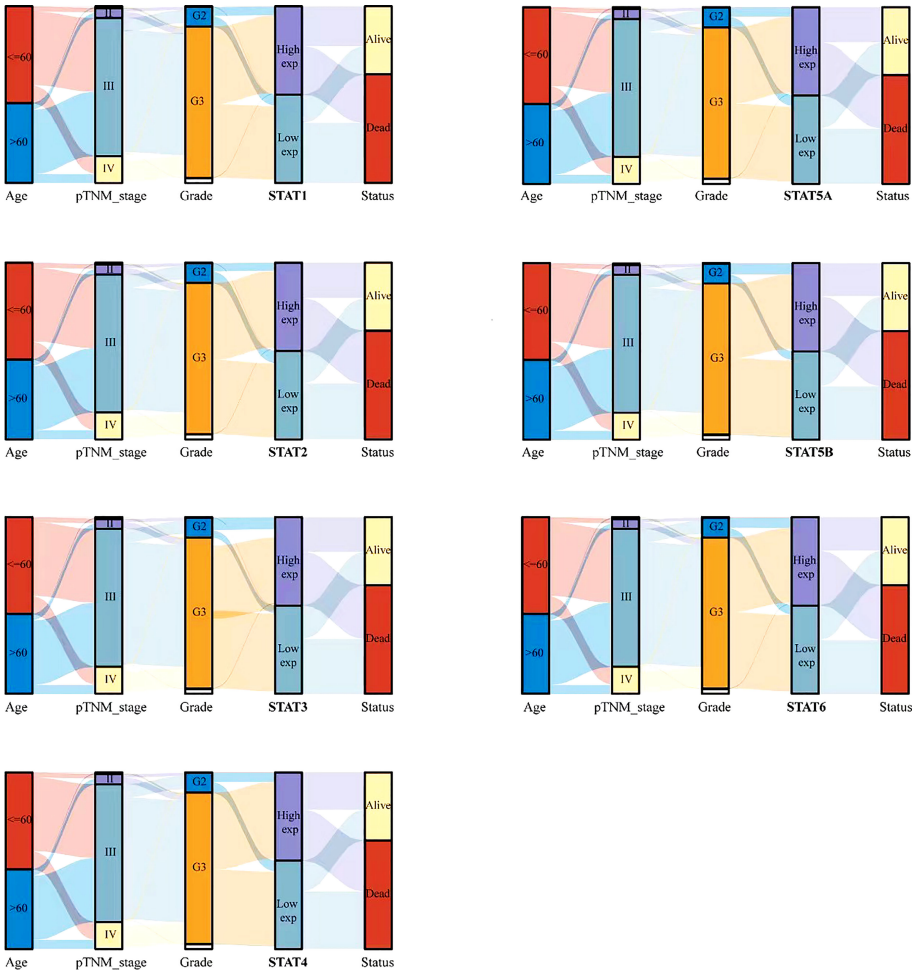


FIGURE 4
Relationship between STAT family and clinical characteristics of ovarian cancer patients. Rows represent feature variables, different color represents different age (<=60 years, >60 years) or pTNM_stage (I, II, III, IV) or Grade (G1, G2, G3) or expression level (High exp, Low exp) or survival status (Alive, Dead). Lines show how the same sample is distributed across different feature variables.

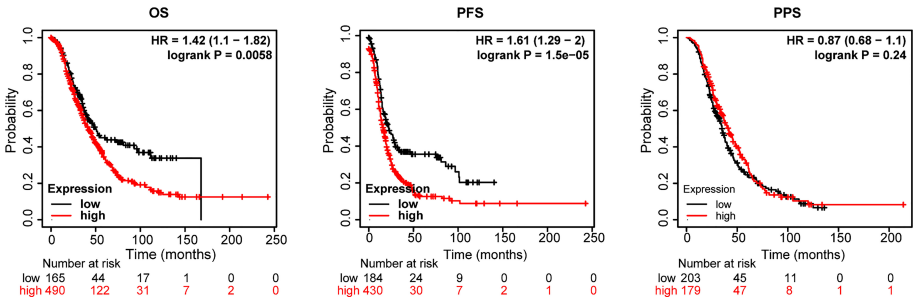


FIGURE 5
Relationship between the STATs family and survival of ovarian cancer patients. Probe Id (Gene symbol): 200887_s_at (ISGF-3, STAT91, STAT1), 225636_at (STAT2), 225289_at (STAT3), 206118_at (STAT4), 203010_at (STAT5, MGF, STAT5A), 212549_at (STAT5B), 201331_s_at (STAT6, IL-4-STAT, D12S1644). OS, overall survival; PFS, progression-free survival; PPS, post-progression survival, HR= hazard ratio.

TABLE 1 Correlation between the expression of STATs and OS or PFS in ovarian cancer patients.

| | OS | | | | PFS | | | |
|---|---|---|---|---|---|---|---|---|
| | MST (months) | | HR (95% CI) | *P*-Value | MST (months) | | HR (95% CI) | *P*-Value |
| | Low | High | | | Low | High | | |
| **STAT1** | 44.13 | 50 | 0.84 (0.72-0.98) | 0.023 | 22.13 | 19.09 | 1.19 (1.04-1.37) | 0.011 |
| **STAT2** | 48 | 40.4 | 1.32 (1.05-1.66) | 0.016 | 22.6 | 15 | 1.63 (1.30-2.05) | 1.7e-05 |
| **STAT3** | 40 | 48 | 0.89 (0.71-1.12) | 0.32 | 18 | 16.03 | 1.27 (1.05-1.54) | 0.016 |
| **STAT4** | 43 | 46 | 0.84 (0.73-0.96) | 0.09 | 18.79 | 26.06 | 0.85 (0.74-0.97) | 0.02 |
| **STAT5A** | 42.17 | 46.82 | 0.89 (0.77-1.02) | 0.082 | 19.23 | 20.43 | 1.07 (0.94-1.21) | 0.33 |
| **STAT5B** | 44.3 | 45.97 | 0.88 (0.78-1.01) | 0.059 | 19.09 | 20.93 | 0.93 (0.82-1.06) | 0.3 |
| **STAT6** | 43 | 50.3 | 0.79 (0.69-0.91) | 0.0012 | 20 | 20 | 1.09 (0.96-1.25) | 0.17 |

MST, median survival time; Low, Low expression cohort; High, High expression cohort; HR, hazard ratio, 95% CI, 95% Confidence interval.

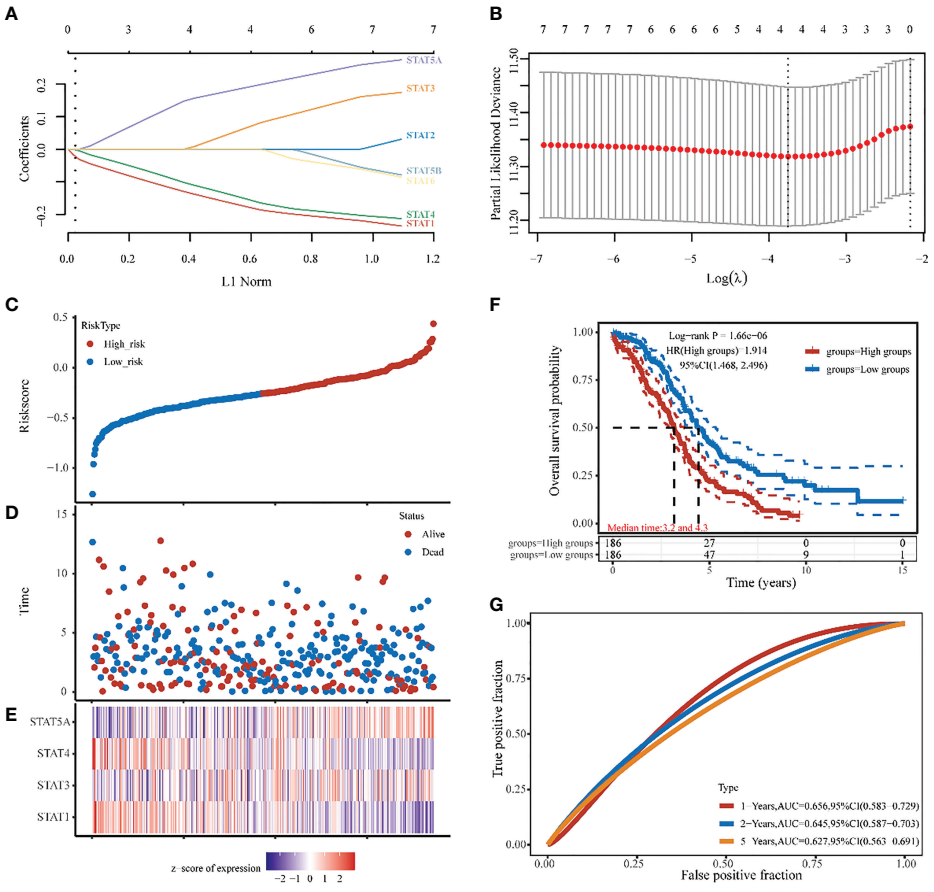


FIGURE 6
Ovarian cancer survival prediction and STAT genes selection. **(A)** The coefficients of 7 STATs in the LASSO model were screened by 10-fold cross-validation. **(B)** Analysis of the seven selected STATs by X-tile. **(C, D)** The selected dataset's risk score, survival time, and survival status. **(E)** The heatmap was the gene expression from the signature. **(F)** A risk model for signature OV patients with Kaplan-Meier survival analysis. HR (High exp) represents the hazard ratio of the low-expression sample relatives to the high-expression sample. **(G)** ROC curves of 1,2,5 years, 1-, 2-, and 5-year overall survival probability based on the STATs Risk score.

STAT1, STAT3, STAT4, and STAT5A as filter variables (Figures 6A, B). The Risk score was calculated as follows: (-0.1694) * *STAT1* + (0.0554) * *STAT3* + (-0.1447) * *STAT4* + (0.1837) * *STAT5A*. Smooth curve fitting provided the following results, which showed the Risk score from low (blue spot) to high (blue spot), thus based on the Risk score median, a cut-off value was determined (high risk: score > -0.257, low risk: score < -0.257) (Figure 6C). As shown in scatter plots and also Kaplan-Meier plots Figures 6D, F), patients with a high-Risk score had a short median survival time (median time=3.2 vs. 4.3 years, hazard ratio [HR] =1.914, $P$ = 1.66e-06). The heatmap was the gene expression of STAT1, 3, 4, and 5A from the signature. In the high-risk group, the protective STAT1 and STAT4 genes were low expressed, whereas STAT3 and 5A, the risk genes, were significantly higher expressed (Figure 6E). In terms of time-dependent ROC curves, 1-, 2-, and 5- years of survival were assessed using Area Under Curve (AUC) values of 0.659, 0.645, and 0.627, respectively (Figure 6G). A prognostic model based on disease-specific survival (DSS) was also constructed through STAT1, 4, 5A. Compared to the low-risk group with STAT1,4, the high-risk group with STAT5A was closely linked with a worse 1-, 2-, 5- years DSS of ovarian cancer patients (median time=3.4 vs. 4.7 years, HR =1.831, $P$ = 3.31e-05 in Figure S2). Finally, as revealed by univariate analysis, Age, Race, and STAT 1, 4, and 5A were significantly related to OS based on the TCGA cohort (Figure S3A). Using the factors aforementioned above, we performed a multivariate Cox regression analysis. As a result, STAT5A was still an independent predictor of outcome for this cohort of patients (hazard ratio [HR] = 1.3, $P$ < 0.001), which was consistent with LASSO analysis (Figure S3B). Additionally, Figures 3C, D displayed the cohort's 1-, 2-, and 5-years OS Nomograms. As STAT5A was the gene with the highest risk score in the OV prognostic model, it had become the focus of follow-up research.

## STAT5A gene mutation analysis in ovarian cancer

STAT5A was altered (73%) in 272 samples from 374 patients with ovarian serous cystadenocarcinoma. The somatic mutation rate of STAT5A was only 0.37%, which was manifested as a gene missense mutation, leading to abnormal amino acid coding in the SH2 domain (Figure 7A). The panoramic waterfall mutation

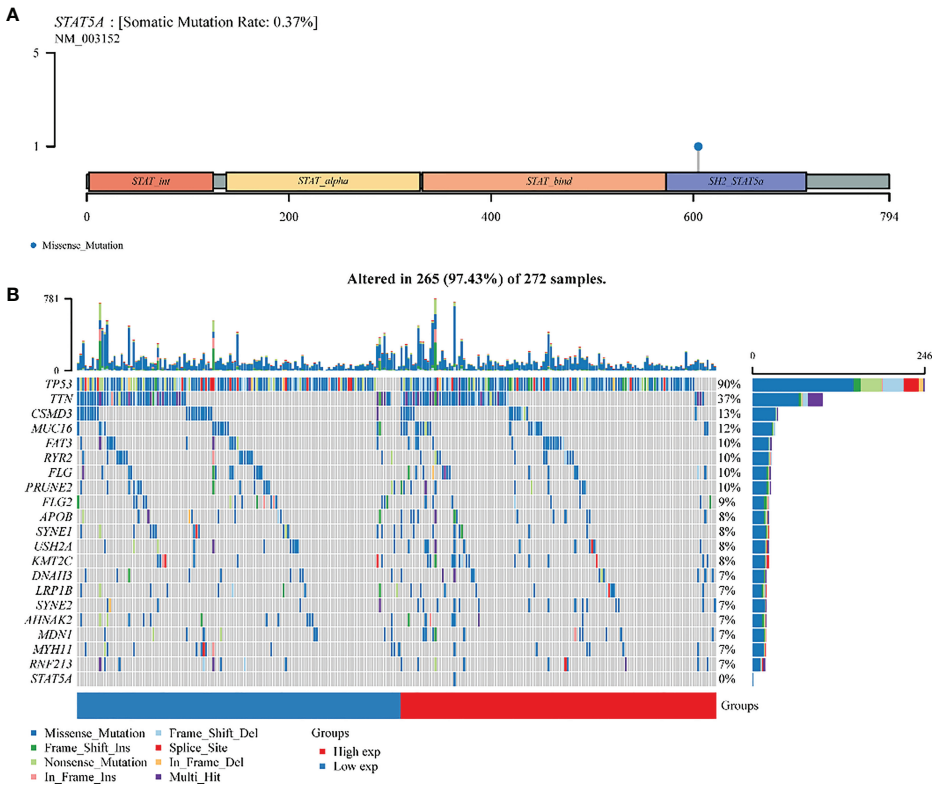


FIGURE 7
A landscape analysis of STAT5A gene mutations in ovarian cancer. **(A)** Lollipop charts of the mutated STAT5A gene. **(B)** Oncoplot displays the somatic landscape of OV TCGA cohorts. The genes and samples are sorted according to their mutation frequency and histology; Above the legend, the bar plot shows the number of mutations burdened.

type diagram shows that each sample's mutation load was different, and the median value was 82. TP53 had the highest mutation rate (90%), and the top ten mutated genes included TTN (37%), MUC16(12%), CSMD (13%), FAT3 (10%), FLG (10%), RYR2 (10%), PRUNE2 (10%). FLG2 (9%) and APOB (8%). However, STAT5A mutation only occurred in the group with high STAT5A expression, so there should be no mutation in ovarian cancer with relatively low STAT5A expression (Figures 3, 7B S4B). A missense mutation was the main classification of gene mutation in each sample. Single nucleotide polymorphisms (SNPs) were the most common mutation type. Cytosine (C > T, C > A, C > G) and thymine (T > A, T > C, T > G) are the main types of single nucleotide mutation (SNV) mutations (Figure S4A).

## Correlation between STAT5A and the functional states of OV cells

To further study the role of STAT5A in OV, GSEA online database-Linkedomics (http://linkedomics.org) was used to explore the pathways and functions involved in STAT5A. We first analyzed the 50 most positively and negatively affecting genes related to STAT5A expression, as shown in the heat map in Figures S5A, B. Then GO and KEGG analysis of STAT5A in patients with OV was carried out in Figures S5C, D which revealed significant enrichment in mitochondrial gene expression, mitochondrial respiratory complex assembly, adaptive immune response, Oxidative phosphorylation, Chemokine signaling pathway, NF-kappa B signaling pathway, and JAK-STAT signaling pathway. From this, it can be concluded that the transcription factor STAT5A may affect the oxidative phosphorylation process of cells through the negative regulation of the mitochondrial respiratory chain complex and then interfere with the immune regulation and signal molecule transmission process of the body. Next, we conducted a more in-depth analysis of the function of STAT5A in OV using the CancerSEA single cell sequencing database (http://biocc.hrbmu.edu.cn/CancerSEA). Single gene analysis of STAT5A from different cell groups, which denoted different OV patients-derived xenograft samples, was performed. There are 7 functional states including Quiescence (R=0.28), Hypoxia (R=0.28), Apoptosis (R=0.24), Angiogenesis (R=0.23), Cell Cycle (R=-0.30), DNA repair (R=-0.36) and Invasion (R=-0.38) that are significantly related to STAT5A ($P < 0.05$, Figure S6). Specifically, a significant inverse relationship was found between STAT5A expression and invasive behaviors and DNA damage repair (Figure 8, $P < 0.01$), indicating that lower STAT5A expression could promote ovarian cancer cell invasion as well as improve the ability of cells to repair DNA damage, thus participating in the process of metastasis and recurrence of ovarian cancer.

## Analysis of the expression of STAT5A on OV tissues and cell lines

For further validation of the main conclusion in Figure 8, we first verified the expression of STAT5A and P-STAT5A in ovarian cancer from tissue microarray (TMA). In the detection of 45 pairs of ovarian cancer and adjacent normal tissues, the expression levels of both in cancer were significantly lower than those in para-cancerous tissues (Figure 9A, $P<0.0001$). The receiver operating characteristics (ROC) curves on independent tests of STAT5A and P-STAT5A are illustrated in Figure 9B. The optimal cut-off value for STAT5A was < 0.04375 (sensitivity 73.33%, specificity 73.33%, AUC=0.744, $P<0.0001$), while that for P-STAT5A was < 0.0125 (sensitivity 83.37%, specificity 83.72%, AUC =0.920, $P<0.0001$). Kaplan-Meier survival plots revealed that OV patients with high STAT5A expression had longer survival times than those with low STAT5A levels ($P$ =0.039). However, high expression of P-STAT5A seems to be a better prognostic indicator of ovarian Cancer ($P$ =0.0042, Figure 9C). Consistently, the univariate and multivariate Cox regression analyses of OS in paired ovarian cancer and para-cancerous tissues showed that P-STAT5A rather than STAT5A could be an independent risk factor ($P$=0.032, Supplementary Material Table 6 in Supporting Information). Next, to address the role of STAT5A in OV cell invasiveness, human ovarian serous cell line HO8910 was used as the research object and normal ovarian epithelial cell IOSE80 as the control. First, we explored the baseline expression of transcription factor STAT5A, the activated form P-STAT5A and matrix metalloproteinases 2 (MMP2) and MMP12. The latter is involved in the degradation of extracellular matrix (ECM), in turn, mediates the epithelial-to-mesenchymal transition (EMT) process, which is known as one of the primary mechanisms for tumor invasion and metastasis. Compared to IOSE80 cells, the levels of STAT5A, P-STAT5A, and MMP12 proteins decreased significantly in HO8910 cells, while MMP2 levels increased (Figure 9D). After that, STAT5A overexpression plasmids were transiently transfected into HO8910 cells. The transfection efficiency was verified by quantitative real-time PCR (qRT–PCR) (Figure 9E, $P<0.0001$) and Western blotting analysis (Figure 9F). HO8910 cells overexpressing STAT5A exhibited increased MMP12 expression, while MMP2 was significantly suppressed. Compared with the control and the negative vector transfection group, a significant reduction was observed in the migration ability of cells transfected with cDNA-STAT5A. It can be seen by the area of wound-healing (marked by the yellow line in the figures) significantly decreased from the initial scratch time (0 h) to 48 h post-scratching (Figure 9G, $P<0.0001$).

Furthermore, HO8910 cells were seeded in the upper compartments of Matrigel-coated transwell chambers to assess cell invasion ability. After 48 h, the number of cells that invaded

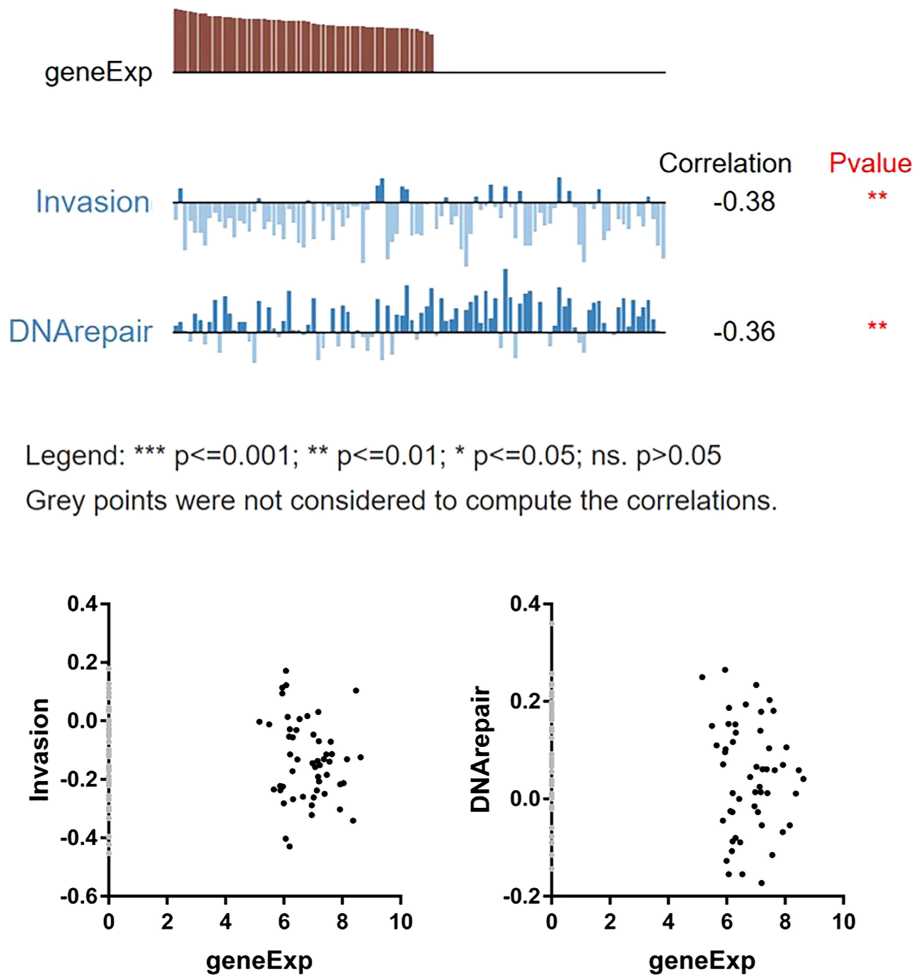


FIGURE 8
Correlation between STAT5A and functional states of OV cells.

the lower chamber in the STAT5A-PcDNA transfected group was less than 30% of the control group (Figure 9H, $P<0.0001$). These results suggested that low expressed STAT5A may directly or indirectly regulate the expression of MMP2 and promote the invasion and metastasis of ovarian serous cystadenocarcinoma cells.

## Discussion

STAT5 consists of two isoforms, STAT5A and STAT5B, each encoded by a different gene, although they share 94% of the same structure (35). STAT5A was cloned from the lactation tissue of sheep in 1994 and was initially called mammary gland factor (MGF) (36), which could initiate milk protein expression and modulate prolactin action (37). As part of the classical JAK2-STAT5A/5B signal pathway, the activated STAT5A/5B dimer in the cytoplasm was required to travel into the nucleus. An eight to ten base pair reverse repetitive DNA sequence known as TTC (C/T) N (G/A) GAA was recognized by the nuclear STAT5A/5B (38). structurally active Mutations of STAT5 caused carcinogenesis *in vitro* and *in vivo* (39). So far, STAT5B mutations are rare and tend only to be found in human myeloid leukemia such as $CD4^+$ T-cell prominent granular lymphocytic (T-LGL) leukemia, chronic natural killer lymphoproliferative disorders (CLPD-NK), Acute promyelocytic leukemia (APL) (40, 41). Most mutations in STAT5B occurred in the SH2 region (42). In this study, the mutation frequency of STAT5A in ovarian cancer was found to be extremely low, mainly missense mutation in the SH2 domain (Figure 7).

In much the same way as other STAT family members, the structural activation of STAT5 contributes to tumor survival, growth, metastasis, and chemotherapy resistance. As mentioned earlier, activated STAT5B is involved in maintaining ovarian CSCs; chemotherapy resistance and tumor immune response are closely related. Nevertheless, little information was available

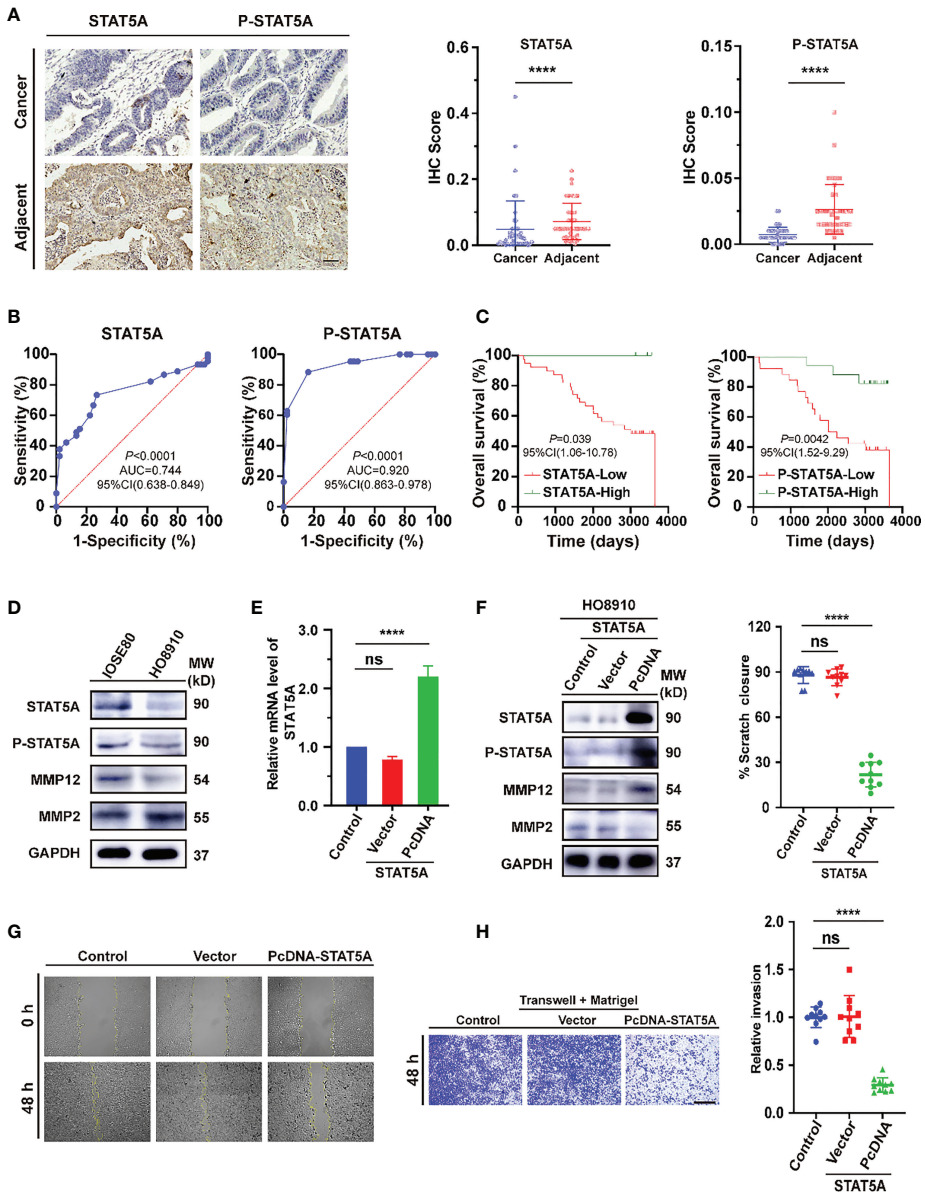


FIGURE 9
Evaluation of STAT5A expression in ovarian cancer tissues and cell lines. **(A)** Immunohistochemical staining of STAT5A and p-STAT5A on ovarian cancer and adjacent tissues from TMA samples (n=90). Black scale bar, 50 μm. **(B)** The ROC curves of STAT5A and P-STAT5A are based on independent tests. **(C)** Kaplan–Meier OS curves based on STAT5A or P-STAT5A level. **(D)** Immunoblots illustrating the basal expression of STAT5A, P-STAT5A (Tyr 694), MMP12, and MMP2 in the indicated human ovarian serous adenocarcinoma cell (HO8910) and normal ovarian epithelial cell line (IOSE80). **(E, F)** The mRNA and corresponding protein expression levels of SATAT5A were determined 48 h post-transfection with pcDNA-STAT5A plasmids in HO8910 cells. For normalization, GAPDH was used as an internal reference. MW: molecular weight. **(G)** Scratch-wound assay to quantify HO8910 cell migration ability. The scratches were recorded at 0 h and 48 h after scratching. Yellow lines indicated the scratched edges. White scale bar, 100 μm. **(H)** Transwell invasion assay with Matrigel. Cell invasion abilities were measured 48 h after cells or STAT5A overexpressing cells seeding onto a Matrigel-coated transwell filter. Black scale bar, 200 μm. **** $P<0.0001$, ns: not significantly determined by one-way ANOVA **(E, F, H)**, Mann-Whitney test **(B)**, Chi-square test, Kaplan-Meier survival analysis, and Log-rank statistical test **(C)**.

about how STAT5A affected ovarian cancer development and progression. Interestingly, mice carrying STAT5 homozygous deletion (STAT5A−/− 5B −/−) were shown to be sterile, deficient in luteal functional differentiation, and disrupted ovarian development (43). Besides, STAT5 can be activated by various cytokines and hormones. The interaction between steroid receptors such as progesterone and estrogen receptors and nuclear STAT5 stimulates its activity, showing the importance of STAT5

expression in maintaining the ovary's normal structure and functional integrity (44). According to a study on non-coding RNA transcripts involved in the pathogenesis of ovarian endometriosis (OEM), it was found that STAT5A can be used as a diagnostic marker of OME, and its overexpression was associated with a positive outcome for EOC (45), which was inconsistent with our experimental results. As shown in Figure 8, STAT5A expression and ovarian cancer invasion were negatively correlated (R= -0.38). Despite STAT5A/5B being active in most leukemia and some solid tumors, the role of STAT5A/5B in tumor invasion was complicated (46). Data from murine breast cancer studies suggested that STAT5A had dual efficacy in malignant mammary epithelial cells. In the early stage of breast cancer, STAT5A/5B promoted malignant transformation of breast epithelial cells and accelerated tumor growth. In advanced breast cancer, STAT5 was a key molecule regulating and promoting the differentiation of mammary epithelial cells, which can effectively delay the invasion and metastasis of tumors (47). And in the breast cancer clinical sample activated STAT5A/5B was positively correlated with the differentiation status of breast cancer, but it can also prevent the dissemination of confirmed breast cancer, which was a sign of good outcome for breast cancer with negative lymph nodes (48). Phenotypic analysis of TRAM mouse models of prostate cancer and STAT5 knockout mice indicated that STAT5A/5B activation was essential for the growth and survival of prostate cancer. Further studies showed that CyclinD1 and Bcl-xl were the target genes of STAT5 in prostate cancer, which was a potential mechanism of STAT5 regulating prostate cancer (49). Nuclear STAT5A/5B expression predicted early disease recurrence and enhanced the ability of prostate cancer cells to metastasize *in vivo* and *in vitro* (50). Prostate cancer distant clinical metastases were overexpressed with nuclear STAT5A/5B in 61% of cases, which consequently made prostate cancer cells migrate and invade more readily with the aid of microtubule network rearrangement. Importantly, in an experimental *in vivo* metastasis test, activated STAT5 resulted in a ten-fold increase in lung metastasis. In addition, constitutive activation of STAT5 signaling also enhanced cell invasion, migration, and EMT of head and neck squamous cell carcinoma (51). In the subsequent verification, we also confirmed that the expression of STAT5A and P-STAT5A was significantly lower in OV tissues and cell lines, which was closely correlated to the beneficial prognosis in OV patients, especially the low level of P-STAT5A (Figures 9A–D). Besides, STAT5A was negatively related to tumor-promoting MMP2 expression in human ovarian serous cystadenocarcinoma cell line HO8910 (Figures 9D–F). It is speculated that MMP2 may act as a direct or indirect effect molecule of transcription factor STAT5A to promote the invasion and migration of ovarian cancer, which was in line with previous studies on esophageal cancer (52). Other researchers had suggested that STAT5A activation was related to the regulation of angiogenesis in ovarian cancer, because VEGF secreted by ovarian cancer cells can activate STAT *via* VEGFR in the cancer cells (53). The dual role of activated STAT5A in ovarian cancer invasion demonstrated the complexity of STAT5A function. Of course, we had to admit that there are individual differences among ovarian cancer cell lines, which will be further checked in various human serous cancer cell lines (e.g., SK-OV-3, Shin-3, OVCA-3). We will expand the sample size appropriately to increase the rigor of this validation. In addition, we will construct an ovarian cancer xenograft tumor model and introduce STAT5A or JAK2 recombinant protein to verify the inhibition of MMP2 by high expression of STAT5A, thus affecting the invasion and migration ability of ovarian cancer.

Furthermore, in this study single-cell sequencing data in Figure 8 also demonstrated that in ovarian cancer cells, STAT5A expression was negatively related to DNA repair (R= -0.36). STAT5A-overexpressed ovarian cancer patients can benefit from multiple types of treatment, including chemotherapy, radiotherapy, and immunotherapy because an essential limiting factor in tumor therapeutic efficacy is tumor cells' ability to repair DNA damage. In a study of radiation resistance and glutamine anabolism, STAT5 regulated the transcriptional level of glutamine synthetase (GS), then promoted nucleotide metabolism, accelerated DNA damage repair, and eventually made cancer cells more resistant to radiation. In turn, radiation-resistant cells exhibited high glutamine anabolic, including nasopharyngeal carcinoma cells (CNE2-IRR) and glioma cells (U251-IRR) (54). However, a novel class III RKT inhibitor-AIU2001 reduced DNA damage repair genes expression by downregulating STAT5 mRNA level in lung cancer cells (55). Moreover, STAT5A/5B participated in the regulation of DNA repair using homologous recombination in prostate cancer by inducing the RAD51 mRNA level while blocking of JAK2-STAT5A/5B signal pathway sensitized prostate cancer to radiotherapy (56). To sum up, the relationship between STAT5 expression and DNA damage and repair of tumor cells may vary with tumor types.

An integrated prognostic model that includes STAT1, STAT3, STAT4, and STAT5A may be more accurate than one based on a single biomarker. Transcriptional factor families, such as E2F and Forkhead box O (FOXO) transcription factors, have demonstrated outstanding potential as a predictor of cancer outcomes recently. The above studies preliminarily proved that STATs expression had an essential impact on ovarian cancer progression. Mainly, STAT5A affected cell invasion and DNA damage repair, which can be an essential tool to predict ovarian cancer prognosis. However, there are limitations to the current research. Data for this study were derived from the TCGA

database and single-cell sequencing, and no independent cohort studies were available. As a next step, we will collect enough clinical samples to validate the effect of STAT family expression on the clinical parameters of ovarian cancer patients.

# Conclusion

Here, a comprehensive analysis of STATs expression and its prognostic value has been carried out to construct an ovarian prognosis model. These results provided a basis for realizing personalized and accurate treatment of ovarian cancer and improving predictive biomarkers. Based on our findings, STAT1, STAT4, and STAT6 may be viable therapeutic targets for ovarian cancer. Low P-STAT5A, but not STAT5A, was a favorable prognostic indicator in human OV. Since STAT5A expression was negatively correlated with ovarian cancer cell invasion and DNA repair, STAT5A/P-STAT5A activators or inducers may increase ovarian cancer survivorship and allow more of them to benefit from radiotherapy and chemotherapy, molecular targeted drug therapy, or immunotherapy.

# Materials and methods

## Source of the data

RNA-sequencing profiles and relevant clinical data consisting of 374 OV tissues came from the TCGA dataset (https://portal.gdc.com). 180 normal control samples were accessed from Genome Type tissue expression (GTEx) datasets (V8) (https://www.gtexportal.org/home/datasets). Additionally, various clinical parameters were collected, including survival status, age, race, pTNM stage, and grade collected in Table 1. We used R software v4.0.3 (R Foundation for Statistical Computing, Vienna, Austria) for our statistical analyses. Statistical significance was deemed to be $p$-value <0.05.

The Sankey diagram was constructed with the R software package ggalluvial. The gene mutation data were downloaded and visualized by the map tools package in R software. Genes with higher mutational frequency detected in an ovarian cancer patient in histogram were shown.

## GEPIA2 dataset

A total of 9736 tumors and 8587 normal samples based on the TCGA and GTEx projects were analyzed using the GEPIA2 analyzer. Through the multiple gene comparison columns in the expression analysis plate, the STATs expression level in various tumors was investigated. Besides, we profiled the expression of STATs in the significant stage of ovarian cancer using a box plot in the "pathological stage plot" column.

## Metascape database

Metascape database is a highly effective tool for studying functional gene annotations. Genes and proteins can be analyzed in batches to understand better how genes or proteins work. First, the members of the STAT family were input into the "multiple gene list" text box, and the species "H.sapines" was selected for custom analysis. Findings from the gene ontology enrichment analysis were obtained in the analysis report.

## Kaplan-Meier Plotter

Based on ovarian cancer gene chip data, Kaplan-Meier Plotter analysis was conducted to determine how STAT's gene expression affects ovarian cancer survival rates. The prognostic value (mainly OS and PFS of ovarian cancer patients) of each member of the STATs family was analyzed, respectively. According to the median values of the expression levels of the samples of the ovarian cancer patients, groups with high and low expression were created. Comparing the two cohorts yielded an HR with 95% confidence intervals (CIs) and a log-rank $P$-value using the Kaplan-Meier survival plot, indicated at the top right of the main graph (57).

## Prognostic value assessment of STATs

The ovarian RNA sequencing data from the TCGA database were converted into transcripts per million (TPM), the data log2 (TPM+1) was normalized, and the clinical information samples were retained for follow-up analysis. An analysis of survival rates among groups by the log-rank test was conducted. The prediction accuracy and risk score of STATs gene were analyzed and compared by time ROC (v0.4).

In this study, the LASSO regression algorithm was employed as a feature selection algorithm, along with 10-fold cross-validation, and a glmnet package in R was performed for the analysis. Multivariate cox regression analysis was used to construct a prognostic model, and first, the multi-factor Cox regression was used to analyze the data, and then the step function performed the iteration. Finally, the optimal model was selected as the final model. Kaplan-Meier curves plotting standard was the same as that described above.

The analyses and R packages were all developed with R (foundation for statistical computing 2020) version 4.0.3. Statistical significance was deemed to be $P$-value <0.05.

## LinkedOmics database

LinkedOmics is a database based on multiple group association data analysis for TCGA. The ovarian cancer data set (TCGA-OV)

was selected, and RNAseq was chosen as the data type in the searching and targeting data sets. The target gene STAT5A was input; then, the Pearson Correlation test statistical method was selected for correlation analysis. Finally, we obtained the heat map of the genes positively and negatively related to STAT5A. Moreover, the above results were analyzed by GSEA enrichment analysis in the LinkInterpreter plate based on WebGestalt. In the Enrichment Analysis column, select the KEGG pathway and GO Analysis (Biological process) for further analysis.

## CancerSEA single cell state atlas

The database collects 72 single-cell datasets, totaling 41,900 single cells of 25 human cancers, Mapping the functional states of a single cell of these 14 functional states related to cancer in different cancers. These functional states were also associated with 18,895 protein-coding genes (PCGs) and 15,571 LncRNAs on the single cell level to understand the mechanisms underlying functional differences in cancer cells (58). By inputting the STAT5A gene, the heat map of its correlation with 14 states of ovarian cancer cells was plotted. The status of ovarian cancer cells with a high correlation with the STAT5A gene was filtered by limiting the correlation strength ($R > 0.3$), and the corresponding scatters plot was generated automatically.

## Cell lines and culture

Human ovarian cancer cell line HO8910 was obtained from the American Type Culture Collection (ATCC). Human normal ovarian epithelial cells (IOSE80) were a kind gift from Hanqing Hong (International Peace Maternity and Child Health Hospital, China). The two kinds of cells were incubated in DMEM High Glucose medium and DMEM-F12medium (HyClone, SH30234.01), respectively, with 10% Foetal Bovine Serum (FBS), 1% penicillin, and 1% streptomycin at 37°C in 5% CO2.

HO8910 cells were transiently transfected with pcDNA3.1-STAT5A-C-3Fla or empty vector plasmids using Lipofectamine™ 3000 Transfection Reagent (Thermo L3000015) according to the manufacturer's instructions. The total RNA and whole-cell lysates were then harvested for Western blots analysis 48 h after transfection.

## RT-PCR

Total RNA was extracted from HO8910 cells by the Trizol method. According to TAKARA reverse transcription kit instructions, the reaction solution was prepared in a 0.2 mL Ep tube. The reverse transcription conditions were as follows: 37 ℃ for 15 min. The target gene and internal reference gene expression in the cell sample were detected by qPCR. RT$^2$Profiler PCR Array Data Analysis system of QIAGEN Company was used for data analysis. Primer sequence for STAT5A and GAPDH (5'to 3'):

STAT5A-human-F: GCAGAGTCCGTGACAGAGG;
STAT5A-human-R: CCACAGGTAGGGACAGAGTCT.
GAPDH-human-F: TCAACGACCACTTTGTCAAGCTCA;
GAPDH-human-R: GCTGGTGGTCCAGGGGTCTTACT.

PCR reaction condition was as follows: 10 min 95°C pre-denaturation; 95°C 15 s, 60°C 60 s PCR cycles for 40 cycles, 60 → 95°C for dissociation curves.

## Western blots

Above $110^7$ IOSE80 and HO8910 cells were collected, respectively. Western blotting analysis was carried out using whole-cell extracts lysed with RIPA lysis buffer (Thermo 89901). The above two cell protein lysates were electrophoresed with 10% sodium dodecyl sulfate-polyacrylamide gel electrophoresis (SDS-PAGE) (Concentration: 100V, 15min; Separation: 120V, 60min) and then transferred to nitrocellulose (NC) membranes (Merck, filter type 0.45μm). Next, all the NC membranes were blocked with 1×protein-free rapid blocking buffer (Epizyme, Shanghai) in a room temperature setting for 40 min. A further incubation step was taken with anti-STAT5A (Proteintech 13179-1-AP), anti-P-STAT5A (Signalway Antibody, 11048), anti-MMP2 (Proteintech, 10373-2-AP), anti-MMP12 (Proteintech, 22989-1-AP), and HRP-conjugated mouse anti-GAPDH (Yeasen Biotech, #30203ES10) diluted to 1:1000 at room temperature for 2 hours. Wash three times in Tris-buffered saline containing 0.1% Tween-20 (TBST) for five minutes each; incubation of the membranes with corresponding secondary antibodies (diluted to 1:10000) followed for 1 hour. The enhanced chemiluminescence (ECL) reagent (Millipore WBKLS0500) was used to visualize protein signals on an Image Quant LAS4000 system (GE Healthcare). These images were analyzed semi-quantitatively using ImageJ 1.8.0 (USA) software, then normalized to a background image.

## Scratch wound assay

HO8910 cells, after different treatments, were seeded in 48-well plates with $1.5x10^5$ cells per well and incubated overnight in DMEM High Glucose medium supplemented with 2%FBS. Then the cell monolayer was scraped horizontally with a 200 μL pipette tip and scratches were immediately generated and washed twice with 1XPBS. 2 ml of fresh DMEM High Glucose medium containing 2% FBS was added, and cells were continued

to be cultured for 48 h. Images of cells using an inverted microscope (Leica DMi8) by a 10X objective. Image J software quantified and analyzed the scratch area (freeware http://fiji.sc).

## Transwell invasion assay

The Matrigel was placed in the refrigerator at 4° C overnight from -20° C, and the upper chamber surface of the bottom membrane of the Transwell chamber was coated with 50 mg/L Matrigel (1:8 diluent) and air-dried at 4° C. HO8910 cells after different treatments were digested with trypsin and resuspended with serum-free medium. The cell density was adjusted to $5\times10^5$ cells/mL. 200 μL of cell suspension was added into the upper compartment of the Transwell chamber, and 500 μL of culture medium containing 10% FBS was added into the lower chamber of the 24-well plate. The culture plates were placed in a $CO_2$ incubator at 37° C for 48 h. The chambers were taken out, and 1 x PBS was washed twice. The cells in the upper layer of the chamber's membrane were removed carefully using a cotton swab. 4% paraformaldehyde-fixed for 20 min. Crystal violet solution stained for 15 min. Images were taken under an inverted microscope (Leica DMi8) by a 4X objective. 10 fields of view were counted randomly for each sample by Image J software (freeware http://fiji.sc) and then analyzed statistically.

## IHC assay

Ovarian Cancer and adjacent normal tissue microarray (TMA, n=90) were obtained from Shanghai Outdo Biotechnology Company, Ltd (SHXC2021YF01). IHC was carried out as described previously (59). The TMA was placed in an oven at 68°C for 2 h. Dewaxing was completed in the automatic dyeing machine, and the slides were placed in the antigen retrieval instrument to initiate the repair. Then, they were allowed to cool naturally for more than 10 minutes and washed with PBS buffer. The working solution of primary antibodies, including anti-STAT5A (Proteintech 13179-1-AP), anti-P-STAT5A (Signalway Antibody, 11048), anti-MMP2 (Proteintech, 10373-2-AP) diluted 1:200 was added respectively. The slides were kept at 4°C overnight and then rewarmed at room temperature for 45 min, washed with PBS buffer, and put into DAKO automatic IHC instrument. The blocking, secondary antibody binding, and DAB color development procedures were selected according to the "Autostainer Link 48 Use Guide". The slides were stained with hematoxylin for 1min, immersed in 0.25% alcohol hydrochloric acid (400ml 70% alcohol +1ml concentrated hydrochloric acid) for about 10 s, and rinsed with tap water for 5 min. Then, the slides were dried at room temperature and sealed with neutral resin.

## Statistical analysis

All the experiments were performed independently, at least in triplicate. All the data were expressed as mean ± standard deviation (SD). Statistical analyses were carried out with GraphPad Prism software version 8.0. Multiple group comparisons were performed using a one-way ANOA test. Mann-Whitney test was used to analyze the expression of molecules in tissues. The correlation between molecular and clinical indicators was evaluated by the Chi-square test, Kaplan-Meier survival analysis, and Log-rank Statistical test. $P < 0.05$ was considered statistically significant.

# Data availability statement

The original contributions presented in the study are included in the article/Supplementary Material. Further inquiries can be directed to the corresponding authors.

# Author contributions

XG and XL conceived and designed the research. XG performed the experiments, analyzed the data, and wrote the manuscript. Both authors contributed to the article and approved the submitted version.

# Conflict of interest

The authors declare that the research was conducted in the absence of any commercial or financial relationships that could be construed as a potential conflict of interest.

# Publisher's note



# Supplementary material

The Supplementary Material for this article can be found online at: https://www.frontiersin.org/articles/10.3389/fonc.2022.1054647/full#supplementary-material

# References


1. Siegel RL, Miller KD, Fuchs HE, Jemal A. Cancer statistics, 2022. *CA Cancer J Clin* (2022) 72:7–33. doi: 10.3322/caac.21708

2. Groen RS, Gershenson DM, Fader AN. Updates and emerging therapies for rare epithelial ovarian cancers: one size no longer fits all. *Gynecol Oncol* (2015) 136:373–83. doi: 10.1016/j.ygyno.2014.11.078

3. Chang SJ, Hodeib M, Chang J, Bristow RE. Survival impact of complete cytoreduction to no gross residual disease for advanced-stage ovarian cancer: a meta-analysis. *Gynecol Oncol* (2013) 130:493–8. doi: 10.1016/j.ygyno.2013.05.040

4. Robson M, Im SA, Senkus E, Xu B, Domchek SM, Masuda N, et al. Olaparib for metastatic breast cancer in patients with a germline BRCA mutation. *N Engl J Med* (2017) 377:523–33. doi: 10.1056/NEJMoa1706450

5. Darnell JEJr., Kerr IM, Stark GR. Jak-STAT pathways and transcriptional activation in response to IFNs and other extracellular signaling proteins. *Sci* (1994) 264:1415–21. doi: 10.1126/science.8197455

6. Gao B. Cytokines, STATs, and liver disease. *Cell Mol Immunol* (2005) 2:92–100.

7. Machida K, Tsukamoto H, Liu JC, Han YP, Govindarajan S, Lai MM, et al. C-jun mediates hepatitis c virus hepatocarcinogenesis through signal transducer and activator of transcription 3 and nitric oxide-dependent impairment of oxidative DNA repair. *Hepatology* (2010) 52:480–92. doi: 10.1002/hep.23697

8. Calò V, Migliavacca M, Bazan V, Macaluso M, Buscemi M, Gebbia N, et al. STAT proteins: from normal control of cellular events to tumorigenesis. *J Cell Physiol* (2003) 197:157–68. doi: 10.1002/jcp.10364

9. Lu T, Bankhead A, Ljungman M3rd, Neamati N. Multi-omics profiling reveals key signaling pathways in ovarian cancer controlled by STAT3. *Theranostics* (2019) 9:5478–96. doi: 10.7150/thno.33444

10. Huang D, Chen X, Zeng X, Lao L, Li J, Xing Y, et al. Targeting the regulator of G protein signaling 1 in tumor-specific T cells enhances their trafficking to breast cancer. *Nat Immunol* (2021) 22:865–79. doi: 10.1038/s41590-021-00939-9

11. Hu F, Zhao Y, Yu Y, Fang JM, Cui R, Liu ZQ, et al. Docetaxel-mediated autophagy promotes chemoresistance in castration-resistant prostate cancer cells by inhibiting STAT3. *Cancer Lett* (2018) 416:24–30. doi: 10.1016/j.canlet.2017.12.013

12. Geiger JL, Grandis JR, Bauman JE. The STAT3 pathway as a therapeutic target in head and neck cancer: Barriers and innovations. *Oral Oncol* (2016) 56:84–92. doi: 10.1016/j.oraloncology.2015.11.022

13. Burke AJ, Garrido P, Johnson C, Sullivan FJ, Glynn SA. Inflammation and nitrosative stress effects in ovarian and prostate pathology and carcinogenesis. *Antioxid Redox Signal* (2017) 26:1078–90. doi: 10.1089/ars.2017.7004

14. Kielbik M, Szulc-Kielbik I, Klink M. The potential role of iNOS in ovarian cancer progression and chemoresistance. *Int J Mol Sci* (2019) 20(7):1751. doi: 10.3390/ijms20071751

15. Li L, Zhu L, Hao B, Gao W, Wang Q, Li K, et al. iNOS-derived nitric oxide promotes glycolysis by inducing pyruvate kinase M2 nuclear translocation in ovarian cancer. *Oncotarget* (2017) 8:33047–63. doi: 10.18632/oncotarget.16523

16. Leung EL, Fraser M, Fiscus RR, Tsang BK. Cisplatin alters nitric oxide synthase levels in human ovarian cancer cells: involvement in p53 regulation and cisplatin resistance. *Br J Cancer* (2008) 98:1803–9. doi: 10.1038/sj.bjc.6604375

17. Tian X, Guan W, Zhang L, Sun W, Zhou D, Lin Q, et al. Physical interaction of STAT1 isoforms with TGF-β receptors leads to functional crosstalk between two signaling pathways in epithelial ovarian cancer. *J Exp Clin Cancer Res* (2018) 37:103. doi: 10.1186/s13046-018-0773-8

18. Au K, Peterson N, Truesdell P, Reid-Schachter G, Khalaj K, Ren R, et al. CXCL10 alters the tumor immune microenvironment and disease progression in a syngeneic murine model of high-grade serous ovarian cancer. *Gynecol Oncol* (2017) 145:436–45. doi: 10.1016/j.ygyno.2017.03.007

19. Frank S, Stallmeyer B, Kämpfer H, Kolb N, Pfeilschifter J. Nitric oxide triggers enhanced induction of vascular endothelial growth factor expression in cultured keratinocytes (HaCaT) and during cutaneous wound repair. *FASEB J* (1999) 13:2002–14. doi: 10.1096/fasebj.13.14.2002

20. Zhang Y, Liu Z. STAT1 in cancer: friend or foe? *Discovery Med* (2017) 24:19–29.

21. Au KK, Le Page C, Ren R, Meunier L, Clément I, Tyrishkin K, et al. STAT1-associated intratumoral T(H)1 immunity predicts chemotherapy resistance in high-grade serous ovarian cancer. *J Pathol Clin Res* (2016) 2:259–70. doi: 10.1002/cjp2.55

22. Wang Z, Chen W, Zuo L, Xu M, Wu Y, Huang J, et al. The fibrillin-1/VEGFR2/STAT2 signaling axis promotes chemoresistance *via* modulating glycolysis and angiogenesis in ovarian cancer organoids and cells. *Cancer Commun (Lond)* (2022) 42:245–65. doi: 10.1002/cac2.12274

23. Seo JM, Park S, Kim JH. Leukotriene B4 receptor-2 promotes invasiveness and metastasis of ovarian cancer cells through signal transducer and activator of transcription 3 (STAT3)-dependent up-regulation of matrix metalloproteinase 2. *J Biol Chem* (2012) 287:13840–9. doi: 10.1074/jbc.M111.317131

24. Jia ZH, Jia Y, Guo FJ, Chen J, Zhang XW, Cui MH. Phosphorylation of STAT3 at Tyr705 regulates MMP-9 production in epithelial ovarian cancer. *PloS One* (2017) 12:e0183622. doi: 10.1371/journal.pone.0183622

25. Yue P, Zhang X, Paladino D, Sengupta B, Ahmad S, Holloway RW, et al. Hyperactive EGF receptor, jaks, and Stat3 signaling promote enhanced colony-forming ability, motility, and migration of cisplatin-resistant ovarian cancer cells. *Oncogene* (2012) 31:2309–22. doi: 10.1038/onc.2011.409

26. Xu Q, Briggs J, Park S, Niu G, Kortylewski M, Zhang S, et al. Targeting Stat3 blocks both HIF-1 and VEGF expression induced by multiple oncogenic growth signaling pathways. *Oncogene* (2005) 24:5552–60. doi: 10.1038/sj.onc.1208719

27. Park J, Park SY, Kim JH. Leukotriene B4 receptor-2 contributes to chemoresistance of SK-OV-3 ovarian cancer cells through activation of signal transducer and activator of a transcription-3-linked cascade. *Biochim Biophys Acta* (2016) 1863:236–43. doi: 10.1016/j.bbamcr.2015.11.011

28. McLean K, Tan L, Bolland DE, Coffman LG, Peterson LF, Talpaz M, et al. Leukemia inhibitory factor functions in parallel with interleukin-6 to promote ovarian cancer growth. *Oncogene* (2019) 38:1576–84. doi: 10.1038/s41388-018-0523-6

29. Zhao L, Ji G, Le X, Luo Z, Wang C, Feng M, et al. An integrated analysis identifies STAT4 as a key regulator of ovarian cancer metastasis. *Oncogene* (2017) 36:3384–96. doi: 10.1038/onc.2016.487

30. Lee H, Kim JW, Choi DK, Yu JH, Kim JH, Lee DS, et al. Poziotinib suppresses ovarian cancer stem cell growth *via* inhibition of HER4-mediated STAT5 pathway. *Biochem Biophys Res Commun* (2020) 526:158–64. doi: 10.1016/j.bbrc.2020.03.046

31. Jinawath N, Vasoontara C, Jinawath A, Fang X, Zhao K, Yap KL, et al. Oncoproteomic analysis reveals co-upregulation of RELA and STAT5 in carboplatin resistant ovarian carcinoma. *PloS One* (2010) 5:e11198. doi: 10.1371/journal.pone.0011198

32. Lieber S, Reinartz S, Raifer H, Finkernagel F, Dreyer T, Bronger H, et al. Prognosis of ovarian cancer is associated with effector memory CD8(+) T cell accumulation in ascites, CXCL9 levels and activation-triggered signal transduction in T cells. *Oncoimmunol* (2018) 7:e1424672. doi: 10.1080/2162402x.2018.1424672

33. Bai Y, Yin K, Su T, Ji F, Zhang S. CTHRC1 in ovarian cancer promotes M2-like polarization of tumor-associated macrophages *via* regulation of the STAT6 signaling pathway. *Onco Targets Ther* (2020) 13:5743–53. doi: 10.2147/ott.S250520

34. Ruan Z, Yang X, Cheng W. OCT4 accelerates tumorigenesis through activating JAK/STAT signaling in ovarian cancer side population cells. *Cancer Manag Res* (2019) 11:389–99. doi: 10.2147/cmar.S180418

35. Liu X, Robinson GW, Gouilleux F, Groner B, Hennighausen L. Cloning and expression of Stat5 and an additional homologue (Stat5b) involved in prolactin signal transduction in mouse mammary tissue. *Proc Natl Acad Sci U.S.A.* (1995) 92:8831–5. doi: 10.1073/pnas.92.19.8831

36. Schmitt-Ney M, Doppler W, Ball RK, Groner B. Beta-casein gene promoter activity is regulated by the hormone-mediated relief of transcriptional repression and a mammary-gland-specific nuclear factor. *Mol Cell Biol* (1991) 11:3745–55. doi: 10.1128/mcb.11.7.3745-3755.1991

37. Wakao H, Gouilleux F, Groner B. Mammary gland factor (MGF) is a novel member of the cytokine regulated transcription factor gene family and confers the prolactin response. *EMBO J* (1994) 13:2182–91. doi: 10.1002/j.1460-2075.1994.tb06495.x

38. Darnell JEJr. STATs and gene regulation *Science* (1997) 277:1630–5 doi: 10.1126/science.277.5332.1630

39. Moriggl R, Sexl V, Kenner L, Duntsch C, Stangl K, Gingras S, et al. Stat5 tetramer formation is associated with leukemogenesis. *Cancer Cell* (2005) 7:87–99. doi: 10.1016/j.ccr.2004.12.010

40. Arnould C, Philippe C, Bourdon V, Gr goire MJ, Berger R, Jonveaux P. The signal transducer and activator of transcription STAT5b gene is a new partner of retinoic acid receptor alpha in acute promyelocytic-like leukaemia. *Hum Mol Genet* (1999) 8:1741–9. doi: 10.1093/hmg/8.9.1741

41. Dong S, Tweardy DJ. Interactions of STAT5b-RARalpha, a novel acute promyelocytic leukemia fusion protein, with retinoic acid receptor and STAT3 signaling pathways. *Blood* (2002) 99:2637–46. doi: 10.1182/blood.v99.8.2637

42. Shahmarvand N, Nagy A, Shahryari J, Ohgami RS. Mutations in the signal transducer and activator of transcription family of genes in cancer. *Cancer Sci* (2018) 109:926–33. doi: 10.1111/cas.13525

43. Teglund S, McKay C, Schuetz E, van Deursen JM, Stravopodis D, Wang D, et al. Stat5a and Stat5b proteins have essential and nonessential, or redundant, roles in cytokine responses. *Cell* (1998) 93:841–50. doi: 10.1016/s0092-8674(00)81444-0

44. Ferbeyre G, Moriggl R. The role of Stat5 transcription factors as tumor suppressors or oncogenes. *Biochim Biophys Acta* (2011) 1815:104–14. doi: 10.1016/j.bbcan.2010.10.004

45. Wang K, Sun Y, Wang Y, Liu L. An integration analysis of mRNAs and miRNAs microarray data to identify key regulators for ovarian endometriosis based on competing endogenous RNAs. *Eur J Obstet Gynecol Reprod Biol* (2020) 252:468–75. doi: 10.1016/j.ejogrb.2020.06.046

46. Nikitakis NG, Siavash H, Sauk JJ. Targeting the STAT pathway in head and neck cancer: recent advances and future prospects. *Curr Cancer Drug Targets* (2004) 4:637–51. doi: 10.2174/1568009043332736

47. Vafaizadeh V, Klemmt P, Brendel C, Weber K, Doebele C, Britt K, et al. Mammary epithelial reconstitution with gene-modified stem cells assigns roles to Stat5 in luminal alveolar cell fate decisions, differentiation, involution, and mammary tumor formation. *Stem Cells* (2010) 28:928–38. doi: 10.1002/stem.407

48. Cotarla I, Ren S, Zhang Y, Gehan E, Singh B, Furth PA. Stat5a is tyrosine phosphorylated and nuclear localized in a high proportion of human breast cancers. *Int J Cancer* (2004) 108:665–71. doi: 10.1002/ijc.11619

49. Rouet V, Bogorad RL, Kayser C, Kessal K, Genestie C, Bardier A, et al. Local prolactin is a target to prevent expansion of basal/stem cells in prostate tumors. *Proc Natl Acad Sci U S A.* (2010) 107:15199–204. doi: 10.1073/pnas.0911651107

50. Li H, Zhang Y, Glass A, Zellweger T, Gehan E, Bubendorf L, et al. Activation of signal transducer and activator of transcription-5 in prostate cancer predicts early recurrence. *Clin Cancer Res* (2005) 11:5863–8. doi: 10.1158/1078-0432.Ccr-05-0562

51. Koppikar P, Lui VW, Man D, Xi S, Chai RL, Nelson E, et al. Constitutive activation of signal transducer and activator of transcription 5 contributes to tumor growth, epithelial-mesenchymal transition, and resistance to epidermal growth factor receptor targeting. *Clin Cancer Res* (2008) 14:7682–90. doi: 10.1158/1078-0432.Ccr-08-1328

52. Shi F, Shang L, Pan BQ, Wang XM, Jiang YY, Hao JJ, et al. Calreticulin promotes migration and invasion of esophageal cancer cells by upregulating neuropilin-1 expression *via* STAT5A. *Clin Cancer Res* (2014) 20:6153–62. doi: 10.1158/1078-0432.Ccr-14-0583

53. Chen H, Ye D, Xie X, Chen B, Lu W. VEGF, VEGFRs expressions and activated STATs in ovarian epithelial carcinoma. *Gynecol Oncol* (2004) 94:630–5. doi: 10.1016/j.ygyno.2004.05.056

54. Fu S, Li Z, Xiao L, Hu W, Zhang L, Xie B, et al. Glutamine synthetase promotes radiation resistance *via* facilitating nucleotide metabolism and subsequent DNA damage repair. *Cell Rep* (2019) 28:1136–1143.e1134. doi: 10.1016/j.celrep.2019.07.002

55. Ryu H, Choi HK, Kim HJ, Kim AY, Song JY, Hwang SG, et al. Antitumor activity of a novel tyrosine kinase inhibitor AIU2001 due to abrogation of the DNA damage repair in non-small cell lung cancer cells. *Int J Mol Sci* (2019) 20(19):4728. doi: 10.3390/ijms20194728

56. Maranto C, Udhane V, Hoang DT, Gu L, Alexeev V, Malas K, et al. STAT5A/B blockade sensitizes prostate cancer to radiation through inhibition of RAD51 and DNA repair. *Clin Cancer Res* (2018) 24:1917–31. doi: 10.1158/1078-0432.Ccr-17-2768

57. Gyorffy B, Lánczky A, Szállási Z. Implementing an online tool for genome-wide validation of survival-associated biomarkers in ovarian-cancer using microarray data from 1287 patients. *Endocr Relat Cancer* (2012) 19:197–208. doi: 10.1530/erc-11-0329

58. Yuan H, Yan M, Zhang G, Liu W, Deng C, Liao G, et al. CancerSEA: a cancer single-cell state atlas. *Nucleic Acids Res* (2019) 47:D900–d908. doi: 10.1093/nar/gky939

59. Li B, Dewey CN. RSEM: accurate transcript quantification from RNA-seq data with or without a reference genome. *BMC Bioinf* (2011) 12:323. doi: 10.1186/1471-2105-12-323

frontiers | Frontiers in Oncology

TYPE Case Report
PUBLISHED 13 January 2023
DOI 10.3389/fonc.2022.1088962



OPEN ACCESS

EDITED BY
Sarah M. Temkin,
National Institutes of Health (NIH),
United States

REVIEWED BY
Nicola Fusco,
University of Milan, Italy
Antonio Giuseppe Naccarato,
University of Pisa, Italy

*CORRESPONDENCE
Anna Passarelli
passarellian@libero.it;
anna.passarelli@istitutotumori.na.it

SPECIALTY SECTION
This article was submitted to Gynecological Oncology, a section of the journal Frontiers in Oncology

RECEIVED 03 November 2022
ACCEPTED 12 December 2022
PUBLISHED 13 January 2023

CITATION
Passarelli A, Ventriglia J, Pisano C, Cecere SC, Napoli MD, Rossetti S, Tambaro R, Tarotto L, Fiore F, Farolfi A, Bartoletti M and Pignata S (2023) The way to precision medicine in gynecologic cancers: The first case report of an exceptional response to alpelisib in a *PIK3CA*-mutated endometrial cancer.
*Front. Oncol.* 12:1088962.
doi: 10.3389/fonc.2022.1088962



# The way to precision medicine in gynecologic cancers: The first case report of an exceptional response to alpelisib in a *PIK3CA*-mutated endometrial cancer

Anna Passarelli[1]*, Jole Ventriglia[1], Carmela Pisano[1], Sabrina Chiara Cecere[1], Marilena Di Napoli[1], Sabrina Rossetti[1], Rosa Tambaro[1], Luca Tarotto[2], Francesco Fiore[2], Alberto Farolfi[3], Michele Bartoletti[4] and Sandro Pignata[1]

[1]Department of Urology and Gynecology, Istituto Nazionale Tumori, Istituto di Ricovero e Cura a Carattere Scientifico (IRCCS) Fondazione G. Pascale, Naples, Italy, [2]Interventional Radiology Unit, Istituto Nazionale Tumori, Istituto di Ricovero e Cura a Carattere Scientifico (IRCCS) Fondazione G. Pascale, Naples, Italy, [3]Department of Medical Oncology, Istituto Nazionale Tumori, Istituto di Ricovero e Cura a Carattere Scientifico (IRCCS) Istituto Romagnolo per lo Studio dei Tumori Dino Amadori, Meldola, Emilia-Romagna, Italy, [4]Unit of Medical Oncology and Cancer Prevention, Department of Medical Oncology, Centro di Riferimento Oncologico di Aviano (CRO), Aviano, Italy

Endometrial cancer (EC) is the most common gynecologic cancer in Europe and its prevalence is increasing. EC includes a biological and clinical heterogeneous group of tumors, usually classified as type I (endometrioid) or type II (non-endometrioid) based on the histopathological characteristics. In 2013, a new molecular classification was proposed by The Cancer Genome Atlas (TCGA) based on the comprehensive molecular profiling of EC. Several molecular somatic alterations have been described in development and progression of EC. Using these molecular features, EC was reclassified into four subgroups: POLE ultra-mutated, MSI hypermutated, copy-number low, and copy-number high that correlate with the prognosis. To this regard, it is widely reported that EC has more frequent mutations in the phosphatidylinositol 3-kinase (PI3K) pathway signaling than any other tumor. *PIK3CA* is the main significant mutated gene after *PTEN* alterations. Overall, over 90% of endometrioid tumors have activating PI3K molecular alterations that suggests its critical role in the EC pathogenesis. Thus, the dysregulation of PI3K pathway represents an attractive target in EC treatment. Herein, we report a radiological and clinically meaningful response to a selective PIK3 inhibitor in a patient with extensively pre-treated advanced endometrioid EC harboring a somatic activating *PIK3CA* hotspot mutation. These evidences provide the rational for translational strategies of the PI3K inhibition and could support the clinical

usefulness of *PIK3CA* genotyping in advanced EC. To our knowledge, this is the first clinical case of *PIK3CA*-mutated EC successfully treated with alpelisib.

KEYWORDS

**alpelisib, endometrial cancer, phosphatidylinositol 3-kinase (PI3K) pathway, genomic profiling, PI3K inhibitor, PIK3CA mutation**

## Introduction

Endometrial cancer (EC) is the only gynecological tumor that is rising in terms of incidence and associated mortality worldwide (1). EC is typically diagnosed in the early stages when the disease is confined to the uterus. EC patients affected by early-stage disease have a good prognosis, and for all patients with EC in Europe (all disease stages) have been reported 5-years survival rates of 76% (2). Anyway, women with advanced or recurrent EC show lower response rates to the standard treatments, and clinical outcomes are extremely poor.

Therefore, the development of further therapeutic strategies for these patients is needed, hopefully based on the novel aspects of precise molecular pathogenesis of EC.

Historically, EC have been classified into two different groups (3). Type I endometrioid tumors are linked to hormone-receptor positivity, estrogen excess, obesity, and favorable prognosis compared with type II tumors that are more frequent in non-obese women, older, and have a worse outcome. In 2013, the Cancer Genome Atlas (TCGA) proposed a new classification through the evaluation of the genomic and epigenomic landscapes of primary EC. In specific, TCGA delineated four molecular entities: polymerase ϵ (POLE)-mutant/hypermutated, microsatellite instability-high (MSI-H), copy number high, and copy number low (4),. Interestingly, this new classification is related to the underlying tumor biology and promising therapeutic strategies.

In recent years several somatic mutations have been identified and related targeted therapies have shown promising success.

For example, the molecular subtype with Mismatch Repair Deficiency (dMMR)/or MSI-H occurs in 23-36% of EC and is associated with immune activation (5). Therefore, in August 2021 the Food and Drug Administration (FDA) has granted accelerated approval for the anti-PD-1 dostarlimab in recurrent dMMR/MSI EC, based on a phase I trial (6).

Interestingly, the phosphatidylinositol 3-kinase (PI3K)/mammalian target of rapamycin (mTOR) pathway is frequently dysregulated in EC, often due to activating mutations or amplification of PIK3CA (7–9). PI3K alpha is a heterodimeric protein complex comprised of the catalytic p110 alpha subunit and the regulatory p85a subunit, which are encoded by the PIK3CA and PIK3R1 genes respectively. The common mechanisms of the PI3K alpha activation in carcinogenesis are the acquisition of somatic gain-of-function mutations within PIK3CA or loss of PTEN activity. Several studies revealed that over 80% of all *PIK3CA* mutations occurred within exons 9 and 20, while only in 20% within exons 1-7.

Therefore, targeting the PI3K/mTOR pathway is an attractive strategy and may be particularly active in solid tumors that signal heavily through PI3Ka such as those harboring PIK3CA alterations.

Mutations in *PIK3CA* lead to increased activation of the PI3K/AKT/mTOR pathway, occurring in 93% of type 1 and 33% to 38% of type 2 EC (10). In addition, as reported by Stelloo and colleagues in a retrospective molecular analyses study of samples of EC (11), *PIK3CA* alterations were reported in the four molecular subtype, in specific in 23.9% of copy number high, in 33% in MSI, in 51.1% in POLE-hypermutated, and in 31.6% in copy number low subgroup.

It has been reported that the overactivation of this pathway in association to loos of PTEN function, is associated with poor survival in advanced solid tumors (12).

To this regard, alpelisib, an oral PI3K alpha-selective inhibitor, showed preliminary encouraging activity results in a selected population of advanced solid tumors harboring *PIK3CA* alterations, supporting the rationale for the use of PI3K pathway inhibition for the treatment of *PIK3CA*-mutant tumors (13).

We report a *PIK3CA*-mutated advanced endometrioid EC case extensively pre-treated that responded favorably to PI3K alpha-selective inhibitor namely alpelisib.

To our knowledge, this is the first clinical case of *PIK3CA*-mutated advanced EC successfully treated with alpelisib.

## Case presentation

In March 2022, a 51-year-old woman was referred to our institution for a *second opinion*.

Her past medical history was significant for the diagnosis, at the age of 47 years, of endometrial cancer. In April 2018, she underwent a radical hysterectomy with pelvic lymphadenectomy. Histology revealed an intermediate differentiated endometrioid EC,

10.3389/fonc.2022.1088962

FIGO stage IIIC1 (pT3pN1). Estrogen and progesterone receptors were positive. Mismatch-Repair-Proteins such as mutL homolog 1 (MLH1), postmeiotic segregation increased 2 (PMS2), mutS homolog 2 (MSH2) and mutS homolog 6 (MSH6) were expressed.

The risk factors suggested the need of adjuvant chemoradiation treatment.

Following multi-disciplinary discussion, a sequential adjuvant radio-chemotherapy was proposed to the patient. She consented to a course of 4 cycles of 3 weekly Carboplatin (AUC 5) and Paclitaxel (175 mg/m$^2$), which she received from May to July 2018, and external beam radiotherapy completed in November 2018. Three months after finishing the adjuvant therapy cycle a follow-up thoracic and abdominal computed tomography (CT) scan showed complete remission.

Ten months after stopping adjuvant therapy, the patient showed a radiological disease progression to the peritoneal carcinomatosis nodules. In consideration of the platinum free-interval, the patient was treated with carboplatin plus paclitaxel chemotherapy at standard dose for a total of six cycles.

After approximately 2 months, she experienced disease progression with increased of peritoneal nodules for which she was subjected to cytoreductive surgery on peritoneum. The histological examination confirmed the diagnosis of endometrioid EC with a high expression of hormone receptors, microsatellite stability.

The patient then received hormonal therapy with megestrol acetate for 9 months until new peritoneal disease progression.

Therefore, from January to April 2021, the patient underwent second-line chemotherapy with liposomal doxorubicin until disease progression.

From April to July 2021, the patient received intravenous weekly topotecan without any benefit.

In August 2021 started fourth-line of oral chemotherapy with cyclophosphamide until the progression of disease.

In November 2021, a new clinical progression associated to radiologic progression to peritoneum occurred. Thus, the patient received a fifth-line therapy with oral etoposide.

In January 2022, for a new lymph node and peritoneal progression associated to painful abdominal symptoms, the patient started hormone therapy with letrozole at the dosage of 2,5 mg daily.

A timeline overview of the patient's management is summarized in Figure 1.

In March 2022, the patient referred to our institution in order to evaluate the potential enrollment in experimental clinical trials. Given the unavailability of clinical trials in our Institute for this type of patient, we proposed to perform a comprehensive genomic profiling through next generation sequencing (NGS) on archival tumor tissue from the last surgery. Importantly, the combination of pembrolizumab and lenvatinib was not yet available in Italy for patients with advanced EC that is not MSI-H or dMMR, who have disease progression following prior systemic therapy in any setting (14).

The patient had a personal history of hypertensive heart disease in pharmacological therapy, and iatrogenic hypothyroidism currently treated with thyroid hormone replacement. The patient was functioning well, as indicated by an Eastern Cooperative Oncology Group performance status of 1.

The NGS (*FoundationOne CDx* assay) was performed on tumor sample and showed microsatellite stability and low Tumor Mutational Burden (TMB) (1 mut/Mb) (see Table 1). Moreover, the data analysis revealed several genomic alterations (Table 1) including *PIK3CA* mutation in exon 20 (*H1047R*, variant allele frequency 78.2%), which was considered targetable.

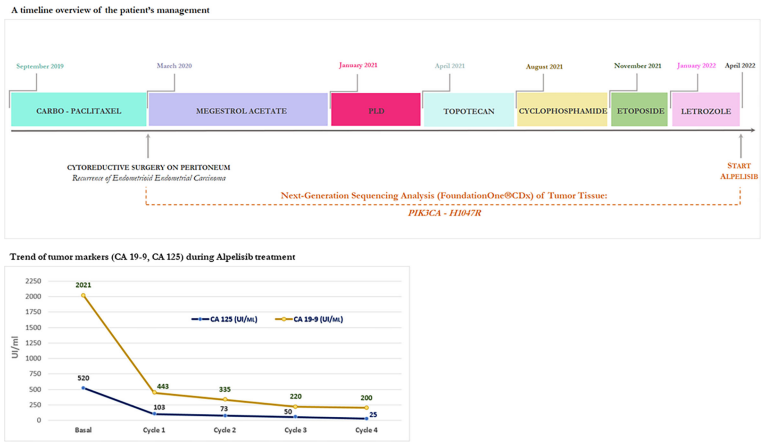


FIGURE 1
A timeline overview of the patient's management and trend of tumor markers (CA 19-9, CA 125) during Alpelisib treatment.

TABLE 1 Summary of molecular analysis – variants identified through test NGS (FoundationOne®CDx).

| GENOMIC SIGNATURES: | Result | Therapy and Clinical Trial Implications |
|---|---|---|
| Microsatellite Status – MS | MS-Stable | No therapies or clinical trials |
| Tumor Mutational Burden | 1 Muts/Mb | No therapies or clinical trials |

| GENE ALTERATIONS: | Alteration | Coding Sequence Effect | VAF (%) | Therapy and Clinical Trial Implications |
|---|---|---|---|---|
| **PIK3CA** | H1047R | 314OA>G | 78.2% | In patient' tumor type: None.<br>In other tumor type: Temsirolimus; Everolimus; Alpelisib. |
| **ARID1A** | Q507*<br>Y1279* | 1519C>T<br>3837T>G | 37.9%<br>38.5% | No therapies or clinical trials<br>No therapies or clinical trials |
| **CTNNB1** | S37C | 110C>G | 37.5% | No therapies or clinical trials |
| **NOTCH1** | R1594Q - subclonal | 4781G>A | 1.3% | Gene alteration with no reportable therapeutic or clinical trial options |

| VARIANT OF UNKNOWN SIGNIFICANCE (VUS) | | | |
|---|---|---|---|
| **ATM**<br>L2492R | ERBB2<br>Amplification | **KDR**<br>R842H | **KIT**<br>T67S |
| **NKKBIA**<br>P65A | **PDGFRB**<br>S1006A | **ROS1**<br>G1027D and T299I | |

NGS, next-generation sequencing; VAF, variant allele frequency.

In April 2022, given the lack of validated standard treatment, following discussion in the Molecular Tumor Board (MTB) of MITO for gynecological cancer patients (15), the patient started treatment with oral PI3K alpha-selective inhibitor namely alpelisib at the standard dose of 300 mg once daily on a continuous schedule in 28-day cycles until disease progression, unacceptable toxicity, or withdrawal of consent.

Following approval by the Institute's ethics committee, alpelisib was provided for compassionate use by Novartis.

A CT scan at baseline revealed two bulky nodules of peritoneal carcinomatosis (83 mm, 85 mm), a 15 mm mass in the paraaortic lymph node, and a 22 mm mass in the right inguinal lymph node (see Figures 2, 3).

During the course of alpelisib treatment, the patient experienced minimal toxicity, including fatigue (grade 1), and decreased appetite (grade 1), based on the CTCAE (version 5.0). Interestingly, the patient not experienced the onset of adverse events as hyperglycemia and skin reactions. To reduce the onset of skin adverse events, the patient was taking prophylactic non-sedating antihistamines such as cetirizine 10 mg once daily during the first 8 weeks of therapy then taper off.

Unfortunately, the patient developed grade 3 diarrhea (increase of ≥7 stools/day) at 30 days of alpelisib requiring treatment with loperamide and temporary interruption of alpelisib until recovery to grade ≤1. Then, the dose of alpelisib was reduced from 300 mg to 200 mg daily, which was well tolerated.

In terms of effectiveness, after just completing one 28-day cycle, she obtained a clinical benefit with meaningful improvement in her abdominal distension and discomfort, size reduction of peritoneal lesions associated to rapid and progressive reduction of tumor marker (CA 125, CA 19-9), as shown in Figure 1.

After only 4 months of alpelisib treatment, she achieved a partial radiologic response with complete disappearing of one of two nodules of peritoneal carcinomatosis and dimensional reduction of para-aortic and inguinal lymph nodes, as shown by the CT-scan (see Figures 2, 3).

Therefore, in consideration of the objective and radiological partial response, the clinical benefit and the absence of unacceptable toxicity, by the time of writing (7 months after the start of treatment), the patient is still on therapy with alpelisib 200 mg daily.

## Discussion

In advanced EC setting, the strategy based on the use of platinum-regimens is the most active. Advanced EC patients who progress after fist line therapy have a poor prognosis and the subsequent options available are disappointing.

10.3389/fonc.2022.1088962

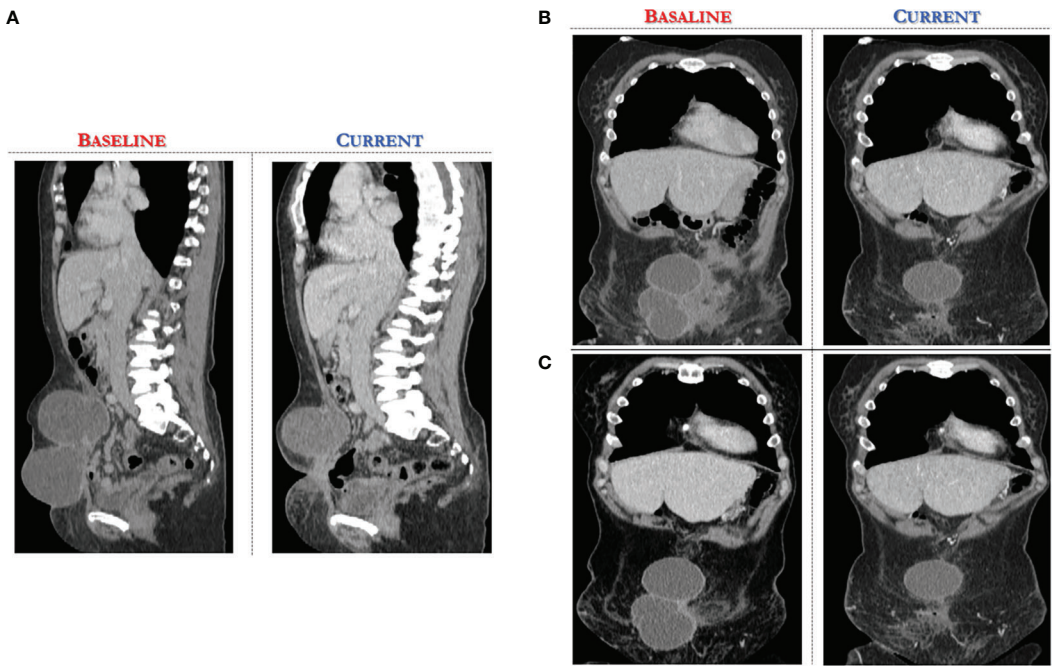


FIGURE 2
Computed Tomography scan demonstrates significant reduction of target lesions after 4 months of Alpelisib treatment compared with the corresponding pre-treatment scan. **(A)** sagittal section of CT abdomen/pelvis revealing at baseline two bulky nodules of peritoneal carcinomatosis (83 mm, 85 mm). **(B, C)** coronal view of CT abdomen/pelvis, different scans.

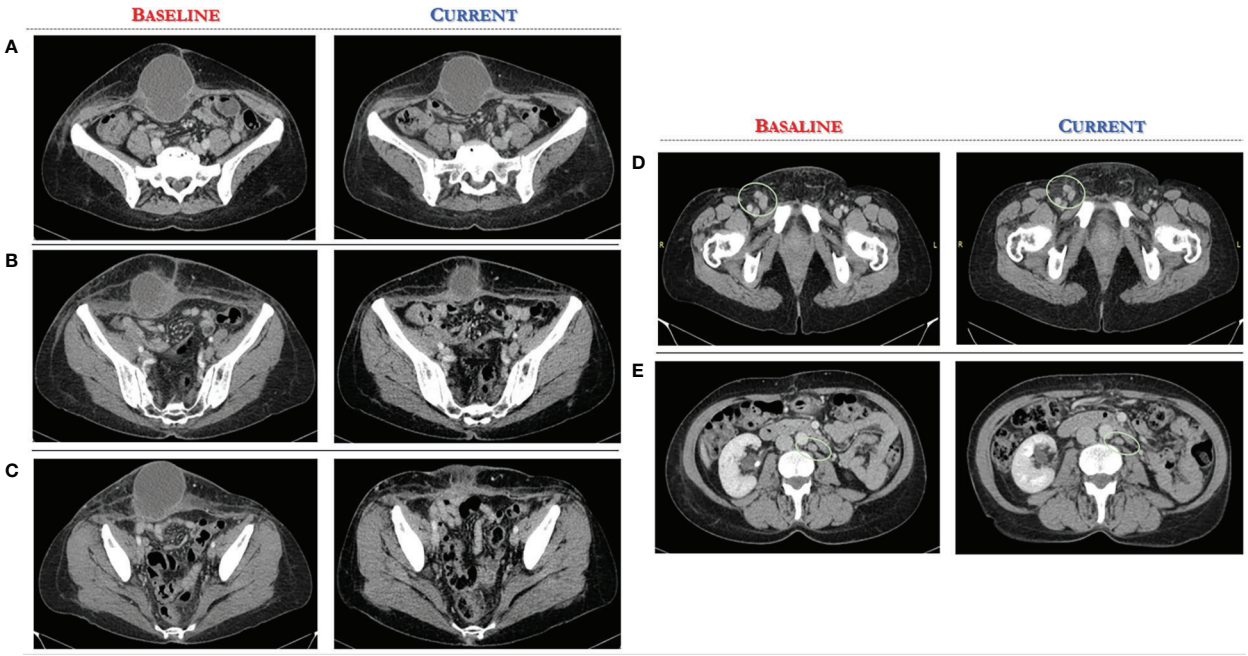


FIGURE 3
Computed Tomography scan demonstrates significant reduction of target lesions after 4 months of Alpelisib treatment compared with the corresponding pre-treatment scan. **(A-C)** axial CT scan, several sections of peritoneal carcinomatosis pre and post alpelisib treatment. **(D, E)** axial CT scan, several sections of secondary lymph nodes in the right inguinal and paraaortic region pre and post alpelisib treatment.

Given that PIK3 pathway activation is involved in the pathogenesis of EC, PIK3 pathway inhibitors are often investigated in this setting.

Here we report an emblematic case of patient with extensively pre-treated advanced endometrioid EC harboring a somatic activating *PIK3CA* mutation in exon 20 (*H1047R*), effectively treated with alpelisib as a part of a compassionate use program.

It is now known that EC harbors more frequent mutations in the PI3K/AKT pathway than any other tumor type analyzed by TCGA so far (4). *PIK3CA* and *PIK3R1* mutations were frequent and showed a strong trend for mutual exclusivity in all molecular subgroups, but they occurred with *PTEN* mutations in the MSI and copy-number low subgroups.

Previously, it has been also reported that the increased PI3K/AKT/mTOR signaling in EC is associated with aggressive phenotype disease and a poor prognosis, regardless of endometrial cancer type (16).

The PI3K pathway represents a target highly druggable and several classes of agents including rapalogs, PI3K isoform-specific inhibitors, dual PI3K/mTOR catalytic inhibitors, pan-PI3K inhibitors, mTOR-specific catalytic inhibitors, and AKT inhibitors, are in clinical development. There are several registered clinical trials of PI3K/mTOR inhibitors as a single drug or in combination for the treatment of EC.

Robust preliminary data have shown that the PI3K/AKT/mTOR pathway inhibition may be effective in patients with activating mutations in *PIK3CA* and/or loss of PTEN. In patients with breast and gynecologic malignancies, a retrospective phase I clinical trial reported significantly higher response rates in cancers with *PIK3CA* mutations (30%) compared with non-*PIK3CA* mutated tumors (10%) treated with PI3K/AKT/mTOR inhibitors as single agents or in combination with alternative therapies. The response rate was 33%, when considering only patients with EC (17). Although these data suggest *PIK3CA* mutations may have a predictive role of response, only 6 patients with EC and *PIK3CA* mutations were evaluable for response, thus further prospective clinical trials are required to conclude regarding the predictive role of *PIK3CA* mutations.

Regarding the specific function of PI3K isoform-specific inhibitors, alpelisib has demonstrated anti-cancer activity in several cancer cell lines and tumor xenograft models, in particular those harboring *PIK3CA* mutations or amplifications, underlining the enhanced clinical effectiveness in patients with PIK3CA-altered advanced solid tumors.

Our decision to manage this case with alpelisib was based on the positive preliminary NCT01219699 trial results.

In fact, in 2018 Juric and colleagues reported in the first-in-human study (NCT01219699) a favorable safety profile and encouraging signs of anti-tumor activity of alpelisib, an oral PI3K alpha-selective inhibitor, in patients with *PIK3CA*-mutant, ER-positive/HER2-negative breast cancer and other *PIK3CA*-altered advanced solid cancers (13). In this small study, the enrolled patients with diagnosis of advanced endometrial cancer were three. Interestingly, the only complete response was reported in a patient with endometrial cancer. In detail, overall response rate was 6%, stable disease was achieved in 70 patients (52.2%) and was maintained >24 weeks, disease control rate (complete and partial responses and stable disease) was 58.2%.

In addition, although the sample size was small, patients with *PIK3CA* helical domain mutations (E545K or E542K), unusual kinase mutations, or PTEN loss had partial or complete response, whereas no responses were observed in patients with kinase mutations on H1047 contrarily to our case report. PTEN mutations, which potentially may contribute to PI3K inhibitor resistance, were detected in five patients, including three whose disease progressed during the first two treatment cycles.

Since the predictive nature of these biomarkers remains not well defined, selected patients with advanced EC should be enrolled in clinical trials, and tumor samples should be collected for definition of PI3K/AKT/mTOR pathway activation status.

In gynecologic oncology, the role of predictive molecular biomarkers will continue to expand and to provide new therapeutic approaches for the management of EC patients with subsequently improvement of outcomes of efficacy and safety. To this regard, several interesting phase II basket-trials as TAPISTRY (NCT04589845) and ROME trial (NCT04591431) are ongoing and test specific targeted drugs based on molecular tumor profiling, also in pre-treated gynecologic tumors (for instance, TAPISTRY trial: *PIK3CA*➔drug Inavolisib; ROME trial: *PIK3CA*➔drug Ipatasertib) (18).

The experience in this case suggests that the precision medicine in gynecologic oncology through the detection of molecular tumor biomarkers could significantly downstage tumors also in advanced stage of disease and in extensively pre-treated patients.

Indeed, MTB can identify innovative pharmacological approaches, expanded access program or ongoing clinical trials based on tumor NGS data in patients for which there are no valid therapeutic alternatives.

Specifically, based on the effectiveness data of alpelisib in our case, we recommend referral to specialized centers the advanced EC patients and incorporation of the comprehensive NGS into care in order to offer the best chance of treatment. In consideration of the high frequency of *PIK3CA* tumor alterations in advanced EC, the genomic sequencing of the tumor tissue should be performed to evaluate for a druggable targets. To this regard, additional prospective trials are underway and needed.

## Conclusion

To our knowledge, we report for the first time a case of advanced endometrioid EC harboring a somatic *PIK3CA* mutation with an exceptional response and a good tolerance to a PI3K alpha-selective inhibitor. Our study provides unequivocal clinical evidence for the alpelisib effectiveness in treating EC cancer patients with *PIK3CA* mutation.

Future prospective studies are warranted to validate both efficacy and safety of therapy with PIK3-inhibitors in patients harboring activating *PIK3CA* mutation.

## Data availability statement

The original contributions presented in the study are included in the article/supplementary material. Further inquiries can be directed to the corresponding author.

## Ethics statement

The patient provided their written informed consent to participate in this study. Written informed consent was obtained from the individual for the publication of any potentially identifiable images or data included in this article.

## Author contributions

Experimental study design: AP and SP. Writing of the manuscript: AP and SP. Data analysis and interpretation: AP, SP and LT. Revision of the manuscript: AP, SP, LT, FF, JV, AF, MB, CP, SC, MN, RT, SR. All authors contributed to the article and approved the submitted version.

## Acknowledgments

The authors wish to acknowledge Elisabetta Coppola, Angela Maria Trujillo, Gelsomina Iovane, and Margherita Tambaro for the research assistance.

## Conflict of interest

SP received honoraria from MSD, Pfizer, AZ, Roche, Clovis, and GSK. MB reports advisory board from G.S.K. outside this work.

The remaining authors declare that the research was conducted in the absence of any commercial or financial relationships that could be construed as a potential conflict of interest.

## Publisher's note



## References

1. Sung H, Ferlay J, Siegel RL, Laversanne M, Soerjomataram I, Jemal A, et al. Global cancer statistics 2020: GLOBOCAN estimates of incidence and mortality worldwide for 36 cancers in 185 countries. *CA Cancer J Clin* (2021) 71:209–49. doi: 10.3322/caac.21660

2. Concin N, Matias-Guiu X, Vergote I, Cibula D, Mirza MR, Marnitz S, et al. ESGO/ESTRO/ESP guidelines for the management of patients with endometrial carcinoma. *Int J Gynecol Cancer* (2021) 31:12–39. doi: 10.1136/ijgc-2020-002230

3. Bokhman JV. Two pathogenetic types of endometrial carcinoma. *Gynecol Oncol* (1983) 15(1):10–7. doi: 10.1016/0090-8258(83

4. Kandoth C, Schultz N, Cherniack AD, Akbani R, Liu Y, Shen H, et al. Integrated genomic characterization of endometrial carcinoma. *Nature* (2013) 497:67–73. doi: 10.1038/nature12113

5. Passarelli A, Pisano C, Cecere SC, Di Napoli M, Rossetti S, Tambaro R, et al. Targeting immunometabolism mediated by the IDO1 pathway: A new mechanism of immune resistance in endometrial cancer. *Front Immunol* (2022) 13:953115. doi: 10.3389/fimmu.2022.953115

6. Oaknin A, Tinker AV, Gilbert L, Samoueülian V, Mathews C, Brown J, et al. Clinical activity and safety of the anti–programmed death 1 monoclonal antibody dostarlimab for patients with recurrent or advanced mismatch repair–deficient endometrial cancer: A nonrandomized phase 1 clinical trial. *JAMA Oncol* (2020) 6:1766–72. doi: 10.1001/jamaoncol.2020.4515

7. Kyo S, Nakayama K. Endometrial cancer as a metabolic disease with dysregulated PI3K signaling: Shedding light on novel therapeutic strategies. *Int J Mol Sci* (2020) 21:6073. doi: 10.3390/ijms21176073

8. Myers A. New strategies in endometrial cancer: Targeting the PI3K/mTOR pathway - the devil is in the details. *Clin Cancer Res* (2013) 19(19):5264–74.

9. Pavlidou A, Vlahos NF. Molecular alterations of PI3K/Akt/mTOR pathway: A therapeutic target in endometrial cancer. *Sci World J* (2014) 709736. doi: 10.1155/2014/709736

10. Slomovitz BM, Coleman RL. The PI3K/AKT/mTOR pathway as a therapeutic target in endometrial cancer. *Clin Cancer Res* (2012) 18(21):5856–64.

11. Stelloo E, Nout RA, Osse EM, Jurgenliemk-Schulz IJ, Jobsen JJ, Lutgens LC, et al. Improved risk assessment by integrating molecular and clinicopathological factors in early-stage endometrial cancer–combined analysis of the PORTEC cohorts. *Clin Cancer Res* (2016) 22(16):4215–24. doi: 10.1158/1078-0432.CCR-15-2878

12. Ocana A, Vera-Badillo F, Al-Mubarak M, Templeton AJ, Corrales-Sanchez V, Diez-Gonzalez L, et al. Activation of the PI3K/mTOR/ AKT pathway and survival in solid tumors: systematic review and meta-analysis. *PloS One* (2014) 9(4): e95219. doi: 10.1371/journal.pone.0095219.eCollection

13. Juric D, Rodon J, Tabernero J, Janku F, Burris HA, Schellens JHM, et al. Phosphatidylinositol 3-kinase a-selective inhibition with alpelisib (BYL719) in PIK3CA-altered solid tumors: Results from the first-in-Human study. *J Clin Oncol* (2018) 36:1291–9. doi: 10.1200/JCO.2017

14. Makker V, Colombo N, Casado Herráez A, Santin AD, Colomba E, Miller DS, et al. Lenvatinib plus pembrolizumab for advanced endometrial cancer. *N Engl J Med* (2022) 386:437–48. doi: 10.1056/NEJMoa2108330

15. Bartoletti M, Bergamini A, Giannone G, Nero C, Musacchio L, Farolfi A, et al. A fully virtual and nationwide molecular tumor board for gynecologic cancer patients: the virtual experience of the MITO cooperative group. *Int J Gynecol Cancer* (2022). doi: 10.1136/ijgc-2022-003425

16. Holst F, Werner HMJ, Mjos S, Hoivik EA, Kusonmano K, Wik E, et al. PIK3CA amplification associates with aggressive phenotype but not markers of AKT-MTOR signaling in endometrial carcinoma. *Clin Cancer Res* (2019) 25 (1):334–45. doi: 10.1158/1078-0432

17. Janku F, Wheler JJ, Westin SN, Moulder SL, Naing A, Tsimberidou AM, et al. PI3K/AKT/mTOR inhibitors in patients with breast and gynecologic malignancies harboring PIK3CA mutations. *J Clin Oncol* (2012) 30:777–82. doi: 10.1200/JCO.2011.36.1196

18. Drilon AE, Liu H, Wu F, Chen D, Wilson TR, Simmons BP, et al. Tumor-agnostic precision immuno-oncology and somatic targeting rational for you (TAPISTRY): a novel platform umbrella trial. *J Clin Oncol* (2021) 39:15_suppl:TPS3154–TPS3154.

frontiers | Frontiers in Oncology

TYPE Original Research
PUBLISHED 10 March 2023
DOI 10.3389/fonc.2023.1104521



OPEN ACCESS

EDITED BY
Pierluigi Giampaolino,
University of Naples Federico II, Italy

REVIEWED BY
Roberto C. Delgado Bolton,
Hospital San Pedro, Spain
Laura Rosanò,
Department of Biomedical Sciences,
National Research Council (CNR), Italy

*CORRESPONDENCE
Jae-Hoon Kim
jaehoonkim@yuhs.ac

SPECIALTY SECTION
This article was submitted to Gynecological Oncology, a section of the journal Frontiers in Oncology

RECEIVED 21 November 2022
ACCEPTED 13 February 2023
PUBLISHED 10 March 2023

CITATION
Ryu J-W, Shin H-Y, Kim H-S, Han GH, Kim JW, Lee H-N, Cho H, Chung J-Y and Kim J-H (2023) Prognostic value of β-Arrestins in combination with glucocorticoid receptor in epithelial ovarian cancer. *Front. Oncol.* 13:1104521. doi: 10.3389/fonc.2023.1104521



# Prognostic value of β-Arrestins in combination with glucocorticoid receptor in epithelial ovarian cancer

Ji-Won Ryu[1], Ha-Yeon Shin[1], Hyo-Sun Kim[1], Gwan Hee Han[2], Jeong Won Kim[3], Hae-Nam Lee[4], Hanbyoul Cho[1,5,6], Joon-Yong Chung[7] and Jae-Hoon Kim[1,5,6]*

[1]Department of Obstetrics and Gynecology, Yonsei University College of Medicine, Seoul, Republic of Korea, [2]Department of Obstetrics and Gynecology, Kyung Hee University Hospital at Gangdong, Seoul, Republic of Korea, [3]Department of Pathology, Kangnam Sacred Heart Hospital, Hallym University College of Medicine, Seoul, Republic of Korea, [4]Department of Obstetrics and Gynecology, Catholic University of Korea Bucheon St. Mary's Hospital, Bucheon, Republic of Korea, [5]Department of Obstetrics and Gynecology, Gangnam Severance Hospital, Yonsei University College of Medicine, Seoul, Republic of Korea, [6]Institute of Women's Life Medical Science, Yonsei University College of Medicine, Seoul, Republic of Korea, [7]Molecular Imaging Branch, National Cancer Institute, Center for Cancer Research, National Institutes of Health, Bethesda, MD, United States

Hormones may be key factors driving cancer development, and epidemiological findings suggest that steroid hormones play a crucial role in ovarian tumorigenesis. We demonstrated that high glucocorticoid receptor (GR) expression is associated with a poor prognosis of epithelial ovarian cancer. Recent studies have shown that the GR affects β-arrestin expression, and vice versa. Hence, we assessed the clinical significance of β-arrestin expression in ovarian cancer and determined whether β-arrestin and the GR synergistically have clinical significance and value as prognostic factors. We evaluated the expression of β-arrestins 1 and 2 and the GR in 169 patients with primary epithelial ovarian cancer using immunohistochemistry. The staining intensity was graded on a scale of 0–4 and multiplied by the percentage of positive cells. We divided the samples into two categories based on the expression levels. β-arrestin 1 and GR expression showed a moderate correlation, whereas β-arrestin 2 and GR expression did not demonstrate any correlation. Patients with high β-arrestin 1 and 2 expression exhibited improved survival rates, whereas patients with low GR expression showed a better survival rate. Patients with high β-arrestin 1 and low GR levels had the best prognosis among all groups. β-arrestin is highly expressed in ovarian cancer, suggesting its potential as a diagnostic and therapeutic biomarker. The combination of β-arrestin and GR demonstrated greater predictive prognostic power than GR expression alone, implicating another possible role in prognostication.

KEYWORDS

**β-arrestin, glucocorticoid receptor, epithelial ovarian cancer, prognostic power, steroid hormones**

# 1 Introduction

The 5-year relative survival rate of patients with various cancers has increased by 20% over the last 30 years (1). Despite this improvement, the survival rate of patients with ovarian cancer remains limited compared to that of patients with other cancers (2, 3). Ovarian cancer is the fifth leading cause of cancer-related deaths among women worldwide and the most lethal of all gynecological cancers (4). Although patients with early-stage disease have a survival rate of approximately 90%, most women are diagnosed in stage III/IV, and more than 75% of them die from this disease (5). Cytoreductive surgery and chemotherapy, the standard treatments for ovarian cancer, are accompanied by a high risk of relapse and resistance to chemotherapy (6). Although trials to overcome these limitations, including the use of bevacizumab, poly(ADP-ribose) polymerase inhibitors, and programmed cell death protein 1 blockers, are ongoing, early results indicate that these therapies cannot effectively reduce disease-specific mortality, despite their success against other advanced cancers (7–10). Therefore, the mechanisms that can overcome chemotherapy resistance and relapse in ovarian cancer must be better defined.

Ovarian cancer is a hormone-dependent malignancy, and its progression is affected by steroid hormones and their receptors (8). Nevertheless, the efficacy of hormone therapy in ovarian cancer remains limited due to the various histopathological types, the diversity of hormone receptor expression, and the lack of molecular markers (8). However, the dysregulation of steroid hormone receptor (SHR) signaling in cancer can be exploited as a treatment strategy (11). Hence, we investigated the expression of SHRs and their clinical significance in patients with ovarian cancer and reported that the expression of the GR modifies the role of the progesterone receptor (PR) and affects the androgen receptor (AR) (12). The GR is a major transcription factor regulating gene expression after glucocorticoid binding. Glucocorticoid-mediated transcription regulates selective gene transcription, although the mechanism remains nebulous (13). GR activation by dexamethasone inhibits the cell death in breast, cervical, and ovarian cancer cell lines and xenograft models (14). Currently, the GR is not used as a therapeutic or diagnostic marker in clinical practice, although high GR expression is associated with a poor prognosis of ovarian cancer (15). Co-factors or co-regulators of the GR have to be identified to unravel its role in ovarian cancer.

Recent studies have demonstrated the mutual relationship between β-arrestins and the GR (13, 16–18). The GR enhances the expression of β-arrestins, and in turn, β-arrestins are highly correlated with GR stability, affecting GR protein turnover (16). β-arrestins are scaffolding proteins involved in the negative signaling of G-protein-coupled receptors, affecting cell proliferation, cytoskeletal rearrangement, and cell motility (19). β-arrestins are also involved in cancer cell phenotypes, such as cancer cell migration, invasion, and metastasis, in various cancers (20–22). Additionally, β-arrestins play ambivalent roles in promoting or inhibiting tumor growth (23), with their overall effect depending on the tumor microenvironment and interactions with various receptors or signaling systems (24, 25). Studies on the expression of β-arrestins and their effects on prognosis are being conducted in several tumor types, but the role of β-arrestins in ovarian cancer treatment response and survival is not yet well understood. In the present study, we aimed to investigate the expression of β-arrestins in ovarian cancer and assess their prognostic value in combination with GR expression.

# 2 Materials and methods

## 2.1 Patients and tumor specimens

We obtained 169 formalin-fixed paraffin-embedded surgical specimens of ovarian cancer and 66 normal ovarian epithelial tissues from the Departments of Obstetrics and Gynecology of Gangnam Severance Hospital and Yonsei University College of Medicine, and the Korea Gynecologic Cancer Bank through the Bio and Medical Technology Development Program of the Ministry of Education, Science and Technology, Korea (NRF-2017M3A9B8069610). The surgical specimens were tissues from patients with ovarian cancer who underwent surgery at the Gangnam Severance Hospital and Bucheon St. Mary's Hospital between 1997 and 2012. The exclusion criteria included a diagnosis of recurrent ovarian cancer, peritoneal and fallopian tube cancers, or any other invasive cancers as well as the use of immunosuppression therapies. A retrospective chart review was conducted to obtain patients' clinical information, including age and disease stage at the time of diagnosis (according to FIGO stage), cell type, tumor grade, tissue differentiation status, surgery date, blood test results before surgery, and sensitivity to chemotherapy. Recurrence and treatment response were determined using Response Evaluation Criteria in Solid Tumors (RECIST; version 1.1) on computed tomography scans. Patient status was assessed at the last follow-up visit, and patients lost to follow-up were interviewed *via* telephone. Recurrence-free survival (RFS) was calculated from the date of surgery to the date when recurrence was confirmed or the last follow-up visit in cases without recurrence. Overall survival (OS) was calculated from the date of surgery to the date of confirmed death or the last follow-up visit for patients who were alive. We used all patients' tissues and medical records after disseminating notice to the patients and obtaining their informed consent according to the guidelines of the Gangnam Severance Hospital institutional review board (IRB 3-2021-0361, Seoul, Korea).

## 2.2 Tissue microarray-based immunohistochemistry

We prepared human ovarian tissue microarrays as previously reported (12). In brief, we sectioned the formalin-fixed paraffin-embedded tumor tissue blocks to a thickness of 5 μm. The sections were deparaffinized in xylene and rehydrated using a graded ethanol series. Antigen retrieval was performed by incubating the samples in antigen retrieval buffer, pH 6.0 (Dako, Carpinteria, CA, USA) for β-arrestin 1 and pH 9.0 (Dako) for β-arrestin 2 for 20 min. We

quenched endogenous peroxidase activity with 3% hydrogen peroxide for 15 min. Protein blocking was performed for 20 min.

The sections were incubated with rabbit monoclonal anti-β-arrestin 1 (Cat. No. ab32099; 1:2,000; Abcam, Cambridge, MA, USA) and goat polyclonal anti-β-arrestin 2 (Cat. No. ab31294; 1:400; Abcam) at room temperature for 1 h. Antigen–antibody reactions were detected with EnVision+ Rabbit-HRP (Dako) or LSAB (Dako) and visualized with 3,3-diaminobenzidine (Dako). The sections were counterstained with hematoxylin and then mounted. Appropriate positive and negative controls were run concurrently.

## 2.3 Evaluation of immunohistochemical staining

The stained tissue microarray sections were scanned with a high-resolution optical scanner (NanoZoomer 2.0 HT; Hamamatsu Photonic K.K., Hamamatsu City, Japan) at 20× objective magnification (0.5-mm resolution). The scanned sections were analyzed using VIS Image Analysis Software, version 4.5.1.324 (Visiopharm, Hørsholm, Denmark). β-arrestin 1 was stained in 149 ovarian cancer specimens and 49 non-adjacent normal epithelial tissues, whereas β-arrestin 2 was stained in 114 ovarian cancer specimens and 34 non-adjacent normal epithelial tissues. The expression of the GR was examined based on a study at our institute published in 2021 (12). Staining intensity was scored on a scale of 0–4 (0 = negative, 1 = weak, 2 = moderate, 3 = strong), and immunoreactivity score was calculated by multiplying the intensity score with the percentage of positive cells (possible range, 0–300). The Contal & O'Quigley method was used to obtain the optimal cutoffs to divide the expression levels into two groups (OS cut-off histoscore: β-arrestin 1 = 28.385, β-arrestin 2 = 69.632, RFS cut-off histoscore: β-arrestin 1 = 31.96, β-arrestin 2 = 69.632). For the GR, the cut-off values from the 2021 study were used OS and recurrence free survival (RFS) cut-offs = 6.85] (12).

## 2.4 *In silico* analysis of β-arrestin and GR expression

Data from the Gene Expression Omnibus (GEO), the Gene Expression Profiling Interactive Analysis (GEPIA), and The Cancer Genome Atlas (TCGA) were used in this study. The datasets GSE14407 (serous type; normal = 12, cancer = 12), GSE26712 (serous type; normal = 10, cancer = 185), and GSE29450 (clear cell type; normal = 12, cancer = 20) were used. Correlations among β-arrestin 1, β-arrestin 2, and GR expression were determined based on TCGA and the genotype-tissue expression data in the GEPIA. Kaplan–Meier survival curves were generated using TCGA data in cBioPortal (http://www.cbioportal.org).

## 2.5 Statistical analysis

β-arrestin 1, β-arrestin 2, and GR expression data were statistically analyzed using Mann–Whitney or independent *t*-test, as appropriate. The chi-square test or Fisher's exact test was used for patient characteristics. Survival was analyzed using the log-rank test with the cut-off values determined using the Contal & O'Quigley method and Kaplan–Meier plots. Spearman correlation was used to assess the relationships among β-arrestins 1, β-arrestin 2, and the GR. Cox proportional hazard models were used to estimate the Hazard Ratios(HRs) and confidence intervals (CIs) for univariate and multivariate models. We performed a C-index comparison to determine whether the predictive power of the models would increase when independent variables were combined. We performed statistical analyses using SPSS version 26.0 (IBM SPSS Statistics, Chicago, IL, USA), SAS version 9.4 (SAS Institute, Cary, NC, USA), and R version 4.0.3 (http://www.r-project.org). Statistical significance was set at $P < 0.05$.

# 3 Results

## 3.1 Clinicopathological characteristics

The mean age of the 169 patients was 51.7 ( ± 11.9) years. The serous type accounted for the largest proportion of cases (n = 110, 65.1%), followed by the endometrioid type (n = 23, 13.6%), mucinous type (n = 19, 11.2%), clear cell type (n = 13, 7.7%), and transitional cell type (n = 4, 2.4%). Fifty-seven patients (33.7%) had stage I or II tumors at the time of diagnosis, whereas 112 patients (66.3%) were diagnosed with stage III or higher disease. Among the 169 patients, tumor recurrence was recorded in 93 patients, and 61 patients died of ovarian cancer. The mean follow-up period was 94 months (range, 1–385 months, Supplementary Table S1).

Patients with clinical stage I ovarian cancer at the time of diagnosis showed the highest β-arrestin 1 expression. In contrast, patients with stage II disease exhibited the lowest β-arrestin 1 expression. Interestingly, β-arrestin 2 expression varied by stage (Supplementary Figures S1A, B). Low β-arrestin 1 expression was observed slightly more often than high β-arrestin 1 expression in advanced stages (stages III and IV, $P = 0.010$). However, there were no significant differences in β-arrestin 1's expression level according to other factors, including age, CA125 level, chemotherapy resistance, cell differentiation at the time of diagnosis, and cell type. β-arrestin 2 expression was not significantly different when considering all clinicopathological characteristics within the cohort. The patients' clinicopathological characteristics and β-arrestin 1 and 2 expression levels are presented in Table 1A.

## 3.2 Expression of β-arrestins 1 and 2

We performed immunohistochemistry analysis of cancer and the non-adjacent normal tissues to determine the expression pattern of β-arrestin. β-arrestins 1 and 2 were observed in the cytoplasm (Figure 1C). For β-arrestin 1, 149 ovarian cancer tissue specimens were interpretable, and 49 non-adjacent normal epithelial tissues were identified using immunohistochemistry. For β-arrestin 2, 114 ovarian cancer tissues were interpretable, and 34 non-adjacent normal epithelial tissues were identified using immunohistochemistry. β-

TABLE 1

A. The association between clinicopathologic features and β-arrestin 1,2 expression.

| Patient characteristic | β-Arrestin 1 lown = 74 (%) | β-Arrestin 1 highn = 75 (%) | *P*-value | β-Arrestin 2 lown = 30 (%) | β-Arrestin 2 highn = 84 (%) | *P*-value |
|---|---|---|---|---|---|---|
| Age (years) | | | 0.356 | | | 0.534 |
| <50 | 29 (39.19) | 35 (46.67) | | 13 (43.33) | 31 (36.90) | |
| ≥50 | 45 (60.81) | 40 (53.33) | | 17 (56.67) | 53 (63.10) | |
| CA125 (mmol/L) | | | 0.826 | | | >0.999 |
| <35 | 12 (16.22) | 13 (17.57) | | 3 (10.00) | 10 (11.90) | |
| ≥35 | 62 (83.78) | 61 (82.43) | | 27 (90.00) | 74 (88.10) | |
| Chemosensitivity | | | 0.589 | | | 0.233 |
| Sensitive | 57 (85.07) | 60 (88.24) | | 20 (74.07) | 67 (85.90) | |
| Resistant | 10 (14.93) | 8 (11.76) | | 7 (25.93) | 11 (14.10) | |
| Stage | | | 0.010* | | | 0.757 |
| I, II | 17 (22.97) | 32 (42.67) | | 7 (23.33) | 22 (26.19) | |
| III, IV | 57 (77.03) | 43 (57.33) | | 23 (76.67) | 62 (73.81) | |
| Cell type | | | 0.816 | | | 0.809 |
| Others | 27 (36.49) | 26 (34.67) | | 10 (33.33) | 26 (30.95) | |
| Serous | 47 (63.51) | 49 (65.33) | | 20 (66.67) | 58 (69.05) | |
| Grade | | | 0.116 | | | 0.200 |
| Well–moderate | 31 (43.06) | 42 (56.00) | | 12 (40.00) | 44 (53.66) | |
| Poor | 41 (56.94) | 33 (44.00) | | 18 (60.00) | 38 (46.34) | |

*P < 0.05, chi-square test or Fisher's exact test. Optimal cut-off points were determined using the Contal & O'Quigley method. The cut-off value for β-arrestin 1 expression was 28.38 and that for β-arrestin 2 expression was 69.93.

B. Correlation between clinicopathological characteristics of patients and combined β-arrestin 1 and GR expression.

| Patient characteristic | β-Arrestin 1 low[a] & GR high n = 63 (%) | β-Arrestin 1 low & GR low n = 10 (%) | β-Arrestin 1 high[a] & GR low n = 9 (%) | β-Arrestin 1 high & GR high n = 66 (%) | *P*-value |
|---|---|---|---|---|---|
| Age (years) <50 | 25 (39.68) | 4 (40.00) | 5 (55.56) | 30 (45.45) | 0.794 |
| ≥50 | 38 (60.32) | 6 (60.00) | 4 (44.44) | 36 (54.55) | |
| CA125 level (mmol/L) <35 | 8 (12.70) | 4 (40.00) | 1 (11.11) | 12 (18.46) | 0.188 |
| ≥35 | 55 (87.30) | 6 (60.00) | 8 (88.89) | 53 (81.54) | |
| Chemosensitivity Sensitive | 46 (82.14) | 10 (100.00) | 6 (100.00) | 54 (87.10) | 0.508 |
| Resistant | 10 (17.86) | 0 (0.00) | 0 (0.00) | 8 (12.90) | |
| Stage I, II | 13 (20.63) | 4 (40.00) | 6 (66.67) | 26 (39.39) | 0.012* |
| III, IV | 50 (79.37) | 6 (60.00) | 3 (33.33) | 40 (60.61) | |
| Cell type Others | 22 (34.92) | 5 (50.00) | 5 (55.56) | 21 (31.82) | 0.400 |

*(Continued)*

Continued

| Patient characteristic | β-Arrestin 1 low[a] & GR high n = 63 (%) | β-Arrestin 1 low & GR low n = 10 (%) | β-Arrestin 1 high[a] & GR low n = 9 (%) | β-Arrestin 1 high & GR high n = 66 (%) | *P*-value |
|---|---|---|---|---|---|
| Serous | 41 (65.08) | 5 (50.00) | 4 (44.44) | 45 (68.18) | |
| Grade Well–moderate | 24 (38.71) | 7 (70.00) | 5 (55.56) | 37 (56.06) | 0.120 |
| Poor | 38 (61.29) | 3 (30.00) | 4 (44.44) | 29 (43.94) | |

[a] β-Arrestin 1 expression was categorized as high and low expression according to an optimal cut-off point of 28.38 determined using the Contal & O'Quigley method.

C. Correlation between clinicopathological characteristics of patients and combined β-arrestin 2 and GR expression.

| Patient characteristic | β-Arrestin 2 low[b] & GR high n = 28 (%) | β-Arrestin 2 low & GR low n = 0 | β-Arrestin 2 high[b] & GR low n = 10 (%) | β-Arrestin 2 high & GR high n = 72 (%) | *P*-value |
|---|---|---|---|---|---|
| Age (years) <50 | 13 (46.43) | NA | 3 (30.00) | 27 (37.50) | 0.589 |
| ≥50 | 15 (53.57) | NA | 7 (70.00) | 45 (62.50) | |
| CA125 (mmol/L) <35 | 3 (10.71) | NA | 2 (20.00) | 8 (11.11) | 0.726 |
| ≥35 | 25 (89.29) | NA | 8 (80.00) | 64 (88.89) | |
| Chemosensitivity Sensitive | 20 (80.00) | NA | 9 (100.00) | 56 (83.58) | 0.478 |
| Resistant | 5 (20.00) | NA | 0 (0.00) | 11 (16.42) | |
| Stage I, II | 7 (25.00) | NA | 5 (50.00) | 17 (23.61) | 0.203 |
| III, IV | 21 (75.00) | NA | 5 (50.00) | 55 (76.39) | |
| Cell type Others | 8 (28.57) | NA | 5 (50.00) | 21 (29.17) | 0.390 |
| Serous | 20 (71.43) | NA | 5 (50.00) | 51 (70.83) | |
| Grade well–moderate | 11 (39.29) | NA | 6 (60.00) | 38 (53.52) | 0.362 |
| Poor | 17 (60.71) | NA | 4 (40.00) | 33 (46.48) | |

[b] β-arrestin 2 expression was categorized as high or low according to an optimal cut-off point of 69.93 determined using the Contal & O'Quigley method.
NA, not applicable.

arrestin 1 was significantly more highly expressed in cancer tissues than in the non-adjacent normal tissues (mean histoscore 47.66 vs. 28.85, $P = 0.02$), whereas β-arrestin 2 expression was not significantly different between cancer and non-adjacent normal tissues (mean histoscore 84.48 vs. 79.52, $P = 0.36$) (Figures 1A, B). We further analyzed β-arrestin expression using GEO data (Supplementary Figure S2). In GSE14407, the expression of β-arrestins 1 and 2 was higher in tumor specimens than in normal tissues, which is consistent with the present study findings (Supplementary Figure S2A). However, in GSE26712, β-arrestin 1 was expressed at lower levels in tumor specimens than in normal tissues (Supplementary Figure S2B). In GSE16570, containing data of clear cell tumors, β-arrestin 2 was expressed at lower levels in tumor specimens than in normal tissues (Supplementary Figure S2C).

## 3.3 Correlations between clinicopathological characteristics and combined β-arrestin and GR expression

We examined the correlations between combined β-arrestin and GR expression and clinicopathological characteristics in the patient cohort (Tables 1B, C). The specimens were categorized into high and low expression groups and then further subdivided into four groups. When evaluating β-arrestin 1 and GR expression combined, clinical stage was significant ($P = 0.012$), whereas, age, CA125 level, chemosensitivity, grade, and cell type were not (Table 1B). Consistent with prior results, β-arrestin 2 and GR combination did not reveal any significant differences among the clinicopathological characteristics in the cohort (Table 1C).

## 3.4 Correlations between β-arrestin and GR expression

β-Arrestin 1 and GR expression showed a moderate correlation (r = 0.274, $P$ = 0.001), whereas β-arrestin 2 expression showed no correlation with GR expression (r = 0.044, $P$ = 0.660) (Supplementary Figures S3A, B). GR expression was higher in stage I than in stages II and III. GR expression and β-arrestin 1 gradually increased from stages II to IV (Supplementary Figure S1C). Next, we compared the correlation between β-arrestin and GR expression using public data. Correlations among the expression of GR, β-arrestin 1, and β-arrestin 2 were determined using the GEPIA (Supplementary Figure S4). β-arrestin 1 expression had a significant positive correlation with GR expression (r = 0.38, $P$ < 0.001). β-Arrestin 2 expression had a moderate correlation with GR expression (r = 0.28, $P$ < 0.001).

## 3.5 Prognostic significance of β-arrestins 1 and 2

The RFS and OS according to β-arrestin 1 and 2 expression levels were determined using Kaplan–Meier curves. The group with high β-arrestin 1 expression had significantly better RFS ($P$ = 0.013) and OS ($P$ = 0.037) than the group with low β-arrestin 1 expression (Figures 2A, D). Similarly, the group with high β-arrestin 2 expression had significantly better RFS ($P$ = 0.008) and OS ($P$ = 0.007) than the group with low β-arrestin 2 expression (Figures 2B, E). Consistent with previous study's findings, the group with high GR expression demonstrated significantly worse RFS ($P$ = 0.037) and OS ($P$ = 0.065) than the group with low GR expression (Figures 2C, F).

A Cox regression analysis was performed to examine whether β-arrestins were independent factors for prognostication. High β-arrestin 1 expression was a significant prognostic factor for RFS (univariate HR: 0.537, 95% CI: 0.340–0.849, $P$ = 0.008; multivariate HR: 0.459, 95% CI: 0.275–0.765, $P$ = 0.003). High β-arrestin 2 expression was an independent prognostic factor indicating a better prognosis (univariate HR: 0.507, 95% CI: 0.302–0.8505, $P$ = 0.010; multivariate HR: 0.456, 95% CI: 0.263–0.789, $P$ = 0.0051).

## 3.6 Prognostic significance of the combination of β-arrestins and the GR

We examined differences in the survival rate based on the expression of β-arrestins 1 and 2 and the GR. After classifying the data into four groups based on expression levels, differences in the survival rate were compared using Kaplan–Meier curves. The survival rate was the lowest when β-arrestin 1 expression was low and GR expression was high, and the highest when β-arrestin 1 expression was high and GR expression was low (log-rank $P$ = 0.009 for OS, log-rank $P$ = 0.003 for RFS) (Figures 3A, C). Similarly, the survival rate was the lowest when β-arrestin 2 expression was low and GR expression was high, and the highest when β-arrestin 2 expression was high and GR expression was low (log-rank $P$ = 0.013 for both OS and RFS) (Figures 3B, D).

We examined the effect of β-arrestin and GR expression levels on prognosis using the Cox regression model. When using the group with low β-arrestin 1 and high GR expression as the reference arm, the risk was lower in the group with high β-arrestin 1 and GR expression (multivariate HR: 0.459, 95% CI: 0.272–0.775, $P$ = 0.003). The risk was also lower, albeit not significantly, in the group with high β-arrestin 1 expression and low GR expression (HR: 0.182, 95% CI: 0.025–1.335, $P$ = 0.093). When using the group with low β-arrestin 2 and high GR expression as the reference arm, the risk was lower in the group with high β-arrestin 2 and GR expression (multivariate HR: 0.491, 95% CI: 0.277–0.870, $P$ = 0.014). The risk was the lowest in the group with high β-arrestin 2 expression and low GR expression (multivariate HR: 0.159, 95% CI: 0.036–0.700, $P$ = 0.015) (Table 2).

## 3.7 Predictive power of β-arrestins and the GR

Harrell's C-index analysis was performed to determine whether the combination of β-arrestins and the GR improved prognostication. The combination of β-arrestin 1 and the GR demonstrated greater predictive power in terms of both RFS and OS than the GR alone (C-index for β-arrestin 1 and GR = 0.626, 95% CI: 0.559–0.693, $P$ = 0.0427; C-index for GR = 0.600, 95% CI: 0.567–0.673, $P$ = 0.009). Interestingly, the addition of β-arrestin 2 expression did not significantly affect the prognostic value of GR expression (C-index for β-arrestin 2 and GR = 0.606, 95% CI: 0.543–0.669, $P$ = 0.137; C-index for GR = 0.599, 95% CI: 0.538–0.660, $P$ = 0.091) (Figures 4A, B).

# 4 Discussion

In general, the expression signatures of specific genes or proteins can not only explain the development of certain diseases, but also be utilized as diagnostic biomarkers and treatment targets. The present study demonstrated that the expression of β-arrestin 1 was higher in ovarian cancer specimens than in normal tissues. Furthermore, the combination of β-arrestin 1 and GR expression had a greater predictive prognostic value than GR expression alone, suggesting that β-arrestin 1 may potentially serve as a biomarker in clinical practice and as a therapeutic target. Although further studies are needed to elucidate whether targeting β-arrestin can actually result in improved outcomes, the present study highlights the contribution of β-arrestins in the pathophysiology of ovarian cancer.

Hormones contribute to cancer incidence and mortality; they exert a considerable effect on gynecologic cancers. It is well established that hormones released from the hypothalamic-pituitary-ovarian axis can stimulate or suppress ovarian cancer progression (8, 26, 27). Gonadotropins, estrogens, and androgens may promote ovarian cancer progression, whereas gonadotropin-releasing hormone and progesterone may protect against ovarian

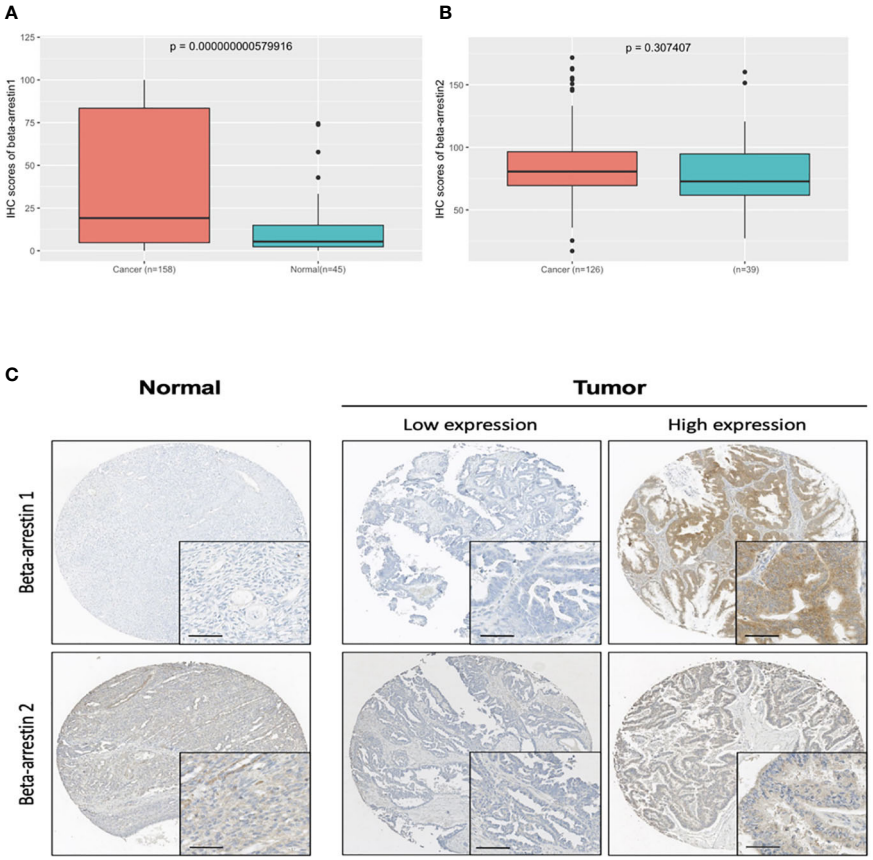


FIGURE 1
β-Arrestin expression in ovarian cancer tissues. **(A)**, β-Arrestin 1 expression was significantly increased in cancer tissue (*P* = 5.79e−10). **(B)**, β-Arrestin 2 expression in cancer tissue did not differ from that in the nonadjacent normal tissue (*P* = 0.307). **(C)**, Immunohistochemical images of β-arrestins 1 and 2 in ovarian cancer tissues. β-Arrestins 1 and 2 were detected in the cytoplasm. (scale bar: 50 μm).

cancer (8, 28, 29). Empirical studies have corroborated that hormone receptors are expressed in both normal and ovarian cancer surface epithelium (30) and they may be associated with carcinogens and result in ovarian cancer (31, 32). Although clinical trials using hormonal therapeutic agents in patients with ovarian cancer have been conducted (33, 34), their results have been inconclusive.

Hormone receptors are transcription factors that regulate diverse physiological functions and have decisive roles in hormone-driven cancers. For example, the estrogen receptor (ER) is expressed in 50%–88% of all breast cancers and therefore has served as a primary therapeutic target (35, 36). ER antagonists have demonstrated excellent curative efficacy in patients with ER-positive breast cancer (37); while ovarian cancer is also hormone-driven, the expression and role of hormone receptors in its pathogenesis remain poorly elucidated. We previously assessed the expression levels of ER-α, ER-β, AR, GR, and PR in ovarian cancer tissues and determined their association with the survival rate. The GR was more highly expressed in ovarian cancer tissues than in the non-adjacent normal tissues, and elevated GR levels were associated with a poor prognosis. The GR also affected the expression of the AR and PR (12). High GR expression is associated with an increased risk of disease progression in gynecological and untreated, early-stage, triple-negative breast cancer (38). GR actions can be regulated in a cell type-specific manner, and GR may be a useful therapeutic target in cancer treatment. Upon steroid binding, the GR undergoes activation, dissociates from the chaperone complex, and exerts its various effects (39). The latter requires the translocation of the receptor to the nucleus, where it can bind to glucocorticoid-responsive elements or tether with other transcription factors (40, 41), resulting in a cross-talk between the receptor and an array of elements, such as co-modulators, co-activators, co-repressors, and DNA-remodeling factors (13, 42). β-arrestin 1 has been recently shown to bind to the GR to stabilize the GR protein (16). Accordingly, loss of β-arrestin 1 increases GR protein turnover by promoting its degradation (13).

β-arrestin has been shown to play a key role in various signaling pathways. The binding of β-arrestin 1 to the endothelin-1 (ET-1)/ET A-type receptor (ETAR) signaling complex, and the activation of β-catenin promote the migration, invasion, and progression of ovarian cancer cells (43). Furthermore, β-arrestins activate NF-kB in ovarian cancer cells, thereby enhancing their survival. It has also been reported that β-arrestin 1 is involved in the activation of the YAP/mutant p53 complex in high-grade serous ovarian cancer cells and is associated with increased cancer cell proliferation (44, 45). ETAR antagonists (e.g., ZD4054) can inhibit metastatic progression

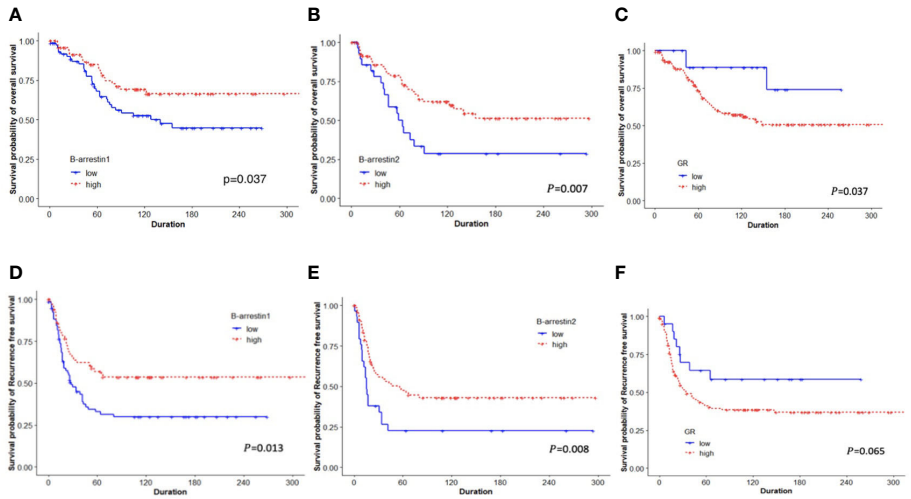


FIGURE 2
Kaplan–Meier plots for OS and RFS based on categorized β-arrestin 1 and 2 and GR expression. **(A, B)**, Low β-arrestin 1 and 2 expression was associated with shorter OS (log-rank $P$ = 0.037, $P$ = 0.007, respectively). **(C, F)**, Low GR expression was associated with better OS (log-rank $P$ = 0.037), but not with RFS (log-rank $P$ = 0.065). **(D, E)**, Patients with low expression of β-arrestins 1 and 2 had significantly shorter RFS than those with high expression (log-rank $P$ = 0.013, $P$ = 0.008).

by interfering with β-arrestin 1 signaling (46). Although the roles of β-arrestin in various signaling systems are being actively studied, there are only a few studies on its survival implication and clinical significance in patients with ovarian cancer.

Therefore, we investigated the relationship between β-arrestin expression and the survival of patients with ovarian cancer. Notably, we found a positive relation between β-arrestin expression levels and the survival of patients with ovarian cancer.

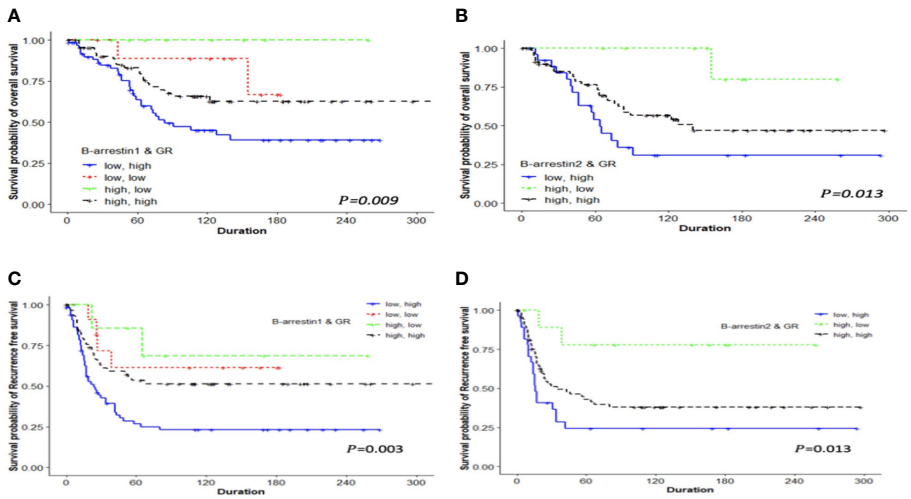


FIGURE 3
Kaplan–Meier analysis of patients with ovarian cancer based on the combination of β-arrestin 1, β-arrestin 2, and GR expression. OS and RFS differences were observed among the four groups classified according to high or low expression levels. **(A)**, The OS of patients with low β-arrestin 1 expression and high GR expression was shorter (median 63 months) than that of patients with high β-arrestin 1 expression and high GR expression (median 94 months), low β-arrestin 1 expression and low GR expression (median 138.5 months), or high β-arrestin 1 expression and low GR expression (median 85 months) (log-rank $P$ = 0.009). **(B)**, Patients with low β-arrestin 2 expression and high GR expression had a significantly shorter OS (median 64 months) than those with high β-arrestin 2 expression and high GR expression (median 140 months) or high β-arrestin 2 expression and low GR expression (median not reached) (log-rank $P$ = 0.013). **(C)**, The RFS of patients with low β-arrestin 1 expression and high GR expression was significantly shorter (median 18.5 months) than that of patients with high β-arrestin 1 expression and high GR expression (median 52 months), low β-arrestin 1 expression and low GR expression (median 106 months), or high β-arrestin 1 expression and low GR expression (median 66 months) (log-rank $P$ = 0.003). **(D)**, Patients with low β-arrestin 2 expression and high GR expression had a significantly shorter RFS (median 16 months) than those with high β-arrestin 2 expression and high GR expression (median 35 months) or high β-arrestin 2 expression and low GR expression (median 118.5 months) (log-rank $P$ = 0.013).

TABLE 2 Associations between prognostic variables and recurrence-free survival in primary epithelial ovarian cancer.

| Risk factor | Univariate regression | | Multivariate regression | |
|---|---|---|---|---|
| | HR | *P* | HR | *P* |
| β-Arrestin 1 (high[a]) | 0.537 (0.340–0.849) | 0.007* | 0.459 (0.275–0.765) | 0.002* |
| β-Arrestin 2 (high[b]) | 0.507 (0.302–0.850) | 0.010* | 0.456 (0.263–0.789) | 0.005* |
| GR (high[c]) | 1.943 (0.940–4.018) | 0.073 | 1.549 (0.708–3.386) | 0.273 |
| β-Arrestin 1 low & GR high | Ref. | | Ref. | |
| β-Arrestin 1 high & GR high | 0.485 (0.301–0.780) | 0.002* | 0.459 (0.272–0.775) | 0.003* |
| β-Arrestin 1 low & GR low | 0.323 (0.116–0.897) | 0.030* | 0.525 (0.185–1.492) | 0.226 |
| β-Arrestin 1 high & GR low | 0.224 (0.054–0.924) | 0.038* | 0.182 (0.025–1.335) | 0.093 |
| β-Arrestin 2 low & GR high | Ref. | | | |
| β-Arrestin 2 high & GR high | 0.485 (0.301–0.780) | 0.002* | 0.491 (0.277–0.870) | 0.014* |
| β-Arrestin 2 low & GR low | NA | | NA | |
| β-Arrestin 2 high & GR low | 0.224 (0.054–0.924) | 0.038* | 0.159 (0.036–0.700) | 0.015* |
| Age (≥50 years) | 1.481 (0.973–2.254) | 0.066 | 1.905 (1.041–3.487) | 0.036* |
| CA125 (≥35 mmol/l) | 2.801 (1.356–5.788) | 0.005* | 1.105 (0.500–2.442) | 0.805 |
| Cell type (serous) | 2.583 (1.572–4.245) | 0.0002* | 1.504 (0.819–2.762) | 0.188 |
| Grade (poor) | 1.890 (1.247–2.863) | 0.002* | 1.640 (1.005–2.678) | 0.047 |
| Chemosensitivity (resistant) | 17.154 (9.371–31.404) | <0.0001* | 16.398 (7.442–36.135) | <0.0001* |
| FIGO Stage (≥III) | 6.122 (3.249–11.536) | <0.0001* | 3.726 (1.819–7.634) | 0.0003* |

[a]cut-off of β-arrestin 1 expression = 31.96 established by the Contal & O'Quigley method, [b]cut-off of β-arrestin 2 expression = 69.32 established by the Contal & O'Quigley method, [c]cut-off of GR expression = 6.85 according to [(12)].
*P < 0.05.
Ref, reference arm; NA, not applicable.

Therefore, TCGA data were used to analyze the expression of β-arrestin genes *ARRB1* and *ARRB2* and the survival of patients with ovarian cancer. OS was more favorable when β-arrestins 1 and 2 were highly expressed, whereas lower expression resulted in high RFS (Supplementary Figure S4).

These results have also been reported in other cancer types. In lung cancer, high β-arrestin 1 expression was associated with a poor prognosis (20), whereas low β-arrestin 2 expression was associated with a poor prognosis as β-arrestin 2 inhibits lung cancer metastasis (47). In colorectal cancer, high β-arrestin 2 expression inhibits NF-kB activation and is associated with a favorable prognosis (48). β-arrestin 1 has also been shown to play a decisive role in colorectal cancer metastasis by forming a signaling complex with prostaglandin E and c-Src (49). Therefore, it is important to elucidate the tissue-specific roles of β-arrestins and their interactions with key signaling cascades in each tumor type.

In conclusion, we evaluated the expression of β-arrestin in ovarian cancer tissues and observed that its increased expression was associated

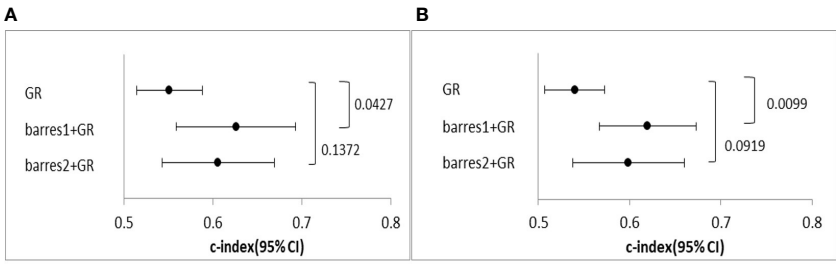


FIGURE 4
Comparison of the predictive power of the GR and the GR and β-arrestin combination. **(A)**, C-index of univariate Cox regression analysis for OS. **(B)**, C-index of univariate Cox regression analysis for PFS. The GR and β-arrestin 1 expression combination showed a better predictive power than GR expression alone. However, the GR and β-arrestin 2 expression combination showed similar predictive power as GR expression alone.

with a good prognosis and had clinical significance in epithelial ovarian cancer. However, it should be noted that this was a retrospective study with several inherent biases and limitations, such as a low number of patients and a broad timeline of inclusion of cases. Additionally, no cellular experiments were conducted to validate our results. Despite these limitations, our study suggests that β-arrestin, in combination with the GR, may have enhanced predictive power for patients with epithelial ovarian cancer, implicating a possible role in prognostication.

A marker that can predict prognosis or treatment response can be an essential clue to providing more differentiated and effective treatment for each individual. There is a need for more powerful markers for the treatment of ovarian cancer. In oncology, efforts have been made to identify non-invasive and more efficient markers. Recently, 2-$^{18}$FDG PET/CT has been known to have recurrence detection and prognostic values, and expectations for their role as an imaging biomarker are growing (50, 51). Attempts to combine new biomarkers with clinical features or imaging technique provide an opportunity to predict the patient's prognosis and offer improved individualized treatment. This potential was observed in the case of the epithelial ovarian cancer biomarkers, β-arrestin and GR, in this study.

## Data availability statement

The datasets presented in this study can be found in online repositories. The names of the repository/repositories and accession number(s) can be found in the article/Supplementary Material.

## Author contributions

Conceptualization: J-WR, GH, and J-HK. Data curation: J-WR, H-SK, JK, H-NL, and J-YC. Methodology: J-WR, J-YC, and J-HK. Funding acquisition: HC, J-HK. Resource: GH, H-SK. Visualization: H-Y.S, J-YC. Writing-original draft: J-WR. Writing-review and editing: J-HK, J-YC, and J-WR. Supervision: HBC, J-HK. All authors have read and agreed to the published version of the manuscript. All authors contributed to the article and approved the submitted version.

## Funding

This study was supported by the National Research Foundation of Korea (NRF) through the Basic Science Research Program funded by the Ministry of Education (NRF-2021R1A2B5B02001915).

## Acknowledgments

Paraffin blocks were provided by the Korea Gynecologic Cancer Bank through Bio & Medical Technology Development Program of the Ministry of Education, Science and Technology, Korea (NRF-2017M3A9B8069610), and were obtained from the Human Tissue Bank of Gangnam Severance Hospital, Yonsei University College of Medicine.

## Conflict of interest

The authors declare that the research was conducted in the absence of any commercial or financial relationships that could be construed as a potential conflict of interest.

## Publisher's note



## Supplementary material

The Supplementary Material for this article can be found online at: https://www.frontiersin.org/articles/10.3389/fonc.2023.1104521/full#supplementary-material

## References

1. Siegel RL, Miller KD, Jemal A. Cancer statistics, 2018. *CA Cancer J Clin* (2018) 68:7–30. doi: 10.3322/caac.21442

2. Lheureux S, Braunstein M, Oza AM. Epithelial ovarian cancer: Evolution of management in the era of precision medicine. *CA Cancer J Clin* (2019) 69:280–304. doi: 10.3322/caac.21559

3. Peres LC, Cushing-Haugen KL, Köbel M, Harris HR, Berchuck A, Rossing MA, et al. Invasive epithelial ovarian cancer survival by histotype and disease stage. *J Natl Cancer Inst* (2019) 111:60–8. doi: 10.1093/jnci/djy071

4. Stewart C, Ralyea C, Lockwood S. Ovarian cancer: An integrated review. *Semin Oncol Nurs* (2019) 35:151–6. doi: 10.1016/j.soncn.2019.02.001

5. Banerjee S, Kaye SB. New strategies in the treatment of ovarian cancer: Current clinical perspectives and future potential. *Clin Cancer Res* (2013) 19:961–8. doi: 10.1158/1078-0432.CCR-12-2243

6. Roett MA, Evans P. Ovarian cancer: an overview. *Am Fam Phys* (2009) 80:609–16.

7. Haunschild CE, Tewari KS. Bevacizumab use in the frontline, maintenance and recurrent settings for ovarian cancer. *Future Oncol* (2020) 16:225–46. doi: 10.2217/fon-2019-0042

8. Li H, Liu Y, Wang Y, Zhao X, Qi X. Hormone therapy for ovarian cancer: emphasis on mechanisms and applications [Review]. *Oncol Rep* (2021) 46:223. doi: 10.3892/or.2021.8174

9. Wan C, Keany MP, Dong H, Al-Alem LF, Pandya UM, Lazo S, et al. Enhanced efficacy of simultaneous PD-1 and PD-L1 immune checkpoint blockade in high-grade serous ovarian cancer. *Cancer Res* (2021) 81:158–73. doi: 10.1158/0008-5472.CAN-20-1674

10. Mirza MR, Coleman RL, González-Martín A, Moore KN, Colombo N, Ray-Coquard I, et al. The forefront of ovarian cancer therapy: update on PARP inhibitors. *Ann Oncol* (2020) 31:1148–59. doi: 10.1016/j.annonc.2020.06.004

11. Ahmad N, Kumar R. Steroid hormone receptors in cancer development: A target for cancer therapeutics. *Cancer Lett* (2011) 300:1–9. doi: 10.1016/j.canlet.2010.09.008

12. Han GH, Hwang I, Cho H, Ylaya K, Choi JA, Kwon H, et al. Clinical significance of tumor infiltrating lymphocytes in association with hormone receptor expression patterns in epithelial ovarian cancer. *Int J Mol Sci* (2021) 22:5714. doi: 10.3390/ijms22115714

13. Petrillo MG, Oakley RH, Cidlowski JA. β-Arrestin-1 inhibits glucocorticoid receptor turnover and alters glucocorticoid signaling. *J Biol Chem* (2019) 294:11225–39. doi: 10.1074/jbc.RA118.007150

14. Schlossmacher G, Stevens A, White A. Glucocorticoid receptor-mediated apoptosis: mechanisms of resistance in cancer cells. *J Endocrinol* (2011) 211:17–25. doi: 10.1530/JOE-11-0135

15. Fang YY, Li D, Cao C, Li CY, Li TT. Glucocorticoid receptor repression mediated by BRCA1 inactivation in ovarian cancer. *BMC Cancer* (2014) 14:188. doi: 10.1186/1471-2407-14-188

16. Oakley RH, Revollo J, Cidlowski JA. Glucocorticoids regulate arrestin gene expression and redirect the signaling profile of G protein-coupled receptors. *Proc Natl Acad Sci U.S.A.* (2012) 109:17591–6. doi: 10.1073/pnas.1209411109

17. Zhang M, Teng H, Shi J, Zhang Y. Disruption of β-arrestins blocks glucocorticoid receptor and severely retards lung and liver development in mice. *Mech Dev* (2011) 128:368–75. doi: 10.1016/j.mod.2011.07.003

18. Purayil HT, Daaka Y. βArrestin1 regulates glucocorticoid receptor mitogenic signaling in castration-resistant prostate cancer. *Prostate* (2022) 82:816–25. doi: 10.1002/pros.24324

19. Laporte SA, Scott MGH. β-arrestins: multitask scaffolds orchestrating the where and when in cell signalling. *Methods Mol Biol* (2019) 1957:9–55. doi: 10.1007/978-1-4939-9158-7_2

20. Sobolesky PM, Moussa O. The role of β-arrestins in cancer. *Prog Mol Biol Transl Sci* (2013) 118:395–411. doi: 10.1016/B978-0-12-394440-5.00015-2

21. Dasgupta P, Rizwani W, Pillai S, Davis R, Banerjee S, Hug K, et al. ARRB1-mediated regulation of E2F target genes in nicotine-induced growth of lung tumors. *J Natl Cancer Inst* (2011) 103:317–33. doi: 10.1093/jnci/djq541

22. Buchanan FG, Gorden DL, Matta P, Shi Q, Matrisian LM, DuBois RN. Role of β-arrestin 1 in the metastatic progression of colorectal cancer. *Proc Natl Acad Sci U.S.A.* (2006) 103:1492–7. doi: 10.1073/pnas.0510562103

23. Song Q, Ji Q, Li Q. The role and mechanism of β_arrestins in cancer invasion and metastasis (Review). *Int J Mol Med* (2018) 41:631–9. doi: 10.3892/ijmm.2017.3288

24. Lin EW, Karakasheva TA, Hicks PD, Bass AJ, Rustgi AK. The tumor microenvironment in esophageal cancer. *Oncogene* (2016) 35:5337–49. doi: 10.1038/onc.2016.34

25. Kim JI, Lakshmikanthan V, Frilot N, Daaka Y. Prostaglandin E2 promotes lung cancer cell migration *via* EP4-barrestin1-c-Src signalosome. *Mol Cancer Res* (2010) 8:569–77. doi: 10.1158/1541-7786.MCR-09-0511

26. Gründker C, Emons G. Role of gonadotropin-releasing hormone (GnRH) in ovarian cancer. *Cells* (2021) 10:292. doi: 10.3390/cells10020437

27. Paleari L, DeCensi A. Endocrine therapy in ovarian cancer: Where do we stand? *Curr Opin Obstet Gynecol* (2018) 30:17–22. doi: 10.1097/GCO.0000000000000423

28. Bose CK. Follicle stimulating hormone receptor in ovarian surface epithelium and epithelial ovarian cancer. *Oncol Res* (2008) 17:231–8. doi: 10.3727/096504008786111383

29. Kim O, Park EY, Kwon SY, Shin S, Emerson RE, Shin YH, et al. Targeting progesterone signaling prevents metastatic ovarian cancer. *Proc Natl Acad Sci U.S.A.* (2020) 117:31993–2004. doi: 10.1073/pnas.2013595117

30. Ko YJ, Balk SP. Targeting steroid hormone receptor pathways in the treatment of hormone dependent cancers. *Curr Pharm Biotechnol* (2004) 5:459–70. doi: 10.2174/1389201043376616

31. Ajani MA, Salami A, Awolude OA, Oluwasola AO. Hormone-receptor expression status of epithelial ovarian cancer in ibadan, south-Western Nigeria. *Pan Afr Med J* (2017) 27:259. doi: 10.11604/pamj.2017.27.259.11883

32. Tan J, Song C, Wang D, Hu Y, Liu D, Ma D, et al. Expression of hormone receptors predicts survival and platinum sensitivity of high-grade serous ovarian cancer. *Biosci Rep* (2021) 41:BSR20210478. doi: 10.1042/BSR20210478

33. Lee JY, Shin JY, Kim HS, Heo JI, Kho YJ, Kang HJ, et al. Effect of combined treatment with progesterone and tamoxifen on the growth and apoptosis of human ovarian cancer cells. *Oncol Rep* (2012) 27:87–93. doi: 10.3892/or.2011.1460

34. Wuntakal R, Seshadri S, Montes A, Lane G. Luteinising hormone releasing hormone (LHRH) agonists for the treatment of relapsed epithelial ovarian cancer. *Cochrane Database Syst Rev* (2016) 6):CD011322. doi: 10.1002/14651858.CD011322.pub2

35. Yip CH, Rhodes A. Estrogen and progesterone receptors in breast cancer. *Future Oncol* (2014) 10:2293–301. doi: 10.2217/fon.14.110

36. Bai Z, Gust R. Breast cancer, estrogen receptor and ligands. *Arch Pharm (Weinheim)* (2009) 342:133–49. doi: 10.1002/ardp.200800174

37. Chlebowski RT, Aragaki AK, Pan K. Breast cancer prevention: Time for change. *JCO Oncol Pract* (2021) 17:709–16. doi: 10.1200/OP.21.00343

38. Bakour N, Moriarty F, Moore G, Robson T, Annett SL. Prognostic significance of glucocorticoid receptor expression in cancer: A systematic review and meta-analysis. *Cancers (Basel)* (2021) 13:1649. doi: 10.3390/cancers13071649

39. Kadmiel M, Cidlowski JA. Glucocorticoid receptor signaling in health and disease. *Trends Pharmacol Sci* (2013) 34:518–30. doi: 10.1016/j.tips.2013.07.003

40. Cain DW, Cidlowski JA. Immune regulation by glucocorticoids. *Nat Rev Immunol* (2017) 17:233–47. doi: 10.1038/nri.2017.1

41. Monczor F, Chatzopoulou A, Zappia CD, Houtman R, Meijer OC, Fitzsimons CP. A model of glucocorticoid receptor interaction with coregulators predicts transcriptional regulation of target genes. *Front Pharmacol* (2019) 10:214. doi: 10.3389/fphar.2019.00214

42. Petta I, Dejager L, Ballegeer M, Lievens S, Tavernier J, De Bosscher K, et al. The interactome of the glucocorticoid receptor and its influence on the actions of glucocorticoids in combatting inflammatory and infectious diseases. *Microbiol Mol Biol Rev* (2016) 80:495–522. doi: 10.1128/MMBR.00064-15

43. Rosanò L, Cianfrocca R, Tocci P, Spinella F, Di Castro V, Spadaro F, et al. β-arrestin-1 is a nuclear transcriptional regulator of endothelin-1-induced β-catenin signaling. *Oncogene* (2013) 32:5066–77. doi: 10.1038/onc.2012.527

44. Tocci P, Cianfrocca R, Di Castro V, Rosanò L, Sacconi A, Donzelli S, et al. β-arrestin1/YAP/mutant p53 complexes orchestrate the endothelin a receptor signaling in high-grade serous ovarian cancer. *Nat Commun* (2019) 10:3196. doi: 10.1038/s41467-019-11045-8

45. Tocci P, Cianfrocca R, Sestito R, Rosanò L, Di Castro V, Blandino G, et al. Endothelin-1 axis fosters YAP-induced chemotherapy escape in ovarian cancer. *Cancer Lett* (2020) 492:84–95. doi: 10.1016/j.canlet.2020.08.026

46. Morris CD, Rose A, Curwen J, Hughes AM, Wilson DJ, Webb DJ. Specific inhibition of the endothelin a receptor with ZD4054: clinical and pre-clinical evidence. *Br J Cancer* (2005) 92:2148–52. doi: 10.1038/sj.bjc.6602676

47. Wu Z, Tong W, Tan Z, Wang S, Lin P. The clinical significance of β-arrestin 2 expression in the serum of non-small cell lung cancer patients. *Zhongguo Fei Ai Za Zhi* (2011) 14:497–501. doi: 10.3779/j.issn.1009-3419.2011.06.04

48. Ren W, Wang T, He X, Zhang Q, Zhou J, Liu F, et al. β–arrestin 2 promotes 5-FU–induced apoptosis *via* the NF-κB pathway in colorectal cancer. *Oncol Rep* (2018) 39:2711–20. doi: 10.3892/or.2018.6340

49. Buchanan FG, Lee Gorden D, Matta P, Shi Q, Matrisian LM, DuBois RN. Role of beta-arrestin 1 in the metastatic progression of colorectal cancer. *Proc Natl Acad Sci U.S.A.* (2006) 103(5):1492–7. doi: 10.1073/pnas.0510562103

50. Delgado Bolton RC, Aide N, Colletti PM, Ferrero A, Paez D, Skanjeti A, et al. EANM guideline on the role of 2-[(18)F]FDG PET/CT in diagnosis, staging, prognostic value, therapy assessment and restaging of ovarian cancer, endorsed by the American college of nuclear medicine (ACNM), the society of nuclear medicine and molecular imaging (SNMMI) and the international atomic energy agency (IAEA). *Eur J Nucl Med Mol Imaging* (2021) 48(10):3286–302. doi: 10.1007/s00259-021-05450-9

51. Delgado Bolton RC, Calapaquí Terán AK, Pellet O, Ferrero A, Giammarile F. The search for new 2-18F-FDG PET/CT imaging biomarkers in advanced ovarian cancer patients: Focus on peritoneal staging for guiding precision medicine and management decisions. *Clin Nucl Med* (2021) 46(11):906–7. doi: 10.1097/RLU.0000000000003784

frontiers | Frontiers in Oncology

TYPE Case Report
PUBLISHED 13 March 2023
DOI 10.3389/fonc.2023.1108586



OPEN ACCESS

EDITED BY
Pierluigi Giampaolino,
University of Naples Federico II, Italy

REVIEWED BY
Luigi Della Corte,
University of Naples Federico II, Italy
Komsun Suwannarurk,
Thammasat University, Thailand

*CORRESPONDENCE
Yue Shi
shiyue7467@fckyy.org.cn
Yan Ning
ningyan1370@fckyy.org.cn

†These authors have contributed equally to this work and share first authorship

SPECIALTY SECTION
This article was submitted to Gynecological Oncology, a section of the journal Frontiers in Oncology

RECEIVED 26 November 2022
ACCEPTED 13 February 2023
PUBLISHED 13 March 2023

CITATION
Lu L, Wang S, Shen H, Zhang F, Ma F, Shi Y and Ning Y (2023) Case Report: A case of *COL1A1–PDGFB* fusion uterine sarcoma at cervix and insights into the clinical management of rare uterine sarcoma. *Front. Oncol.* 13:1108586. doi: 10.3389/fonc.2023.1108586



# Case Report: A case of *COL1A1–PDGFB* fusion uterine sarcoma at cervix and insights into the clinical management of rare uterine sarcoma

Linghui Lu[1†], Shunni Wang[1†], Haoran Shen[2], Feiran Zhang[1], Fenghua Ma[3], Yue Shi[2*] and Yan Ning[1*]

[1]Department of Pathology, Obstetrics and Gynecology Hospital of Fudan University, Shanghai, China, [2]Department of Gynecological Oncology, Obstetrics and Gynecology Hospital of Fudan University, Shanghai, China, [3]Department of Radiology, Obstetrics and Gynecology Hospital of Fudan University, Shanghai, China

*COL1A1–PDGFB* gene fusion uterine sarcoma is an especially rare malignant mesenchymal tumor that was previously classified as an undifferentiated uterine sarcoma due to the lack of specific features of differentiation. Till now, only five cases have been reported, and here we presented another case recently diagnosed in a Chinese woman who had vaginal bleeding. She presented with a cervical mass at the anterior lip of the cervix invading the vagina and was treated with laparoscopic total hysterectomy plus bilateral salpingo-oophorectomy (TH+BSO) and partial vaginal wall resection with the final pathology of *COL1A1–PDGFB* fusion uterine sarcoma. Our aim is to emphasize the importance of differential diagnosis of this rare tumor, as early precise diagnosis may allow patients to benefit from the targeted therapy imatinib. This article also serves as further clinical evidence of this disease, serving to increase clinical awareness of this rare sarcoma to avoid misdiagnosis.

KEYWORDS

**COL1A1-PDGFB fusion, uterine sarcoma, RNA sequencing, dermatofibrosarcoma protuberans (DFSP), NTRK fusion, target therapy**

## Introduction

Uterine mesenchymal tumors consist of a group of heterogeneous tumors with various morphological features, immunohistochemical (IHC) presentations, and genetic mutations. Undifferentiated uterine sarcomas are malignant mesenchymal tumors that lack specific features of differentiation and are diagnosed with the exclusion of others. With the rapid development of molecular technology including fluorescence *in situ* hybridization (FISH) and next-generation sequencing (NGS), the pathological classification and prognosis assessment of these tumors achieved remarkable progression (1, 2).

*COL1A1* gene is located at chromosomes 17q21.3 to q22.1 with 52 exons. The gene is highly variable, as it contains multiple fragile breakpoints spanning a wide range. *PDGFB* gene is located at chromosomes 22q12.3 to q13.1 containing 7 exons. Its breakpoint is consistently present in intron 1. When these two genes merged, the expression of *PDGFB* would be muted from the regulation of upstream inhibitory factors, and *COL1A1–PDGFB* chimeric mRNAs would be generated, resulting in *PDGFB* and its receptor (*PDGFBRB*) stimulating cell proliferation in an autocrine or paracrine manner, which was reported to be oncogenic (3–5).

According to the previous literature, *COL1A1–PDGFB* gene fusion occurred mainly in soft tissue dermatofibrosarcoma protuberans (6–8) and pediatric giant cell fibroblastoma (9), while it was rarely reported in the female genital tract. Croce (10) first reported three cases with *COL1A1–PDGFB* fusion in uterine sarcomas in 2019, and subsequently, Samuel and Adriana respectively reported one case each in 2020 and 2022 (11, 12).

The relevant literature had been reviewed, and no reports in China had been found on this tumor so far. Here, we presented the first uterine sarcoma located at the cervix with *COL1A1–PDGFB* gene fusion in China.

# Case report

## Clinical presentation

A 57-year-old woman presented with uninduced post-menopausal vaginal bleeding for 2 weeks. Gynecological examination revealed a 4-cm mass on the anterior lip of the cervix protruding to the vagina. Pelvic ultrasound showed a 51 × 45 × 35 $mm^3$ hypoechoic mass in the lower segment of the uterus extending to the anterior lip of the cervix with a rich blood supply. MRI displayed an irregular exophytic mass on the cervix that presented slightly high signal intensity on T2-weighted imaging (T2WI) with significant enhancement (Supplementary Figure 1), and cervical myoma was suspected for which malignancy could not be excluded. As for medical history, she had undergone surgery for papillary thyroid cancer in another hospital with iodine-131 radiation after an operation in 2011, and regular follow-ups showed no abnormality currently. She denied any family history. For obstetric history, she was G2P2 with two children born through vaginal delivery in her 30s. She denied any unprotected sex, and no bleeding was noticed during intercourse. The pre-op tumor markers were all within normal range. A comprehensive pre-op evaluation was performed with the human papillomavirus (HPV) test as negative, liquid based cytology test (LCT) as negative for intraepithelial lesion or malignancy (NILM), and abdominal +chest CT with contrast showing no suspicious lymph node or any other abnormality.

As cervical myoma was considered and malignancy could not be excluded, total hysterectomy plus bilateral salpingo-oophorectomy (TH+BSO) plus partial vaginal wall resection was suggested for this patient who has had menopause for 11 years already. The patient received laparoscopic surgery with frozen pathology reported as cervical myoma, and the whole specimen was extracted through the vagina. As the tumor size was slightly too big to pass through the atrophic vagina, the uterus was dissected under the protection of a specimen bag, and there was no dissemination of the tumor during the operation. The tumor was completely resected, and no extrauterine lesions were detected during the operation. Postoperative RNA sequencing of tumor tissue was performed, which supported the diagnosis of *COL1A1–PDGFB* fusion uterine sarcoma. Considering the rarity of this tumor and limited data available as to the treatment and prognosis, thorough communication with the patient was conducted, and the decision was reached as no further adjuvant therapy was given post-operation and close follow-up was required. The patient was suggested to undergo follow-ups every 3–6 months in the first 2 years post-operation, and the frequency could be extended to 6–12 months since the third year after surgery. The patient was recommended to undergo lifelong follow-ups, and the latest follow-up at 6 months after surgery showed no abnormality. The patient had been compliant with regular follow-ups, and no adverse events have been reported so far.

## Methods

The IHC staining was performed on formalin-fixed and paraffin-embedded (FFPE) tissue blocks automatically (Leica Bond Max, Wetzlar, Germany), and then antibodies (Table 1) were applied according to the manufacturer's instructions. RNA extraction, RNA-seq library preparation, sequencing, and analysis were carried out as previously described (13–15). Total RNA was extracted from FFPE tissue blocks, and rRNA was removed to obtain mRNA, which was then processed into short fragments. The interrupted mRNA segments were reverse-transcribed with random primers. After the synthesis of the first strand of cDNA by reverse transcription, the second strand of cDNA was synthesized, which became double-stranded cDNA. cDNA was purified by Beckman AMPPure XP magnetic beads and repaired at the end, and a sequencing joint was added. The target fragments were recovered by purifying magnetic beads and then amplified by PCR. The library constructed was sequenced by Illumina HiSeq2000.

## Pathologic analyses

### Histopathologic findings

A gross examination of the specimen revealed a 5.5-cm mass at the anterior lip of the cervix protruding toward the vagina. The tumor cross-section was firm, white, and whorled with relatively clear boundaries (Supplementary Figure 2). Microscopically, the tumor boundary was generally clear, while infiltration into the cervical mucosa and fibromyometrium was noticed locally (Figure 1A). The tumor consisted of relatively uniform spindle cells densely arranged in more prominent storiform or herringbone patterns. The nuclei were oval- to spindle-shaped, and the cytoplasm was eosinophilic and scarce, with blurred cell boundaries (Figure 1B). However, some minor regions with sparse cell distribution and dilated small blood vessels were also

TABLE 1 Details of immunohistochemical results in this case presentation.

| Primary antibody | Tumor stain | Clone | Dilution | Manufacturer |
|---|---|---|---|---|
| CD34 | + | QBEND/10 | 1:200 | Changdao |
| S-100 | – | Polyclonal antibody | 1:200 | DAKO |
| ER | – | 6F11 | 1:200 | Leica |
| PR | – | PgR636 | 1:200 | DAKO |
| Desmin | – | D33 | 1:1,000 | DAKO |
| Caldesmon | – | h-CD | 1:200 | GT |
| SMA | – | 1A4 | 1:100 | DAKO |
| CD10 | – | 56C6 | 1:1 | Leica |
| TRK | – | EPR17341 | 1:100 | Abcam |
| P16 | + | 6H12 | 1:1,000 | Maixin |
| P53 | Wild type | DO-7 | 1:300 | DAKO |
| Ki-67 | 30% + | MIB-1 | 1:150 | DAKO |
| PHH3 | 25/10 HPF | Polyclonal antibody | 1:50 | Zhongshan |
| CCND1 | 5% + | EP12 | 1:100 | Zhongshan |
| BCOR | – | C-10 | 1:50 | Santa |
| ALK | – | 5A4 | 1:200 | Leica |
| MeLan-A | – | A103 | 1:100 | DAKO |
| HMB-45 | – | Polyclonal antibody | 1:100 | Changdao |
| NSE | – | BBS/NS/VI-H14 | 1:100 | DAKO |
| SMARCA4 | + | EPNCIR111A | 1:200 | Abcam |
| INI1 | + | MRQ-27 | 1:1 | Maixin |
| CD99 | – | O 13 | 1:100 | GT |

seen (Figure 1C). Mitoses were relatively active, up to 30 per 10 high-power fields (HPF), with mild-to-moderate nuclear heteromorphism (Figure 1D).

### Immunohistochemical findings

The tumor cells were stained positive for CD34, P16, SMARCA4, and INI1 and scattered weak-positive for CCND1. S-100, estrogen receptor (ER), progesterone receptor (PR), desmin, caldesmon, SMA, CD10, BCOR, ALK, TRK, Melan-A, HMB-45, NSE, and CD99 were stained negative. P53 was stained as wild type, and Ki-67 was expressed in 30% of tumor cells (Figures 1E–L).

### Molecular findings

Illumina NextSeq RNA sequencing was adopted, which covered all exons including 632 genes, and special attention was focused on 148 genes (listed in the Supplementary Material), and *COL1A1* (NM_000088.3: Exon45)–*PDGFB* (NM_002608.2: Exon2) gene fusion was detected in this case (Figure 2).

## Discussion

In 2019, Croce recommended that uterine spindle cell sarcomas could be divided into three categories: *NTRK* fusion group, *COL1A1–PDGFB* fusion group, and a group that was tentatively classified as malignant peripheral nerve sheath tumor as positively stained with S100 and contained neither of the molecular abnormalities above (10), a category that excluded leiomyosarcoma (LMS) and high-grade endometrial stromal sarcoma (HGESS). Identification of gene fusion-associated sarcomas is extremely important, as patients can potentially benefit from specific targeted treatments. The first drug that targeted *NTRK* gene fusion-positive tumors and received approval from the Food and Drug Administration (FDA) was larotrectinib in 2018, which had an overall response rate (ORR) of 75% (95% CI: 61–85%, independent review) in a pooled analysis of three phase I and II single-arm trials of 55 combined pediatric and adult patients (16). An updated pooled analysis from three phase I and II clinical trials of larotrectinib (NCT02122913, TNCT02637687, and

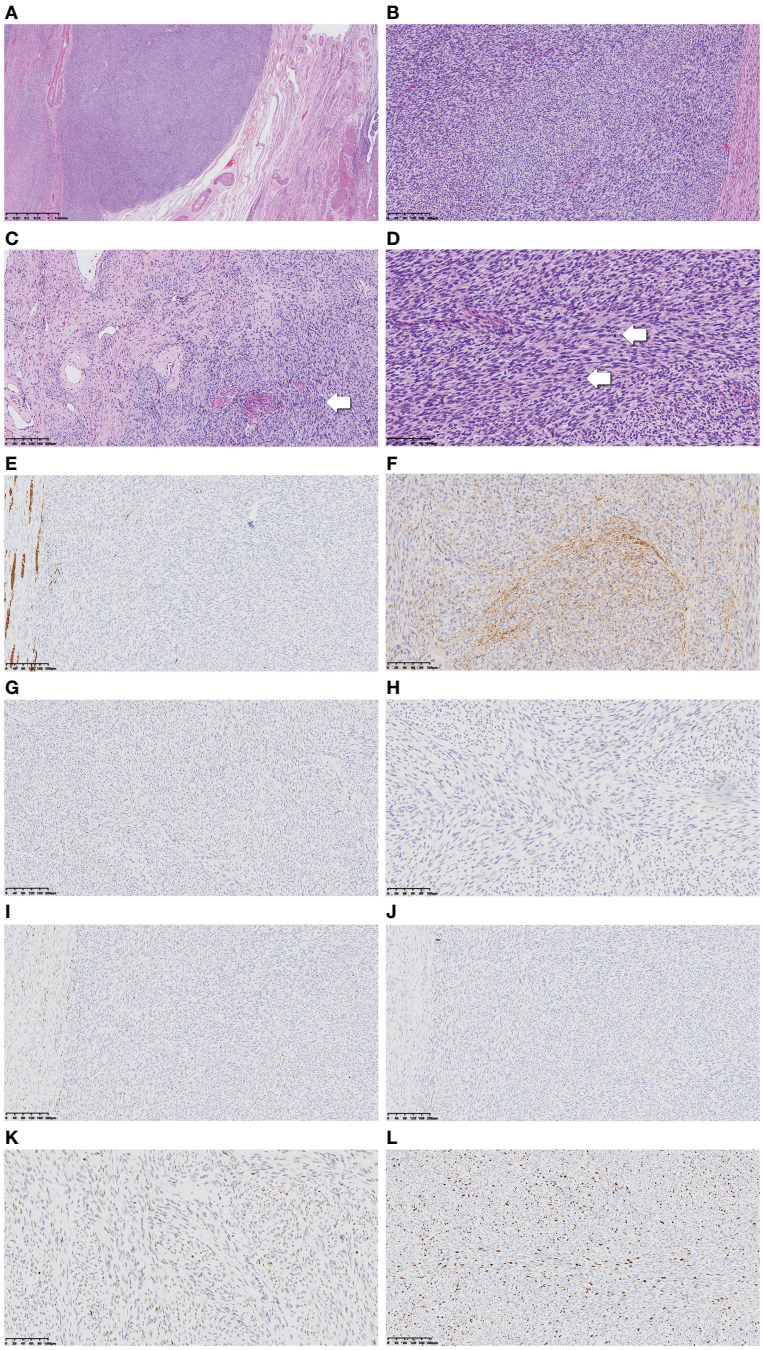


FIGURE 1
Low-power view of the tumor revealed relatively clear boundary (**A**, ×40). Tumor cells were arranged in a more prominent storiform or herringbone pattern in the cellular view (**B**, ×100), whereas in the cell-sparse area, more dilated small blood vessels can be seen. Normal cervical fibromuscular tissue not invaded by the tumor as pointed by the arrow (**C**, ×100). Tumor nuclei in oval to spindle shape are shown in high-power view, and the cytoplasm appears sparse and eosinophilic. The nuclear heteromorphism appears mild to moderate, while mitoses are numerous and obvious (arrow) (**D**, ×200). Immunohistochemical results including desmin, CD34, TRK, S100, ER, PR, and P53 are displayed (**E–K**, ×200). The Ki-67 proliferation index was high (**L**, ×200).

NCT02576431) resulted in an ORR of 75% (95% CI: 68–81%) based on an investigator review of 206 patients evaluable for response (17). In 2019, entrectinib was also approved, and a pooled analysis of three phase I and II studies showed an ORR of 57% (95% CI: 43–71%, independent review) in 54 adult patients (18). As ORRs for larotrectinib and entrectinib were averaged across different tumor types, the underlying assumption was that the efficacy or effectiveness was the same regardless of histology. As for uterine cancer, the National Comprehensive Cancer Network (NCCN) Clinical Practice Guidelines in Uterine Neoplasms (NCCN Guidelines®) explicitly recommended trying either larotrectinib or entrectinib for *NTRK 1/2/3* fusion-positive uterine sarcoma (19). Imatinib was first approved by the FDA for the treatment of patients with soft tissue tumors bearing *COL1A1–PDGFB* fusion in

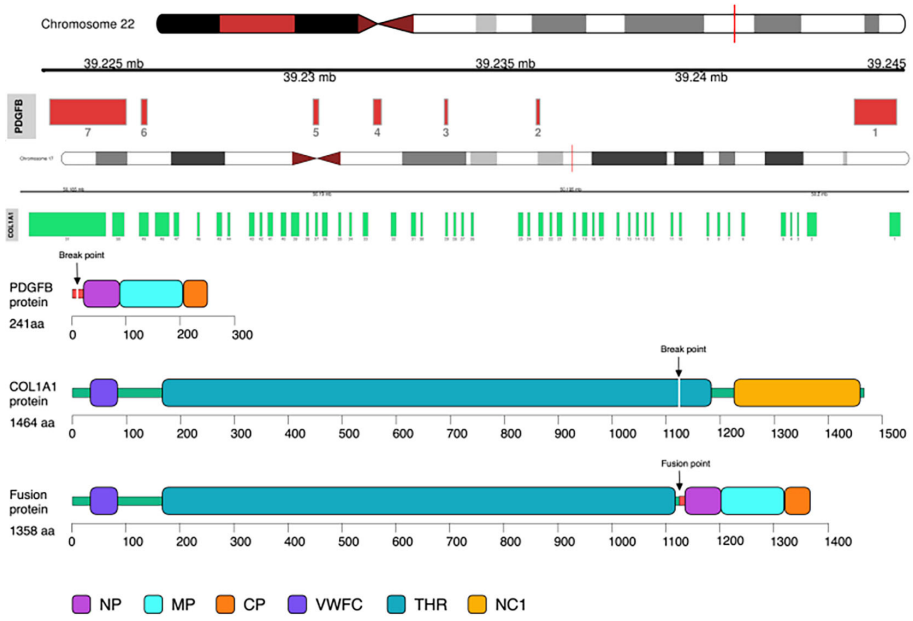


FIGURE 2
*COL1A1–PDGFB* gene fusion was detected by RNA sequencing. Note the unbalanced breakpoints (arrows) on CH17q (*COL1A1*) and 22q (*PDGFB*).

2006 and, according to a recent systematic review, was associated with objective responses in more than 60% of advanced cases (20).

*COL1A1–PDGFB* fusion uterine sarcomas were often reported to be asymptomatic. Patient 4 was noticed to have a palpable mass on physical examination, and the tumor grew rapidly during follow-up. The patient in the fifth case came with vaginal bleeding and lower abdominal pain. A cervical mass was found on vaginal examination. The fourth case described that the tumor had a pink–tan–white whorled appearance with areas of necrosis. Our case shared a similar gross appearance, with no obvious necrotic area. Interestingly, our case had a relatively clear boundary and mainly invaded in an expansive manner, compressing on surrounding normal tissue, while local infiltration was seen. Further comparisons between our case and patients reported previously are discussed in detail in Table 2 (10–12).

In our case, the uterine sarcoma displayed relatively uniform spindle cells with elongated nuclei, uniform chromatin, sparse cytoplasm, and poorly defined cell boundaries. The nuclei were mildly anomalous, and mitoses were relatively active with up to 30 per 10 HPF, which looked like dermatofibrosarcoma protuberans (DFSP). Previous studies (3, 21, 22) suggested DFSP is a relatively inert, low-to-moderate-malignant soft tissue tumor of the dermis. The morphological feature was poorly defined nodular masses infiltrating subcutaneous or skeletal muscle. The morphology is usually presented with a uniform arrangement of spindle-shaped cell bundles in a typical storiform pattern. Particular attention should be paid to the presence of fibrosarcomatous change or other high-risk features, and CD34 is often highly and diffusely expressed in the cytoplasm. Both histomorphologic manifestations and IHC staining of CD34 overlap with *COL1A1–PDGFB* fusion uterine sarcomas. DFSP has a characteristic molecular feature of t (17;22) (q22; q13), and therefore, *COL1A1–PDGFB* fusion could be detected in more than 90% of DFSP cases. For DFSP without *COL1A1–PDGFB* fusion, the molecular assay showed multiple gene translocations, *P53* mutation or overexpression, or *murine double minute 2* (*MDM2*) overexpression. The most common sites of DFSP were the torso of the body and extremities, and in rare cases, it could also occur at the head and neck, while DFSP in the female genital tract was only reported in the vulvar region. Therefore, although some scholars prefer to refer to uterine tumors bearing *COL1A1–PDGFB* fusion as dermatofibrosarcoma in the uterus (considering the morphologic and IHC similarity), the nomenclature of uterine sarcoma with *COL1A1–PDGFB* fusion seems more appropriate.

In a pathological setting, leiomyoma, LMS, HGESS, and undifferentiated uterine sarcoma should be considered as the main differential diagnosis of *COL1A1–PDGFB* fusion uterine sarcomas, and *NTRK* fusion uterine sarcoma should be the most challenging one to be differentiated (23–25). *NTRK* fusion uterine sarcoma was first reported in 2011 (24, 26) and mainly occurred in young women, with an age range of 23–60 years (average 35 years). The lesions were mostly located at the cervix instead of the corpus, which is the same for *COL1A1–PDGFB* fusion uterine sarcomas. The morphology usually presented with fibrosarcoma-like spindle cells arranged in a storiform or fishbone pattern. Other features such as vascular hyalinosis and hemangiopericytoma-like changes, vascular infiltration, and significant inflammatory cell infiltration are rarely seen in *COL1A1–PDGFB* fusion uterine sarcomas. IHC markers could be critical clues for diagnosis; usually, TRK, S100, and CD34 were stained positive, with markers of smooth muscle (desmin and caldesmon) and hormone receptors (ER and PR) stained negative for *NTRK* fusion uterine sarcoma. However, the absence or weak expression of TRK cannot rule out the *NTRK* fusion uterine sarcoma due to the poor sensitivity and specificity of

TABLE 2 Clinicopathological findings of *COL1A1–PDGFB* fusion uterine sarcoma in this case and comparison with previous cases in the literature.

| Author and Year | Case Number | Age (years) | Tumor size (cm) | Tumor location | Clinical signs and symptoms | Clinical staging | Follow-up time (months) | Macroscopic appearance | Nuclear atypia | Mitotic figures (per/ 10HPF) | Tumor Border | Necrosis | Molecular detection method |
|---|---|---|---|---|---|---|---|---|---|---|---|---|---|
| SabrinaCroce 201910 | 1<br>2<br>3 | 82<br>60<br>48 | 8.2<br>5.8<br>12 | Cervical<br>Cervical<br>Corpus | Not available | IB<br>IIIB<br>IB | 10ms NED<br>60ms DOD<br>NA | NA | Mild<br>Moderate<br>Mild | 8<br>20<br>20 | Infiltrating<br>Infiltrating<br>NE | YES<br>NO<br>NO | Array-CGH genomic profile and FISH dual fusion |
| Samuel L 2020 11 | 4 | 43 | 12 | Corpus | Physical examination accidentally found | IVA | 34ms DOD | Pink-tan, white whorled | mild | 45 | Infiltrating | YES | Gene fusion study (RNA sequencing) |
| Adriana Hogeboom 2022 12 | 5 | 50 | 12 | Posterior uterine isthmus extending towards the cervix | Metrorrhagia and lower abdominal pain | IB | 2ms NED | Firm, multinodular with white whorled | Moderate | 54 | Predominant expansile growth | YES | FISH |
| This study | 6 | 57 | 5.5 | Cervical | Irregular vaginal bleeding | IB | 6ms NED | Firm, White whorled | Mild to moderate | 30 | Infiltrating | NO | Gene fusion study (RNA sequencing) |

NED, no evidence of disease; DOD, died of disease; NA, not available; NE, not evaluable; CGH, comparative genomic hybridization; FISH, fluorescence in situ hybridization; HPF, high-power field.



10.3389/fonc.2023.1108586

IHC staining of TRK, which should be verified by molecular testing if necessary. Of cases of *NTRK* fusion uterine sarcomas, 90% were found to be confined to the uterus at the time of initial clinical evaluation and were potentially responsive to anticancer therapy (27). Boyle and Rabban reported four cases of uterine sarcoma with *NTRK* fusion presented as rare cervical polypoid masses, which could be easily confused with adenosarcoma with stromal overgrowth. However, adenosarcoma usually presented with negative S100 and TRK on IHC, and molecular detection without *NTRK* rearrangement should be the gold standard to facilitate differentiation (28, 29). Similar to *COL1A1–PDGFB* fusion uterine sarcomas, both were more common in the cervix and shared similar morphological manifestations. However, the age onset of *COL1A1–PDGFB* fusion uterine sarcomas was older, ranging from 43 to 82 years (average at 56.7 years, median at 53.5 years). IHC features usually provided more clues for differential diagnosis, as CD34 was usually stained remarkably positive, while TRK, S100, myogenic markers, and hormone receptors were often stained negative. Although in most cases IHC staining is a simple and cost-effective method to assist diagnosis, confirmatory FISH or gene sequencing is mandatory in cases that are hard to identify. Due to the rarity of this tumor, limited experience with clinical treatment and prognosis, and lack of knowledge about the effectiveness of targeted therapy, it was particularly critical to correctly identify the tumor as the first step.

Under a microscope, a relatively sparse area of tumor cells with rare mitoses inspected could also be confused with leiomyoma. However, IHC markers for smooth muscle differentiation (desmin, caldesmon, and SMA) stained negative could exclude benign leiomyoma. LMS usually displayed moderate-to-severe nuclear heteromorphism, active mitoses, and remarkable necrosis and stained positive for the markers of smooth muscle differentiation (23), which were inconsistent with *COL1A1–PDGFB* fusion uterine sarcomas. The tumor cells of HGESS were often smaller with irregular or tongue-like invasion into the myometrium, and CCND1 and BCOR were often positive on IHC. They usually presented with specific gene fusion of *YWHAE–NUTM2 A/B* fusion and *ZC3H7B–BCOR* fusion. Other mutations such as *EPC1*, *SUZ12*, *BRD8*, *PHF1*, *TPR*, *LMNA*, *TPM3*, *RBPMS*, *EML4*, and *STRN* were also reported (30–32).

The prognosis for *COL1A1–PDGFB* fusion uterine sarcomas does not seem optimistic so far, as two patients of the five cases reported before have died. Both of them were at advanced clinical stages IIIB and IVA. Our patient (case 6 in Table 2) did not show any recurrence or progression for the past 6 months. The rarity of *COL1A1–PDGFB* fusion uterine sarcomas occurring in the female genital tract and unspecific morphology, especially without molecular tests, resulted in frequent misdiagnosis. Misdiagnosis could be one of the main reasons for poor prognosis, as adequate adjuvant therapy was delayed or missed for these patients. Therefore, awareness is encouraged when morphology and IHC markers do not match, and assistance from molecular tests (especially RNA sequencing for gene fusion in sarcoma) is critical for precise diagnosis.

As the clinical signs and symptoms in patients with *COL1A1–PDGFB* fusion uterine sarcomas in the female genital tract were usually silent in early stages, two out of six patients were initially diagnosed at late stages (IIIB and IVA in cases 2 and 4) as shown in Table 2. These two patients died of the disease at 60 and 34 months on follow-up. In case 4, the lack of response to chemotherapy prompted genomic testing for potential targeted therapies. It was at that time the *COL1A1–PDGFB* fusion was identified. Treatment with imatinib was initiated and continued for 6 months. The effects lasted and achieved the peak at the 11-month follow-up, as the intrabdominal mass reduced in size from 22.4 to 6.5 cm. CT progression was noticed at the 14-month follow-up after initiation of imatinib, as multiple abdominal masses that previously decreased in size grew back rapidly. Further investigations of more targeted therapy at *COL1A1–PDGFB* fusion are urgently needed to improve prognosis. Routine physical examination and clinical identification with the coordination of gynecologists and radiologists are crucial to guarantee early diagnosis and prompt treatment.

As for the surgical approach, the risk of inadvertent dissemination of occult malignancies of presumed benign tissue must be considered, as *COL1A1–PDGFB* fusion uterine sarcomas could be judged as benign leiomyoma on imaging (33). Morcellation should be avoided or carefully performed under the protection of a specimen bag. Laparotomy, colpotomy, or laparoscopic hysterectomy with contained specimen extraction through the vagina is appropriate.

This study expands the clinicopathological features of *COL1A1–PDGFB* fusion uterine sarcomas of the cervix, adding the first Chinese case to the five reported cases and highlighting a potential pitfall in the morphological differential diagnosis with *NTRK* fusion uterine sarcoma, leiomyoma, LMS, HGESS, and undifferentiated uterine sarcoma. A lack of knowledge has been seldom discussed previously. The prognosis for *COL1A1–PDGFB* fusion uterine sarcomas does not seem optimistic so far, as the current clinical evidence, long-term follow-up of these patients, and more clinical analyses with bigger sample size are urgently needed to better study the prognosis of this particularly rare type of uterine sarcoma. More investigations are warranted to clarify the pathogenesis and development of this disease and help improve the prognosis.

## Conclusion

The new categorization of uterine spindle cell sarcomas in 2009 started a new era of pathological diagnosis depending on molecular features from classical morphology. With only five cases previously reported, we presented the sixth case of *COL1A1–PDGFB* fusion uterine sarcoma in the female genital tract. Its pathological morphology is easily confused with benign uterine leiomyoma. Moreover, other mesenchymal malignancies such as *NTRK* fusion uterine sarcoma, LMS, and HGESS also need to be differentiated. The assistance by immunohistochemistry and molecular detection is critical for precise pathological diagnosis of different categories of uterine sarcoma. Precise identification could allow patients to benefit from further treatment, especially targeted therapy such as imatinib.

## Data availability statement

The original contributions presented in the study are included in the article/Supplementary Material. Further inquiries can be directed to the corresponding authors.

## Ethics statement

Written informed consent was obtained for the publication of this case report.

## Author contributions

Author Contributions: Conceptualization, YN and YS. Methodology, YN and LL. Software, LL. Clinical resources, YN and LL. Lab work, SW, FZ and LL. Writing—original draft preparation, YS and LL. Writing—review and editing, YN and YS. Visualization, HS and FM. Supervision, YN and YS. All authors contributed to the article and approved the submitted version.

## Conflict of interest

The authors declare that the research was conducted in the absence of any commercial or financial relationships that could be construed as a potential conflict of interest.

## Publisher's note

All claims expressed in this article are solely those of the authors and do not necessarily represent those of their affiliated organizations, or those of the publisher, the editors and the reviewers. Any product that may be evaluated in this article, or claim that may be made by its manufacturer, is not guaranteed or endorsed by the publisher.

## Supplementary material

The Supplementary Material for this article can be found online at: https://www.frontiersin.org/articles/10.3389/fonc.2023.1108586/full#supplementary-material

SUPPLEMENTARY INFORMATION OF GENES COVERED BY THE SARCOMA GENE PANEL

*AKT2, AKT3, ALK, AR, AXL, BCL2, BCOR, BCR, BRAF, BRCA1, BRCA2, BRD4, CD74, CDK12, CDKN2A, CIC, CTNNB1, DDR2, EGFR, ERBB2, ERBB4, ERG, ESR1, ETV1, ETV6, FGFR1, FGFR2, FGFR3, FGR, FLT3, FOXO1, GLI1, JAK2, JAK3, KIT, KMT2A, KRAS, MDM4, MET, MSH2, MYC, NF1, NOTCH1, NOTCH2, NRG1, NTRK1, NTRK2, NTRK3, PDGFB, PDGFRA, PDGFRB, PIK3CA, PPARG, PTEN, RAD51B, RAF1, RARA, RB1, RET, ROS1, SMARCB1, STK11, TERT, TFE3, TMPRSS2, WT1, ETV4, ETV5, EWSR1, MYB, NUTM1, EZR, SLC34A2, SDC4, ACTB, ATF1, CAMTA1, COL1A1, COL1A2, CREB3L1, CREB3L2, CSF1, DNAJB1, FEV, FLI1, FUS, JAZF1, LPP, MGEA5, NAB2, NCOA2, NOTCH4, NR4A3, PHF1, PLAG1, PRKACA, RANBP2, RELA, RIPK4, RPS6KB2, SS18, SSX1, USP6, YWHAE, HMGA2, TAF15, TFG, CCNB3, EPC1, MEAF6, MKL2, STAT6, TCF12, NUP214, PRKACB, PRKCA, TACC3, DDIT3, SLC45A3, NCOA1, EIF3E, RSP02, PAX8, MAML2, PAX3, PAX7, PTPRK, RSPO3, NUP107, PBX1, C110RF95, COL6A3, MAML3, MYBL1, PLK2, PRDM10, PRKCB, TFEB, TRIO, VGLL2, GRB7, MAST1, MAST2, BRD3, CDH11, ESRP1, MYH9, YAP1.*

SUPPLEMENTARY FIGURE 1

Pelvic MRI showed that an oval mass protruding from the cervix to the vagina and compressed on the anterior bladder with a slightly higher signal **(A)**. The mass was significantly enhanced, remarkably higher than that of the uterus post-enhancement **(B)**.

SUPPLEMENTARY FIGURE 2

On gross examination of the specimen, the tumor was mainly located on anterior lip of the cervix, growing in a pushing manner toward the vagina. The cross-section of the mass was firm and white-whorled with relatively clear boundary.

## References

1. Momeni-Boroujeni A, Chiang S. Uterine mesenchymal tumours: recent advances. *Histopathology* (2020) 76(1):64–75. doi: 10.1111/his.14008

2. Chiang S, Oliva E. Recent developments in uterine mesenchymal neoplasms. *Histopathology* (2013) 62(1):124–37. doi: 10.1111/his.12048

3. Thway K, Noujaim J, Jones RL, Fisher C. Dermatofibrosarcoma protuberans: pathology, genetics, and potential therapeutic strategies. *Ann Diagn Pathol* (2016) 25:64–71. doi: 10.1016/j.anndiagpath.2016.09.013

4. Simon MP, Navarro M, Roux D, Pouysségur J. Structural and functional analysis of a chimeric protein COL1A1-PDGFB generated by the translocation t(17;22) (q22;q13.1) in dermatofibrosarcoma protuberans (DP). *Oncogene* (2001) 20(23):2965–75. doi: 10.1038/sj.onc.1204426

5. Takahira T, Oda Y, Tamiya S, Higaki K, Yamamoto H, Kobayashi C, et al. Detection of COL1A1-PDGFB fusion transcripts and PDGFB/PDGFRB mRNA expression in dermatofibrosarcoma protuberans. *Mod Pathol* (2007) 20(6):668–75. doi: 10.1038/modpathol.3800783

6. Pedeutour F, Simon MP, Minoletti F, Barcelo G, Terrier-Lacombe MJ, Combemale P, et al. Translocation, t(17;22) (q22;q13), in dermatofibrosarcoma protuberans: A new tumor-associated chromosome rearrangement. *Cytogenet Cell Genet* (1996) 72(2-3):171–4. doi: 10.1159/000134178

7. Simon MP, Pedeutour F, Sirvent N, Grosgeorge J, Minoletti F, Coindre JM, et al. Deregulation of the platelet-derived growth factor b-chain gene *via* fusion with collagen gene COL1A1 in dermatofibrosarcoma protuberans and giant-cell fibroblastoma. *Nat Genet* (1997) 15(1):95–8. doi: 10.1038/ng0197-95

8. Karanian M, Pérot G, Coindre JM, Chibon F, Pedeutour F, Neuville A. Fluorescence *in situ* hybridization analysis is a helpful test for the diagnosis of dermatofibrosarcoma protuberans. *Mod Pathol* (2015) 28(2):230–7. doi: 10.1038/modpathol.2014.97

9. Maire G, Martin L, Michalak-Provost S, Gattas GJ, Turc-Carel C, Lorette G, et al. Fusion of COL1A1 exon 29 with PDGFB exon 2 in a der(22)t(17;22) in a pediatric giant cell fibroblastoma with a pigmented bednar tumor component. evidence for age-related chromosomal pattern in dermatofibrosarcoma protuberans and related tumors. *Cancer Genet Cytogenet* (2002) 134(2):156–61.

10. Croce S, Hostein I, Longacre TA, Mills AM, Pérot G, Devouassoux-Shisheboran M, et al. Uterine and vaginal sarcomas resembling fibrosarcoma: a clinicopathological and molecular analysis of 13 cases showing common NTRK-rearrangements and the description of a COL1A1-PDGFB fusion novel to uterine neoplasms. *Mod Pathol* (2019) 32(7):1008–22. doi: 10.1038/s41379-018-0184-6

11. Grindstaff SL, DiSilvestro J, Hansen K, DiSilvestro P, Sung CJ, Quddus MR. COL1A1-PDGFB fusion uterine fibrosarcoma: A case report with treatment implication. *Gynecol Oncol Rep* (2020) 31:100523. doi: 10.1016/j.gore.2019.100523

12. Hogeboom A, Bárcena C, Parrilla-Rubio L, Revilla E, Ruano Y, Gallego-Gutiérrez I, et al. A case of COL1A1-PDGFB fusion uterine sarcoma. *Int J Gynecol Pathol* (2022) 42(2):147–50. doi: 10.1097/PGP.0000000000000875

13. Ren H, Li Y, Yao Q, Lv H, Tang S, Zhou X, et al. Epithelioid leiomyosarcoma of broad ligament harboring PGR-NR4A3 and UBR5-PGR gene fusions: a unique case report. *Virchows Arch* (2022) 480(4):933–8. doi: 10.1007/s00428-021-03169-4

14. Cloutier JM, Allard G, Bean GR, Hornick JL, Charville GW. PDGFB RNA *in situ* hybridization for the diagnosis of dermatofibrosarcoma protuberans. *Mod Pathol* (2021) 34(8):1521–9. doi: 10.1038/s41379-021-00800-2

15. Zhu R, Yan J, Li B, Tan F, Yan W, Shen J, et al. Determination of COL1A1-PDGFB breakpoints by next-generation sequencing in the molecular diagnosis of dermatofibrosarcoma protuberans. *Exp Mol Pathol* (2021) 122:104672. doi: 10.1016/j.yexmp.2021.104672

16. Hong DS, DuBois SG, Kummar S, Farago AF, Albert CM, Rohrberg KS, et al. Larotrectinib in patients with TRK fusion-positive solid tumours: a pooled analysis of three phase 1/2 clinical trials. *Lancet Oncol* (2020) 21(4):531–40. doi: 10.1016/S1470-2045(19)30856-3

17. Doebele RC, Drilon A, Paz-Ares L, Siena S, Shaw AT, Farago AF, et al. Entrectinib in patients with advanced or metastatic NTRK fusion-positive solid tumours: integrated analysis of three phase 1–2 trials. *Lancet Oncol* (2020) 21 (2):271–82. doi: 10.1016/S1470-2045(19)30691-6

18. Cocco E, Scaltriti M, Drilon A. NTRK fusion-positive cancers and TRK inhibitor therapy. *Nat Rev Clin Oncol* (2018) 15(12):731–47. doi: 10.1038/s41571-018-0113-0

19. Abu-Rustum NR, Yashar CM, Bradley K, Campos SM, Chino J, Chon HS, et al. NCCN guidelines® insights: Uterine neoplasms, version 3.2021. *J Natl Compr Canc Netw* (2021) 19(8):888–95. doi: 10.6004/jnccn.2021.0038

20. Navarrete-Dechent C, Mori S, Barker CA, Dickson MA, Nehal KS. Imatinib treatment for locally advanced or metastatic dermatofibrosarcoma protuberans: a systematic review. *JAMA Dermatol* (2019) 155(3):361–9. doi: 10.1001/jamadermatol.2018.4940

21. Allen A, Ahn C, Sangueza OP. Dermatofibrosarcoma protuberans. *Dermatol Clin* (2019) 37(4):483–8. doi: 10.1016/j.det.2019.05.006

22. Hao X, Billings SD, Wu F, Stultz TW, Procop GW, Mirkin G, et al. Dermatofibrosarcoma protuberans: Update on the diagnosis and treatment. *J Clin Med* (2020) 9(6):1752. doi: 10.3390/jcm9061752

23. Chiang S, Cotzia P, Hyman DM, Drilon A, Tap WD, Zhang L, et al. NTRK fusions define a novel uterine sarcoma subtype with features of fibrosarcoma. *Am J Surg Pathol* (2018) 42(6):791–8. doi: 10.1097/PAS.0000000000001055

24. Croce S, Hostein I, McCluggage WG. NTRK and other recently described kinase fusion positive uterine sarcomas: A review of a group of rare neoplasms. *Genes Chromosomes Cancer* (2021) 60(3):147–59. doi: 10.1002/gcc.22910

25. Markl B, Hirschbuhl K, Dhillon C. NTRK-fusions - a new kid on the block. *Pathol Res Pract* (2019) 215(10):152572. doi: 10.1016/j.prp.2019.152572

26. Mills AM, Karamchandani JR, Vogel H, Longacre TA. Endocervical fibroblastic malignant peripheral nerve sheath tumor (neurofibrosarcoma): report of a novel entity possibly related to endocervical CD34 fibrocytes. *Am J Surg Pathol* (2011) 35(3):404–12. doi: 10.1097/PAS.0b013e318208f72e

27. Chiang S. S100 and pan-trk staining to report NTRK fusion-positive uterine sarcoma: Proceedings of the ISGyP companion society session at the 2020 USCAP annual meeting. *Int J Gynecol Pathol* (2021) 40(1):24–7. doi: 10.1097/PGP.0000000000000702

28. Boyle W, Williams A, Sundar S, Yap J, Taniere P, Rehal P, et al. TMP3-NTRK1 rearranged uterine sarcoma: A case report. *Case Rep Womens Health* (2020) 28:e00246. doi: 10.1016/j.crwh.2020.e00246

29. Rabban JT, Devine WP, Sangoi AR, Poder L, Alvarez E, Davis JL, et al. NTRK fusion cervical sarcoma: a report of three cases, emphasising morphological and immunohistochemical distinction from other uterine sarcomas, including adenosarcoma. *Histopathology* (2020) 77(1):100–11. doi: 10.1111/his.14069

30. Kim Y, Kim D, Jung Sung W, Hong J. High-grade endometrial stromal sarcoma: Molecular alterations and potential immunotherapeutic strategies. *Front Immunol* (2022) 13:837004. doi: 10.3389/fimmu.2022.837004

31. Hoang L, Chiang S, Lee CH. Endometrial stromal sarcomas and related neoplasms: new developments and diagnostic considerations. *Pathology* (2018) 50 (2):162–77. doi: 10.1016/j.pathol.2017.11.086

32. Chiang S, Lee CH, Stewart CJR, Oliva E, Hoang LN, Ali RH, et al. BCOR is a robust diagnostic immunohistochemical marker of genetically diverse high-grade endometrial stromal sarcoma, including tumors exhibiting variant morphology. *Mod Pathol* (2017) 30(9):1251–61. doi: 10.1038/modpathol.2017.42

33. Mercorio A, Della Corte L, Vetrella M, Russo M, Serafino P, Palumbo M, et al. Uterine fibroids morcellation: a puzzle topic. *Minim Invasive Ther Allied Technol* (2022) 31(7):1008–16. doi: 10.1080/13645706.2022.2095872

frontiers | Frontiers in Oncology

TYPE Review
PUBLISHED 17 March 2023
DOI 10.3389/fonc.2023.1138142



OPEN ACCESS

EDITED BY
Umberto Malapelle,
University of Naples Federico II, Italy

REVIEWED BY
Kanagaraj Palaniyandi,
SRM Institute of Science and Technology, India
Sapna Deo,
University of Miami, United States

*CORRESPONDENCE
Lianwen Zheng
davezheng@sohu.com

SPECIALTY SECTION
This article was submitted to Gynecological Oncology, a section of the journal Frontiers in Oncology

RECEIVED 05 January 2023
ACCEPTED 06 March 2023
PUBLISHED 17 March 2023

CITATION
Wang M, Fu L, Xu Y, Ma S, Zhang X and Zheng L (2023) A comprehensive overview of exosome lncRNAs: Emerging biomarkers and potential therapeutics in gynecological cancers.
*Front. Oncol.* 13:1138142.
doi: 10.3389/fonc.2023.1138142



# A comprehensive overview of exosome lncRNAs: Emerging biomarkers and potential therapeutics in gynecological cancers

Min Wang, Lulu Fu, Ying Xu, Shuai Ma, Xueying Zhang and Lianwen Zheng*

Reproductive Medical Center, Department of Obstetrics and Gynecology, The Second Hospital of Jilin University, Changchun, China

Ovarian, endometrial, and cervical cancer are common gynecologic malignancies, and their incidence is increasing year after year, with a younger patient population at risk. An exosome is a tiny "teacup-like" blister that can be secreted by most cells, is highly concentrated and easily enriched in body fluids, and contains a large number of lncRNAs carrying some biological and genetic information that can be stable for a long time and is not affected by ribonuclease catalytic activity. As a cell communication tool, exosome lncRNA has the advantages of high efficiency and high targeting. Changes in serum exosome lncRNA expression in cancer patients can accurately reflect the malignant biological behavior of cancer cells. Exosome lncRNA has been shown in studies to have broad application prospects in cancer diagnosis, monitoring cancer recurrence or progression, cancer treatment, and prognosis. The purpose of this paper is to provide a reference for clinical research on the pathogenesis, diagnosis, and treatment of gynecologic malignant tumors by reviewing the role of exosome lncRNA in gynecologic cancers and related molecular mechanisms.

KEYWORDS

**exosome lncRNA, expression, biomarkers, therapeutics, gynecological cancers**

## 1 Introduction

An exosome is a cell-secreted nanoscale vesicle containing DNA, proteins, lipids, RNA, metabolites, cytokines, transcription factor receptors, and other biologically active substances (1). Its composition is similar to that of parental cells and can be used as a "fingerprint" to identify relevant cells and provide specific signals that can be traced in circulating blood (2). The composition is similar to that of parental cells and can be used to identify relevant cells by providing specific signals that can be traced in circulating blood.

Long noncoding RNAs (lncRNAs) are noncoding RNAs that are abundant in the cytoplasm and nucleus (3). They do not have protein-coding functions, but they can influence cancer development in a variety of ways and can be specifically sorted into the exosome (4). Despite the presence of RNA enzymes in the blood, lncRNAs can persist due to exosome protection (5, 6). Tumor-derived exosomes (TDE) lncRNAs can contribute to cancer progression in a variety of ways by altering the tumor microenvironment, the epithelial-mesenchymal transition (EMT), and angiogenesis, as well as playing a role in cancer growth maintenance and stabilization. Because cancer invasion, metastasis, treatment, and drug resistance are all intertwined, it is of great scientific importance to mine and explores the exosome lncRNAs that affect malignant biological behavior, as this can help to further investigate the mechanism of cancer development and provide new ideas and strategies for cancer treatment (7, 8).

# 2 Overview of the exosome

## 2.1 Discovery and distribution of exosome

Exosomes were discovered by Johnstone et al. in the study of extracellular cytoplasmic fusion of reticulocyte multivesicular bodies (9), are 30-150 nm in diameter (10), have a phospholipid bilayer structure, and belong to the extracellular vesicle family. Exosomes released from cells into the extracellular compartment are found in a variety of body fluids, including saliva, breast milk, blood, urine, amniotic fluid, and vaginal/alveolar lavage fluid (11). The endosomal sorting complex required for transport (ESCRT) is made up of the complexes ESCRT-0, I, II, and III, as well as co-proteins like apoptosis-linked gene 2-interacting protein X (ALIX) and vacuolar protein sorting 4 (VPS4). Several studies have confirmed the importance of ESCRT in exosome biosynthesis (12). Exosome production, on the other hand, is not entirely dependent on ESCRT mechanisms such as the ceramide mechanism. It was discovered that mouse oligodendrocytes secreted lipoprotein-carrying exosomes normally even after ESCRT inhibition and that cellular exosome secretion was reduced after ceramide synthesis inhibition, implying a regulatory role for ceramide in exosome synthesis. Exosomes are produced by cellular self-selection, and exosomes from different cells can carry different "cargo" (13). Under various physiological and pathological conditions, the same cell can produce multiple exosomes containing additional genetic information (14) (Figure 1).

## 2.2 Functions of exosome

Exosomes can create a pre-metastatic microenvironment suitable for cancer cell growth, regulate the glucose and lipid metabolism of target cells, counteract the body's immune defense, and promote and cooperate with cancer development by transferring lncRNA to recipient cells and mediating material transport and information exchange.

Exosome has been confirmed as a circulating biomarker for various breast, colorectal, and bladder cancers in numerous studies (15). On January 21, 2016, the first exosome-based cancer diagnostic product was launched in the United States (16). The exosome is a natural lipid vesicle that can be used as a gene therapy carrier and has significant development potential in the field of cancer therapy (17). Exosomes can cross the blood-brain barrier and transport drugs and genes (e.g., proteins, lipids, DNA, and RNA) into tissues, effectively preventing their degradation (18). The drugs could not penetrate the blood-brain barrier in the control group of zebrafish embryos treated with conventional drugs, but in the experimental group, in which the anti-cancer drugs adriamycin and paclitaxel were integrated into the exosome and then introduced into zebrafish embryos, large number of exosomes could penetrate the blood-brain barrier and allow the drugs to reach the cancer cells directly (19). In advanced cancers, clinical trials targeting dendritic cell-derived exosomes (DEX) have been conducted (20). Cancer exosomes are known to play an essential role in the distant compartment effect, a recently discovered mechanism that effectively targets cancers and inhibits distant metastasis (21); As a result, the exosome is expected to be a novel and efficient drug delivery system. Exosomes can be used for gene therapy by transfecting siRNA into the exosome and successfully silencing genes using the exosome as a vector, according to research (22).

# 3 Overview of lncRNAs

## 3.1 Biogenesis of lncRNAs

The noncoding region of the human genome contains approximately 88% of single nucleotide polymorphisms. Non-coding RNA is classified into two types based on its length: LncRNA and short-stranded noncoding RNA. LncRNA is a class of single-stranded RNA molecules with sizes less than 200 nt, the majority of which are found in the nucleus and some in the cytoplasm, and are classified as sense lncRNA, antisense lncRNA (AS lncRNA), bidirectional lncRNA, intronic lncRNA, and intergenic lncRNA (23). When compared to most protein-coding genes, lncRNAs have better cell specificity and relatively stable local secondary and tertiary structures, making them easier to detect in body fluids and capable of interacting with DNA, RNA, or proteins. They play an essential role in the physiological and pathological processes of the body (24). LncRNAs participate in a variety of biological pathways, including cell growth, by regulating gene transcription and post-translational expression. By regulating innate and adaptive immunity, lncRNAs can participate in a variety of immune pathways, and dysregulation of their expression levels can disrupt immune homeostasis. It is anticipated that it will be one of the most promising biomarkers for disease diagnosis and prognosis (25) (Figure 2).

## 3.2 LncRNAs are involved in gene expression

LncRNAs are important regulators at the epigenetic, transcriptional, and post-transcriptional levels (26). Epigenetic

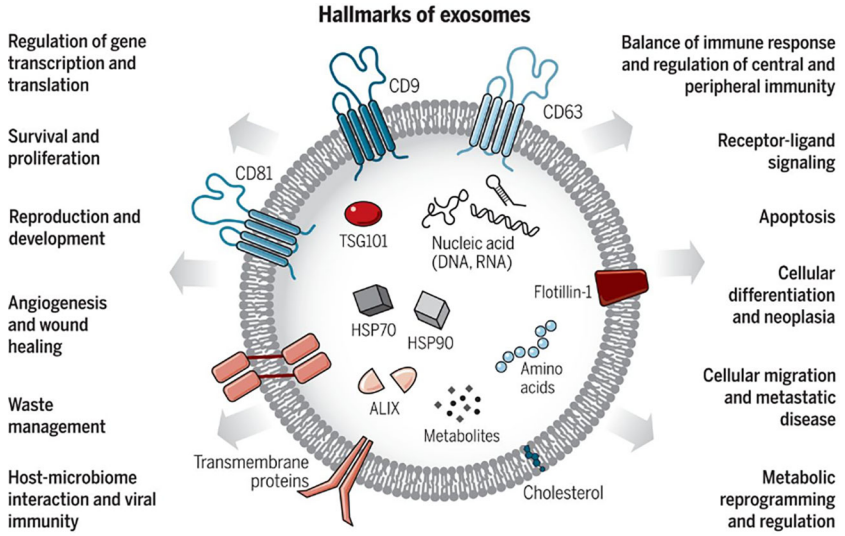


FIGURE 1
Exosomes: A cell-to-cell transit system in the human body with pleiotropic functions. Exosomes are extracellular vesicles generated by all cells and they carry nucleic acids, proteins, lipids, and metabolites. They are mediators of near and long-distance intercellular communication in health and disease and affect various aspects of cell biology (1).

silencing or activation of target genes: lncRNAs can regulate gene expression at the epigenetic level *via* DNA methylation, demethylation, histone modification, and chromosome remodeling (27). MEG3 expression was found to be significantly reduced in glioblastoma due to DNA methyltransferase I-mediated hypermethylation of the MEG3 promoter, which downregulated MEG3 expression in glioblastoma and inhibited p53 protein activation.

Transcriptional level: Long noncoding RNAs (lncRNAs) can interact with transcription factors, enhancers, and promoters to regulate RNA transcription, localization, and stability (28). The lncRNA Gas5 can compete with the glucocorticoid response element (GRE) for binding to the glucocorticoid receptor (GR), preventing GR transcriptional activation and resulting in an autoimmune response. In breast cancer, low Gas5 expression increased cancer cells' survival during starvation. P21-associated noncoding RNA with DNA damage activation (lncRNA PANDA) was found to promote osteosarcoma cell proliferation. Further research revealed that the lncRNA PANDA inhibited apoptosis in normal human fibroblasts by binding to transcription factors that prevented it from binding to apoptosis-related gene promoters. Long noncoding RNA homeobox (HOX) A11 antisense lncRNA (HOXA11-AS) was discovered to bind to transcription factor WD repeat domain 5 (WDR5) in the promoter region, promote -catenin transcription, and activate the Wingless-Type MMTV Integration Site Family (WNT) signaling pathway, accelerating cancer metastasis *in vivo*.

Post-transcriptionally, lncRNAs can form RNA dimers with target mRNAs *via* complementary base pairing, obstruct transcription factor binding, or directly recruit specific translation repressor proteins to regulate mRNA shearing, translation, and degradation (29). KLF4 is a transcriptional activator of vascular endothelial growth factor (VEGF). The lncRNA H19 can bind to miR-7, allowing miR-competitive endogenous RNA (ceRNA-7) to release translational repression of KLF4 and activate the KLF4/VEGF signaling pathway. Stable knockdown of exosome lncRNA H19 can significantly affect KLF4 and VEGF mRNA and protein expression levels, which affect the formation of the pre-metastatic microenvironment, inhibit cancer cell migration and invasion, and regulate the tumor microenvironment and vascular normalization. During the progression of hepatocellular carcinoma, the expression level of long noncoding RNA-activated by transforming growth factor beta (lncRNA-ATB) was increased and directly linked to IL-11, which altered IL-11 tertiary structure, increased the stability of IL-11 mRNA, induced IL-11 autocrine, triggered the signal transducer and activator of transcription 3 (STAT3) pathway, and promoted cancer metastasis and organ colonization. The first lncRNA with trans-activation, HOX transcript antisense RNA (HOTAIR), acts as a pro-oncogene in a variety of cancer cells, including breast cancer and hepatocellular carcinoma (30). HOTAIR, a lncRNA with sponge adsorption for miR-122, can regulate cancer cell epithelial-mesenchymal transition (31).

## 4 Exosome lncRNAs and tumor

The early and precise diagnosis of malignant cancers has become a hot research topic. Cancer occurrence and progression are dependent on the interaction between cancer cells and the tumor microenvironment. In addition to intercellular contact and the

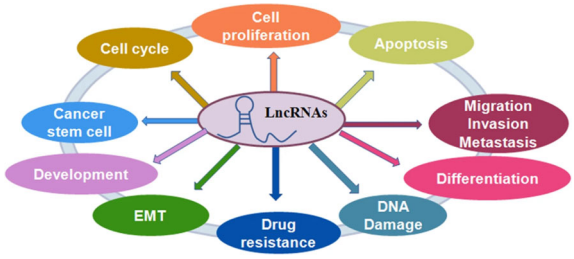


FIGURE 2
The role of lncRNAs in regulating cellular processes. LncRNAs play a critical role in the regulation of cell proliferation, cell apoptotic death, cell cycle, cell migration and invasion, epithelial-mesenchymal transition (EMT), cancer stem cells, DNA damage and drug resistance in cancer (25).

release of soluble factors, cancer cells can communicate with the tumor microenvironment *via* exosomes (32). The TDE transports molecules such as content DNA, miRNA, and lncRNA that reflect genetic or signaling changes originating in cancer cells (33). lncRNA enters the recipient cells *via* the exosome and acts as a signaling mediator to coordinate cellular functions among cancer cells, creating a microenvironment conducive to cancer cell metastasis at a distant site (34–36). In cancer progression, lncRNAs can serve two purposes. MALAT1 (metastasis-associated lung adenocarcinoma transcript1) can promote or inhibit breast cancer metastasis by activating or inactivating neighboring prometastatic transcription factors (37). DEAD-box RNA helicase 3 (DDX3) also plays a dual role in the progression of lung cancer. On the one hand, DDX3 can activate the WNT signaling pathway, facilitating lung cancer metastasis. DDX3, on the other hand, can inhibit lung cancer progression by activating the MDM2/Slug/E-cadherin signaling pathway (38). The lncRNA HOTAIR can affect the co-localization and activity of vesicle-associated membrane protein 3 (VAMP3) and synaptosomal-associated protein 23 (SNAP23) to promote the fusion of MVB with the plasma membrane to promote HCC exosome secretion, confirming that lncRNAs have the function of promoting cancer exosome secretion and providing a new idea for the study of cancer lncRNAs (Figure 3).

## 4.1 Exosome lncRNAs and tumor microenvironment

The tumor microenvironment is made up of a variety of cells, including cancer cells and stromal cells like endothelial cells, fibroblasts, adipocytes, and mesenchymal stem cells (39). Tumorigenesis, progression, and metastasis are all affected by the characteristics of cancer cells as well as the interaction between cancer cells and stromal cells in the tumor microenvironment (40). The exosome, which is released into the extracellular environment *via* paracrine or autocrine signaling pathways and causes receptor cell-related phenotypic changes (27), is a critical communication mediator for primary tumor microenvironment alterations. Different exosome lncRNA sources play different roles (41). Cancer cells and tumor-associated macrophages (TAMs) may be important sources of exosomes in the tumor microenvironment (42). TDE, by remodeling the extracellular matrix (ECM) and inducing angiogenesis, creates a microenvironment favorable for cancer cell metastasis at distant sites (43). Cancer parenchymal cells use the exosome to transport biogenetic information to the extracellular space, transforming normal stromal cells and promoting cancer cell proliferation, apoptosis, migration, invasion, and prognosis (44, 45). Carcinoma-associated fibroblasts (CAFs), macrophages, and other cells secrete lncRNA-containing exosomes to promote cancer development and malignancy (46). LINC00092 was found to be significantly elevated in paraneoplastic fibroblasts in OC, along with elevated chemokine (C-X-C motif) ligand 14 (CXCL14), which was associated with metastasis and poor prognosis in OC (47).

## 4.2 Exosome lncRNA and tumor angiogenesis

The formation of neovascularization is an important environment for cancer genesis and development, and blood vessels provide sufficient oxygen and nutrients for cancer cell metastasis and growth (48). TDE can help with cancer angiogenesis and extracellular matrix remodeling by dynamically regulating different cells in the tumor microenvironment. The cancer vasculature is typically disorganized as a result of adjacent cancer cells compressing new blood vessels, resulting in tortuous and malformed vessels. Endothelial cells are loosely connected, and permeability and leakiness increase, allowing cancer cells to spread quickly into the vasculature and then develop distant metastases (49). As a result, anti-cancer cell angiogenesis will emerge as a novel therapeutic strategy. Cancer cells' exosome lncRNA can act on endothelial cells in the microenvironment to promote cancer angiogenesis. Exosomes secreted by cancer stem cells invade endothelial cells, deliver lncRNA H19 to their target cells, and stimulate HUVEC angiogenesis by synthesizing and releasing VEGF (50). In preparation for cancer growth and metastasis, glioma cells were found to promote angiogenesis by increasing the expression of endothelial cell pro-angiogenic factor VEGFA *via* exosome lncRNA CCAT and lncRNA HOTAIR (51). The exosome lncRNA Small nucleolar RNA host gene 16 (SNHG16)/miR-4500/N-acetylgalactosamine-transferase 1 (GALNT1) axis has been linked to tumor angiogenesis.

## 4.3 Exosome lncRNAs and tumor metastasis

Metastasis is a fundamental challenge in cancer therapy because cancer cells and the tumor microenvironment regulate cancer proliferation and metastasis (52). TDE lncRNAs can promote malignant growth by interacting with the microenvironment and cancer cells, resulting in increased cancer proliferation and metastasis (53). During rapid growth, cancer cells cause internal tissue hypoxia and promote upregulation of hypoxia-inducible factor (HIF-1) expression, stimulating cancer cells to secrete

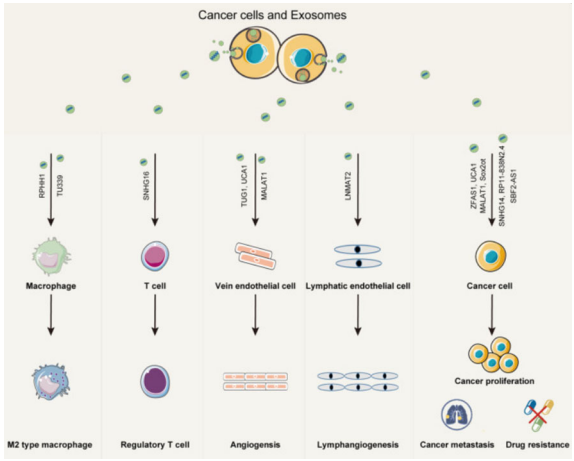


FIGURE 3
Exosomes play an important role in mediating the interaction between cancer cells and both immune cells and stromal cells within the cancer microenvironment. Exosomal lncRNAs from cancer cells can promote immune modulation, angiogenesis, cancer proliferation, metastasis, and drug resistance (35).

exosomes with enhanced angiogenic and metastatic potential and promoting cancer invasion and metastasis (54). According to studies, exosome lncRNA 91H is highly expressed in patients' serums with colorectal cancer and usually decreases after surgery. lncRNA 91H has been shown to promote cancer migration and invasion by regulating the expression of heterogeneous nuclear ribonucleoprotein K (HNRNPK) (55). HOTAIR, an exosome lncRNA, has been linked to bladder cancer progression, and knocking it out in uroepithelial bladder cancer cell lines inhibits EMT (56). MALAT1, an exosome-derived lncRNA that promotes cancer cell migration and prevents cancer cell apoptosis, was found to be positively related to the TNM stage and lymph node metastasis in NSCLC (57). It has been demonstrated that exosome-derived epidermal growth factor receptor (EGFR) protein in lung cancer cells induces the formation of tolerogenic dendritic cells (DCs), which in turn inhibits the anti-cancer effects of CD8+ T cells by inducing the production of regulatory T cells (Treg), and ultimately Treg promotes cancer immune escape (58). Elucidating the molecular mechanisms of cancer metastasis may lead to the development of more effective cancer therapeutic strategies (59).

## 4.4 Exosome lncRNA and cancer drug resistance

It is critical to investigate the specific mechanisms of innate or acquired drug resistance in cancer cells (60); Cancer cells and stromal cells in the tumor microenvironment can help spread cancer drug resistance by secreting exosomes (61). Exosomes can affect cell sensitivity to drugs *via* the following mechanisms (62). Exosomes directly wrap anti-cancer drugs, reducing their effectiveness. Exosomes transport bioactive molecules that compete for binding targets with anti-cancer drugs. Drug-resistant cells transmit drug-resistance information to sensitive cells *via* exosome-derived bioactive small molecules. Drug sensitivity information is transmitted from sensitive cells to drug-resistant cells *via* exosome-derived bioactive small molecules. Resistance to chemotherapeutic drugs could be improved by interfering with receptor cells with lncRNA, which could be a new therapeutic approach (63). lncRNA regulators of reprogramming (ROR) were found to be highly expressed in hepatocellular carcinoma cells (64). Drug resistance was found to be increased when hepatocellular carcinoma cells were treated with exosomes containing a high concentration of lncRNA ROR (65). Infection of lncRNA ROR in hepatocellular carcinoma cells with RNAi resulted in adriamycin sensitivity, and cancer cells may use exosomes and lncRNA to enhance drug resistance in nearby cells. Celastrol is thought to be therapeutic for a variety of cancers. When compared to free celastrol and celastrol exosome preparations, anti-cancer activity was significantly increased, with no liver or nephrotoxicity (66). Paclitaxel-resistant breast cancer cells can be induced by delivering the lncRNA SNHG15 to sensitive cells *via* exosomes. The exosome lncRNA KCNQ1OT1 is a critical molecule mediating radiotherapy resistance in lung cancer A549 cells. The use of CAFs as an entry point for reversing radiotherapy resistance in lung cancer cells provides a critical theoretical foundation. Investigating the effect of exosome lncRNAs on drug resistance will aid in elucidating the molecular mechanism of cancer drug resistance and provide new ideas for overcoming or reversing drug resistance (67).

# 5 Exosome lncRNA and gynecologic malignancies

## 5.1 Exosome lncRNA and ovarian cancer

Ovarian cancer (OC) is the most difficult to diagnose and has the worst prognosis of all malignant cancers of the female reproductive system, causing serious health problems in women (68). The pathogenesis of OC is complex, the early clinical symptoms are subtle, and the metastatic potential is high. When most patients are diagnosed, they are already in an advanced stage of the disease (69), so radical surgery cannot be used, the treatment effect is inadequate, and more than 70% of OC patients have a recurrence. The Food and Drug Administration (FDA) has approved only two biomarkers, CA125 and HE4, as diagnostic biomarkers for OC (70). CA125 is widely used in clinical settings, but it has some limitations (71). CA125, for example, is less sensitive in early-stage OC and can be elevated in pregnancy, pelvic inflammatory disease, endometriosis, and other conditions. In the presence of conditions such as acute and chronic renal insufficiency, HE4 can also indicate gynecological diseases and abnormal changes (72). As a result, a new reliable marker is required for the early detection of OC (73).

Exosome lncRNA can be used as a non-invasive diagnostic and screening tool, requiring only a small amount of fresh or frozen blood from OC patients and simultaneously analyzing for DNA,

RNA, and protein. Exosomes can be extracted from the urine and blood of OC patients using a human recombinant S100A8 protein aptamer bound to cell membrane HSP70 (74). CD24 was found in exosomes from malignant ascites and *in vitro* cancer cells. This marker has been used to predict the prognosis of OC, demonstrating the exosome's utility as a minimally invasive biopsy (75). Experiments with magnetic nanobeads revealed that many HER2-positive exosomes were found in the serum of OC patients (76). Chen et al. (77) discovered that CA125 levels were higher in exosomes than in serum, that serum exosome-derived CA125 improved the sensitivity of OC diagnosis, and that serum HE4 combined with exosome CA125 improved the diagnostic efficiency of OC. Zhang et al. (78) examined the circulating exosomes in the plasma of OC patients and identified seven biomarkers with diagnostic ability, including HER2, EGFR, Folate Receptor (FR), CA-125, Epithelial Cell Adhesion Molecule (EpCAM), CD24, and (CD9+CD63), and demonstrated that these exosome biomarkers not only distinguished OC patients from benign subjects but also differentiated early and advanced OC, indicating the MALAT1 is a long noncoding RNA that is involved in the angiogenesis and metastasis of OC. Sun et al. (79) discovered that the lncRNA MALAT1 plays an important role in the development of OC by mediating the Janus kinase 2 (JAK2)/STAT3 signaling pathway, promoting OC cell proliferation, and inhibiting cancer cell apoptosis. Jin et al. (80) discovered that the lncRNA MALAT1 could increase OC cell proliferation while inhibiting cancer cell apoptosis *via* the PI3K-protein kinase B (PKB, AKT) signaling pathway, enhancing OC cell invasion, migration, and EMT function. Some researchers discovered that the expression level of serum exosomes (81) was higher when testing the expression of serum exosome MALAT1. MALAT1 expression was significantly higher in epithelial OC patients than in controls, and it was associated with an advanced International Federation of Gynecology and Obstetrics (FIGO) stage, a high histological grade, and lymph node metastasis. Increased serum exosomeMALAT1 expression was associated with a progressive metastatic epithelial OC phenotype and a poor prognosis, suggesting that it could be used as a prognostic or predictive biomarker for epithelial OC. The HOXA transcript at the distal tip (HOTTIP), a homeobox lncRNA, is critical in the progression of OC. HOTTIP overexpression was found to increase IL-6 expression and secretion in OC cells. IL-6 activated the STAT3 pathway by binding to IL-6 receptors on the surface of neutrophils surrounding cancer cells, increasing the expression of PD-L1 on the surface of neutrophils, inhibiting T cell activity further, accelerating OC immune escape, and ultimately promoting cancer cell growth and metastasis (82). The lncRNA NEAT1 was found to be significantly overexpressed in ovarian cancer cells compared to normal human ovarian epithelial cells. Through sponge adsorption of miR-36, lncRNA NEAT1 may promote ovarian cancer cell proliferation by upregulating fibroblast growth factor (FGF) 9.

The use of exosomes for vaccine preparation is a novel approach in cancer immunotherapy. TDE has low immunogenicity, a low drug attrition rate, and easy tissue diffusion, making it suitable for use as a drug or gene carrier for targeting OC and as a cancer vaccine to inhibit cancer growth. The cytotoxicity of paclitaxel-loaded macrophage exosomes against drug-resistant P-gp transfected Manin-Darby canine kidney epithelial cells (MDCKMDR1) cell line was increased more than 50-fold, and the anti-cancer effect of the drug-loaded exosomes was demonstrated (83). Farrukh et al. (84) discovered that exosome delivery of anthocyanin had a strong therapeutic effect on both drug-sensitive and drug-resistant human ovarian cancer cells and that its therapeutic activity was synergistically enhanced when combined with cisplatin. The co-culture of the hypoxic OC cell line exosome (HEX) with cancer cells during cisplatin treatment improved cell survival, according to Kalpana et al. (85). Simultaneously, a known inhibitor, STAT3, inhibited exosome release. Exosome release and cisplatin treatment increased apoptosis, indicating that HEX can promote OC metastasis and increase chemoresistance, and could be a new mechanism for cancer metastasis and chemoresistance, as well as a therapeutic intervention to improve clinical outcomes.

## 5.2 Exosome lncRNA and endometrial carcinoma

Endometrial carcinoma (EC) is one of the most common malignant cancers of the female reproductive system (86), accounting for 20%–30% of all malignancies of the female genital tract. In recent years, the incidence of EC has been increasing year after year, and the age of onset has gotten younger. EC can be diagnosed clinically based on symptoms such as vaginal bleeding or increased fluid discharge, but a definitive diagnosis requires further examination improvement. Fear of diagnostic scraping and hysteroscopy causes some patients to postpone their investigation, delaying the best time for diagnosis and treatment. Those who do not receive timely treatment at an early stage frequently have poor prognoses and survival rates. When the presence of lesions in the endometrium is determined through diagnostic scraping, the distribution of lesions cannot be accurately grasped, and small local lesions may be missed, increasing the rate of EC misdiagnosis. The clinical treatment of EC is primarily surgical, with the decision to combine radiotherapy based on high-risk factors. There are few adjuvant treatment options for advanced and recurrent cancers. As a result, identifying practical early diagnostic markers and precise therapeutic targets is critical.

Exosome lncRNA regulates EC proliferation and invasion primarily through angiogenesis, EMT, and immune regulation, among other things. Exosome lncRNA promotes the formation of a tumor microenvironment by transforming related cells, which not only speeds up normal cell proliferation but also changes the biological characteristics of nearby and distant non-cancer cells, allowing cancer cells to spread. Through related signaling pathways, some lncRNAs can effectively promote EC cell proliferation and enhance EC cell invasion, migration, and EMT function, thereby promoting cancer growth (87). Some lncRNAs, on the other hand, can effectively inhibit cancer cell proliferation, block the cell cycle process, and promote cancer cell apoptosis *via* related signaling pathways, which may be related to the composition of the tumor microenvironment, particularly CAFs (88).

MEG3 is a long noncoding RNA with anti-cancer properties (89). Reduced expression of MEG3, which inhibits cancer cell proliferation, migration, and invasion and promotes apoptosis, has been linked to cancer development and progression (90, 91). MEG3 activity is controlled by both TP53-dependent and TP53-independent mechanisms. The TP53 gene is mutated in the majority of human cancers, and it functions as a transcription factor, controlling the expression of many target genes and thus inhibiting cancer development and growth. The differential expression of TP53 in normal and cancerous tissues suggests that MEG3 could be used to assess cancer staging and prognosis (92). Guo et al. examined the expression of MEG3 and Notch signaling molecules in EC tissues and cell lines using real-time quantitative PCR and Western blotting. MEG3 expression was found to be significantly downregulated in EC tissues, whereas Notch protein expression was found to be upregulated in both. MEG3 downregulation inhibits EC proliferation by inhibiting the Notch signaling pathway (93). In EC patients, low expression of exosome lncRNA MEG3 in plasma predicts more high-risk factors, a higher recurrence rate, and a worse prognosis. By comparing the serum expression levels of lncRNA ROR and miR-29 in EC patients and healthy women and using ROC curves to assess the diagnostic value of both in EC, Serum lncRNA ROR and miR-29 levels were found to be significantly higher in EC patients than in healthy women. The expression levels in patients with TNM stages I–II increased dramatically, indicating the combined serum level (94). MALAT1 overexpression is associated with a poor prognosis for EC, implying that MALAT1 could be used as a novel biomarker and diagnostic target for EC (95).

The primary issue with cancer drug therapy is cancer drug resistance, particularly in recurrent cancers where acquired drug resistance renders the therapeutic effect ineffective. Exosome-mediated lncRNA communication in the tumor microenvironment has been shown in studies to be one of the reasons for increased drug resistance. It is possible to inhibit the production or uptake of an exosome-carrying "oncogene" and promote the production or uptake of an exosome-carrying "oncogene" based on the fact that exosomes can transport proteins and nucleic acids related to cancer invasion, metastasis, angiogenesis, and drug resistance. This opens up a new avenue for the future use of exosomes in the treatment of EC. The engineered exosome is more effective in targeting therapy than the original exosome, and it also reduces cytotoxicity and significantly inhibits tumor growth (96). Exosome lncRNAs play an important role in the development of EC, opening up new avenues for the early diagnosis and treatment of EC patients. They may also become an important tool in monitoring the progression and prognosis of EC in the future.

## 5.3 Exosome lncRNA and cervical cancer

Cervical cancer (CC) is one of the most common cancers in women. According to data, more than 500,000 people are diagnosed with CC each year, with the majority of deaths occurring in developing countries (97, 98). As a result, CC is a global public health issue that should not be underestimated (99). Despite the fact that chemotherapy combined with targeted therapy can improve overall survival (OS), progression-free survival (PFS), and cancer mortality in CC patients, cancer incidence continues to rise. The prognosis of advanced CC, which has a low local control rate and is prone to distant metastasis, is influenced by high-risk factors. The treatment effect is frequently poor, with only a 60% 5-year survival rate (100). As a result, improving early diagnosis of CC, identifying therapeutic targets, and investigating biomarkers that can indicate prognosis have emerged as top priorities in CC basic and clinical research (101).

Because of the impact of exosome LncRNA on the tumor microenvironment and its biological properties, it has the potential to become a cancer biomarker for CC patients, which has important clinical implications in cancer screening, treatment detection, and prognosis evaluation (102). Exosomes from HeLa cells in CC have been shown to promote distant metastasis by inducing endothelial cell endoplasmic reticulum stress and disrupting vascular endothelial cell integrity, thereby disrupting tight endothelial junctions (103). When CC HeLa cell exosomes were injected into mice, they found increased vascular permeability and cancer metastasis. The primary mechanism involved the CC HeLa cell exosome regulating the expression of closed junction proteins. Immunity against CC was improved in a mouse model of CC by increasing the cytotoxic activity of DEX-induced CD8+ T cells against cancer cells, prompting CD8+ T cell proliferation, and increasing IFN secretion (104).

HOXA11 is a recently discovered and researched lncRNA (105). HOXA11-AS has been shown in studies to promote cancer cell proliferation by regulating the expression of miR-124, miR-140-5p, LATS1, PADI2, and other genes (106–108). Exosome lncRNA HOXA11-AS may increase the expression of SRY-related high-mobility group box 4 (SOX4) in endothelial cells, increasing the proliferative capacity of endothelial cells involved in cervical cancer. According to the ROC curve, the specificity of lncRNA gradually increased during hepatocarcinogenesis (GIHCG), and the sensitivity was 88.75% in distinguishing between healthy people and CC patients. In the future, lncRNA GIHCG could be used to predict CC (109). HOTAIR and MALAT1 lncRNAs were found to be significantly overexpressed in exosomes isolated from the lavage fluid of CC patients (111.112). The lncRNA MEG3 was found to be significantly reduced and correlated with cancer stage, metastasis, and other factors. Chen et al. demonstrated that MEG3 can inhibit cervical cancer cell proliferation, invasion, and migration by regulating the Rac1 and PI3K/AKT/MMP-2/9 signaling pathways (110). When compared to non-neoplastic cervical tissues, the expression of lncRNA MEG3 was significantly downregulated in the histopathological grading of cervical intraepithelial neoplasia (CIN) in CIN 2 and CIN3. According to one study, MEG3 expression was reduced in cervical tissues, and it was associated with cancer size, lymph node metastasis, high-risk HPV infection, and the FIGO stage. *In vitro*, ectopic expression of MEG3 may inhibit the proliferation of human CC cells HeLa and C-33A. The researchers discovered that NF-kappaB interacting lncRNA (NKILA) inhibits proliferation and promotes apoptosis in cervical squamous cells by down-regulating miRNA-21 expression.

LncRNA ArfGAP with the RhoGAP domain, ankyrin repeat, and PH domain 1 antisense RNA (ARAP1-AS1) can promote proto-oncogene c-Myc translation in cervical cancer by separating dimers and promoting tumorigenesis (59). Furthermore, through interactions with recombinant Polypyrimidine Tract Binding Protein 1 (PTBP1), LncRNA surfactant associated 1 (SFTA1P) promoted the degradation of tropomyosin 4 (TPM4) mRNA and the progression of cervical cancer (52). These findings support MEG3's critical role in the molecular etiology of CC and point to MEG3's potential use in the treatment of CC (111) (Table 1).

## 6 Conclusion

Exosomal lncRNA has a wide range of research applications (114). Exosome lncRNAs regulate a variety of pathophysiological processes, including cancer cell genesis, invasion, metastasis, and vascular neogenesis, as well as mediate cancer drug resistance and play an important role in cancer development. Exosome lncRNA is thought to be a novel marker for gynecologic cancer diagnosis, efficacy evaluation, and prognosis prediction. Exosome lncRNA research is still in its early stages, and its functions are not fully understood. There are the following flaws: The specificity of exosome lncRNA as a molecular marker for gynecological tumor diagnosis has yet to be determined; The technology of exosome *in vitro* synthesis as a carrier of targeted therapeutic drugs has yet to be improved; Exosome lncRNAs play a role in a variety of cancers, and multiple exosome lncRNAs have the same cancer action target, but their interaction is still unknown, making it difficult to fully resolve their regulatory network. The above problems can be solved one by one with the rapid development of proteomics, high-throughput sequencing, transcriptomics, and bioinformatics analysis, and researchers will have a better understanding of the mechanisms of exosome-derived lncRNAs in the development of gynecological malignancies and their clinical applications.

TABLE 1 The expression and functions of exosomal lncRNAs in gynecological cancers.

| Cancer types | Specimen source | Exosomal lncRNAs | Functions | References |
|---|---|---|---|---|
| OC | Cells | LINC00092 | Metastasis | (47) |
| OC | Cells | MALAT1 | Proliferation | (79) |
| OC | Cells | HOTTIP | Metastasis | (82) |
| OC | Cells | MEG3 | Drug resistance | (36) |
| OC | Cells | GIHCG | Proliferation | (34) |
| OC | Cells | PTAR | Metastasis | (34) |
| OC | Cells | MORT | proliferation | (73) |
| OC | Cells | HOTAIR | Metastasis | (86) |
| OC | Cells | NEAT1 | proliferation | (86) |
| OC | Cells | H19 | Proliferation | (86) |
| OC | Cells | HOXA11 | Biomarkers | (105) |
| EC | Cells | MEG3 | Proliferation | (93) |
| EC | Cells | ROR | Proliferation | (94) |
| EC | Cells | MALAT1 | Biomarkers | (95) |
| EC | Cells | DLEU1 | Metastasis | (87) |
| EC | Cells | HOTAIR | Metastasis | (86) |
| EC | Cells | NEAT1 | Metastasis | (86) |
| EC | Cells | H19 | Proliferation | (86) |
| CC | Cells | ARAP1-AS1 | Proliferation | (59) |
| CC | Cells | NKILA | Proliferation | (59) |
| CC | Cells | MORT | proliferation | (73) |
| CC | Cells | HOXA11 | Proliferation | (105) |
| CC | Cells | GIHCG | Biomarkers | (109) |

*(Continued)*

TABLE 1 Continued

| Cancer types | Specimen source | Exosomal lncRNAs | Functions | References |
|---|---|---|---|---|
| CC | Vaginal Douche | HOTAIR | Metastasis | (112) |
| CC | Vaginal Douche | MALAT1 | Metastasis | (113) |
| CC | Vaginal Douche | MEG3 | Metastasis | (110) |
| CC | Cells | LINC01305 | Metastasis | (102) |
| CC | Cells | NEAT1 | Proliferation | (86) |
| CC | Serum | H19 | Biomarkers | (101) |
| CC | Cells | SPRY4-IT1 | Proliferation | (111) |
| CC | Cells | GAS5 | Proliferation | (111) |
| CC | Cells | PVT1 | Proliferation | (111) |
| CC | Cells | LINC00675 | Metastasis | (111) |
| CC | Cells | CCST1 | Proliferation | (111) |
| CC | Cells | ZEB1-AS1 | Metastasis | (111) |

## Author contributions

MW, LF, YX, SM, XZ, and LZ performed literature searches and selected the studies and reviews discussed in the manuscript. The first draft of the manuscript was prepared by MW, LF, YX, SM, and XZ and made subsequent amendments. LZ revised the manuscript. All authors contributed to the article and approved the submitted version.

## Funding

Funding for this work was provided by the Natural Science Foundation of Jilin Province (No.20210101268JC and No.20210101462JC).

## Conflict of interest

The authors declare that the research was conducted in the absence of any commercial or financial relationships that could be construed as a potential conflict of interest.

## Publisher's note



## References

1. Kalluri R, LeBleu VS. The biology, function, and biomedical applications of exosomes. *Science* (2020) 367(6478):640. doi: 10.1126/science.aau6977

2. Simona F, Laura S, Simona T, Riccardo A. Contribution of proteomics to understanding the role of tumor-derived exosomes in cancer progression: state of the art and new perspectives. *Proteomics* (2013) 14(10-11):1581–94. doi: 10.1002/pmic.201200398

3. Wu P, Mo Y, Peng M, Tang T, Zhong Y, Deng X, et al. Emerging role of tumor-related functional peptides encoded by lncRNA and circRNA. *Mol Cancer* (2020) 19 (1):22. doi: 10.1186/s12943-020-1147-3

4. Schmitz SU, Grote P, Herrmann BG. Mechanisms of long noncoding RNA function in development and disease. *Cell Mol Life Sci* (2016) 73(13):2491–509. doi: 10.1007/s00018-016-2174-5

5. Zhan Y, Du L, Wang L, Jiang X, Zhang S, Li J, et al. Expression signatures of exosomal long noncoding RNAs in urine serve as novel non-invasive biomarkers for diagnosis and recurrence prediction of bladder cancer. *Mol Cancer* (2018) 17(1):142. doi: 10.1186/s12943-018-0893-y

6. Takahashi K, Ota Y, Kogure T, Suzuki Y, Iwamoto H, Yamakita K, et al. Circulating extracellular vesicle-encapsulated HULC is a potential biomarker for human pancreatic cancer. *Cancer Sci* (2020) 111(1):98–111. doi: 10.1111/cas.14232

7. Morse MA, Garst J, Osada T, Khan S, Hobeika A, Clay TM, et al. A phase I study of dexosome immunotherapy in patients with advanced non-small cell lung cancer. *J Trans Med* (2005) 3(1):9. doi: 10.1186/1479-5876-3-9

8. Cheng J, Meng JL, Zhu L, Peng Y. Exosomal noncoding RNAs in glioma: biological functions and potential clinical applications. *Mol Cancer* (2020) 19(1):66. doi: 10.1186/s12943-020-01189-3

9. Pan BT, Johnstone RM. Fate of the transferrin receptor during maturation of sheep reticulocytes *in vitro*: selective externalization of the receptor. *Cell* (1983) 33 (3):967–78. doi: 10.1016/0092-8674(83)90040-5

10. Farooqi AA, Desai NN, Qureshi MZ, Nogueira Librelotto DR, Gasparri ML, Bishayee A, et al. Exosome biogenesis, bioactivities and functions as new delivery systems of natural compounds. *Biotechnol Adv: Int Rev J* (2018) 36(1):328–34. doi: 10.1016/j.biotechadv.2017.12.010

11. Hannafon BN, Gin AL, Xu YF, Bruns M, Calloway CL, Ding WQ. Metastasis-associated protein 1 (MTA1) is transferred by exosomes and contributes to the regulation of hypoxia and estrogen signaling in breast cancer cells. *Cell Communi Signaling CCS* (2019) 17:13. doi: 10.1186/s12964-019-0325-7

12. Henne WM, Stenmark H, Emr SD. Molecular mechanisms of the membrane sculpting ESCRT pathway. *Cold Spring Harbor Perspect Biol* (2013) 5(9):a016766. doi: 10.1101/cshperspect.a016766

13. Pegtel DM, Gould SJ. Exosomes. *Annu Rev Biochem* (2019) 88(1):487–514. doi: 10.1146/annurev-biochem-013118-111902

14. van Niel G, D'Angelo G, Raposo G. Shedding light on the cell biology of extracellular vesicles. *Nat Rev Mol Cell Biol* (2018) 19(4):213–28. doi: 10.1038/nrm.2017.125

15. Melo S, Sugimoto H, O'Connell J, Kato N, Villanueva A, Vidal A, et al. Cancer exosomes perform cell-independent MicroRNA biogenesis and promote tumorigenesis. *Cancer Cell* (2014) 26(5):707–21. doi: 10.1016/j.ccell.2014.09.005

16. Sheridan C. Exosome cancer diagnostic reaches market. *Nat Biotechnol* (2016) 34(4):358–9. doi: 10.1038/nbt0416-359

17. Sun ZQ, Yang SX, Zhou QB, Wang GX, Song JM, Li Z, et al. Emerging role of exosome-derived long noncoding RNAs in tumor microenvironment. *Mol Cancer* (2018) 17(1):82. doi: 10.1186/s12943-018-0831-z

18. Hu Y, Rao SS, Wang ZX, Cao J, Tan YJ, Luo J, et al. Exosomes from human umbilical cord blood accelerate cutaneous wound healing through miR-21-3p-mediated promotion of angiogenesis and fibroblast function. *Theranostics* (2018) 8 (1):169–84. doi: 10.7150/thno.21234

19. Yang TZ, Martin P, Fogarty B, Brown A, Schurman K, Phipps R, et al. Exosome delivered anti-cancer drugs across the blood-brain barrier for brain cancer therapy in danio rerio. *Pharm Res* (2015) 32(6):2003–14. doi: 10.1007/s11095-014-1593-y

20. Viaud S, Terme M, Flament C, Taieb J, André F, Novault S, et al. Dendritic cell-derived exosomes promote natural killer cell activation and proliferation: A role for NKG2D ligands and IL-15Rα. *PloS One* (2009) 4(3):e4942. doi: 10.1371/journal.pone.0004942

21. Shan ZC, Wang HM, Zhang YJ, Min WP. The role of tumor-derived exosomes in the abscopal effect and immunotherapy. *Life-Basel* (2021) 11(5):381. doi: 10.3390/life11050381

22. Luan X, Sansanaphongpricha K, Myers I, Chen H, Yuan H, Sun D. Engineering exosomes as refined biologica nanoplatforms for drug delivery. *Acta Pharmacol Sin* (2017) 38):763. doi: 10.1038/aps.2017.12

23. St Laurent G, Wahlestedt C, Kapranov P. The landscape of long noncoding RNA classification. *Trends Genet* (2015) 31(5):239–51. doi: 10.1016/j.tig.2015.03.007

24. Bonasio R, Shiekhattar R. Regulation of transcription by long noncoding RNAs. *Annu Rev Genet* (2014) 48:433–55. doi: 10.1146/annurev-genet-120213-092323

25. Chen S, Shen X. Long noncoding RNAs: functions and mechanisms in colon cancer. *Mol Cancer* (2020) 19(1):167. doi: 10.1186/s12943-020-01287-2

26. de Almeida VD. Role of lncRNA alterations in cervical oncogenesis. *Eurasian J Med Oncol* (2022) 6(2):111–20. doi: 10.14744/ejmo.2022.74937

27. Zhao W, Liu Y, Zhang C, Duan C. Multiple roles of exosomal long noncoding RNAs in cancers. *BioMed Res Int* (2019) 2019:1–12. doi: 10.1155/2019/1460572

28. Brandenburger T, Somoza AS, Devaux Y, Lorenzen JM. Noncoding RNAs in acute kidney injury. *Kidney Int* (2018) 94(5):870–81. doi: 10.1016/j.kint.2018.06.033

29. Tripathi V, Ellis JD, Shen Z, Song DY, Prasanth KV. The nuclear-retained noncoding RNA MALAT1 regulates alternative splicing by modulating SR splicing factor phosphorylation. *Mol Cell* (2010) 39(6):925–38. doi: 10.1016/j.molcel.2010.08.011

30. Wu YS, Zhang L, Wang Y, Li H, Ren XB, Wei F, et al. Long noncoding RNA HOTAIR involvement in cancer. *Tumor Biol* (2014) 35(10):9531–8. doi: 10.1007/s13277-014-2523-7

31. Cheng D, Deng JG, Zhang B, He XY, Meng Z, Li GL, et al. LncRNA HOTAIR epigenetically suppresses miR-122 expression in hepatocellular carcinoma *via* DNA methylation. *Ebiomedicine* (2018) 36:159–70. doi: 10.1016/j.ebiom.2018.08.055

32. Kirave P, Gondaliya P, Kulkarni B, Rawal R, Kalia K. Exosome mediated miR-155 delivery confers cisplatin chemoresistance in oral cancer cells via epithelial-mesenchymal transition. *Oncotarget* (2020) 11(13):1157–71. doi: 10.18632/oncotarget.27531

33. Zhang L, Yu D. Exosomes in cancer development, metastasis, and immunity. *Biochim Biophys Acta (BBA) - Rev Cancer* (2019) 1871(2):455–68. doi: 10.1016/j.bbcan.2019.04.004

34. Han SQ, Qi YQ, Luo YM, Chen XP, Liang HF. Exosomal long noncoding RNA: Interaction between cancer cells and non-cancer cells. *Front Oncol* (2021) 10. doi: 10.3389/fonc.2020.617837

35. Zhang WW, Wang QS, Yang Y, Zhou SY, Zhang P, Feng TB. The role of exosomal lncRNAs in cancer biology and clinical management. *Exp Mol Med* (2021) 53 (11):1669–73. doi: 10.1038/s12276-021-00699-4

36. Zhang J, Liu JY, Xu XY, Li L. Curcumin suppresses cisplatin resistance development partly *via* modulating extracellular vesicle-mediated transfer of MEG3 and miR-214 in ovarian cancer. *Cancer Chemother Pharmacol* (2017) 79(3):479–87. doi: 10.1007/s00280-017-3238-4

37. Kim J, Piao HL, Kim BJ, Yao F, Han Z, Wang Y, et al. Long noncoding RNA MALAT1 suppresses breast cancer metastasis. *Nat Genet* (2018) 50:1705–15. doi: 10.1038/s41588-018-0252-3

38. Bol GM, Xie M, Raman V. DDX3, a potential target for cancer treatment. *Mol Cancer* (2015) 14:188. doi: 10.1186/s12943-015-0461-7

39. Hanahan D, Weinberg RA. Hallmarks of cancer: The next generation. *Cell* (2011) 144(5):646–74. doi: 10.1016/j.cell.2011.02.013

40. Wu Q, Wu X, Xiang Y, Zhu Q, Wang X. Suppression of endothelial cell migration by tumor associated macrophage-derived exosomes is reversed by epithelial ovarian cancer exosomal lncRNA. *Cancer Cell Int* (2017) 17(1):62. doi: 10.1186/s12935-017-0430-x

41. Chen C-W, Fu M, Du Z-H, Zhao F, Yang W-W, Xu L-H, et al. Long noncoding RNA MRPL23-AS1 promoteoid cystic carcinoma lung metastasis. *Cancer Res* (2020) 80 (11):2273–85. doi: 10.1158/0008-5472.CAN-19-0819

42. Dong R, Zhang B, Tan B, Lin N. Long noncoding RNAs as the regulators and targets of macrophage M2 polarization. *Life Sci* (2021) 266:118895. doi: 10.1016/j.lfs.2020.118895

43. Guo H, Chitiprolu M, Roncevic L, Javalet C, Hemming FJ, Trung MT, et al. Atg5 disassociates the V1V0-ATPase to promote exosome production and tumor metastasis independent of canonical macroautophagy. *Dev Cell* (2017) 43(6):716–30.E7. doi: 10.1016/j.devcel.2017.11.018

44. Hoshino A, Costa-Silva B, Shen T-L, Rodrigues G, Hashimoto A, Mark MT, et al. Tumour exosome integrins determine organotropic metastasis. *Nature* (2015) 527 (7578):329–35. doi: 10.1038/nature15756

45. Rashed MH, Bayraktar E, Helal GK, Abd-Ellah MF, Amero P, Chavez-Reyes A, et al. Exosomes: From garbage bins to promising therapeutic targets. *Int J Mol Sci* (2017) 18(3):538. doi: 10.1158/0008-5472.CAN-16-1615

46. Bradford JR, Cox A, Bernard P, Camp NJ. Consensus analysis of whole transcriptome profiles from two breast cancer patient cohorts reveals long noncoding RNAs associated with intrinsic subtype and the tumour microenvironment. *PloS One* (2016) 11(9):e0163238. doi: 10.1371/journal.pone.0163238

47. Zhao L, Ji G, Le X, Wang C, Xu L, Feng M, et al. Long noncoding RNA LINC00092 acts in cancer-associated fibroblasts to drive glycolysis and progression of ovarian cancer. *Cancer Res* (2017) 77(6):1369–82. doi: 10.1002/jcp.10133

48. Lang HL, Hu GW, Chen Y, Liu Y, Tu W, Lu YM, et al. Glioma cells promote angiogenesis through the release of exosomes containing long noncoding RNA POU3F3. *Eur Rev Med Pharmacol Sci* (2017) 21(5):959–72. doi: 10.1186/s12943-015-0426-x

49. Martin TA, Mansel RE, Jiang WG. Antagonistic effect of NK4 on HGF/SF induced changes in the transendothelial resistance (TER) and paracellular permeability of human vascular endothelial cells. *J Cell Physiol* (2002) 192(3):268–75. doi: 10.3892/or.2017.5742

50. Conigliaro A, Costa V, Lo Dico A, Saieva L, Buccheri S, Dieli F, et al. CD90+liver cancer cells modulate endothelial cell phenotype through the release of exosomes containing H19 lncRNA. *Mol Cancer* (2015) 14:155. doi: 10.1038/s41419-022-05359-7

51. Lang H-L, Hu G-W, Zhang B, Kuang W, Chen Y, Wu L, et al. Glioma cells enhance angiogenesis and inhibit endothelial cell apoptosis through the release of exosomes that contain long noncoding RNA CCAT2. *Oncol Rep* (2017) 38(2):785–98. doi: 10.1186/s12943-021-01411-w

52. Luo AR, Lan XX, Qiu QZ, Zhou Q, Li J, Wu MT, et al. LncRNA SFTA1P promotes cervical cancer progression by interaction with PTBP1 to facilitate TPM4 mRNA degradation. *Cell Death Dis* (2022) 13(11):936. doi: 10.1007/s10555-019-09783-8

53. Jiang CY, Zhang N, Hu XL, Wang HY. Tumor-associated exosomes promote lung cancer metastasis through multiple mechanisms. *Mol Cancer* (2021) 20(1):117. doi: 10.1186/s12935-018-0506-2

54. Logozzi M, Spugnini E, Mizzoni D, Di Raimo R, Fais S. Extracellular acidity and increased exosome release as key phenotypes of malignant tumors. *Cancer Metastasis Rev* (2019) 38(1-2):93–101. doi: 10.1371/journal.pone.0147236

55. Gao T, Liu X, He B, Nie Z, Zhu C, Zhang P, et al. Exosomal lncRNA 91H is associated with poor development in colorectal cancer by modifying HNRNPK expression. *Cancer Cell Int* (2018) 18(1):11. doi: 10.1016/j.bbrc.2017.06.055

56. Berrondo C, Flax J, Kucherov V, Siebert A, Osinski T, Rosenberg A, et al. Expression of the long noncoding RNA HOTAIR correlates with disease progression in bladder cancer and is contained in bladder cancer patient urinary exosomes. *PloS One* (2016) 11(1):e0147236. doi: 10.3109/07357907.2013.789905

57. Zhang R, Xia Y, Wang Z, Zheng J, Chen Y, Li X, et al. Serum long non coding RNA MALAT-1 protected by exosomes is up-regulated and promotes cell proliferation and migration in non-small cell lung cancer. *Biochem Biophys Res Commun* (2017) 490 (2):406–14. doi: 10.1186/s12967-021-02705-9

58. Huang SH, Li Y, Zhang J, Rong J, Ye S. Epidermal growth factor receptor-containing exosomes induce tumor-specific regulatory T cells. *Cancer Invest* (2013) 31 (5):330–5. doi: 10.1158/0008-5472.CAN-14-3525

59. Zhong QH, Lu MZ, Yuan WQ, Cui YY, Ouyang HQ, Fan Y, et al. Eight-lncRNA signature of cervical cancer were identified by integrating DNA methylation, copy number variation and transcriptome data. *J Trans Med* (2021) 19(1):58. doi: 10.1016/j.canlet.2017.10.040

60. Ran S. The role of TLR4 in chemotherapy-driven metastasis. *Cancer Res* (2015) 75(12):2405–10. doi: 10.1186/s12943-019-0991-5

61. Fan Q, Yang L, Zhang XD, Peng XQ, Wei SB, Su DM, et al. The emerging role of exosome-derived noncoding RNAs in cancer biology. *Cancer Letters* (2018) 414:107–15. doi: 10.1016/j.ijbiomac.2018.12.176

62. Mashouri L, Yousefi H, Aref AR, Ahadi AM, Molaei F, Alahari SK. Exosomes: composition, biogenesis, and mechanisms in cancer metastasis and drug resistance. *Mol Cancer* (2019) 18(1):75. doi: 10.1016/j.gene.2019.144044

63. Gao J, Liu L, Li G, Cai M, Tan C, Han X, et al. LncRNA GAS5 confers the radio sensitivity of cervical cancer cells via regulating miR-106b/IER3 axis. *Int J Biol Macromol* (2018) 126:994–1001. doi: 10.1016/j.fob.2014.04.007

64. He XQ, Yu JJ, Xiong L, Liu YS, Fan L, Li Y, et al. Exosomes derived from liver cancer cells reprogram biological behaviors of LO2 cells by transferring linc-ROR. *Gene* (2019) 719:144044. doi: 10.1016/j.yexmp.2016.05.013

65. Takahashi K, Yan IK, Kogure T, Haga H, Patel T. Extracellular vesicle-mediated transfer of long noncoding RNA ROR modulates chemosensitivity in human hepatocellular cancer. *FEBS Open Bio.* (2014) 4:458–67. doi: 10.1186/s13046-018-0845-9

66. Aqil F, Kausar H, Agrawal AK, Jeyabalan J, Kyakulaga AH, Munagala R, et al. Exosomal formulation enhances therapeutic response of celastrol against lung cancer. *Exp Mol Pathol* (2016) 101(1):12–21. doi: 10.1016/j.yexmp.2016.05.013

67. Kang M, Ren MP, Li Y, Fu YQ, Deng MM, Li CP. Exosome-mediated transfer of lncRNA PART1 induces gefitinib resistance in esophageal squamous cell carcinoma via functioning as a competing endogenous RNA. *J Exp Clin Cancer Res* (2018) 37(1):171. doi: 10.1186/s13046-018-0845-9

68. Sung H, Ferlay J, Siegel RL, Laversanne M, Soerjomataram I, Jemal A, et al. Global cancer statistics 2020: GLOBOCAN estimates of incidence and mortality worldwide for 36 cancers in 185 countries. *Ca-a Cancer J Clin* (2021) 71(3):209–49. doi: 10.3322/caac.21660

69. Torre LA, Trabert B, DeSantis CE, Miller KD, Samimi G, Runowicz CD, et al. Ovarian cancer statistics, 2018. *CA A Cancer J Clin* (2018) 68(4):284–96. doi: 10.3322/caac.21456

70. Montagnana M, Benati M, Danese E. Circulating biomarkers in epithelial ovarian cancer diagnosis: from present to future perspective. *Ann Trans Med* (2017) 5(13):276. doi: 10.21037/atm.2017.05.13

71. Dochez V, Caillon H, Vaucel E, Dimet J, Winer N, Ducarme G. Biomarkers and algorithms for diagnosis of ovarian cancer: CA125, HE4, RMI and ROMA, a review. *J Ovarian Res* (2019) 12(1):28. doi: 10.1186/s13048-019-0503-7

72. Wang LS, Sun YH, Cai XA, Fu GF. The diagnostic value of human epididymis protein 4 as a novel biomarker in patients with renal dysfunction. *Int Urol Nephrol* (2018) 50(11):2043–8. doi: 10.1007/s11255-018-1930-x

73. Di Fiore R, Suleiman S, Drago-Ferrante R, Felix A, O'Toole SA, O'Leary JJ, et al. LncRNA MORT (ZNF667-AS1) in cancer-is there a possible role in gynecological malignancies? *Int J Mol Sci* (2021) 22(15):7829. doi: 10.3390/ijms22157829

74. Gobbo J, Marcion G, Cordonnier M, Dias AMM, Pernet N, Hammann A, et al. Restoring anti-cancer immune response by targeting tumor-derived exosomes with a HSP70 peptide aptamer. *J Natl Cancer Inst.* 108(3):11. doi: 10.1093/jnci/djv330

75. Nakamura K, Sawada K, Kobayashi M, Miyamoto M, Shimizu A, Yamamoto M, et al. Role of the exosome in ovarian cancer progression and its potential as a therapeutic target. *Cancers* (2019) 11(8):1147. doi: 10.3390/cancers11081147

76. Kabe Y, Suematsu M, Sakamoto S, Hirai M, Koike I, Hishiki T, et al. Development of a highly sensitive device for counting the number of disease-specific exosomes in human sera. *Clin Chem* (2018) 64(10):1463–73. doi: 10.1039/C9SC00961B

77. Chen ZX, Liang QX, Zeng H, Zhao Q, Guo ZD, Zhong RH, et al. Exosomal CA125 as a promising biomarker for ovarian cancer diagnosis. *J Cancer* (2020) 11 (21):6445–53. doi: 10.2147/OTT.S214689

78. Zhang P, Zhou X, Zeng Y. Multiplexed immunophenotyping of circulating exosomes on nano-engineered ExoProfile chip towards early diagnosis of cancer. *Chem Sci* (2019) 10(21):5495–504. doi: 10.1039/c9sc00961b

79. Sun Q, Li Q, Xie FF. LncRNA-MALAT1 regulates proliferation and apoptosis of ovarian cancer cells by targeting miR-503-5p. *Oncotargets Ther* (2019) 12:6297–307. doi: 10.7150/ijbs.28048

80. Jin Y, Feng SJ, Qiu S, Shao N, Zheng JH. LncRNA MALAT1 promotes proliferation and metastasis in epithelial ovarian cancer *via* the PI3K-AKT pathway. *Eur Rev Med Pharmacol Sci* (2017) 21(14):3176–84. doi: 10.1186/s13046-019-1394-6

81. Qiu JJ, Lin XJ, Tang XY, Zheng TT, Lin YY, Hua KQ. Exosomal metastasis-associated lung adenocarcinoma transcript 1 promotes angiogenesis and predicts poor prognosis in epithelial ovarian cancer. *Int J Biol Sci* (2018) 14(14):1960–73. doi: 10.1016/j.nano.2015.10.012

82. Shang A, Wang W, Gu C, Chen C, Li D. Long non-coding RNA HOTTIP enhances IL-6 expression to potentiate immune escape of ovarian cancer cells by up-regulating the expression of PD-L1 in neutrophils. *J Exp Clin Cancer Res* (2019) 38 (1):411. doi: 10.1039/C7FO00882A

83. Kim MS, Haney MJ, Zhao Y, Mahajan V, Deygen I, Klyachko NL, et al. Development of exosome-encapsulated paclitaxel to overcome MDR in cancer cells. *Nanomed-Nanotechnol Biol Med* (2016) 12(3):655–64. doi: 10.1038/s41388-018-0189-0

84. Aqil F, Jeyabalan J, Agrawal AK, Kyakulaga AH, Munagala R, Parker L, et al. Exosomal delivery of berry anthocyanidins for the management of ovarian cancer. *Food Funct* (2017) 8(11):4100–7. doi: 10.3390/cancers13236102

85. Dorayappan KDP, Wanner R, Wallbillich JJ, Saini U, Zingarelli R, Suarez AA, et al. Hypoxia-induced exosomes contribute to a more aggressive and chemoresistant ovarian cancer phenotype: a novel mechanism linking STAT3/Rab proteins. *Oncogene* (2018) 37(28):3806–21. doi: 10.2147/OTT.S262661

86. Naz F, Tariq I, Ali S, Somaida A, Preis E, Bakowsky U. The role of long noncoding RNAs (lncRNAs) in female oriented cancers. *Cancers* (2021) 13(23):6102. doi: 10.1016/j.canlet.2017.03.004

87. Jia JJ, Guo SQ, Zhang D, Tian XH, Xie XM. Exosomal-lncRNA DLEUI accelerates the proliferation, migration, and invasion of endometrial carcinoma cells by regulating microRNA-E2F3. *Oncotargets Ther* (2020) 13:8651–63. doi: 10.1007/s00011-018-1186-z

88. Zhang ZC, Li X, Sun W, Yue SQ, Yang JY, Li JJ, et al. Loss of exosomal miR-320a from cancer-associated fibroblasts contributes to HCC proliferation and metastasis. *Cancer Letters* (2017) 397:33–42. doi: 10.1007/s12253-019-00614-3

89. Wang JL, Xu WQ, He YK, Xia Q, Liu SW. LncRNA MEG3 impacts proliferation, invasion, and migration of ovarian cancer cells through regulating PTEN. *Inflammation Res* (2018) 67(11-12):927–36. doi: 10.1530/JME-12-0008

90. Al-Rugeebah A, Alanazi M, Parine NR. MEG3: an oncogenic long noncoding RNA in different cancers. *Pathol Oncol Res* (2019) 25(3):859–74. doi: 10.18632/oncotarget.19931

91. Zhou YL, Zhang X, Klibanski A. MEG3 noncoding RNA: a tumor suppressor. *J Mol Endocrinol* (2012) 48(3):R45–53. doi: 10.1016/j.biopha.2016.02.049

92. He YQ, Luo YH, Liang BY, Ye L, Lu GX, He WM. Potential applications of MEG3 in cancer diagnosis and prognosis. *Oncotarget* (2017) 8(42):73282–95. doi: 10.18632/oncotarget.19931

93. Guo QY, Qian ZD, Yan DD, Li L, Huang LL. LncRNA-MEG3 inhibits cell proliferation of endometrial carcinoma by repressing notch signaling. *Biomed Pharmacother* (2016) 82:589–94. doi: 10.3390/cancers11020234

94. Chen J, Xu YX. Differential expression of serum LncRNA ROR and miR-29 in patients with endometrial carcinoma and their diagnostic value. *Int J Lab Med* (2019) 40(04):484–7. doi: 10.1038/nature22341

95. Dong PX, Xiong Y, Yue JM, Hanley SJB, Kobayashi N, Todo Y, et al. Exploring lncRNA-mediated regulatory networks in endometrial cancer cells and the tumor microenvironment: Advances and challenges. *Cancers* (2019) 11(2):234. doi: 10.3390/cancers11020234

96. Kamerkar S, LeBleu VS, Sugimoto H, Yang SJ, Ruivo CF, Melo SA, et al. Exosomes facilitate therapeutic targeting of oncogenic KRAS in pancreatic cancer. *Nature* (2017) 546(7659):498. doi: 10.1016/j.semradonc.2016.05.003

97. Torre LA, Bray F, Siegel RL, Ferlay J, Lortet-Tieulent J, Jemal A. Global cancer statistics, 2012. *Ca-a Cancer J Clin* (2015) 65(2):87–108. doi: 10.3322/caac.21262

98. Ferlay J, Soerjomataram I, Dikshit R, Eser S, Mathers C, Rebelo M, et al. Cancer incidence and mortality worldwide: Sources, methods and major patterns in GLOBOCAN 2012. *Int J Cancer* (2015) 136(5):E359–E86. doi: 10.18632/aging.202565

99. Jiangli D, Shannon R, Cordia C. Review of the cervical cancer burden and population-based cervical cancer screening in China. *Asian Pacific J Cancer prevention: APJCP* (2015) 16(17):7401–7. doi: 10.1080/20013078.2020.1722385

100. Verma J, Monk BJ, Wolfson AH. New strategies for multimodality therapy in treating locally advanced cervix cancer. *Semin Radiat Oncol* (2016) 26(4):344–8. doi: 10.1016/j.ijbiomac.2018.02.034

101. He JX, Huang BY, Zhang K, Liu MB, Xu TM. Long noncoding RNA in cervical cancer: From biology to therapeutic opportunity. *Biomed Pharmacother* (2020) 127:110209. doi: 10.1016/j.ygyno.2016.04.216

102. Huang XX, Liu XM, Du B, Liu XL, Xue M, Yan QX, et al. LncRNA LINC01305 promotes cervical cancer progression through KHSRP and exosome-mediated transfer. *Aging-Us* (2021) 13(15):19230–42. doi: 10.1007/s12013-021-01007-7

103. Lin Y, Zhang C, Xiang PP, Shen J, Sun WJ, Yu H. Exosomes derived from HeLa cells break down vascular integrity by triggering endoplasmic reticulum stress in endothelial cells. *J Extracellular Vesicles* (2020) 9(1):1722385. doi: 10.1089/dna.2017.3805

104. Chen SS, Lv MF, Fang S, Ye WX, Gao Y, Xu YS. Poly(I:C) enhanced anti-cervical cancer immunities induced by dendritic cells-derived exosomes. *Int J Biol Macromol* (2018) 113:1182–7. doi: 10.1016/j.ijbiomac.2018.02.034

105. Kim HJ, Lee JY, Nam EJ, Park SA, Kim S, Kim SW, et al. Upregulation of long noncoding RNA HOXA11 antisense promotes tumor progression and stemness maintenance of cervical cancer cells. *Gynecol Oncol* (2016) 141:75. doi: 10.7150/jca.28525

106. He YS, Qiu XG. Suppression of lncRNA HOXA11-AS/miR-124 axis inhibits glioma progression. *Cell Biochem Biophys* (2021) 79(4):815–22. doi: 10.2147/OTT.S167053

107. Cui Y, Yi L, Zhao JZ, Jiang YG. Long noncoding RNA HOXA11-AS functions as miRNA sponge to promote the glioma tumorigenesis through targeting miR-140-5p. *DNA Cell Biol* (2017) 36(10):822–8. doi: 10.1089/dna.2017.3805

108. Yu J, Hong JF, Kang J, Liao LH, Li CD. Promotion of LncRNA HOXA11-AS on the proliferation of hepatocellular carcinoma by regulating the expression of LATS1. *Eur Rev Med Pharmacol Sci* (2017) 21(15):3402–11.

109. Zhang X, Mao L, Li L, He Z, Wang N, Song Y. Long non-coding RNA GIHCG functions as an oncogene and serves as a serum diagnostic biomarker for cervical cancer. *J Cancer* (2019) 10(3):672–81. doi: 10.1002/jcla.21990

110. Chen XH, Qu JY. Long noncoding RNA MEG3 suppresses survival, migration, and invasion of cervical cancer. *Oncotargets Ther* (2018) 11:4999–5007. doi: 10.7717/peerj.4763

111. Tornesello ML, Faraonio R, Buonaguro L, Annunziata C, Starita N, Cerasuolo A, et al. The role of microRNAs, long noncoding RNAs, and circular RNAs in cervical cancer. *Front Oncol* (2020) 10. doi: 10.3389/fonc.2020.00150

112. Chen WT, Huang LS, Zeng DD, Chen ZP, Wu ZX. Effect and mechanism of LncRNA HOTAIR on proliferation, apoptosis and EMT of cervical cancer hela cells. *Int J Lab Med* (2022) 43(06):710–6. doi: 10.3390/ijms18030538

113. Zhang J, Liu SC, Luo XH, Tao GX, Guan M, Yuan H, et al. Exosomal long noncoding RNAs are differentially expressed in the cervicovaginal lavage samples of cervical cancer patients. *J Clin Lab Analysis* (2016) 30(6):1116–21. doi: 10.3322/caac.21262

114. Abak A, Abhari A, Rahimzadeh S. Exosomes in cancer: small vesicular transporters for cancer progression and metastasis, biomarkers in cancer therapeutics. *Peerj* (2018) 6:e4763. doi: 10.1002/ijc.29210

10.3389/fonc.2023.1138142

# Glossary

| | |
|---|---|
| lncRNAs | Long non-coding RNAs |
| TDE | Tumor-derived exosomes |
| EMT | Epithelial-mesenchymal transition |
| ESCRT | Endosomal sorting complex required for transport |
| ALIX | Apoptosis-linked gene 2-interacting protein X |
| VPS4 | Vacuolar protein sorting 4 |
| DEX | Dendritic cell-derived exosomes |
| AS lncRNA | Antisense lncRNA |
| MEG3 | Maternally expressed gene 3 |
| GRE | Glucocorticoid response element |
| GR | Glucocorticoid receptor |
| PANDA | P21-associated noncoding RNA DNA damage-activated |
| HOX | Homeobox |
| HOXA11-AS | A11 antisense lncRNA |
| WDR5 | WD repeat domain 5 |
| WNT | Wingless-type MMTV Integration Site Family |
| KLF4 | Kruppel like factor 4 |
| VEGF | Vascular endothelial growth factor |
| ceRNA | Competitive endogenous RNA |
| ATB | Activated by transforming growth factor beta |
| HOTAIR | HOX transcript antisense RNA |
| MALAT1 | Metastasis-associated lung adenocarcinoma transcript 1 |
| DDX3 | DEAD-box RNA helicase 3 |
| VAMP3 | Vesicle associated membrane protein 3 |
| SNAP23 | Synaptosomal-associated protein 23 |
| TAMs | Tumor-associated macrophages |
| ECM | Extracellular matrix |
| CAFs | Carcinoma-associated fibroblasts |
| C-X-C motif | Chemokine |
| CXCL14 | ligand 14 |
| SNHG16 | Small nucleolar RNA host gene 16 |
| GALNT1 | N-acetylgalactosaminyltransferase 1 |
| HIF-1α | Hypoxia-inducible factor |
| HNRNPK | Heterogeneous nuclear ribonucleoprotein K |
| EGFR | Epidermal growth factor receptor |
| DCs | Dendritic cells |
| PI3K | Phosphoinositide 3 kinase |
| ROR | Regulators of Reprogramming |

*(Continued)*

Continued

| | |
|---|---|
| OC | Ovarian Cancer |
| FDA | Food and Drug Administration |
| FRα | Folate Receptor-α |
| EpCAM | Epithelial cell adhesion molecule |
| JAK2 | Janus kinase 2 |
| PKB | AKT, PI3K-protein kinase B |
| FIGO | The International Federation of Gynecology and Obstetrics |
| HOTTIP | HOXA transcript at the distal tip |
| FGF | Fibroblast growth factor |
| MDCKMDR1 | P-gp transfected Manin-Darby canine kidney epithelial cells |
| HEX | Hypoxic OC cell line exosome |
| EC | Endometrial Carcinoma |
| CC | Cervical Cancer |
| OS | Overall Survival |
| PFS | Progression-free Survival |
| SOX4 | SRY-related high-mobility-group box 4 |
| GIHCG | Gradual increase during hepatocarcinogenesis |
| CIN | Cervical intraepithelial neoplasia |
| NKILA | NF-kappaB interacting lncRNA |
| ARAP1-AS1 | ArfGAP with RhoGAP domain, ankyrin repeat, and PH domain 1 antisense RNA |
| SFTA1P | Surfactant associated 1, pseudogene |
| TPM4 | Tropomyosin 4 |
| PTBP1 | Polypyrimidine Tract Binding Protein 1. |

frontiers | Frontiers in Oncology

TYPE Original Research
PUBLISHED 30 March 2023
DOI 10.3389/fonc.2023.1143876



OPEN ACCESS

EDITED BY
Umberto Malapelle,
University of Naples Federico II, Italy

REVIEWED BY
Gaia Giannone,
Imperial College London, United Kingdom
Isabel Soto-Cruz,
National Autonomous University of Mexico, Mexico

*CORRESPONDENCE
Weiwei Feng
fww12066@rjh.com.cn
Lin Lin
linlin0415@hotmail.com

†These authors have contributed equally to this work and share first authorship

SPECIALTY SECTION
This article was submitted to Gynecological Oncology, a section of the journal Frontiers in Oncology

RECEIVED 13 January 2023
ACCEPTED 20 March 2023
PUBLISHED 30 March 2023

CITATION
Jiang C, Lu Y, Liu H, Cai G, Peng Z, Feng W and Lin L (2023) Clinical characterization and genomic landscape of gynecological cancers among patients attending a Chinese hospital.
*Front. Oncol.* 13:1143876.
doi: 10.3389/fonc.2023.1143876



# Clinical characterization and genomic landscape of gynecological cancers among patients attending a Chinese hospital

Cen Jiang[1†], Yiyi Lu[1†], Hua Liu[2†], Gang Cai[1], Zhao Peng[3], Weiwei Feng[2*] and Lin Lin[1*]

[1]Department of Laboratory Medicine, Ruijin Hospital, Shanghai Jiaotong University School of Medicine, Shanghai, China, [2]Department of Obstetrics & Gynecology, Ruijin Hospital, Shanghai Jiaotong University School of Medicine, Shanghai, China, [3]Genecast Biotechnology Co., Ltd., Wuxi, China

**Background:** Gynecological cancers are the most lethal malignancies among females, most of which are associated with gene mutations. Few studies have compared the differences in the genomic landscape among various types of gynecological cancers. In this study, we evaluated the diversity of mutations in different gynecological cancers.

**Methods:** A total of 184 patients with gynecological cancer, including ovarian, cervical, fallopian tube, and endometrial cancer, were included. Next-generation sequencing was performed to detect the mutations and tumor mutational burden (TMB). Kyoto Encyclopedia of Genes and Genomes (KEGG) and Gene Ontology (GO) enrichment analyses were also conducted.

**Results:** We found that 94.57% of patients had at least one mutation, among which single nucleotide variants, insertions and InDels were in the majority. *TP53, PIK3CA, PTEN, KRAS, BRCA1, BRCA2, ARID1A, KMT2C, FGFR2*, and *FGFR3* were the top 10 most frequently mutated genes. Patients with ovarian cancer tended to have higher frequencies of *BRCA1* and *BRCA2* mutations, and the frequency of germline *BRCA1* mutations (18/24, 75.00%) was higher than that of *BRCA2* (11/19, 57.89%). A new mutation hotspot in *BRCA2* (I770) was firstly discovered among Chinese patients with gynecological cancer. Patients with *TP53*, *PIK3CA*, *PTEN*, and *FGFR3* mutations had significantly higher TMB values than those with wild-type genes. A significant cross was discovered between the enriched KEGG pathways of gynecological and breast cancers. GO enrichment revealed that the mutated genes were crucial for the cell cycle, neuronal apoptosis, and DNA repair.

**Conclusion:** Various gynecological cancer types share similarities and differences both in clinical characterization and genomic mutations. Taken together with the results of TMB and enriched pathways, this study provided useful information on the molecular mechanism underlying gynecological cancers and the development of targeted drugs and precision medicine.

KEYWORDS

gynecological cancer, next-generation sequencing, TMB, BRCA1, BRCA2, FGFR3

# 1 Introduction

Ovarian (OC), cervical (CC), and endometrial cancer (EC) are the most common gynecological cancers in the female reproductive system (1, 2). OC is the most lethal gynecological malignancy in developed countries (3), with a 5-year survival rate of ~47% (4). Since ovaries are relatively small and located deep in the pelvic cavity, up to 59% of OCs are only detected at advanced stages, with a low survival rate (5). Epithelial ovarian carcinoma (EOC) accounts for the majority of OCs and can be divided into serous, endometrioid, clear cell, and mucinous carcinoma, amongst others. Serous carcinomas constitute about 75% of EOCs and are further divided into low-grade and high-grade serous carcinomas (LGSC and HGSC) depending on their histological differences (6). CC is the fourth most common cancer among females, affecting approximately 600,000 women annually (7). Although screening programs and human papillomavirus (HPV) vaccines have helped reduce its incidence (8), approximately 310,000 patients with CC die annually (9). CC tends to develop at a younger age (10, 11); however, older patients also often have dismal prognoses (12, 13). EC, which is second only to CC in terms of the incidence of reproductive system cancers, ranks seventh among the most prevalent malignancies among females (14–16). EC can be divided into two types: type I estrogen-dependent EC (EEC) and type II non-estrogen-dependent EC (NEEC) (17). The proportion of patients with EEC is higher, and they are often younger and present with hypertension, diabetes, obesity, and infertility (18). NEEC has higher rates of metastasis and recurrence, poorer prognoses, and is more common among older women (19, 20). Fallopian tube cancer (FTC), which originates in the salpingeal mucosa (21), exhibits clinical behaviors similar to that of OC (22). But mutated fallopian tube epithelial cells were reported to form malignant tumors with a shorter latency and higher penetrance than that of ovarian surface epithelium. Although FTC is a relatively rare gynecological cancer, its incidence increased 4.19-fold from 2001 to 2014 (23).

Cancers are genetic diseases. Gene mutations alter the structure or function of related and encoded proteins, resulting in excessive/persistent stimulation signals for cell growth and transformation. With the development of molecular biology, the use of genetic testing to determine mutations in related tumors has become a topic of interest. Targeted drugs for specific genes and mutations are effective ways to treat cancer. Approximately 10 to 15% of OC are reported to be hereditary, and patients with OC are carriers of germline mutations in *BRCA1* and *BRCA2* (24). *BRCA1* and *BRCA2* mutations increase the lifetime risk of peritoneal malignancies and FTC (25, 26). In 2014, olaparib, the first poly ADP-ribose polymerase (PARP) inhibitor, was approved for the treatment of *BRCA*-mutated OC (27). *PPP2R1A* and *TP53* mutations are dramatically higher in patients with advanced-stage EC (19). *PIK3CA, KMT2C*, and *KMT2D* are the most frequently mutated genes in CC (28).

Next-generation sequencing (NGS) is a high-throughput sequencing technology that plays a vital role in cancer research (29). NGS can identify genomic alterations occurring in any region of a target gene, detect one mutated copy among thousands of wild-type copies, and elucidate many types of mutational landscapes of tumors. NGS has become an important aspect of accurate tumor diagnosis and treatment and has a variety of uses, such as tumor-targeted therapy-related driver gene detection, analysis of drug resistance mechanisms, tumor metastasis and prognosis assessment, and molecular diagnostics. In this study, we investigated 184 patients with gynecological malignancies using NGS and created a genomic landscape to show the diversity among different gynecological cancers, providing useful information for future clinical treatment.

# 2 Materials and methods

## 2.1 Patients and sampling

A total of 184 patients diagnosed with gynecological cancers at Ruijin Hospital, Shanghai Jiaotong University School of Medicine between January 2020 and June 2022 were enrolled in this study. All included patients gave their informed consent. The study was reviewed and approved by the Ethical Committee of the Ruijin Hospital, Shanghai Jiaotong University School of Medicine. Tissue samples were collected during surgical

procedures and were subjected to NGS alongside paired blood samples. Patient information was acquired from medical records. Pathology diagnosis including the tumor site, pathological type, tumor differentiation grade, as well as Federation of International of Gynecologists and Obstetricians (FIGO) grade, were reviewed by two expert pathologists from the pathology department.

## 2.2 DNA extraction

Imprint cytology was performed to evaluate tumor purity before DNA extraction. Briefly, freshly cut surfaces of tissue specimens were gently pressed to glass slides. Then the slides was stained with hematoxylin and eosin (HE) after fixing with 95% of ethyl alcohol for 5–6 s. If the percentage of tumor cells was higher than 15%, the specimen was considered qualified for subsequent extraction and sequencing. Genomic DNA was extracted from fresh tumor tissue using the TIANamp Genomic DNA Kit (TIANGEN, China). Genomic DNA from peripheral blood lymphocytes (PBL) was extracted using a TGuide S32 Magnetic Blood Genomic DNA Kit (TIANGEN, China). The concentration of DNA was measured using a Qubit dsDNA HS Assay Kit (Thermo Fisher, USA), whereas the DNA quality was assessed using an Agilent 2100 BioAnalyzer (Agilent, USA). All extractions and assays were conducted according to the manufacturers' instructions supplied in the respective kits used in this study.

## 2.3 Library preparation and sequencing

Genomic DNA extracted from each tumor or PBL sample was sheared with Covaris LE220 to a length of 200 bp, and fragmented DNA was used to construct a library using the KAPA Hyper Preparation Kit (Kapa Biosystems, USA). Target regions were captured using the HyperCap Target Enrichment Kit (Roche, Switzerland). The customized panel used in the capture process includes 543 genes (30), which are tumor-related major genes, and spans around a 1.67 MB genomic region of the human genome (Supplemental Table 1; Genecast Biotechnology Co., Ltd., Beijing, China). Bioinformatic analyses of these 543 genes were carried out at a College of American Pathologists (CAP)-certified laboratory (Genecast Biotechnology). Hybridization and washing were conducted according to the manufacturer's protocol. The captured library was sequenced on the instrument of Illumina Novaseq 6000, which produces paired-end reads with the length of each end as 150bp, according to the manufacturer's protocol.

Clean sequenced reads were mapped to the human reference genome (hg19) using BWA (v0.7.17) (31). VarDict (version 1.5.1) was used to call single nucleotide variant (SNV) mutations (32), whereas compound heterozygous mutations were merged using FreeBayes (version 1.2.0) (33). After annotation using ANNOVAR (2015 Jun17) (34), somatic mutations were selected based on the following standards: (i) located in intergenic/intronic regions; (ii) synonymous SNVs; (iii) allele frequency ≥ 0.002 in Exome Aggregation Consortum (ExAC) and genome aggregation database (gnomAD) (35, 36); (iv) allele frequency <0.05 in the tumor sample/allele frequency <0.01 in the plasma sample; (v) strand bias mutations in the reads; (vi) support reads <5; (vii) depth <30.

## 2.4 Tumor mutational burden calculation

Primarily, dynamic nonsynonymous mutations in the coding regions were selected for the following analysis of TMB, while driver gene mutations and germline alterations in the Single Nucleotide Polymorphism database (dbSNP) were removed. We filtered SNV mutations in all samples according to the following rules: (i) not splicing or exonic; (ii) depth <100 X/allele frequency <0.05; (iii) allele frequency ≥ 0.002 in the ExAC and gnomAD; and (iv) strand bias mutations in the reads. After quantification of the number of somatic nonsynonymous SNVs, the value was extrapolated to the whole exome using a validated algorithm (37). TMB, measured in mutations per Mb, was then calculated after obtaining absolute mutation counts against the mutation spots of the normal samples using the following formula:

$$\mathrm{TMB} = \frac{\text{Absolute mutation counts} \times 1000000}{\text{Panel exonic base number}}$$

## 2.5 Gene ontology and Kyoto encyclopedia of genes and genomes pathway enrichment analyses

GO functional enrichment and KEGG pathway analyses were performed using DAVID tools (https://david.ncifcrf.gov/). For GO analysis, contigs were categorized, and their molecular functions, cellular components, and biological processes were statistically analyzed.

## 2.6 Protein interaction

Search Tool for the Retrieval of Interacting Genes/Proteins (STRING, version 11.0, https://string-db.org) was used to analyze functional interactions with a confidence of 0.7. "Ovarian cancer," "cervical cancer," "fallopian tube cancer," and "endometrial cancer" were used as keywords in Chilibot (http://www.chilibot.net/) to analyze the interaction between genes and different gynecological cancers, excluding abstract co-occurrence relationships.

## 2.7 Statistical analysis

Descriptive statistics were presented as the median (interquartile range; IQR) for continuous variables, and as numbers (percentages) for categorical data. All data were analyzed using SPSS version 26.0 (SPSS Inc., Chicago, IL, USA). Mann–Whitney and Kruskal–Wallis nonparametric tests were conducted for comparisons between groups. Pearson's Chi-square test was used for categorical variables. The Benjamini–Hochberg procedure was conducted to derive significance for enrichment tests. Spearman's correlation coefficients with a two-tailed $p$ value were determined for correlation analyses; $p < 0.05$ indicated significance. Data are visualized in graphs produced using GraphPad Prism version 8.0 and R software version 4.0.5.

# 3 Results

## 3.1 The clinical features of the analyzed cohort

Among the 184 patients, 140 had OC, 12 had CC, 8 had FTC, and 24 had EC. Clinicopathological characteristics are presented in Table 1. The median age at diagnosis was 60 (50–67) years old.

Patients with CC were younger at diagnosis, especially compared with those with OC and FTC. No significant differences were observed in menopausal status. Patients with OC had larger tumors, found at more advanced stages, while patients with CC and EC were diagnosed at earlier stages ($p < 0.05$). Metastasis occurred at both at node and

TABLE 1 Clinical characterization of the population in this study.

| | OC | CC | FTC | EC | *p* value |
|---|---|---|---|---|---|
| | (n = 140) | (n = 12) | (n = 8) | (n = 24) | |
| Age at diagnosis | | | | | *p*=0.008 |
| Median | 61 (51-67) | 48 (39-60) | 67 (61-70) | 57 (46-63) | |
| ≥ 55 years | 91 (65.00%) | 3 (25.00%) | 7 (87.50%) | 14 (58.33%) | |
| Menopausal status | | | | | *p*=0.206 |
| Pre-menopausal | 35 (25.00%) | 5 (41.67%) | 0 (0.00%) | 7 (29.17%) | |
| Post-menopausal | 105 (75.00%) | 7 (58.33%) | 8 (100.00%) | 17 (70.83%) | |
| Tumor size | | | | | *p*=0.01 |
| Median | 5.0 (2.5-8.5) | 3.1 (1.6-4.8) | 3.4 (1.5-4.4) | 4.0 (2.0-5.9) | |
| ≥5 cm | 75 (53.57%) | 3 (25.00%) | 1 (12.50%) | 8 (33.33%) | |
| Metastasis | | | | | *p*=0.027 |
| Node | 23 (16.43%) | 1 (8.33%) | 0 (0.00%) | 4 (16.67%) | |
| Organ | 9 (6.43%) | 2 (16.67%) | 0 (0.00%) | 1 (4.17%) | |
| Both | 73 (51.14%) | 4 (33.33%) | 8 (100.00%) | 7 (29.17%) | |
| None | 35 (25.00%) | 5 (41.67%) | 0 (0.00%) | 12 (50.00%) | |
| FIGO stage | | | | | *p*=0.000 |
| I-II | 39 (27.86%) | 9 (75.00%) | 3 (37.50%) | 16 (66.67%) | |
| III-IV | 101 (71.14%) | 3 (25.00%) | 5 (62.50%) | 8 (33.33%) | |
| Personal history | | | | | |
| Breast cancer | 8 (5.71%) | 0 (0.00%) | 0 (0.00%) | 0 (0.00%) | |
| Thyroid cancer | 2 (1.43%) | 0 (0.00%) | 0 (0.00%) | 0 (0.00%) | |
| Hematologic tumor | 2 (1.43%) | 0 (0.00%) | 0 (0.00%) | 0 (0.00%) | |
| Renal cancer | 1 (0.71%) | 0 (0.00%) | 0 (0.00%) | 0 (0.00%) | |
| Liver cancer | 1 (0.71%) | 0 (0.00%) | 0 (0.00%) | 0 (0.00%) | |
| Colon cancer | 1 (0.71%) | 0 (0.00%) | 0 (0.00%) | 0 (0.00%) | |
| Family history | | | | | |
| Thyroid cancer | 1 (0.71%) | 0 (0.00%) | 0 (0.00%) | 0 (0.00%) | |
| Lung cancer | 1 (0.71%) | 0 (0.00%) | 0 (0.00%) | 0 (0.00%) | |

OC, ovarian cancer; CC, cervical cancer; EC, endometrial cancer; FTC, fallopian tube cancer; FIGO, Federation of International of Gynecologists and Obstetricians.

organs in all patients with FTC. Patients with OC tended to have personal/family histories of cancer, especially breast cancer. Further analysis was performed among patients with OC according to their pathological types (Supplementary Table 2).

## 3.2 Gynecological cancers exhibit various genomic landscapes

Patient DNA from tumor tissues and matched peripheral blood were used for NGS. We detected 529 SNVs, 132 insertions and InDels, 36 truncations, 111 gene amplifications, 36 gene deletions, and 17 splice site mutations. Of all our patients, 94.57% (174/184) had at least one mutation (Figure 1). The top 10 most frequently altered genes in patients with gynecological cancer are presented in Figure 2. Patients with OC and FTC had higher frequencies of *TP53* mutations, while patients with EC showed more *PTEN* alterations. Changes in *KMT2C* and *FGFR3* were more frequent among patients with CC than in the other three types.

Furthermore, different mutation types were uncovered among different genes. *TP53* showed obvious alterations in SNVs and InDels. *PIK3CA* and *PTEN* revealed higher frequencies of copy number variations. *BRCA1* and *BRCA2* had similar patterns with slight differences, such as splice site mutations in *BRCA1* and insertions in *BRCA2*. R273 and V173 in *TP53*, H1047 and E542 in *PIK3CA*, R183 in *PPP2R1A*, and G12 in *KRAS* were hotspots of mutations among these patients (data not shown). The top 10 most frequently altered genes among patients with OC were the same as those in all 184 patients, but in an order with slight changes (Supplementary Figure 1).

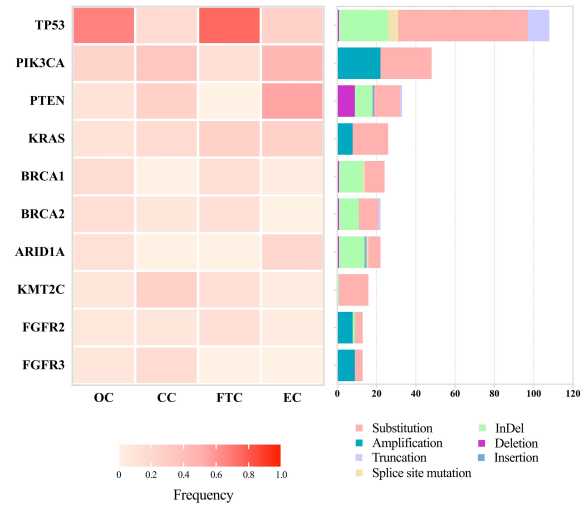


FIGURE 2
Landscapes of the top 10 most frequently mutated genes among 184 patients with gynecological cancer. Next-generation sequencing was performed to detect mutations. Frequencies of mutated genes are listed on the left, and mutation types are shown on the right, with annotation bars at the bottom. OC, ovarian cancer; CC, cervical cancer; EC, endometrial cancer; FTC, fallopian tube cancer.

## 3.3 Analysis of *BRCA1* and *BRCA2* mutations

In total, 24 and 19 mutations were discovered in *BRCA1* and *BRCA2*, respectively, most of which were found in patients with OC (Figure 3). Two patients with OC (HGSC and endometrioid carcinoma, respectively) carried both *BRCA1* and *BRCA2* mutations simultaneously. No *BRCA1* or *BRCA2* mutations were found in patients with CC. The proportion of germline mutations was higher than somatic mutations in *BRCA1* and *BRCA2*. Moreover, the frequency of germline *BRCA1* mutations (18/24, 75.00%) was higher than that of *BRCA2* mutations (11/19, 57.89%). HGSC accounted for the majority of germline mutations in both *BRCA1* and *BRCA2* in patients with OC (Supplementary Figure 2). *BRCA2* mutation c.2307delT p.I770Ffs*2 was the hotspot firstly reported here among Chinese patients with gynecological cancer.

## 3.4 TMB analysis

TMB range in this study spanned 0 to 192.35. To improve the accuracy, the data from one patient with endometrioid OC with

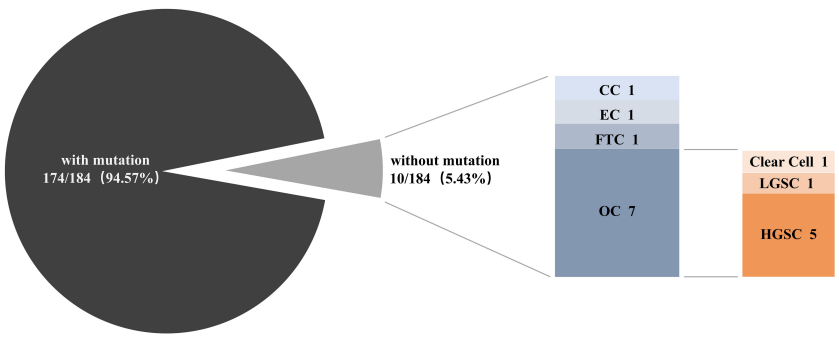


FIGURE 1
The proportion of patients with and without mutations. Next-generation sequencing was performed among 184 gynecological cancer patients to detect genomic alterations. OC, ovarian cancer; CC, cervical cancer; EC, endometrial cancer; FTC, fallopian tube cancer; LGSC, low-grade serous cancer; HGSC, high-grade serous cancer.

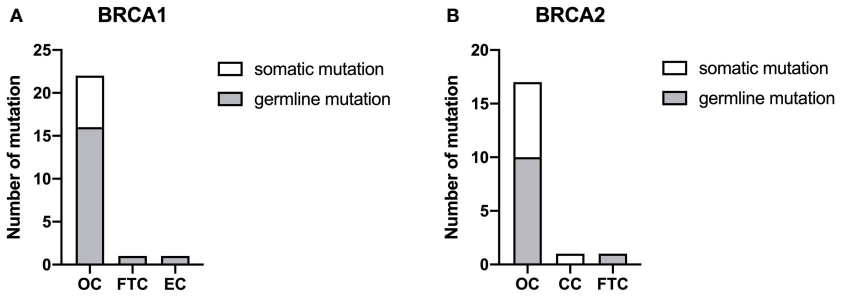


FIGURE 3
The proportion of *BRCA*1 **(A)** and *BRCA2* **(B)** mutations. Somatic and germline mutations were respectively detected by next-generation sequencing among the different types of gynecological cancer. OC, ovarian cancer; CC, cervical cancer; EC, endometrial cancer; FTC, fallopian tube cancer.

statistical outliers (TMB = 192.35) was removed. The median TMB for all remaining patients was 2.94 (1.34–5.17). We ranked the TMB values from the lowest to highest and classified them into low, moderate, and high categories using quantiles ≤ 25%, 25–75%, and ≥75%, respectively. The ratio for TMB-low, TMB-moderate, and TMB-high was 32.79% (60/183), 54.64% (100/183), and 12.57% (23/183), respectively. No difference was observed between the median of the four gynecological cancer types ($p$ = 0.200, Table 2); however, patients with EC tended to have a higher ratio of TMB-high values. Further analysis of TMB among patients with OC is shown in Supplementary Table 3. No correlation was observed between TMB and age, tumor size, menopausal status, metastasis, or FIGO stage (data not shown). Further, we analyzed the association between TMB and the top 10 most frequently changed genes in Figure 2. Compared with the wild-type, significant differences were discovered in the median of TMBs among patients with *TP53*, *PIK3CA*, *PTEN*, and *FGFR3* mutations ($p < 0.05$, Figure 4).

## 3.5 Enrichment analysis and protein interaction

In this cohort, 529 SNVs and 132 insertions and InDels were detected, which accounted for the majority of mutations (661/861, 76.77%). Therefore, we performed an overlap analysis of the SNVs- and insertions and InDels-associated 29 genes. The KEGG and GO analyses of these genes are shown in Figure 5. A significant cross was discovered between the enriched pathways of gynecological and breast cancers (Figure 5A). Enrichment also revealed potential resistance to epidermal growth factor receptor (EGFR) tyrosine kinase inhibitors, endocrine, and platinum drugs. The top five enriched GO terms in biological processes, cellular components, and molecular functions are listed according to their $p$ values (Figure 5B). Results showed that the mutated genes were crucial for neuronal apoptosis and DNA repair, as well as normal cell cycle. Protein interaction analysis identified *TP53* as a crucial protein in the network (Figure 6A). *SRC, RB1, CREBBP, ARID1A, SMARCA4, BRCA1*, and *ATM* also contributed significantly to the interaction net. Chilibot analysis showed that most of these mutated genes had stimulatory or inhibitory relationships with different gynecological cancers (Figure 6B).

# 4 Discussion

Gynecological cancers are among the most common malignancies with significant morbidity and mortality, primarily classified into five major types according to the organ affected (38, 39). In this retrospective study, we investigated 184 Chinese patients with gynecological cancer using NGS. Patients with OC, CC, EC, and FTC shared similarities but also varied both in clinical characterization and genomic landscape. It is worth noting that our research also has some limitations. Firstly, consistent with their clinical incidence, the numbers of patients with CC, EC, and FTC were limited in this study. Therefore, the relevant statistical results among patients with OC were more informative. Secondly, no overall survival data are provided at this time since the most recent patient enrolled was in June 2022. Therefore, this study may provide preliminary information for the clinical features and

TABLE 2 Tumor mutational burden of the population in this study.

| | OC | CC | FTC | EC | $p$ value |
|---|---|---|---|---|---|
| | (n = 139) | (n = 12) | (n = 8) | (n = 24) | |
| Median | 2.94 (1.30-5.17) | 2.10 (0.00-6.02) | 2.76 (1.91-4.19) | 3.85 (2.56-7.44) | $p$=0.200 |
| Low | 50 (35.97%) | 6 (50.00%) | 2 (25.00%) | 2 (8.33%) | |
| Moderate | 74 (53.24%) | 4 (33.33%) | 6 (75.00%) | 16 (66.67%) | |
| High | 15 (10.79%) | 2 (16.67%) | 0 (0.00%) | 6 (25.00%) | |

OC, ovarian cancer; CC, cervical cancer; EC, endometrial cancer; FTC, fallopian tube cancer.

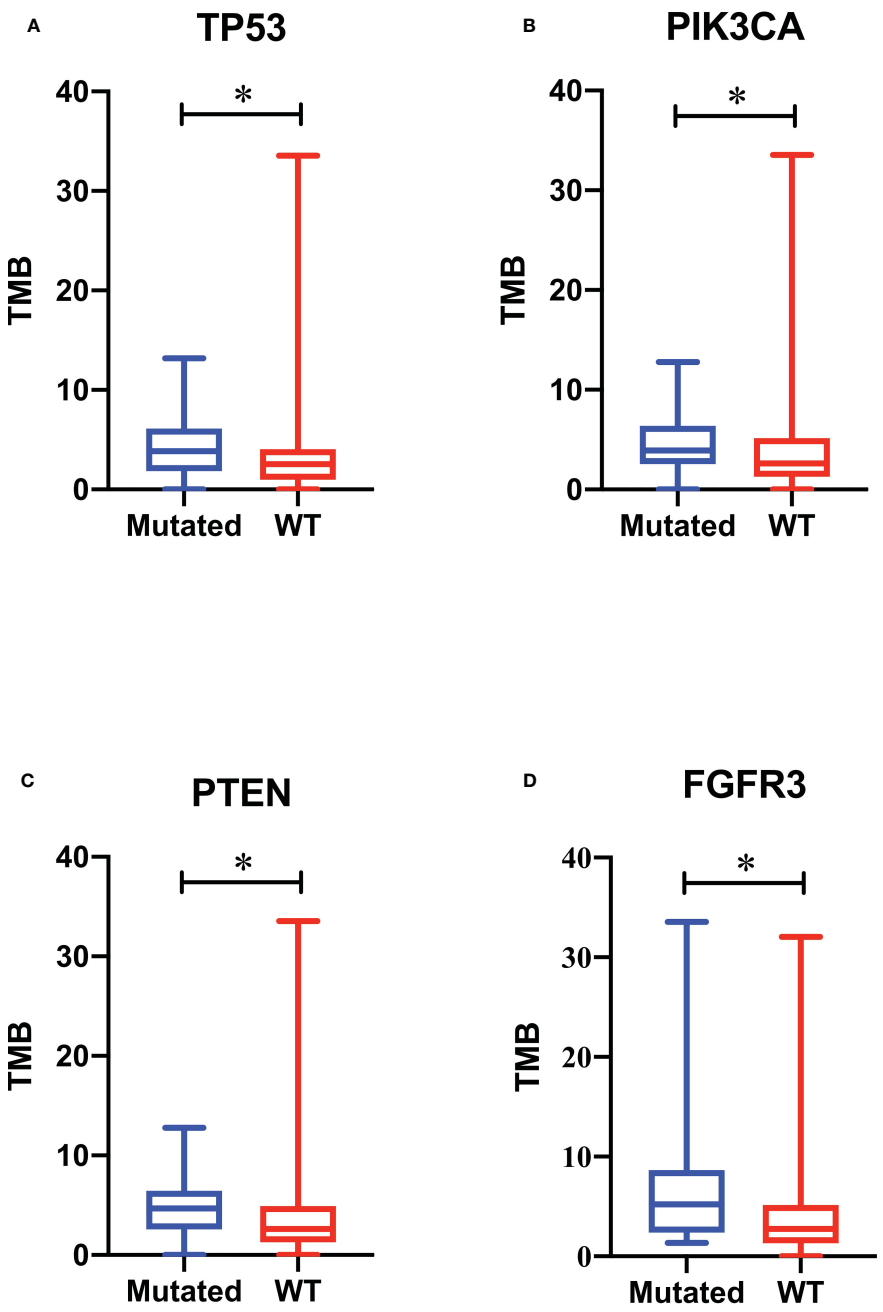


FIGURE 4
Association of gene mutations with tumor mutational burden (TMB). TMB values of patients with *TP53* **(A)**, PIK3CA **(B)**, *PTEN* **(C)**, and *FGFR3* **(D)** mutations are respectively compared with those of patients with wild-type genes. A box plot was used to show the minimum, maximum, median, and interquartile range of the TMB values. The blue box represents patients with mutations, and the red box represents patients with wild-type genes. * $p < 0.05$.

mutations of different types of gynecological tumors, and offer new ideas for future clinical treatment and targeted drug development.

It was reported that women with hereditary breast cancer have a 30–50% chance of developing OC (40). All the patients with a family and personal history of cancer in this study were diagnosed with OC, especially those with breast cancer. Our KEGG enrichment results also showed a significant cross between gynecological cancers and breast cancer (Figure 5A). Therefore, for persons with family history, especially with breast cancer history, it is crucial they undergo gynecological tumor gene screening as early as possible.

NGS technology gives us an opportunity to rapidly sequence multiple genes simultaneously and discover relevant mutations to guide treatment, which is beneficial in the field of precision or personalized medicine (41). *TP53*, the most frequently mutated gene in OC and FTC in our study (Figure 2), was reported in 1979 as the earliest gene to be associated with gynecological cancer (42). Consistently, an analysis from The Cancer Genome Atlas

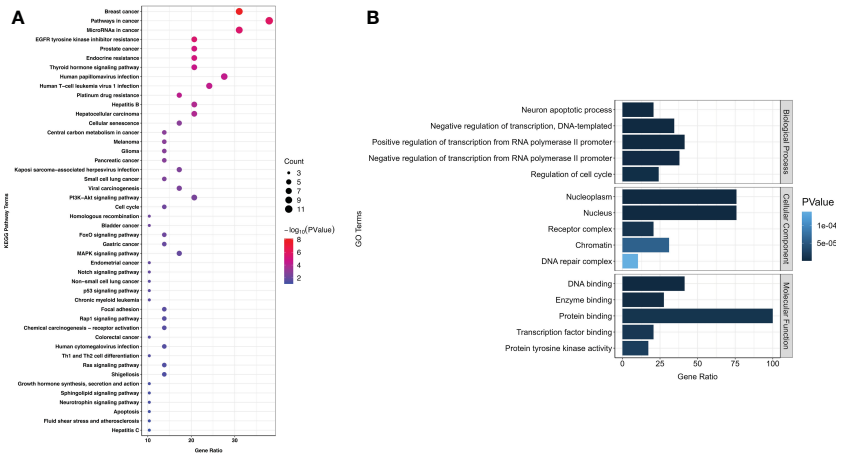


FIGURE 5
KEGG **(A)** and GO **(B)** enrichment among 184 patients with gynecological cancer. Next-generation sequencing was performed to detect mutations. Overlap of SNVs- and insertions and InDels-associated 29 genes was conducted for KEGG and GO enrichment. The size of each dot in KEGG enrichment indicates the number of genes included. The bigger the dot, the more genes are involved in the pathway. The top five GO enrichments are listed according to their *p* values.

demonstrated that 96% HGSC was characterized by *TP53* mutation (43). *KMT2C* and *FGFR3* mutations had higher frequencies among the patients with CC in our study (Figure 2), of which FGFR3-TACC3 fusion was recently reported to be a potential molecular mechanism for inducing small cell cervical carcinoma (44). *PTEN* overexpression was suggested to promote morular differentiation in EC (45), but our results showed that *PTEN* deletion also played an important role (Figure 2). SNV was the most common mutation in our study, followed by insertions and InDels. A combination of these mutation-associated genes and the top 10 most frequent mutations will constitute the potential multi-gene panel to screen gynecological cancers.

*BRCA1* and *BRCA2* mutations are related to the DNA double-strand break repair process, which is also demonstrated in the GO enrichment result (Figure 5B). The process will not proceed normally when these two genes mutate, and the upstream codon will be converted to a stop codon and thus affect the protein formation (40). *BRCA* gene mutations are also indicators for PARP inhibitor (43, 46) and chemotherapy treatment (47). To the best of our knowledge, the mutation hotspot in *BRCA2* (I770) discovered in our study is the first

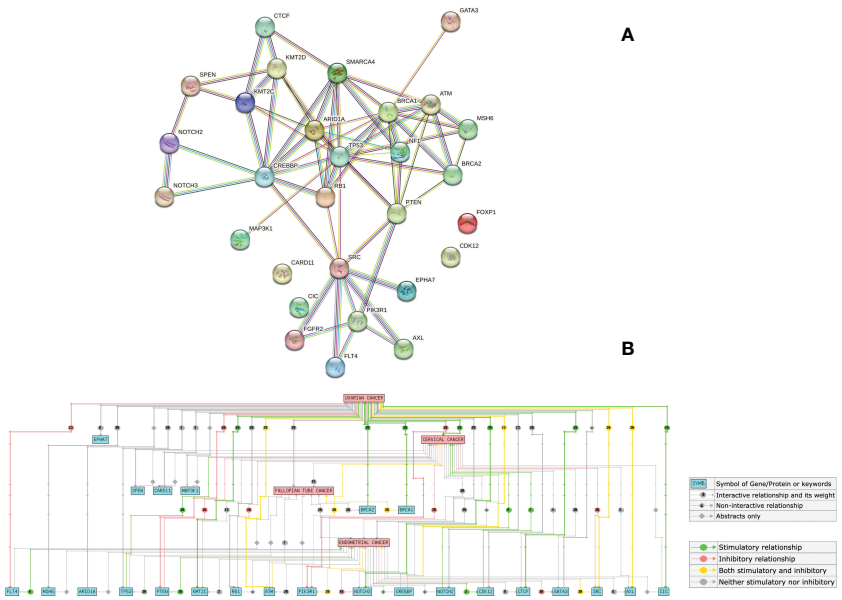


FIGURE 6
Interaction between mutated genes. Overlap analysis of SNVs- and insertions and InDels-associated 29 genes were performed on STRING **(A)** and Chilibot **(B)**. A confidence of 0.7 was used to analyze functional interactions on the STRING website. "Ovarian cancer", "cervical cancer", "fallopian tube cancer", and "endometrial cancer" were used as keywords on Chilibot to analyze the interaction between genes and different gynecological cancers, excluding abstract co-occurrence relationships.

reported among Chinese patients with gynecological cancer (48–50). Patients with *BRCA2* mutations have a better prognosis than those with *BRCA1* mutations (51).

Comprehensive understanding of factors associated with genomic instability is crucial for improving our knowledge of carcinogenesis. TMB is defined as the total number of somatic coding mutations, base substitutions, and insertion–deletion errors per million bases (52). Recently, researchers have identified the crucial role of TMB in response to immunotherapy and patient prognosis (53, 54). Higher TMB is associated with higher-grade, advanced clinical stage, and immunosuppressive phenotypes (55). According to our results, patients with EC (Table 2) and mucinous carcinoma (Supplementary Table 3) tended to have a higher ratio of TMB-high values. Zhu et al. also documented that the TMB of mucinous tumors in their study was higher than that of HGSC and LGSC (56). However, limited by the sample sizes in our study, more patient data in a larger cohort will be collected to verify this conclusion. A TMB value ≥75% level is usually defined as TMB-high (57), and there were 23 (12.57%) patients with TMB-high in this study. Pre-menopause was found to contribute significantly to higher TMB values among these 23 patients ($p < 0.05$, data not shown). Genomic alterations are also documented to be associated with TMB. In this study, besides the most frequently altered genes *TP53*, *PKI3CA*, and *PTEN*, patients with *FGFR3* mutations also tended to have higher TMB values than those with wild-type genes (Figure 4). Erdafitinib has been approved for patients with urothelial carcinomas with select *FGFR3* mutations (58). Therefore, *FGFR3* may also become a potential target for patients with gynecological cancers.

## 5 Conclusions

In summary, our study elucidated the distinct genomic landscapes of various types of gynecological cancers. Taken together with the results of TMB and enriched pathways, this study preliminarily sheds light on the molecular mechanisms of gynecological cancers, and the information gained may contribute to the development of targeted drugs and clinical treatment in precision medicine. Further large-scale and multi-center studies will be performed to validate our findings.

## Data availability statement

The original contributions presented in the study are included in the article/Supplementary Material. Further inquiries can be directed to the corresponding authors.

## Ethics statement

The studies involving human participants were reviewed and approved by Ethics Committee of the Ruijin Hospital, Shanghai Jiao Tong University School of Medicine. The patients/participants provided their written informed consent to participate in this study.

## Author contributions

CJ and LL contributed to study conception and design. HL and WF performed surgeries and enrollment of patients. CJ and YL conducted patient recruitment, data collection and sequencing. ZP and GC performed bioinformatics analysis. CJ and YL drafted the manuscript. WF and LL revised the manuscript. All authors contributed to the article and approved the submitted version.

## Funding

The study is supported by Shanghai "Rising Stars of Medical Talents" youth clinical laboratory practitioner program (SHWRS (2020)_87).

## Acknowledgments

We would like to thank the patients who gave their consent to present data in this study, as well as the investigators and research staff.

## Conflict of interest

ZP is an employee of Genecast Biotechnology Co., Ltd., Wuxi, China.

The remaining authors declare that the research was conducted in the absence of any commercial or financial relationships that could be construed as a potential conflict of interest.

## Publisher's note



## Supplementary material

The Supplementary Material for this article can be found online at: https://www.frontiersin.org/articles/10.3389/fonc.2023.1143876/full#supplementary-material

# References


1. Wang N, Yang Y, Jin D, Zhang Z, Shen K, Yang J, et al. PARP inhibitor resistance in breast and gynecological cancer: Resistance mechanisms and combination therapy strategies. *Front Pharmacol* (2022) 13:967633. doi: 10.3389/fphar.2022.967633

2. Suszynska M, Klonowska K, Jasinska AJ, Kozlowski P. Large-Scale meta-analysis of mutations identified in panels of breast/ovarian cancer-related genes - providing evidence of cancer predisposition genes. *Gynecol Oncol* (2019) 153(2):452–62. doi: 10.1016/j.ygyno.2019.01.027

3. Caro AA, Deschoemaeker S, Allonsius L, Coosemans A, Laoui D. Dendritic cell vaccines: A promising approach in the fight against ovarian cancer. *Cancers (Basel)* (2022) 14(16):4037. doi: 10.3390/cancers14164037

4. Chelariu-Raicu A, Coleman RL. Breast cancer (*BRCA*) gene testing in ovarian cancer. *Chin Clin Oncol* (2020) 9(5):63. doi: 10.21037/cco-20-4

5. American Cancer Society- Cancer Facts and Figures. (2019). Available at: https://www.cancer.org/research/cancer-facts-statistics/all-cancer-facts-figures/cancer-facts-figures-2019.html.

6. Lalwani N, Prasad SR, Vikram R, Shanbhogue AK, Huettner PC, Fasih N. Histologic, molecular, and cytogenetic features of ovarian cancers: Implications for diagnosis and treatment. *Radiographics* (2011) 31(3):625–46. doi: 10.1148/rg.313105066

7. Siegel RL, Miller KD, Fuchs HE, Jemal A. Cancer statistics, 2022. *CA Cancer J Clin* (2022) 72(1):7–33. doi: 10.3322/caac.21708

8. Wen H, Guo QH, Zhou XL, Wu XH, Li J. Genomic profiling of Chinese cervical cancer patients reveals prevalence of DNA damage repair gene alterations and related hypoxia feature. *Front Oncol* (2022) 11:792003. doi: 10.3389/fonc.2021.792003

9. Maluf FC, Dal Molin GZ, de Melo AC, Paulino E, Racy D, Ferrigno R, et al. Recommendations for the prevention, screening, diagnosis, staging, and management of cervical cancer in areas with limited resources: Report from the international gynecological cancer society consensus meeting. *Front Oncol* (2022) 12:928560. doi: 10.3389/fonc.2022.928560

10. Siegel RL, Miller KD, Fuchs HE, Jemal A. Cancer statistics, 2021. *CA Cancer J Clin* (2021) 71(1):7–33. doi: 10.3322/caac.21654

11. Fidler MM, Gupta S, Soerjomataram I, Ferlay J, Steliarova-Foucher E, Bray F. Cancer incidence and mortality among young adults aged 20-39 years worldwide in 2012: a population-based study. *Lancet Oncol* (2017) 18(12):1579–89. doi: 10.1016/S1470-2045(17)30677-0

12. Cohen PA, Jhingran A, Oaknin A, Denny L. Cervical cancer. *Lancet* (2019) 393 (10167):169–82. doi: 10.1016/S0140-6736(18)32470-X

13. Davies-Oliveira JC, Round T, Crosbie EJ. Cervical screening: The evolving landscape. *Br J Gen Pract* (2022) 72(721):364–65. doi: 10.3399/bjgp22X720197

14. Li Y, Feng J, Zhao C, Meng L, Shi S, Liu K, et al. A new strategy in molecular typing: the accuracy of an NGS panel for the molecular classification of endometrial cancers. *Ann Transl Med* (2022) 10(16):870. doi: 10.21037/atm-22-3446

15. Sung H, Ferlay J, Siegel RL, Laversanne M, Soerjomataram I, Jemal A, et al. Global cancer statistics 2020: GLOBOCAN estimates of incidence and mortality worldwide for 36 cancers in 185 countries. *CA Cancer J Clin* (2021) 71:209–49. doi: 10.3322/caac.21660

16. Kasius JC, Pijnenborg JMA, Lindemann K, Forsse D, van Zwol J, Kristensen GB, et al. Risk stratification of endometrial cancer patients: FIGO stage, biomarkers and molecular classification. *Cancers (Basel)* (2021) 13:5848. doi: 10.3390/cancers13225848

17. Urick ME, Bell DW. Clinical actionability of molecular targets in endometrial cancer. *Nat Rev Cancer* (2019) 19:510–21. doi: 10.1038/s41568-019-0177-x

18. Clarfield L, Diamond L, Jacobson M. Risk-reducing options for high-grade serous gynecologic malignancy in BRCA1/2. *Curr Oncol* (2022) 29(3):2132–40. doi: 10.3390/curroncol29030172

19. Hong JH, Cho HW, Ouh YT, Lee JK, Chun Y, Gim JA. Genomic landscape of advanced endometrial cancer analyzed by targeted next-generation sequencing and the cancer genome atlas (TCGA) dataset. *J Gynecol Oncol* (2022) 33(3):e29. doi: 10.3802/jgo.2022.33.e29

20. Feng W, Jia N, Jiao H, Chen J, Chen Y, Zhang Y, et al. Circulating tumor DNA as a prognostic marker in high-risk endometrial cancer. *J Transl Med* (2021) 19(1):51. doi: 10.1186/s12967-021-02722-8

21. Stasenko M, Fillipova O, Tew WP. Fallopian tube carcinoma. *J Oncol Pract* (2019) 15(7):375–82. doi: 10.1200/JOP.18.00662

22. Maeda M, Hisa T, Matsuzaki S, Ohe S, Nagata S, Lee M, et al. Primary fallopian tube carcinoma presenting with a massive inguinal tumor: A case report and literature review. *Medicina (Kaunas)* (2022) 58(5):581. doi: 10.3390/medicina58050581

23. Lõhmussaar K, Kopper O, Korving J, Begthel H, Vreuls CPH, van Es JH, et al. Assessing the origin of high-grade serous ovarian cancer using CRISPR-modification of mouse organoids. *Nat Commun* (2020) 11(1):2660. doi: 10.1038/s41467-020-16432-0

24. Liao CI, Chow S, Chen LM, Kapp DS, Mann A, Chan JK. Trends in the incidence of serous fallopian tube, ovarian, and peritoneal cancer in the US. *Gynecol Oncol* (2018) 149(2):318–23. doi: 10.1016/j.ygyno.2018.01.030

25. Choi MC, Bae JS, Jung SG, Park H, Joo WD, Song SH, et al. Prevalence of germline *BRCA* mutations among women with carcinoma of the peritoneum or fallopian tube. *J Gynecol Oncol* (2018) 29(4):e43. doi: 10.3802/jgo.2018.29.e43

26. Shah S, Cheung A, Kutka M, Sheriff M, Boussios S. Epithelial ovarian cancer: Providing evidence of predisposition genes. *Int J Environ Res Public Health* (2022) 19 (13):8113. doi: 10.3390/ijerph19138113

27. Vicus D, Finch A, Cass I, Rosen B, Murphy J, Fan I, et al. Prevalence of *BRCA1* and *BRCA2* germ line mutations among women with carcinoma of the fallopian tube. *Gynecol Oncol* (2010) 118(3):299–302. doi: 10.1016/j.ygyno.2010.05.011

28. Poveda A, Floquet A, Ledermann JA, Asher R, Penson RT, Oza AM, et al. Olaparib tablets as maintenance therapy in patients with platinum-sensitive relapsed ovarian cancer and a *BRCA1/2* mutation (SOLO2/ENGOT-Ov21): a final analysis of a double-blind, randomised, placebo-controlled, phase 3 trial. *Lancet Oncol* (2021) 22 (5):620–31. doi: 10.1016/S1470-2045(21)00073-5

29. Liu J, Li Z, Lu T, Pan J, Li L, Song Y, et al. Genomic landscape, immune characteristics and prognostic mutation signature of cervical cancer in China. *BMC Med Genomics* (2022) 15(1):231. doi: 10.1186/s12920-022-01376-9

30. Imyanitov E, Sokolenko A. Integrative genomic tests in clinical oncology. *Int J Mol Sci* (2022) 23(21):13129. doi: 10.3390/ijms232113129

31. Jiang T, Jiang L, Dong X, Gu K, Pan Y, Shi Q, et al. Utilization of circulating cell-free DNA profiling to guide first-line chemotherapy in advanced lung squamous cell carcinoma. *Theranostics* (2021) 11(1):257–67. doi: 10.7150/thno.51243

32. Li H. *Aligning sequence reads, clone sequences and assembly contigs with BWA-MEM*. arXiv preprint (2013). doi: 10.48550/arXiv.1303.3997

33. Lai Z, Markovets A, Ahdesmaki M, Chapman B, Hofmann O, McEwen R, et al. VarDict: a novel and versatile variant caller for next-generation sequencing in cancer research. *Nucleic Acids Res* (2016) 44(11):e108. doi: 10.1093/nar/gkw227

34. Garrison E, Marth G. *Haplotype-based variant detection from short-read sequencing*. arXiv preprint (2012). doi: 10.48550/arXiv.1207.3907

35. Wang K, Li M, Hakonarson H. ANNOVAR: Functional annotation of genetic variants from high-throughput sequencing data. *Nucleic Acids Res* (2010) 38(16):e164. doi: 10.1093/nar/gkq603

36. Karczewski KJ, Weisburd B, Thomas B, Solomonson M, Ruderfer DM, Kavanagh D, et al. The ExAC browser: Displaying reference data information from over 60 000 exomes. *Nucleic Acids Res* (2017) 45(D1):D840–5. doi: 10.1093/nar/gkw971

37. Karczewski KJ Francioli L. The genome aggregation database (gnomAD). *MacArthur Lab* (2017). Available at: https://macarthurlab.org/2017/02/27/the-genome-aggregation-database-gnomad/

38. Chalmers ZR, Connelly CF, Fabrizio D, Gay L, Ali SM, Ennis R, et al. Analysis of 100,000 human cancer genomes reveals the landscape of tumor mutational burden. *Genome Med* (2017) 9(1):34. doi: 10.1186/s13073-017-0424-2

39. Daoud T, Sardana S, Stanietzky N, Klekers AR, Bhosale P, Morani AC. Recent imaging updates and advances in gynecologic malignancies. *Cancers (Basel)* (2022) 14 (22):5528. doi: 10.3390/cancers14225528

40. Therachiyil L, Anand A, Azmi A, Bhat A, Korashy HM, Uddin S. Role of RAS signaling in ovarian cancer. *F1000Res* (2022) 11:1253. doi: 10.12688/f1000research.126337.1

41. Xie C, Luo J, He Y, Jiang L, Zhong L, Shi Y. *BRCA2* gene mutation in cancer. *Med (Baltimore)* (2022) 101(45):e31705. doi: 10.1097/MD.0000000000031705

42. Johansen EL, Thusgaard CF, Thomassen M, Boonen SE, Jochumsen KM. Germline pathogenic variants associated with ovarian cancer: A historical overview. *Gynecol Oncol Rep* (2022) 44:101105. doi: 10.1016/j.gore.2022.101105

43. Kanchi KL, Johnson KJ, Lu C, McLellan MD, Leiserson MD, Wendl MC, et al. Integrated analysis of germline and somatic variants in ovarian cancer. *Nat Commun* (2014) 5:3156. doi: 10.1038/ncomms4156

44. Cancer Genome Atlas Research Network. Integrated genomic analyses of ovarian carcinoma. *Nature* (2011) 474(7353):609–15. doi: 10.1038/nature10166

45. Wang X, Jia W, Wang M, Liu J, Zhou X, Liang Z, et al. Human papillomavirus integration perspective in small cell cervical carcinoma. *Nat Commun* (2022) 13 (1):5968. doi: 10.1038/s41467-022-33359-w

46. Yokoi A, Minami M, Hashimura M, Oguri Y, Matsumoto T, Hasegawa Y, et al. PTEN overexpression and nuclear β-catenin stabilization promote morular differentiation through induction of epithelial-mesenchymal transition and cancer stem cell-like properties in endometrial carcinoma. *Cell Commun Signal* (2022) 20 (1):181. doi: 10.1186/s12964-022-00999-w

47. Li N, Liu Q, Tian Y, Wu L. Overview of fuzuloparib in the treatment of ovarian cancer: Background and future perspective. *J Gynecol Oncol* (2022) 33(6):e86. doi: 10.3802/jgo.2022.33.e86

48. Vencken PMLH, Kriege M, Hoogwerf D, Beugelink S, van der Burg MEL, Hooning MJ, et al. Chemosensitivity and outcome of *BRCA1*- and *BRCA2*-associated ovarian cancer patients after first-line chemotherapy compared with sporadic ovarian cancer patients. *Ann Oncol* (2011) 22(6):1346–52. doi: 10.1093/annonc/mdq628

49. Kwong A, Shin VY, Ma ES, Chan CT, Ford JM, Kurian AW, et al. Screening for founder and recurrent BRCA mutations in Hong Kong and US Chinese populations. *Hong Kong Med J* (2018) 24 Suppl 3(3):4–6.

50. de Juan Jiménez I, García Casado Z, Palanca Suela S, Esteban Cardeñosa E, López Guerrero JA, Segura Huerta Á, et al. Novel and recurrent *BRCA1/BRCA2* mutations in early onset and familial breast and ovarian cancer detected in the program of genetic counseling in cancer of valencian community (eastern Spain). *Relationship Family phenotypes Mutat prevalence Fam Cancer* (2013) 12(4):767–77. doi: 10.1007/s10689-013-9622-2

51. Zhang Y, Wu H, Yu Z, Li L, Zhang J, Liang X, et al. Germline variants profiling of BRCA1 and BRCA2 in Chinese hakka breast and ovarian cancer patients. *BMC Cancer* (2022) 22(1):842. doi: 10.1186/s12885-022-09943-0

52. Bolton KL, Chenevix-Trench G, Goh C, Sadetzki S, Ramus SJ, Karlan BY, et al. Association between BRCA1 and BRCA2 mutations and survival in women with invasive epithelial ovarian cancer. *JAMA* (2012) 307(4):382–90. doi: 10.1001/jama.2012.20

53. Hu-Lieskovan S, Bhaumik S, Dhodapkar K, Grivel JJB, Gupta S, Hanks BA, et al. SITC cancer immunotherapy resource document: A compass in the land of biomarker discovery. *J Immunother Cancer* (2020) 8(2):e000705. doi: 10.1136/jitc-2020-000705

54. Yarchoan M, Hopkins A, Jaffee EM. Tumor mutational burden and response rate to PD-1 inhibition. *N Engl J Med* (2017) 377(25):2500–1. doi: 10.1056/NEJMc1713444

55. Samstein RM, Lee CH, Shoushtari AN, Hellmann MD, Shen R, Janjigian YY, et al. Tumor mutational load predicts survival after immunotherapy across multiple cancer types. *Nat Genet* (2019) 51(2):202–6. doi: 10.1038/s41588-018-0312-8

56. Wang H, Liu J, Yang J, Wang Z, Zhang Z, Peng J, et al. A novel tumor mutational burden-based risk model predicts prognosis and correlates with immune infiltration in ovarian cancer. *Front Immunol* (2022) 13:943389. doi: 10.3389/fimmu.2022.943389

57. Zhu S, Zhang C, Cao D, Bai J, Yu S, Chen J, et al. Genomic and TCR profiling data reveal the distinct molecular traits in epithelial ovarian cancer histotypes. *Oncogene* (2022) 41(22):3093–103. doi: 10.1038/s41388-022-02277-y

58. Jiang T, Chen J, Xu X, Cheng Y, Chen G, Pan Y, et al. On-treatment blood TMB as predictors for camrelizumab plus chemotherapy in advanced lung squamous cell carcinoma: Biomarker analysis of a phase III trial. *Mol Cancer* (2022) 21(1):4. doi: 10.1186/s12943-021-01479-4

59. Huang RSP, Haberberger J, Harries L, Severson E, Duncan DL, Ferguson NL, et al. Clinicopathologic and genomic characterization of PD-L1 positive urothelial carcinomas. *Oncologist* (2021) 26(5):375–82. doi: 10.1002/onco.13753

frontiers | Frontiers in Oncology

TYPE Original Research
PUBLISHED 14 April 2023
DOI 10.3389/fonc.2023.1134763



OPEN ACCESS

EDITED BY
Umberto Malapelle,
University of Naples Federico II, Italy

REVIEWED BY
Kazunori Nagasaka,
The University of Tokyo, Japan
Roger Chammas,
University of São Paulo, Brazil
Min Kyu Kim,
Sungkyunkwan University, Republic of Korea
Yiran Li,
Tongji University, China

*CORRESPONDENCE
H. Uri Saragovi
Uri.Saragovi@mcgill.ca

†These authors share first authorship

SPECIALTY SECTION
This article was submitted to Gynecological Oncology, a section of the journal Frontiers in Oncology

RECEIVED 30 December 2022
ACCEPTED 24 March 2023
PUBLISHED 14 April 2023

CITATION
Galan A, Papaluca A, Nejatie A, Matanes E, Brahimi F, Tong W, Hachim IY, Yasmeen A, Carmona E, Klein KO, Billes S, Dawod AE, Gawande P, Jeter AM, Mes-Masson A-M, Greenwood CMT, Gotlieb WH and Saragovi HU (2023) GD2 and GD3 gangliosides as diagnostic biomarkers for all stages and subtypes of epithelial ovarian cancer.
*Front. Oncol.* 13:1134763.
doi: 10.3389/fonc.2023.1134763



# GD2 and GD3 gangliosides as diagnostic biomarkers for all stages and subtypes of epithelial ovarian cancer

Alba Galan[1†], Arturo Papaluca[1,2†], Ali Nejatie[1,2†], Emad Matanes[1,3], Fouad Brahimi[1], Wenyong Tong[1,2], Ibrahim Yaseen Hachim[4], Amber Yasmeen[3], Euridice Carmona[5], Kathleen Oros Klein[6,7], Sonja Billes[8], Ahmed E. Dawod[8], Prasad Gawande[8], Anna Milik Jeter[8], Anne-Marie Mes-Masson[5,9], Celia M. T. Greenwood[6,7], Walter H. Gotlieb[1,3] and H. Uri Saragovi[1,2,10*]

[1]Translational Cancer Center, Lady Davis Institute-Jewish General Hospital, McGill University, Montreal, QC, Canada, [2]Pharmacology and Therapeutics, McGill University, Montreal, QC, Canada, [3]Department of Ob-Gyn, Jewish General Hospital, McGill University and Segal Cancer Center, Lady Davis Institute of Medical Research, Montreal, QC, Canada, [4]Clinical Sciences Department, College of Medicine, University of Sharjah, Sharjah, United Arab Emirates, [5]Centre de recherche du Centre Hospitalier de l'Université de Montréal (CRCHUM) and Institut du Cancer de Montréal, Montreal, QC, Canada, [6]Division of Gynecologic Oncology, Department of Obstetrics and Gynecology, Université de Montréal, Montreal, QC, Canada, [7]Gerald Bronfman Department of Oncology, McGill University, Montreal, QC, and Department of Epidemiology, Biostatistics and Occupational Health, McGill University, Montreal, QC, Canada, [8]R&D Department, AOA Dx Inc, Cambridge, MA, United States, [9]Department of Medicine, Université de Montréal, Montreal, QC, Canada, [10]Ophthalmology and Vision Science. McGill University, Montreal, QC, Canada

**Background:** Ovarian cancer (OC) is the deadliest gynecological cancer, often diagnosed at advanced stages. A fast and accurate diagnostic method for early-stage OC is needed. The tumor marker gangliosides, GD2 and GD3, exhibit properties that make them ideal potential diagnostic biomarkers, but they have never before been quantified in OC. We investigated the diagnostic utility of GD2 and GD3 for diagnosis of all subtypes and stages of OC.

**Methods:** This retrospective study evaluated GD2 and GD3 expression in biobanked tissue and serum samples from patients with invasive epithelial OC, healthy donors, non-malignant gynecological conditions, and other cancers. GD2 and GD3 levels were evaluated in tissue samples by immunohistochemistry (n=299) and in two cohorts of serum samples by quantitative ELISA. A discovery cohort (n=379) showed feasibility of GD2 and GD3 quantitative ELISA for diagnosing OC, and a subsequent model cohort (n=200) was used to train and cross-validate a diagnostic model.

**Results:** GD2 and GD3 were expressed in tissues of all OC subtypes and FIGO stages but not in surrounding healthy tissue or other controls. In serum, GD2 and GD3 were elevated in patients with OC. A diagnostic model that included serum levels of GD2+GD3+age was superior to the standard of care (CA125, $p<0.001$) in diagnosing OC and early-stage (I/II) OC.

**Conclusion:** GD2 and GD3 expression was associated with high rates of selectivity and specificity for OC. A diagnostic model combining GD2 and GD3 quantification in serum had diagnostic power for all subtypes and all stages of OC, including early stage. Further research exploring the utility of GD2 and GD3 for diagnosis of OC is warranted.

KEYWORDS

tumor marker, diagnostic test, cancer screening, ovarian cancer, ELISA, immunohistochemistry, ganglioside, liquid and tissue biopsy

# 1 Introduction

Ovarian cancer (OC) is the most lethal gynecologic cancer and accounts for an estimated 239,000 new cases and 152,000 deaths worldwide each year (1). The current 5-year survival rate is <50%, and 15% of patients die within 2 months of diagnosis. The high mortality rate is in part related to lack of effective diagnostics because delays in diagnosis consequently delay therapeutic intervention (2, 3).

Although OC is often labeled as a silent killer, 95% of all OC patients experience symptoms for many months prior to diagnosis (4, 5). Indeed, 72% of patients with high-grade serous OC exhibit symptoms at early FIGO stages (6), and 84% consult with a doctor (2). Despite the presence of symptoms, the average delay in receiving a diagnosis is 9 months (2, 7). A delay in the diagnosis of as little as 3 months has been shown to allow cancer progression (3, 5, 8, 9) and to reduce 5-year overall survival (10).

Despite advances in treatment of OC, there continues to be a lack of early and effective diagnostic tools (11). The diagnosis of OC is commonly made using a combination of imaging (pelvic ultrasonography), tumor markers, and morphological and clinical findings. Tumor biomarkers used to aid in diagnosis include cancer antigen 125 (CA125) and human epididymis protein 4 (HE4) (4, 5, 12). However, there are currently no tumor markers that are completely specific, and all diagnostics are inadequate at detecting early-stage OC (2). Thus, the majority of women are diagnosed at late stages, and long-term OC survival rates remain low (2, 13). Improved diagnostic tools are necessary to enable earlier diagnosis and earlier treatment, which is expected to reduce morbidity and mortality, improve quality of life, and reduce health care costs.

Gangliosides are a class of sialic-acid-containing glycolipids that are expressed in plasma membranes of nearly all vertebrate cells. The GD2 and GD3 gangliosides are unique from other gangliosides in that their expression is low/absent in normal cells but high in tumor cells (14–16). GD2 and GD3 are etiological to cancer onset or progression (14, 16, 17) and cause immune suppression, allowing tumors to evade immune responses (14, 18). These features make GD2 and GD3 suitable targets for cancer therapy, and anti-ganglioside therapeutics is an expanding field.

In addition, GD2 and GD3 are shed into the extracellular environment (19–22) and may be measured in blood, which is easier to obtain than tissue biopsies. Biomarkers with these characteristics are preferred over surrogate markers such as CA125 or HE4 that are not etiological or persistent. Despite having characteristics that make them ideal biomarkers for diagnostic tests, GD2 or GD3 has not yet been explored as diagnostic markers in OC (14, 23). Additionally, the means to identify GD2- or GD3-expressing patients would facilitate the clinical use of anti-ganglioside therapeutics by selection of target-expressing patients.

The purpose of our study was to characterize the expression of GD2 and GD3 in the OC tissue and serum and to develop and validate a method to quantify GD2 and GD3 in serum. We then applied this method to develop an algorithm that would allow for the diagnosis of multiple OC subtypes and FIGO stages, including the hard-to-diagnose early stages I/II and low CA125 population.

# 2 Materials and methods

## 2.1 Tissue and blood samples

Tissue and serum samples were procured from biobank sources (see flowchart of the study in Figure 1). No individually identifiable data were used, and ethical approval was obtained from the Institutional Review Boards at each biobank: Jewish General Hospital (JGH, Montreal, QC, Canada, Protocol #15-070), the Centre de recherche du Centre hospitalier de l'Université de Montréal (CRCHUM, Montreal, QC, Canada, Protocol #BD04.002), and the commercial biobank BioIVT (Westbury, NY, USA). Informed consent was obtained from all individuals by the respective institution prior to specimen collection.

Tissue biopsy samples were collected at scheduled surgery, and all were treatment-free except for the neoadjuvant therapy (NACT) group, which received neoadjuvant chemotherapy prior to surgery. Tissue samples for immunohistochemistry were procured from JGH (n=212) and CRCHUM (n=87) for a total of N=299 samples.

Serum samples in the discovery cohort were procured from three biobanks. Samples that were procured from JGH (n=119) and CRCHUM (n=200) were not case-controlled, as there were not sufficient healthy donor samples. Healthy controls (n=60) were procured from BioIVT (total N=379) (Supplementary Table S2).

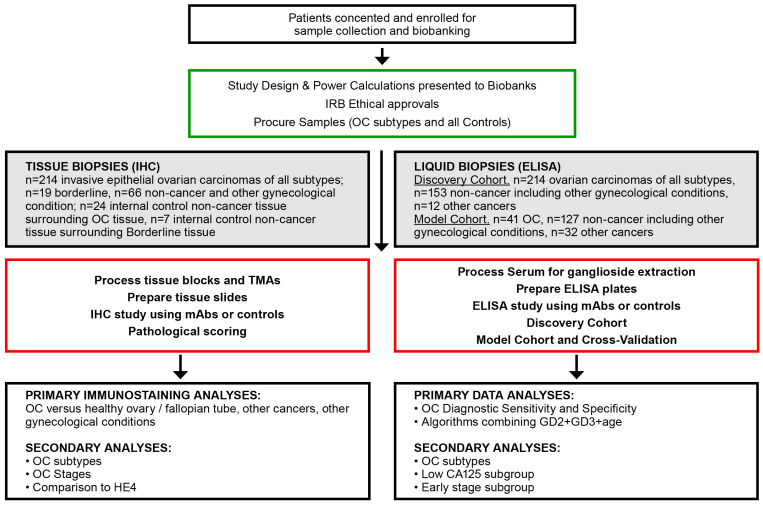


FIGURE 1
Flowchart of experimental approaches and analyses. OC, ovarian cancer; IHC, immunohistochemistry; TMA, tissue microarray; mAb, monoclonal antibody; ELISA, enzyme linked immunosorbent assay.

The model cohort (n=200) included high-quality case-controlled samples obtained from BioIVT. The model cohort only included samples of sufficient quality as defined by a documented storage age of <5 years at −80°C, and a documented maximum of one freeze–thaw cycle, to minimize sample degradation due to age and multiple freeze–thaw cycles. Serum samples were excluded if they were icteric, lipemic, and hemolytic, and had substantial particulates. Serum and tissue samples with insufficient clinical data were also excluded. Serum CA125 and HE4 levels (when available) and other clinical characteristics were obtained from clinical charts. Menopausal status was unknown for many patients; therefore, a cutoff of ≥50 years of age was used as a surrogate for post-menopausal status.

## 2.2 Antibodies

For the immunohistochemistry (IHC) tissue, anti-GD2 14G2a (BD Pharmingen, Cat. 554272, used at 1:400 or 1:1200 depending on lot), anti-GD3 R24 (Abcam, Cat. ab11779, used at 1:400 or 1:200 depending on lot), and anti-human HE4/WFDC2 antibody (R&D systems, MAB6274, used at 1:500) were used. The IHC primary incubation was overnight at 4°C, followed by washing and incubation with secondary reagents for 1–2 h at room temperature. We developed anti-GD2 mAb Clone 19 and anti-GD3 mAb Clone 6 for use in quantitative enzyme linked immunosorbent assay (ELISA) evaluation of serum (characterized in Supplementary Figure S6 and reference (17)). Secondary reagents were as follows. For flow cytometry, anti-mouse IgG conjugated to fluorescein (BD Bioscience, Cat. 554011). For ELISA, anti-mouse IgG conjugated to horseradish peroxidase (HRP) (Sigma, Cat. A0168, used at 1:1,000). For IHC, anti-mouse IgG coupled to horseradish peroxidase (HRP) (Vector Laboratories, ZF0718, used at 1:2,000).

## 2.3 Tissue sample immunohistochemistry

Tissue blocks (paraffin-embedded blocks) and microarrays were procured, and duplicated cores for each sample were studied. The tissue microarrays contained multiple OC subtypes, control healthy fallopian tube, healthy ovarian tissue, and tissue from non-malignant gynecological conditions. A summary of the samples is provided in Supplementary Table S1.

For tissue blocks, paraffin-embedded 4-µm-thick tissue sections were deparaffinized and washed in phosphate-buffered saline (PBS). For tissue microarrays and block tissue, endogenous hydrogen peroxidase and biotin were blocked with 0.3% (v/v) $H_2O_2$ and avidin/biotin blocking kit (Vector Laboratories, Cat. SP-2001), respectively. Unspecific background was blocked with blocking reagent (Vector Laboratories, BMK-2202) followed by overnight incubation with mouse-anti-GD2 mAb or mouse-anti-GD3 primary mAbs at 4°C. Sections were incubated with biotinylated anti-mouse IgG followed by streptavidin coupled to horseradish peroxidase (HRP) (Vector Laboratories, ZF0718), and reactivity was revealed by DAB reaction (Vector Laboratories, SK-4105) and counterstaining with hematoxylin/eosin (Vector Laboratories, H-3502). Sections without primary antibody were used as negative control. Images were taken using a Leica ScanScope AT turbo light microscope scanner.

The tissue from single biopsy blocks was verified pathologically to contain both tumor and healthy tissue (internal control) on the same slide. The immunoreactivity of GD2 and GD3 were reviewed and scored by blinded independent readers (one a certified pathologist) using a semi-quantitative method (24). The independent researchers had a coefficient correlation= 0.70 for GD2 and 0.77 for GD3. Samples were classified according to their intensity: no immunoreactivity (0), 1+ (weak stain), 2+ (stain), and 3+ (strong stain). Scores of 0 or 1+ were considered negative, and scores of 2+ and 3+ were considered positive (Figure 2A). The same scoring method was used for HE4.

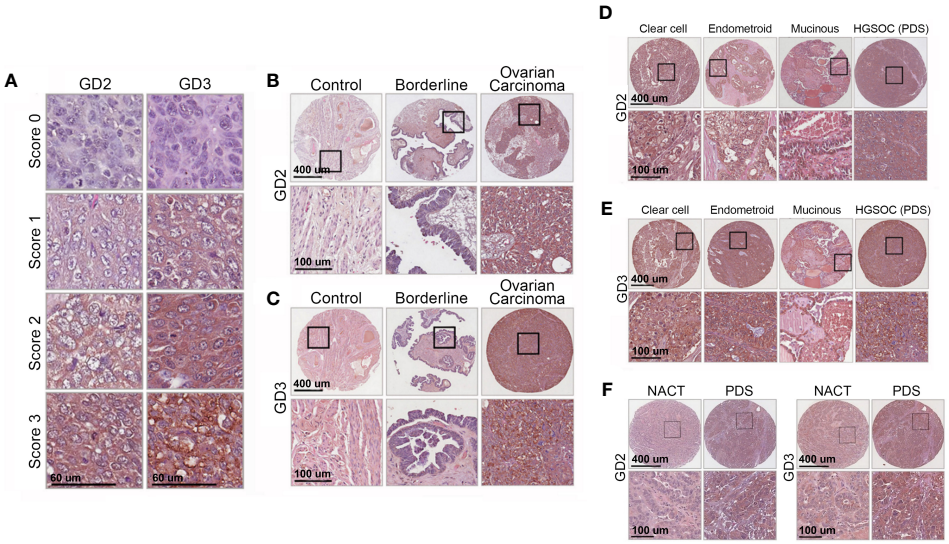


FIGURE 2
Immunohistochemistry shows high GD2 and GD3 in tissues of all OC subtypes. **(A)** Immunohistochemical detection of GD2 and GD3 in OC biopsies. Images show representative pictures of anti-GD2 and anti-GD3 antibody staining, scored as "0" (no staining), "1" (weak staining), "2" (moderate staining), and "3" (strong staining). Scores "0" and "1" were considered negative, and scores "2" and "3" were deemed positive. **(B, C)** Representative images showing GD2 and GD3 immunohistochemistry in normal, borderline ovarian tumor, and OC tissue biopsies. The bottom panels show a higher magnification of tissue within the black boxes (scale bars indicated). **(D, E)** Representative images showing GD2 and GD3 immunohistochemistry in clear cell, endometrioid, and mucinous cancer tissue biopsies, and in primary debulking surgery (PDS) cancer tissue biopsies from high-grade serous cancer (HGSOC) patients. The bottom panels show a higher magnification of tissue within the black boxes (scale bars indicated). (**F**) GD2 and GD3 immunohistochemistry in HGSOC patients with PDS or treated with neoadjuvant therapy (NACT) The bottom panels show a higher magnification of tissue within black boxes (scale bars indicated). See Table 1 for statistical comparisons and summary data.

## 2.4 Extraction of GD2 and GD3 from human serum

Gangliosides GD2 and GD3 were extracted from serum samples following modifications of a described method (18). Briefly, 100 µl of human serum was mixed with 500 µl extraction buffer of chloroform–methanol–water with a ratio of 4:8:3, followed by vigorous vortexing. The sample was centrifuged (3,000*g* for 20 min at 4°C) into aqueous and organic phases, and the aqueous phase (range between 200 and 400 µl) was transferred into a clean tube. After adding sterile water to the collected aqueous phase (for a final ratio of chloroform–methanol–water of 4:8:5.6), a second extraction was performed by repeating the steps above. Organic solvents were removed from the samples under nitrogen gas and resuspended in ethanol.

## 2.5 Indirect enzyme-linked immunosorbent assay

Enzyme-linked immunosorbent assay (ELISA) methods were modified from a previous report (17). After isolation of glycolipids by extraction, samples (10 µl/well) were immobilized onto Clear Flat-Bottom Immuno non-sterile 96-well plates (Thermo Scientific Cat. 3455 Lot X1530419), blocked for 1 h with blocking buffer (PBS+0.1% BSA) followed by three washes with 1× PBS. Wells were then incubated with primary antibodies anti-GD2 or anti-GD3 mAbs (50 µl, 1.7 nM in blocking buffer) or negative control mouse IgG. After 1 h, the wells were washed three times with 1× PBS and then incubated with horseradish peroxidase (HRP)-conjugated anti-mouse IgG secondary antibody (50 µl, 0.06 nM in blocking buffer, Sigma, Cat. A0168) for 1 h. After three washes with 1× PBS, the colorimetric reaction was visualized with 3,3′,5,5′-tetramethylbenzidine substrate solution (TMB, Sigma, Cat. 34028), and the absorbance were read at 450 nm. All tests were performed three independent times for each extracted serum, with each sample in duplicate wells. Each plate had an internal control standard curve of GD2 (Advanced Immunochemical Inc., Cat. 9-IG6-h) or standard curve of GD3 (Avanti Polar Lipids Inc., Cat. 860060) ranging from 0 to 10 ng/well. Background sample controls include non-cancer healthy donors. Background plate controls omitted primary mAb, but with all other reagents added in the proper sequence.

## 2.6 Flow cytometry

Flow cytometry was used to characterize binding activity of proprietary mAbs manufactured in-house for ELISA immunoassays. A total of $2\times10^5$ cells of EL4-GD2+ (EL4 cells expressing surface GD2 but no GD3) and EL4-GD3+ (EL4 cells expressing surface GD3 but no GD2) were studied in binding assays, as described previously (17). Negative control Jurkat and R1.1. cell lines were used, as they do not express GD2 or GD3 but express GM1 and other gangliosides. Cells were incubated for 20 min on ice with positive control anti-GD2 mAb or anti-GD3 mAb (each at 13 nM), or control IgG, followed by fluorescein-conjugated anti-mouse IgG secondary (1.8 nM, Sigma). Cells were

assessed in a flow cytometer (Becton-Dickinson) and data analyzed using CellQuest software.

## 2.7 Quantification of CA125 and HE4 from human serum

CA125 concentrations were available from clinical charts. Where CA125 concentrations were not available, CA125 were quantified using the R&D Systems/Protein Simple Instrument and the Simple Plex Human CA125/MUC16 Cartridge SPCKB-PS-000475. HE4 concentrations were quantified using R&D Systems/Protein Simple Instrument and Simple Plex Human HE4/WFDC2 Cartridge SPCKB-PS-000542).

## 2.8 Statistical analysis

The association of GD2 and GD3 expression with clinicopathological parameters was analyzed using one-sided Kruskal–Wallis test with two-sided Tukey test with significance set at $p<0.05$. One-sided Kruskal–Wallis test was used for multiple comparisons to calculate significance among groups. If Kruskal–Wallis test showed significance, a two-sided Tukey test was done to evaluate significance of specific groups. Two-sided Mann–Whitney U test was used to perform the analysis between two groups. A p-value of <0.05 was considered statistically significant. Statistical differences were calculated using Python 3.8, scipy 1.9.1, scikit-posthocs 0.7.0. Box plots were generated using GraphPad Prism version 8.0.0 for Windows, GraphPad Software, San Diego, CA, USA.

## 2.9 Model cohort power analyses for model building (receiver operating characteristic)

Our performance goal was to achieve sensitivity of 97%. A two-sided power calculation was used to determine the number of cases needed with a minimum effect of 80%, power of 80%, and confidence of 95%. The analysis indicated that 41 confirmed OC samples by histopathology would achieve these targets. Considering a 20% prevalence rate of disease, the total number of individual serum samples needed for developing a model was 200, of which 41 are samples from OC subjects confirmed by histopathology and the rest were controls. Power calculations were performed using Python 3.8, statsmodels 0.12.2.

## 2.10 Model cohort receiver operating characteristic curve analysis

Receiver operating characteristic (ROC) curves were constructed using Python 3.8, Sklearn 0.24.2 for modeling, statsmodels 0.12.2 for power analysis, scikit posthocs 0.7.0, and scipy 1.9.1 for statistical tests to evaluate the diagnostic performance of the biomarkers GD2 and GD3 and to compare with the performance of standard of care biomarkers CA125 and HE4 in ELISA assays. Logistic regression models were estimated for each marker individually and for panels of markers to differentiate between patients with and without OC. For each logistic regression model, ROC curves were constructed, and the area under the curve (AUC-ROC) was compared between two markers or panels of markers using a non-parametric method, which accounts for the correlation induced through the measurement of the two panels on the same set of patients. The area under the curve (ROC-AUC) was calculated with a 95% confidence interval. The model dataset included 200 samples, and the model was cross-validated using a k-fold method. In the overall cohort, the data were randomly divided into fivefold, maintaining a consistent case–control ratio in each subset. In the early-stage (FIGO I/II) cohort, the data were randomly divided into threefold to increase coverage of underrepresented samples. Logistic models were fit leaving out one subset in turn, and performance was evaluated in the samples left out. Multiple training iterations were performed training on k folds and testing on the last one changing the test fold in each iteration. This was repeated, leaving out each group in turn. For cross-validation experiments, an average score for each fold iteration was obtained to calculate an average AUC for each model. Performing a 1,000 k-fold cross-validation tested model stability. The ROC curves produced by the 1,000 k-fold cross-validation confirmed model stability when compared to the reported AUCs. Cross-validation controls the upward bias in estimating operating characteristics of the logistic regression model on the same set of patients from which the model was initially fitted. Discrete cutoffs for each biomarker were not used. The biomarkers were used as continuous variables in the univariate and multivariate logistic regression models, where the binary outcome being presence or absence of OC. For each logistic regression model, a model constant was determined and a weighted coefficient of each variable, which calculated a predicted probability for each patient using each of the logistic regression models, the resulting predicted probability values ranging from 0 to 1 for each model. A test result was considered negative if the predicted probability was less than a selected threshold and positive if it was greater than or equal to a selected threshold. The sensitivity and specificity for all possible predicted probability values (i.e., from 0% to 100%) were determined for each model, and the specificity at 97% sensitivity was reported. The two-sided DeLong method was used to calculate 95% CI and the difference between ROC-AUC curves (25). Sensitivity and specificity were calculated for the overall cohort (n=200) and an early-stage cohort (n=173). Confidence intervals for sensitivity, specificity, and accuracy are used the Clopper–Pearson exact method. p-values were calculated using a two-sided Fisher's exact test. For all statistical comparisons, a p-value of <0.05 was considered statistically significant.

# 3 Results

## 3.1 Immunohistochemical detection of GD2 and GD3 in ovarian cancer

A total of 299 different tissue samples (tissue blocks + microarrays) were evaluated for GD2 and GD3 expression (mean

10.3389/fonc.2023.1134763

TABLE 1 Summary of immunohistochemistry analysis of GD2 and GD3 expression in combined analysis of tissue biopsy block sections and microarrays.

| Parameters | GD2+ expression in tissue | | | GD3+ expression in tissue | | |
|---|---|---|---|---|---|---|
| | Number (positive/total) | % positive | p-value *vs.* control tissue | Number (positive/total) | % positive | p-value *vs.* control tissue |
| Diagnosis | | | | | | |
| **Ovarian Carcinoma (OC)** | (166/214) | 78 | **<0.001** | (167/214) | 78 | **<0.001** |
| HGSOC-PDS | (56/68) | 82 | | (56/68) | 82 | |
| HGSOC-NACT | (34/52) | 65 | | (33/52) | 63 | |
| Clear cell | (29/40) | 73 | | (33/40) | 83 | |
| Endometroid | (33/38) | 87 | | (30/38) | 79 | |
| Mucinous | (14/16) | 88 | | (15/16) | 94 | |
| **Borderline ovarian tumor** | (9/19) | 47 | **0.001** | (8/19) | 42 | **<0.001** |
| **Total control tissues** | (1/97) | 1 | | (1/97) | 1 | |
| **Internal control (from OC patients)** | (0/31) | 0 | | (0/31) | 0 | |
| Non-cancer surrounding OC tumors | (0/24) | 0 | | (0/24) | 0 | |
| Non-cancer surrounding borderline tumors | (0/7) | 0 | | (0/7) | 0 | |
| **External control (from other patients)** | (1/66) | 2 | | (1/66) | 2 | |
| Benign gyn condition ovary | (1/11) | 9 | | (1/11) | 9 | |
| Normal ovary | (0/24) | 0 | | (0/24) | 0 | |
| Normal fallopian tube | (0/9) | 0 | | (0/9) | 0 | |
| Normal tissue (organ not documented) | (0/7) | 0 | | (0/7) | 0 | |
| Normal endometrial tissue | (0/15) | 0 | | (0/15) | 0 | |
| OC FIGO stage | | | | | | |
| I | (42/54) | 78 | **<0.001** | (44/54) | 81 | **<0.001** |
| II | (18/21) | 86 | **<0.001** | (17/21) | 81 | **<0.001** |
| III | (87/118) | 74 | **<0.001** | (87/118) | 74 | **<0.001** |
| IV | (16/18) | 89 | **<0.001** | (16/18) | 89 | **<0.001** |
| Undefined stage | (3/3) | 100 | N/A | (3/3) | 100 | N/A |
| **Primary treatment** | | | p-value *vs* NACT | | | p-value *vs* NACT |
| PDS | (56/68) | 82 | **<0.001** | (56/68) | 82 | **<0.001** |
| NACT | (34/52) | 65 | | (33/52) | 63 | |
| **Menopausal status** | | | p-value *vs* age <50 | | | p-value *vs* age <50 |
| Ovarian carcinoma | | | | | | |
| Post-menopause (age ≥50 years) | (135/172) | 78 | 0.125 | (138/172) | 80 | 0.068 |
| Pre-menopause (age <50 years) | (31/42) | 74 | | (29/42) | 69 | |
| Borderline ovarian tumor | | | | | | |
| Post-menopause (age ≥50 years) | (7/14) | 50 | 0.479 | (6/14) | 43 | 0.437 |
| Pre-menopause (age <50 years) | (2/5) | 40 | | (2/5) | 40 | |

Final GD2 or GD3 scores are shown as a percentage (%) of samples. The total number of tissue samples (N=299) consisted of OC (n=214), borderline ovarian tumor (n=19), and control tissue (n=97). Controls included two types of normal tissues. One is "internal control" and consists of healthy tissue surrounding the OC tumor on block slides from OC patients (n=31). Another is "external control" and consists of cancer-free tissue from non-OC donors (n=66). Statistical significance ($p<0.05$) versus the indicated comparator is highlighted by bold p-values.

patient age, 59 ± 12.4 years; range, 25–91 years) (Table 1). Clinical characteristics of tissue samples used for IHC is presented in Supplementary Table S1. Among tissue block sections, GD2 and GD3 expression was identified in OC tissues (71% positive for GD2 and 63% positive for GD3). In all positive tissue block samples, GD2 and GD3 staining was restricted to tumor cells, whereas the healthy surrounding tissue was negative (Figures 2B, C). In addition, GD2 and GD3 staining was homogeneously distributed in the plasma membrane and in cytoplasmic organelles. Control tissue sections (e.g., healthy fallopian tube, healthy ovary sections, healthy endometrium) did not stain for GD2 or GD3 (Figures 2B, C). Analysis of tissue microarray IHC staining yielded similar results (Figures 2D–F). GD2 was detected in 78% of OC tissues, and GD3 was detected in 80% of OC tissues as single positive. Overall, 88% of OC tissue samples were positive for either GD2 or GD3.

A combined primary analysis was conducted for all IHC tissue (blocks and microarrays) (Table 1). GD2 or GD3 was present in 78% of OC tissues ($p<0.001$ *vs.* control). There was no statistically significant effect of menopausal status (defined as age ≥50 or <50 years) on GD2 and GD3 expression for OC or borderline ovarian tumor. Notably, fallopian tubes that were free of OC were also negative for GD2 and GD3 staining.

A secondary analysis segregated IHC tissue data by OC subtype. Expression of GD2 and GD3 was observed in all OC subtypes compared to the control tissue (Table 1; Supplementary Figure S1). There were statistically significant differences between control and all OC subtypes: high-grade serous ovarian cancer (HGSOC), clear cell, endometrioid, and mucinous (all $p<0.001$ for GD2 and GD3 *vs.* control) (Supplementary Figure S1). There were no differences in GD2 or GD3 expression between OC subtypes.

Another secondary analysis evaluated differences in GD2 and GD3 by FIGO stage. Compared to controls, GD2 or GD3 was significantly elevated in all FIGO stages, including stage I ($p<0.001$) (Table 1). There were no statistical differences among the FIGO stages. Additionally, there was a significant difference in GD2 and GD3 staining scores between OC and borderline ovarian tumors (GD2, $p=0.001$; GD3, $p<0.001$) (Supplementary Figures S1A, B).

Within the HGSOC cohort (representing an aggressive histological subtype), data were segregated for patients who received NACT as compared to patients who had primary debulking surgery (PDS). NACT had a significantly lower (63%–65%) GD2 or GD3 positive staining compared to 82% in PDS (GD2, $p=0.034$; GD3, $p=0.020$) (Table 1). Moreover, NACT biopsies had lower staining intensity for GD2 or GD3 compared to PDS (both $p<0.01$) (Supplementary Figures 1E, F; Figure 2F).

Tissue block sections and tissue microarrays were also evaluated for HE4 immunostaining (Supplementary Figure S2). Expression of HE4 was positive in 83% of OC tissue samples (Supplementary Figure S2C). Among OC subtypes, HE4 was elevated in HGSOC, clear cell, and endometrioid (all $p<0.001$ *vs.* control) but was significantly lower in the mucinous subtype (Supplementary Figure S2D). HE4 staining also spared normal ovaries, but positive staining was observed in normal fallopian tubes (Supplementary Figure S2H). HE4 was significantly elevated only for stages II–IV ($p=0.03$), was not detected in 30% of stage I cases, and had lower statistical significance compared to GD2 or GD3 (Supplementary Figure S2F).

## 3.2 Quantitative ELISA of serum in the discovery cohort showed elevated GD2 and GD3 in all stages and subtypes of ovarian cancer

As primary analyses, ELISA quantification of GD2 and GD3 in the discovery cohort revealed a statistically significant increase in serum levels of GD2 and GD3 in OC compared to healthy controls (both $p<0.001$) (Supplementary Figures S3A, C).

Three subanalyses were done. Subanalysis by OC subtypes revealed that both GD2 and GD3 were significantly elevated in the serum of all invasive OC subtypes compared to healthy donors (both $p<0.001$) (Supplementary Figures S3B, D). Subanalysis of all OC with low levels of CA125 (defined as <35 U/ml at clinical diagnosis, regardless of subtype and stage) showed that GD2 and GD3 were significantly higher compared to healthy donors ($p<0.001$) (Supplementary Figures S4A, C). Lastly, subanalysis according to OC FIGO stages showed that both GD2 and GD3 were elevated in the serum of all OC stages compared to the control (all $p<0.001$). Comparisons of OC FIGO stage to healthy donors were statistically significant for GD2 (FIGO stage I, $p=0.001$; stage II, $p=0.001$; stage III, $p=0.096$; stage IV, $p=0.001$) and for GD3 ($p=0.001$ for all stages) (Supplementary Figures S4B, D).

For specificity controls, in addition to comparing versus healthy donors (Supplementary Figures S3A, C), we evaluated sera from subjects with non-gynecological conditions most likely to be suspected of OC based on symptoms or that can be positive for CA125, as they may be represented in the populations in need of diagnostics. There was no difference in GD2 or GD3 expression between these specificity controls and healthy donors (Supplementary Figures S5A, B), and GD2 and GD3 expression was low in both groups.

## 3.3 Quantitative ELISA of serum in the model cohort showed elevated GD2 and GD3 in ovarian cancer

ELISA quantification of GD2 and GD3 in samples from the model cohort showed statistically significant elevation of GD2 and GD3 in OC compared to the control ($p<0.001$, Figure 3; Supplementary Table S3). Given that quantitative differences in GD2 and GD3 were observed between the discovery *vs.* model cohorts ($p<0.001$ for GD2 and GD3), the data from both cohorts were not combined into a single analysis. Only the data from the model cohort was used for predictive modeling.

In the primary analysis of the model cohort, there was a statistically significant overall difference between the groups for both GD2 and GD3 (both $p<0.001$) (Figure 3). There were statistically significant higher levels of GD2 and GD3 in OC samples compared to all the other groups (e.g., healthy donor,

other cancers, and other gynecological conditions) (Figure 3). Additionally, there was a statistically significant elevation of GD2 and GD3 levels in the "other (non-malignant) gynecological conditions" group *vs.* healthy donor control, but GD2 and GD3 levels remained statistically significant *vs.* OC levels (Figures 3A, C). Notably, there were statistically significant higher levels of GD2 and GD3 in OC compared to all other cancer types (Figures 3B, D).

## 3.4 A diagnostic algorithm combining GD2 and GD3 with CA125, HE4, and/or age

We trained several different predictive models for binary outcomes, including random forest, decision trees, and k-nearest neighbors on the data from the model cohort (n=200), including unbalanced class weighting in the latter two methods. Logistic regression offered the best area under the curve (AUC) in training data and was used thereafter on receiver operator curve (ROC) analysis and cross-validation. The models included GD2, GD3, CA125, HE4, and/or age as predictors in various combinations; and the AUC was calculated for each model to quantify OC detection performance for each analyte independently and in combinations (Table 2).

For the overall population (FIGO stages I–IV, n=41) compared to the control (n=159), the model was validated using the 5× cross-validation method. GD2 (AUC, 0.952) and GD3 (AUC, 0.963) each independently performed significantly better than CA125 (AUC, 0.877) (GD2, p=0.032; GD3, p<0.001) (Figure 4A).

As an important subanalysis, the model cohort was segmented for the early-stage subset (FIGO stage I/II, n=14) versus controls (n=159), and the model was 3× cross-validated. In this early-stage subset, GD2 (AUC, 0.952) and GD3 (AUC, 0.973) each independently performed significantly better than CA125 (AUC, 0.773) (GD2, p=0.033; GD3, p=0.043) (Figure 4B).

The panel combining GD2+GD3+age (AUC, 0.976) was statistically superior to CA125 (AUC, 0.877) for the overall population of the model cohort (FIGO stages I–IV, respectively, p=0.003). Additionally, for the early-stage subset (FIGO stages I–II), the panel combining GD2+GD3+age (AUC, 0.979) was statistically superior to CA125 (AUC, 0.773; p=0.006). Including CA125 and/or HE4 in the GD2+GD3+age panel did not improve predictions (p=0.100); hence, they were omitted from the report. All the analyses are summarized in Table 2.

## 3.5 Sensitivity and specificity performance of the diagnostic algorithm

Metrics were compared at different thresholds of the ROC curve, setting the sensitivity at 97.6% for all models, and performance was compared to the clinically validated threshold of 35 U/ml for CA125.

In the overall population (FIGO I–IV), a combination of GD2 +GD3+age (sensitivity of 97.6%) demonstrated superior sensitivity to CA125 (sensitivity of 63.4%) (p<0.001) with similar specificity

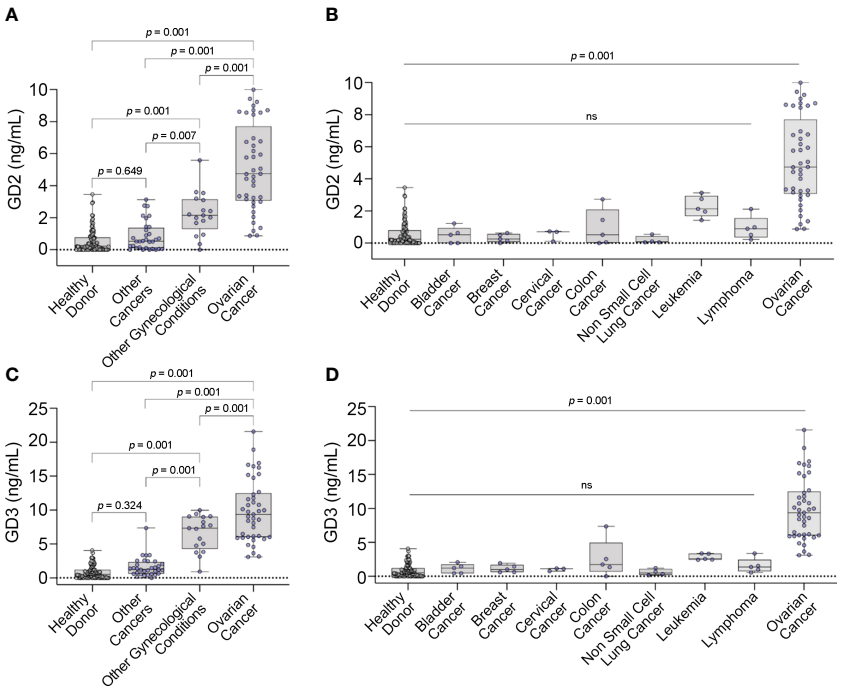


FIGURE 3
GD2 and GD3 expression in serum. Box plots displaying concentrations of **(A)** GD2 and **(C)** GD3 versus different controls. Box plots displaying concentrations of **(B)** GD2 and **(D)** GD3 with other cancers by cancer type. Box plots show median, upper and lower quartiles, and max/min values. Dots represent individual values. ns, not significant.

10.3389/fonc.2023.1134763

TABLE 2 Summary and statistics of ELISA analysis—diagnostic model and cross-validation.

| Overall predictive model (N=200) | | | | | | |
|---|---|---|---|---|---|---|
| | Predictive model AUC | 95% CI | p-value *vs.* CA125 | 5× cross-validation AUC | 95% CI | p-value *vs.* CA125 |
| CA125 | 0.876 | 0.823 – 0.942 | | 0.877 | 0.777-0.977 | |
| HE4 | 0.903 | 0.858 – 0.947 | 0.208 | 0.904 | 0.884 – 0.924 | 0.083 |
| GD2 | 0.957 | 0.928 – 0.985 | **0.010** | 0.952 | 0.922 – 0.982 | **0.032** |
| GD3 | 0.965 | 0.944 – 0.987 | **0.001** | 0.963 | 0.943 – 0.983 | **<0.001** |
| GD2, GD3, age | 0.988 | 0.977 – 0.998 | **<0.001** | 0.976 | 0.956 – 0.996 | **0.002** |
| Early-stage predictive model (N=173) | | | | | | |
| | **Predictive model AUC** | **95% CI** | **p-value *vs.* CA125** | **3× cross-validation AUC** | **95% CI** | **p-value *vs.* CA125** |
| **CA125** | 0.801 | 0.675 – 0.939 | | 0.773 | 0.613 – 0.933 | |
| **HE4** | 0.888 | 0.813 – 0.964 | 0.059 | 0.898 | 0.838 – 0.958 | 0.073 |
| **GD2** | 0.952 | 0.889 – 1.000 | **0.010** | 0.952 | 0.922 – 0.982 | **0.033** |
| **GD3** | 0.967 | 0.936 – 0.997 | **0.014** | 0.973 | 0.963 – 0.983 | **0.043** |
| **GD2, GD3, age** | 0.988 | 0.971 – 1.000 | **0.002** | 0.979 | 0.969 – 0.989 | **0.006** |

Statistical significance ($p<0.05$) indicated by bold p-values.

(91.2% and 91.8%, respectively). In the early-stage subset (FIGO I–II), both GD2+GD3+age and CA125 had similar specificity (91.2% and 91.8%, respectively), but GD2+GD3+age had a sensitivity of 100%, while CA125 had lower sensitivity (57.1%). Including CA125 and/or HE4 to the panel of GD2+GD3+age did not improve predictions for either the overall cohort (FIGO I–IV) or the early-stage subset (FIGO I–II) populations; hence, they are omitted in the report.

## 4 Discussion

We detected consistent and statistically significant increases in expression of GD2 and GD3 in tissue and serum samples from individuals with OC, for all epithelial OC subtypes and FIGO stages, compared to controls. GD2 and GD3 levels were low in all non-OC samples, including healthy tissue, other cancers, and other non-cancerous gynecological conditions. GD2 and GD3 levels were

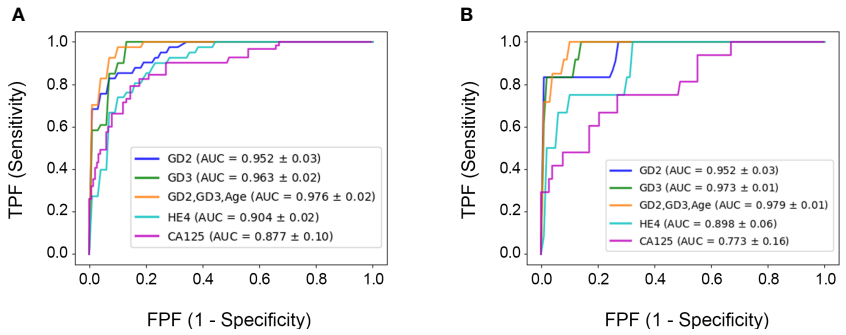


FIGURE 4
Receiver operator curves for each biomarker. **(A)** 5× cross-validation for the overall cohort. **(B)** 3× cross-validation for the segmented early-stage population. The ROC curve and diagnostic performance of GD2 and GD3 was done for all samples FIGO I–IV (n=41) or for segmented data FIGO stages I and II (n=14). The area under the curve (ROC–AUC) values for each test and the p-values of comparisons are listed in the caption and in Table 2.

significantly higher in invasive OC than in borderline (non-invasive) tumor samples.

Using quantitative data from the serum samples, we developed a diagnostic algorithm that included GD2+GD3+age, which is statistically superior in AUC to CA125 and HE4. Reportedly, tumor marker gangliosides can be found in plasma from cancer patients (20, 26), and GD3 expression in OC reportedly may play a role in ovarian cancer immune evasion (18). Our report advances the field, as it is the first study showing that quantification of gangliosides GD2 and GD3 and may be useful in the accurate diagnosis of OC.

## 4.1 GD2 and GD3 were elevated in solid tissues of ovarian cancer patients but not in healthy donors

GD2 and GD3 were detected in the tumor tissue of patients diagnosed with all subtypes of OC studied (clear cell, endometrioid, high-grade serous, low-grade serous, mucinous) and all OC FIGO stages, including early stages. Staining was homogeneously distributed in the plasma membrane and in cytoplasmic organelles, consistent with reports of the cellular distribution of GD2 and GD3 (27, 28). Furthermore, there was no effect of post-menopausal status (defined as age ≥50 years as per literature (29)) on GD2 and GD3 expression in both OC and borderline tumor samples.

Tissue block sections contained large tissue sections that included tumor tissue, and healthy surrounding tissue, e.g., fallopian tube, ovary, and endometrium, that can serve as internal control for the determination of GD2 and GD3 specificity. There was no GD2 and GD3 staining in any of the surrounding healthy tissues or in any other control tissue including fallopian tubes, indicating that GD2 and GD3 are highly selective for ovarian tumor tissue. In parallel, we conducted IHC studies for HE4. HE4 expression was not readily observed in mucinous tumors, or in 30% of stage I OC cases; furthermore, HE4 staining was detected in the normal fallopian tube tissue. These results are consistent with other reports for HE4 (30, 31) and indicate that GD2 and GD3 have higher sensitivity and specificity than HE4.

Tissues from HGSOC patients treated with debulking surgery (PDS) exhibited significantly greater scores and percent positivity for GD2 and GD3 compared to HGSOC patients also treated with chemotherapy (NACT) prior to debulking. It is unlikely that this difference is due to reduced tumor mass in HGSOC-NACT because the percentage of tumor cells in all cores was approximately 90%, regardless of treatment. Rather, we postulate that NACT may possibly reduce the overall density of GD2 or GD3 per cell in the tumor tissues. This hypothesis remains to be investigated.

In summary, GD2 and GD3 expression was detected in all OC subtypes (including mucinous) and all FIGO stages. Incorporating GD2 and GD3 immunostaining may be useful in pathological clinical practice. However, although IHC is informative, it is limited by methodological complications, including a low limit of detection, antigen loss, poor antigen stability or recovery, lack of tumor cells in the section, signal variation across laboratories, and subjective scoring. For these reasons, IHC is a qualitative assay and is rarely used for quantification. In contrast, ELISA is a sufficiently sensitive and quantitative assay where it is possible to establish a baseline that is statistically pre-determined, making it superior to IHC, and was therefore developed for quantification.

## 4.2 A serum-based ELISA quantifies elevated GD2 and GD3 in OC patients compared to healthy donors

We developed a quantitative ELISA to analyze expression of GD2 and GD3 in serum. We observed a statistically significant increase in GD2 and GD3 in OC serum samples compared to the control in both the discovery and model cohorts. Notably, the detection of GD2 and GD3 in serum by ELISA serum yielded higher AUCs than the commonly used biomarkers, CA125 and HE4. We developed an algorithm combining GD2+GD3+age that affords significant sensitivity and specificity for OC. This finding highlights the importance of evaluating multiple data points that include biomarkers and patient health information to increase diagnostic power.

The heterogeneity of ovarian cancer is a major obstacle in discovering novel biomarkers to aid early detection (32). The biomarkers CA125 (and HE4 in some jurisdictions) are typically used during the workup of patients with signs and symptoms of OC (4, 5, 12). Unfortunately, serum levels of these biomarkers often yield unclear results (31, 33). Elevated levels of CA125 are associated with a variety of common benign conditions including uterine leiomyomata, pelvic inflammatory disease, endometriosis, adenomyosis, pregnancy, and even menstruation. A normal CA125 measurement alone does not rule out OC in up to 50% of early-stage cancers and 20%–25% of advanced cancers and has an overall sensitivity and specificity of 80% and 82% (5, 34). Additionally, our results confirm the low specificity of HE4 as a single marker (30, 31). Other markers available today such as carcinoembryogenic antigen (CEA) and cancer antigen 19-9 (CA19-9) may sometimes be used in clinical practice but are not sufficiently sensitive or specific for OC.

Notably, the sensitivity of a combination of GD2+GD3+age for stages I and II (100%) was superior to the sensitivity of CA125 (57%) in the same samples while maintaining equally high specificity. This suggests that GD2 and GD3 may be highly useful in patients with OC and low CA125 levels. This is clinically relevant, as the low CA125 patients are typically harder to diagnose, and up to 50% of women in early-stage OC have normal CA125 levels (35). Indeed, CA125 as a single biomarker for OC may lead to misdiagnosis of OC due to its variability and its presence in many non-cancerous conditions.

Diagnostic algorithms are a unique strategy for improving sensitivity and specificity of diagnosis. Indeed, algorithms combining CA125+HE4 have demonstrated the greatest promise thus far (12, 36), although studies showed low specificity (37). Novel diagnostic algorithms using more sensitivity and specific biomarkers are needed to improve diagnosis accuracy and identification of early-stage OC. In our study, inclusion of CA125

and HE4 to the GD2+GD3+age panel did not improve OC detection. However, it is important to consider inclusion of other biomarkers and patient health information to increase diagnostic power.

Indeed, this is best exemplified by the performance of our algorithm combining GD2+GD3+age. Thus, other OC biomarkers that are currently in development may be considered in a panel, such as RNA (38, 39), DNA methylation (40–42), circulating tumor cells (CTCs), and circulating tumor DNA (ctDNA) (43–45), the Cu isotope, and markers within exosomes, GSTT1, FOLR1, ALDH1, and mRNAs, most likely in conjunction with CA125 (32). Successful development of such combinations would require compatibility with serum biomarkers and preferably be of low cost, allow rapid readouts, and optimally should be amenable to decentralized procedures such as the ELISA presented herein.

Aside from GD2 and GD3 being useful for us to exploit as biomarkers, we posit that the presence of GD2 and GD3 in serum suggests a biological role. Indeed, cell-bound GD2 and GD3 appear to be etiological to cancer onset or progression, lower the threshold for activation of receptor tyrosine kinases, and cause immune suppression allowing tumors to evade immune responses (14, 16, 17). Evidence that shed GD2 and GD3 are at least in part present in extracellular vesicles (ECVs) (46, 47) raises the possibility that horizontal transmission or tissue homing of GD2/3$^{+}$–ECVs may play a role in these biological processes such as immune suppression.

Limitations of this study include the overall relatively small sample size, lack of ethnic diversity, and lack of diversity of benign ovarian tumors/other gynecological conditions that are likely to be represented in the intended target population. Additionally, tissue and blood samples were obtained from three different biobanks to obtain sufficient sample sizes, and not all samples were case controlled. It is possible that different curation practices introduced potential variations depending on the collection procedure, storage conditions, and sample quality. For example, we observed a quantitative difference in GD2 and GD3 levels between the discovery and model cohorts, which are likely attributed to differences in sample quality (the discovery cohort included older samples with an undocumented number of freeze/thaw cycles), while the model cohort contained high-quality case-controlled samples. Finally, menopausal status was not available from all biobanks. Although age is commonly used when menopausal status is unknown, future studies should limit samples to those with documented menopausal status. The introduction of bias was limited by blinding the pathologists who scored the IHC results and blinding ELISA operators to the clinical diagnosis of the samples. The computer modeling used cross-validation to controls for upward bias in estimating operating characteristics of the logistic regression model. Subsequent studies are needed to specifically address more cases of benign ovarian tumors and other gynecological conditions in larger more diverse populations to afford a reliable diagnostic for this unmet clinical need.

In summary, our results demonstrate that GD2 and GD3 are elevated both in tissue and serum samples of OC. Our diagnostic modeling indicates that GD2, GD3, and age are strong candidates for building a diagnostic panel for OC. Our results are a first proof of concept that quantification of GD2 and GD3 in serum afforded significantly better sensitivity than the currently used CA125 and HE4 OC biomarkers for diagnosis of multiple OC subtypes and for all OC stages, including early-stage diagnosis. The quantification of the tumor marker ganglioside family could prove useful for the detection or prognosis of many types of cancer, in a tissue-agnostic manner, from serum. A diagnostic panel could be used in symptomatic patients to facilitate rapid early determination of malignancy, accelerate intervention, and reduce the number of individuals undergoing invasive and expensive diagnostic procedures such as exploratory laparotomy. Validation of such a test could reduce patient wait time, expedite treatments and reduce mortality due to OC.

## Data availability statement

The original contributions presented in the study are included in the article/Supplementary Material. Further inquiries can be directed to the corresponding author.

## Ethics statement

The studies involving human participants were reviewed and approved by Institutional Review Boards at each biobank. TMAs, single biopsy tissue as paraffin-embedded blocks and blood samples were procured from biobank sources. Ethical approval included the Jewish General Hospital biobank, Montreal, QC, Canada (protocol #15-070), and the CRCHUM biobank, Montreal, QC, Canada (protocol #BD04.002). All ethical approval guidelines were followed. Informed consent was obtained from all individuals by the respective institution prior to specimen collection. The patients/participants provided their written informed consent to participate in this study.

## Author contributions

AG, AP and AN conceived, planned, designed, and carried out the experiments and prepared most figures and tables. AG, AP and AN (in order of contribution) curated, analyzed, and cross-validated their data. AG, EM and IH contributed to scoring IHC. JK, KL, AB, BC, EM, AY, EC, A-MM-M, and WG curated and provided clinical serum samples for ELISA. EM, AY and WG curated and provided tissues and tumor microarray samples for IHC. FB and WT generated and characterized the mAbs. KK, CG and AD conducted statistical analysis and the cross-validation. PG, SB and AJ contributed to the analyses and interpretation of the results and prepared some figures and tables. HS generated the concept, helped design experiments, helped with the analyses, and supervised the work. HS, AJ and AG lead the organization and writing of the manuscript, and the iterative editing of versions of the manuscript had contributions primarily by AP and by SB. All authors reviewed and approved the final version of the

manuscript. AG, AP and AN share first authorship, in the order of their relative contributions. The manuscript has value only due to the cooperative and cross-validating nature of their contributions. Authors formally agreed to the order in which they are listed. All authors contributed to the article and approved the submitted version.

## Funding

For this work, HS was funded by the Reseau Quebecois pour le Medicines (RQRM) and the Canadian Institutes of Health Research (CIHR, 202104PQQ).

## Acknowledgments

The authors want to thank the outstanding technical support of Julie Lippens (National Research Council of Canada) towards the production and characterization of anti-GD2 and anti-GD3 mAbs. Dr. Susie Lau, Dr. Liron Kogan, and Dr. Shannon Salvador contributed samples and clinical histories to the JGH tumor biobank. AMMM and DP are researchers of the CRCHUM/ICM, which receive support from the Fonds de recherche du Québec—Santé (FRQS). Selected patient samples used in this study were provided by the CRCHUM ovarian tumor bank, which is supported by Ovarian Cancer Canada (OCC) and by the Banque de tissus et de données of the Réseau de recherche sur le cancer of the FRQS affiliated with the Canadian Tumor Repository Network (CTRNet). We thank Manon de Ladurantaye for assistance with the clinical data and sample selection from the CRCHUM. We thank Dr. Samantha Yee (University of Chicago) for generating the figures.

## Conflict of interest

Authors HS and WT disclose patent filings protecting claims of intellectual property and the monoclonal antibodies within this report, under License to AOA Dx where authors AJ and PG work and where HS, AD and SB served as consultants.

The remaining authors declare that the research was conducted in the absence of any commercial or financial relationships that could be construed as a potential conflict of interest.

## Publisher's note



## Supplementary material

The Supplementary Material for this article can be found online at: https://www.frontiersin.org/articles/10.3389/fonc.2023.1134763/full#supplementary-material

## References

1. Ferlay J, Soerjomataram I, Dikshit R, Eser S, Mathers C, Rebelo M, et al. Cancer incidence and mortality worldwide: Sources, methods and major patterns in GLOBOCAN 2012. *Int J Cancer* (2015) 136(5):E359–86. doi: 10.1002/ijc.29210

2. Reid F, Bhatla N, Oza AM, Blank SV, Cohen R, Adams T, et al. The world ovarian cancer coalition every woman study: Identifying challenges and opportunities to improve survival and quality of life. *Int J Gynecol Cancer* (2021) 31(2):238–44. doi: 10.1136/ijgc-2019-000983

3. Robinson KM, Ottesen B, Christensen KB, Krasnik A. Diagnostic delay experienced among gynecological cancer patients: A nationwide survey in Denmark. *Acta Obstet Gynecol Scand* (2009) 88(6):685–92. doi: 10.1080/00016340902971482

4. Goff BA, Mandel LS, Melancon CH, Muntz HG. Frequency of symptoms of ovarian cancer in women presenting to primary care clinics. *JAMA* (2004) 291 (22):2705–12. doi: 10.1001/jama.291.22.2705

5. American College of Obstetricians anf G. ACOG Committee Opinion: number 280, December 2002. The role of the generalist obstetrician-gynecologist in the early detection of ovarian cancer. *Obstet Gynecol* (2002) 100(6):1413–6. doi: 10.1016/S0029-7844(02)02630-3

6. Chan JK, Tian C, Kesterson JP, Monk BJ, Kapp DS, Davidson B, et al. Symptoms of women with high-risk early-stage ovarian cancer. *Obstet Gynecol* (2022) 139(2):157–62. doi: 10.1097/AOG.0000000000004642

7. Goff BA. Ovarian cancer is not so silent. *Obstet Gynecol* (2022) 139(2):155–6. doi: 10.1097/AOG.0000000000004664

8. Altman AD, Lambert P, Love AJ, Turner D, Lotocki R, Dean E, et al. Examining the effects of time to diagnosis, income, symptoms, and incidental detection on overall survival in epithelial ovarian cancer: Manitoba ovarian cancer outcomes (MOCO) study group. *Int J Gynecol Cancer* (2017) 27(8):1637–44. doi: 10.1097/IGC.0000000000001074

9. Sud A, Torr B, Jones ME, Broggio J, Scott S, Loveday C, et al. Effect of delays in the 2-week-wait cancer referral pathway during the COVID-19 pandemic on cancer survival in the UK: A modelling study. *Lancet Oncol* (2020) 21(8):1035–44. doi: 10.1016/S1470-2045(20)30392-2

10. Gentry-Maharaj A, Burnell M, Dilley J, Ryan A, Karpinskyj C, Gunu R, et al. Serum HE4 and diagnosis of ovarian cancer in postmenopausal women with adnexal masses. *Am J Obstet Gynecol* (2020) 222(1):56 e1– e17. doi: 10.1016/j.ajog.2019.07.031

11. Maringe C, Walters S, Butler J, Coleman MP, Hacker N, Hanna L, et al. Stage at diagnosis and ovarian cancer survival: Evidence from the international cancer benchmarking partnership. *Gynecol Oncol* (2012) 127(1):75–82. doi: 10.1016/j.ygyno.2012.06.033

12. Rosen DG, Wang L, Atkinson JN, Yu Y, Lu KH, Diamandis EP, et al. Potential markers that complement expression of CA125 in epithelial ovarian cancer. *Gynecol Oncol* (2005) 99(2):267–77. doi: 10.1016/j.ygyno.2005.06.040

13. Stedman MR, Feuer EJ, Mariotto AB. Current estimates of the cure fraction: a feasibility study of statistical cure for breast and colorectal cancer. *J Natl Cancer Inst Monogr* (2014) 2014(49):244–54. doi: 10.1093/jncimonographs/lgu015

14. Bartish M, Del Rincon SV, Rudd CE, Saragovi HU. Aiming for the sweet spot: Glyco-immune checkpoints and gammadelta T cells in targeted immunotherapy. *Front Immunol* (2020) 11:564499. doi: 10.3389/fimmu.2020.564499

15. Daniotti JL, Lardone RD, Vilcaes AA. Dysregulated expression of glycolipids in tumor cells: From negative modulator of anti-tumor immunity to promising targets for developing therapeutic agents. *Front Oncol* (2015) 5:300.

16. Gagnon M, Saragovi HU. Gangliosides: Therapeutic agents or therapeutic targets? *Expert Opin Ther Patents* (2002) 12(8):1215–23.

17. Tong W, Maira M, Roychoudhury R, Galan A, Brahimi F, Gilbert M, et al. Vaccination with tumor-ganglioside glycomimetics activates a selective immunity that affords cancer therapy. *Cell Chem Biol* (2019) 26(7):1013–26.e4.

18. Webb TJ, Li X, Giuntoli RL2nd, Lopez PH, Heuser C, Schnaar RL, et al. Molecular identification of GD3 as a suppressor of the innate immune response in ovarian cancer. *Cancer Res* (2012) 72(15):3744–52.

19. Ladisch S, Li R, Olson E. Ceramide structure predicts tumor ganglioside immunosuppressive activity. *Proc Natl Acad Sci USA* (1994) 91(5):1974–8.

20. Santin AD, Ravindranath MH, Bellone S, Muthugounder S, Palmieri M, O'Brien TJ, et al. Increased levels of gangliosides in the plasma and ascitic fluid of patients with advanced ovarian cancer. *BJOG* (2004) 111(6):613–8.

21. Bernhard H, Meyer zum Buschenfelde KH, Dippold WG. Ganglioside GD3 shedding by human malignant melanoma cells. *Int J Cancer* (1989) 44(1):155–60. doi: 10.1002/ijc.2910440127

22. Merritt WD, Der-Minassian V, Reaman GH. Increased GD3 ganglioside in plasma of children with T-cell acute lymphoblastic leukemia. *Leukemia* (1994) 8(5):816–22.

23. Yee SS, Jeter A HUS. Tumor glycolipids, a new frontier for early detection and precision medicine in ovarian cancer and other malignancies. *J Precis Med.* (2021) 7(4):66–71.

24. Orsi G, Barbolini M, Ficarra G, Tazzioli G, Manni P, Petrachi T, et al. GD2 expression in breast cancer. *Oncotarget* (2017) 8(19):31592–600. doi: 10.18632/oncotarget.16363

25. DeLong ER, DeLong DM, Clarke-Pearson DL. Comparing the areas under two or more correlated receiver operating characteristic curves: a nonparametric approach. *Biometrics* (1988) 44(3):837–45. doi: 10.2307/2531595

26. Valentino L, Moss T, Olson E, Wang HJ, Elashoff R, Ladisch S. Shed tumor gangliosides and progression of human neuroblastoma. *Blood* (1990) 75(7):1564–7. doi: 10.1182/blood.V75.7.1564.1564

27. Trinchera M, Pirovano B, Ghidoni R. Sub-Golgi distribution in rat liver of CMP-NeuAc GM3- and CMP-NeuAc:GT1b alpha 2--8sialyltransferases and comparison with the distribution of the other glycosyltransferase activities involved in ganglioside biosynthesis. *J Biol Chem* (1990) 265(30):18242–7. doi: 10.1016/S0021-9258(17)44744-2

28. Chammas R, Sonnenburg JL, Watson NE, Tai T, Farquhar MG, Varki NM, et al. De-n-acetyl-gangliosides in humans: unusual subcellular distribution of a novel tumor antigen. *Cancer Res* (1999) 59(6):1337–46.

29. Hill K. The demography of menopause. *Maturitas* (1996) 23(2):113–27. doi: 10.1016/0378-5122(95)00968-X

30. Galgano MT, Hampton GM, Frierson HF Jr. Comprehensive analysis of HE4 expression in normal and malignant human tissues. *Mod Pathol* (2006) 19(6):847–53. doi: 10.1038/modpathol.3800612

31. Leung F, Bernardini MQ, Brown MD, Zheng Y, Molina R, Bast RC Jr, et al. Validation of a novel biomarker panel for the detection of ovarian cancer. *Cancer Epidemiol Biomarkers Prev* (2016) 25(9):1333–40. doi: 10.1158/1055-9965.EPI-15-1299

32. Atallah GA, Abd Aziz NH, Teik CK, Shafiee MN, Kampan NC. New predictive biomarkers for ovarian cancer. *Diagnostics (Basel)* (2021) 11(3):465–85. doi: 10.3390/diagnostics11030465

33. Anastasi E, Granato T, Coppa A, Manganaro L, Giannini G, Comploj S, et al. HE4 in the differential diagnosis of a pelvic mass: A case report. *Int J Mol Sci* (2011) 12 (1):627–32. doi: 10.3390/ijms12010627

34. Van Gorp T, Cadron I, Despierre E, Daemen A, Leunen K, Amant F, et al. HE4 and CA125 as a diagnostic test in ovarian cancer: Prospective validation of the risk of ovarian malignancy algorithm. *Br J Cancer* (2011) 104(5):863–70. doi: 10.1038/sj.bjc.6606092

35. Muinao T, Deka Boruah HP, Pal M. Multi-biomarker panel signature as the key to diagnosis of ovarian cancer. *Heliyon* (2019) 5(12):e02826. doi: 10.1016/j.heliyon.2019.e02826

36. Yang WL, Lu Z, Bast RCJr. The role of biomarkers in the management of epithelial ovarian cancer. *Expert Rev Mol Diagn* (2017) 17(6):577–91. doi: 10.1080/14737159.2017.1326820

37. Moore RG, Brown AK, Miller MC, Skates S, Allard WJ, Verch T, et al. The use of multiple novel tumor biomarkers for the detection of ovarian carcinoma in patients with a pelvic mass. *Gynecol Oncol* (2008) 108(2):402–8. doi: 10.1016/j.ygyno.2007.10.017

38. Zou M, Du Y, Liu R, Zheng Z, Xu J. Nanocarrier-delivered small interfering RNA for chemoresistant ovarian cancer therapy. *Wiley Interdiscip Rev RNA* (2021) 12 (5):e1648. doi: 10.1002/wrna.1648

39. Gov E, Kori M, Arga KY. RNA-Based ovarian cancer research from 'a gene to systems biomedicine' perspective. *Syst Biol Reprod Med* (2017) 63(4):219–38. doi: 10.1080/19396368.2017.1330368

40. Wittenberger T, Sleigh S, Reisel D, Zikan M, Wahl B, Alunni-Fabbroni M, et al. DNA Methylation markers for early detection of women's cancer: Promise and challenges. *Epigenomics* (2014) 6(3):311–27. doi: 10.2217/epi.14.20

41. Liu MC, Oxnard GR, Klein EA, Swanton C, Seiden MV, Consortium C. Sensitive and specific multi-cancer detection and localization using methylation signatures in cell-free DNA. *Ann Oncol* (2020) 31(6):745–59. doi: 10.1016/j.annonc.2020.02.011

42. Chang CC, Wang HC, Liao YP, Chen YC, Weng YC, Yu MH, et al. The feasibility of detecting endometrial and ovarian cancer using DNA methylation biomarkers in cervical scrapings. *J Gynecol Oncol* (2018) 29(1):e17. doi: 10.3802/jgo.2018.29.e17

43. Zhou Q, Li W, Leng B, Zheng W, He Z, Zuo M, et al. Circulating cell free DNA as the diagnostic marker for ovarian cancer: A systematic review and meta-analysis. *PloS One* (2016) 11(6):e0155495. doi: 10.1371/journal.pone.0155495

44. Diaz LA Jr, Bardelli A. Liquid biopsies: genotyping circulating tumor DNA. *J Clin Oncol* (2014) 32(6):579–86. doi: 10.1200/JCO.2012.45.2011

45. Kamat AA, Baldwin M, Urbauer D, Dang D, Han LY, Godwin A, et al. Plasma cell-free DNA in ovarian cancer: An independent prognostic biomarker. *Cancer* (2010) 116(8):1918–25. doi: 10.1002/cncr.24997

46. Shenoy GN, Loyall J, Berenson CS, Kelleher RJJr., Iyer V, Balu-Iyer SV, et al. Sialic acid-dependent inhibition of T cells by exosomal ganglioside GD3 in ovarian tumor microenvironments. *J Immunol* (2018) 201(12):3750–8. doi: 10.4049/jimmunol.1801041

47. He X, Guan F, Lei L. Structure and function of glycosphingolipids on small extracellular vesicles. *Glycoconj J* (2022) 39(2):197–205. doi: 10.1007/s10719-022-10052-0

frontiers | Frontiers in Oncology

TYPE Original Research
PUBLISHED 01 May 2023
DOI 10.3389/fonc.2023.1117033



OPEN ACCESS

EDITED BY
Umberto Malapelle,
University of Naples Federico II, Italy

REVIEWED BY
Roberto C. Delgado Bolton,
Hospital San Pedro, Spain
Tasaduq H. Wani,
University of Oxford, United Kingdom
Federica Perelli,
Santa Maria Annunziata Hospital, Italy

*CORRESPONDENCE
Xiaoping Song
sxp759823394@163.com

†These authors have contributed equally to this work

RECEIVED 06 December 2022
ACCEPTED 18 April 2023
PUBLISHED 01 May 2023

CITATION
Song X, Qian D, Dai P, Li Q, Xi Q and Sun K (2023) Expression and clinical significance of NCOA5 in epithelial ovarian cancer. *Front. Oncol.* 13:1117033. doi: 10.3389/fonc.2023.1117033



# Expression and clinical significance of NCOA5 in epithelial ovarian cancer

Xiaoping Song[1*†], Da Qian[2†], Ping Dai[2†], Qian Li[1], Qiuping Xi[1] and Kailv Sun[3]

[1]Department of Gynaecology, Changshu Hospital Affiliated to Soochow University, Changshu No.1 People's Hospital, Changshu, Jiangsu, China, [2]Department of Burn and Plastic Surgery-Hand Surgery, Changshu Hospital Affiliated to Soochow University, Changshu No.1 People's Hospital, Changshu, Jiangsu, China, [3]Department of Thyroid and Breast Surgery, Changshu Hospital Affiliated to Soochow University, Changshu No.1 People's Hospital, Changshu, Jiangsu, China

**Background:** Nuclear receptor coactivator 5 (NCOA5) plays a significant role in the progression of human cancer. However, its expression in epithelial ovarian cancer (EOC) is unknown. The current study was designed to explore to investigate the clinical significance of NCOA5 and its correlation with the prognosis of EOC.

**Methods:** Immunohistochemistry was used to detect the expression of NCOA5 in 60 patients with EOC in this retrospective study and statistical analysis was performed to assess its relevance to clinicopathologic features and survival.

**Results:** NCOA5 expression was significantly higher in EOC than in normal ovarian tissues (P < 0.001). Its expression level was significantly correlated with FIGO stage (P <0. 05) and subtypes of ovarian cancer (P < 0.001), while not correlation with age , differentiation and lymph node metastasis (P>0.05). Correlation analysis showed that NCOA5 was significantly correlated with CA125 (P < 0.001) and HE4 (P < 0.01). In a Kaplan-Meier analysis of overall survival rates, the patients with low expression of NCOA5 had significantly longer survival than high expression of NCOA5 (p=0.038).

**Conclusion:** NCOA5 high expression is associated with EOC progression and can be an independent factor affecting the prognosis of EOC patients.

KEYWORDS

**NCOA5, clinical significance, survival, progression, epithelial ovarian cancer**

## Introduction

Ovarian cancer is the seventh most common cancer among women (1). Approximately 90% of ovarian cancers are EOC (2). A total of 23,000 EOC deaths were reported, the crude mortality rate was 3.37/100,000 in females in China (3). Cytoreductive surgery and chemotherapy are the main treatments for ovarian cancer (4). The prognosis and overall survival of ovarian cancer still remains poor due to late diagnosis and chemotherapy

resistance (5, 6). Effective management of epithelial ovarian cancer (EOC) requires a multidisciplinary approach from various disciplines. The multidisciplinary treatment plan may include surgery, chemotherapy, and radiation therapy, among other interventions. Multidisciplinary management of EOC patients is essential for improving the probability of a successful outcome (7). Besides, Goal of multidisciplinary treatment is to not only treat the cancer but also to manage the symptoms of patients and improve their quality of life. The molecular mechanisms of ovarian cancer have not been elucidated. Therefore, highlighting the importance of identifying molecular mechanisms that would improve the prognosis of ovarian cancer is urgently required.

The nuclear receptor coactivator 5(NCOA5), also known as coactivator independent of AF-2, can enhance ER transcription activity (8). Previous studies (9, 10) revealed that NCOA5 insufficiency increases the risk of both glucose intolerance and inflammatory phenotype, resulting in the development of hepatocellular carcinoma (HCC). Identical, NCOA5 low expression is associated with esophageal squamous cell carcinoma (11).However, previous studies have already demonstrated that NCOA5 was involved in tumorigenesis in several types of cancer including breast cancer (12) and colorectal cancer (13). In the present study, we investigated roles of NCOA5 in epithelial ovarian carcinoma.

# Materials and methods

## Patients and samples

In this retrospective study, a total of 60 specimens paraffin sections were obtained from EOC patients who have undergone cytoreductive surgery in the Changshu No.1 People's Hospital from March 2013 to May 2018 for Immunohistochemistry analysis. Meanwhile, twenty specimens paraffin sections of normal ovarian tissues were resected because of uterine or fallopian tube surgery. Pathological staging was reviewed independently by two experienced pathologists according to the 7th edition of the American Joint Committee's Cancer Staging Manual (14). Clinical information was gathered from the patient's records retrospectively. This study was approved in writing by Changshu No.1 People's Hospital's ethics committee(No.87).

## Immunohistochemistry analysis

This study used the method of Sun et al. (12) and the methods description partly reproduced their wording. Formalin-fixed and paraffin-embedded EOC tissues and normal ovarian tissues were cut into 4 μm thick sections. The sections were then deparaffinized and rehydrated. Antigen retrieval was performed by microaving the slides in 0.01 M citrate buffer (pH=6.0) for a total of 10 min. Endogenous peroxidase activity was quenched by treatment with 3% H2O2 for 30 min followed by incubation with goat serum for 15 min. Subsequently, the sections were incubated with rabbit anti-human NCOA5 (1:25; Cat. No.A300-789A, Bethyl, Montgomery, TX, USA) primary antibody in a humidity chamber overnight at 4° C. The primary antibody was omitted for a negative control. Horseradish peroxidase (HRP)-labeled anti-rabbit secondary antibody was then incubated for 1 hour at room temperature and the immunostaining signal was detected using a UltraSensitiveTM SP kit (Maxin, Fuzhou, Guangdong, China). Finally, the slides were counterstained with hematoxylin & eosin (HE) and coverslipped. Immunohistochemistry scores were independently examined by two experienced histopathologists without knowledge of clinicopathological information. The percentage of positive tumor cells and the staining intensity were used to gain the immunohistochemistry scoring. The percentage of positive tumor cells was assigned to 5 categories: ≤5% (0), 5-25% (1), 25-50% (2), 50-75% (3), and ≥75% (4). Positive cells (≤5%) were used as the cut-off to define negative tumors. The intensity of immunostaining was scored as follows: negative (0), weak (1), moderate (2), and strong (3). The percentage of positive tumor cells and staining intensity were added to produce a weighted score for each tumor specimen. The intensity scores were grouped as (-), 0-1; (+), 2-3; (++), 4-5; and (+++), 6-7. It was considered as high expression in tumor specimens when the final scores were ≥4 (++, +++) (15).

## Statistical analysis

SPSS version 23.0 (SPSS Inc., Chicago, IL, USA) and GraphPad Prism version 6.01 (GraphPad Software Inc., La Jolla, CA, USA) were performed to analyze data. Measurement data were described as ± standard deviation, and comparison between groups was performed by independent sample t test or one-way analysis of variance. Pearson correlation coefficient was used to evaluate the correlation between NCOA5 and other tumor markers. Kaplan-Meier survival curve was used to analyze the overall survival (OS) and progression-free survival (PFS) of patients with different NCOA5 expression, and Log-rank test was performed. A two-tailed p-value of less than 0.05 was considered statistically significant.

# Results

## NCOA5 expression in EOC

The study included 60 patients with clinicopathological features representative of EOC. To characterize its expression pattern in EOC, the expression of NCOA5 in human EOC tumor tissues and normal ovarian tissues was evaluated by immunohistochemistry analysis. As shown in Figures 1A–H, NCOA5 protein which was stained yellow brown was detected mainly in the nucleus. We found that NCOA5 expression was significantly higher in EOC than in normal ovarian tissues (Figure 2) ($P < 0.001$, Table 1). What calls for special attention is that the expression level of NCOA5 was significantly higher in serous ovarian cancer than in other EOC ($P<0.001$, Table 2).

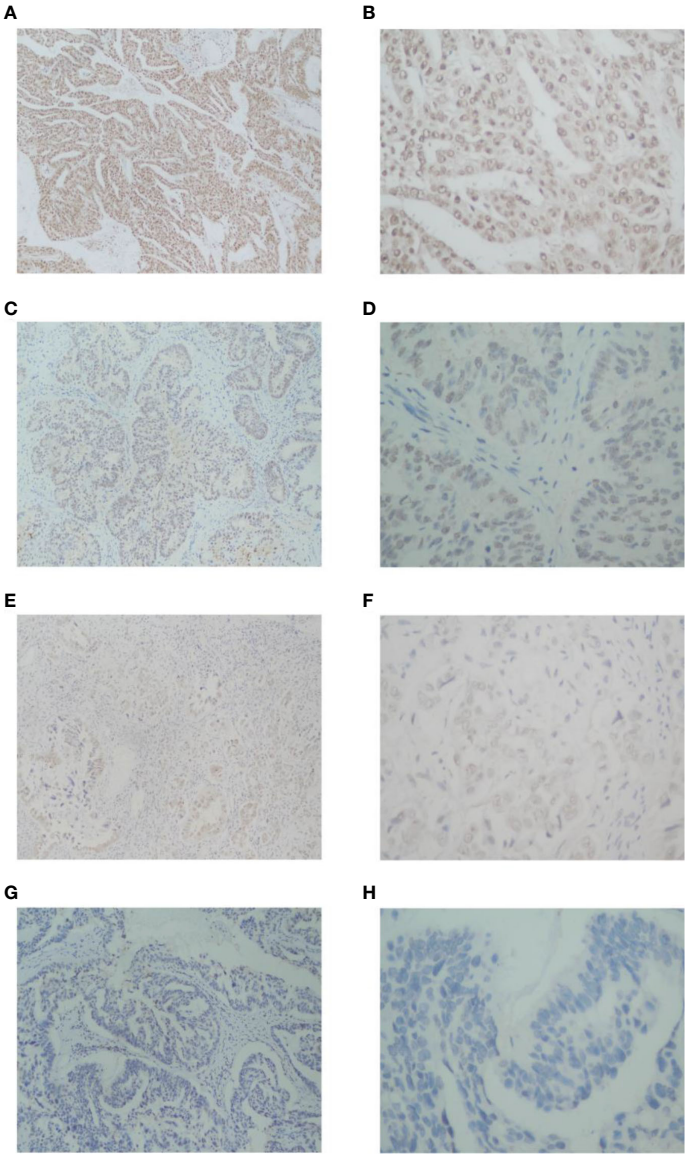


FIGURE 1
Immunohistochemistry analysis of NCOA5 in EOC tissue specimens. The representative pictures +++ (**A**: ×100, **B**: ×400),++ (**C**: ×100, **D**: ×400),+ (**E**: ×100, **F**: ×400) and -(**G**: ×100, **H**: ×400).

## Correlation between NCOA5 expression and prognosis

There was a significant difference in the expression of NCOA5 in FIGO stage of ovarian cancer patients (P<0.001), but there were no significant differences with age, Differentiation degree and lymph node metastasis(P>0.05, Table 2). The association between NCOA5 and CA125 in predicting EOC was 0.719(P<0.001), meanwhile, NCOA5 and human epididymal protein 4(HE4) in predicting EOC was 0.766 (P=0.001, Table 3). OS and PFS for patients after surgery with low expression of NCOA5 had significantly longer survival than high expression of NCOA5 (p=0.038, p=0.049) (Figure 3).

TABLE 1 Comparison of NCOA5 expression between EOC and normal ovarian tissues.

| Groups | Numbers | The expression level of NCOA5 |
|---|---|---|
| EOC | 60 | 1.38 ± 0.14 |
| Normal ovarian tissues | 20 | 0.67 ± 0.10 |
| t value | | 61.02 |
| P value | | 0.000 |

TABLE 2 The relationship of NCOA5 expression with EOC clinicopathological features (Pearson's $\chi^2$ test).

| Variables | Numbers | The expression level of NCOA5 | t value | P value |
|---|---|---|---|---|
| Age (year) | | | 0.895 | 0.314 |
| ≥50 | 34 | 0.27 ± 0.12 | | |
| <50 | 26 | 0.30 ± 0.08 | | |
| Differentiation | | | 0.583 | 0.171 |
| High | 16 | 0.38 ± 0.10 | | |
| Moderately | 21 | 0.29 ± 0.11 | | |
| Poorly | 23 | 0.16 ± 0.09 | | |
| FIGO Stage | | | 0.763 | 0.002 |
| I-II | 26 | 0.59 ± 0.07 | | |
| III-IV | 34 | 1.02 ± 0.05 | | |
| Subtype | | | 0.685 | <0.001 |
| Serous | 40 | 1.97 ± 0.11 | | |
| Non- Serous | 20 | 0.66 ± 0.03 | | |
| Lymph nodes | | | 0.614 | 0.173 |
| Positive | 25 | 0.21 ± 0.09 | | |
| Negative | 35 | 0.35 ± 0.12 | | |

## Discussion

Previous researches revealed that NCOA5 expression were related to breast cancer (12) and colorectal cancer (13). Conversely, It has also been reported that NCOA5 expression is downregulated in hepatocellular carcinoma (9), esophageal squamous cell carcinoma (11), papillary thyroid carcinoma (16), and cervical cancer (17). However, the potential correlation between NCOA5 and clinical outcome in patients with EOC has not been reported. In the present study, NCOA5 expression was significantly increased in EOC compared with normal ovarian tissues, it suggests that NCOA5 is probably involved in the carcinogenesis of EOC.

CA125 has been an established protein marker for the detection and monitoring of ovarian cancer therapy for many years. Since 2003, the increase of serum HE4 level has attracted increasingly attention for predicting ovarian cancer. In addition to finding specific and sensitive markers, ROMA algorithm was developed (18). In our study, the expression of NCOA5 was highly correlated with CA125 and HE4. As suggested by the results above, NCOA5 may meet the criteria of a good diagnostic test for EOC. It is worth noting that the correlation between NCOA5 and pre-Roma is better than that between post-Roma. However, due to the small number of cases, observation after expanding the number of cases may be necessary.

Tan et al. (19) reported that knockdown of NCOA5 in breast cancer cells significantly decreased the expression levels of N-cadherin and Vimentin, whereas increased the expression levels of E-cadherin, on the contrary, upregulation of N-cadherin and Vimentin expression or downregulation of E-cadherin expression contribute to epithelial-mesenchymal transition (20). The expression level of NCOA5 in FIGO stage III/IV was significantly higher than that in FIGO stage I/II patients, indicating that NOCA5 may play a role in the distant metastasis of ovarian cancer, however, it needs to be verified by cell experiments.

This study provides new insights and evidences that NCOA5 is significantly correlated with progression and prognosis in EOC. The expression of NCOA5 in ovarian cancer and its role in tumor development remain unclear. Due to heterogeneity between different databases, differences between study populations NCOA5 is not listed as a prognostic marker in ovarian cancer at present in protein atlas database. Our study reveals that NCOA5 has great potential as a novel prognostic marker in ovarian cancer. There are several limitations of this study have to be pointed out. Firstly, in the present study, we only included a small sample size in this single-center study, whether the research conclusion is

TABLE 3 Correlation analysis between NCOA5 expression and other tumor markers.

| NCOA5 | CA125 | HE4 | Pre-ROMA | Post-ROMA |
|---|---|---|---|---|
| r | 0.719 | 0.766 | 0.711 | 0.802 |
| P | <0.001 | 0.001 | 0.032 | 0.062 |

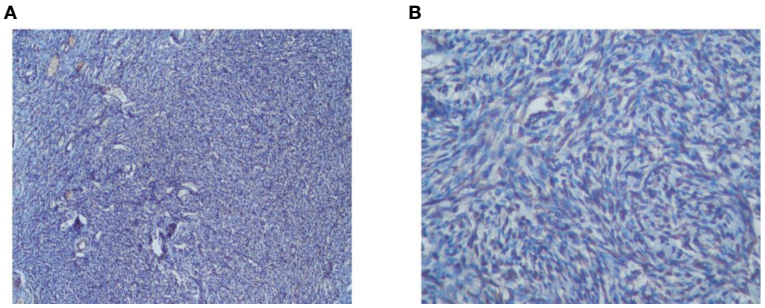


FIGURE 2
Immunohistochemistry analysis of NCOA5 in normal ovarian tissues specimens (**A**: ×100, **B**: ×400).

universal will be verified by accumulating more subjects in the future work. Secondly, several clinical characteristics of enrolled patients were heterogeneous, moreover, we did not study the prognostic values of NCOA5 in patients regarding to the stage of the EOC. Finally, retrospective studies have several inherent biases, including selection bias, recall bias, reporting bias and confounding bias which can affect the reliability of the findings.

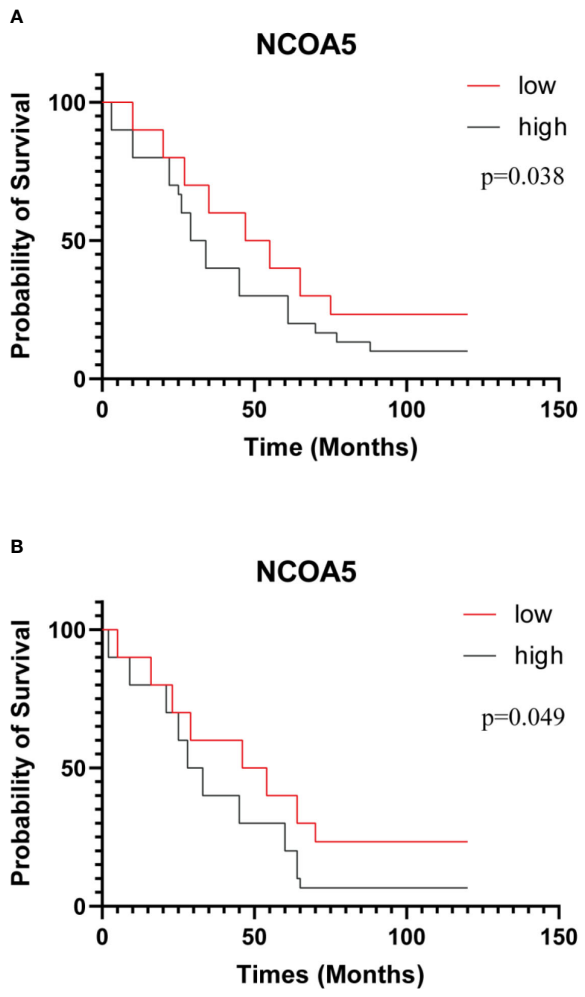


FIGURE 3
Kaplan-Meier curves of OS **(A)** and PFS **(B)** after surgery for all patients. patients with low expression of NCOA5 had significantly longer survival than high expression of NCOA5 (p=0.038、p=0.049).

NCOA5 plays a critical role in the occurrence and development of several cancers by regulating various cellular processes such as cell proliferation, differentiation, and apoptosis. NCOA5 expression is downregulated in breast cancer cells, which promotes the proliferation and survival of cancer cells (19). Moreover, NCOA5 has been found to suppress the expression of cancer stem cell markers, thereby inhibiting tumor growth and metastasis. Moreover, NCOA5 has been shown to suppress the growth and metastasis of colorectal cancer cells by inhibiting the activation of the PI3K/Akt signaling pathway (13). NCOA5 also enhances the sensitivity of colorectal cancer cells to chemotherapy drugs, thereby improving the therapeutic efficacy. Besides, NCOA5 expression is significantly decreased in hepatocellular carcinoma cells compared to normal tissues. It has been demonstrated that NCOA5 inhibits the proliferation, migration, and invasion of gastric cancer cells by suppressing the expression of matrix metalloproteinases (MMPs) (21). Therefore, NCOA5 may serve as a potential therapeutic target for the treatment of cancers. However, the association between NCOA5 and ovarian cancer and its underlying mechanisms has not been reported yet. The overexpression of NOCA5 in patients with advanced stages of ovarian cancer suggests that this gene may play a crucial role in promoting distant metastasis. There are several potential mechanisms by which NOCA5 could contribute to the metastatic spread of ovarian cancer cells. Firstly, NOCA5 may regulate the activity of specific genes involved in the metastatic process, such as genes involved in cell migration, invasion, and adhesion. For instance, NOCA5 may enhance the expression of genes that promote the formation of new blood vessels, which is essential for the growth of metastatic tumors in distant organs. Secondly, NOCA5 could promote the epithelial-mesenchymal transition (EMT), which is a cellular process that allows cancer cells to acquire a more invasive phenotype. During EMT, cancer cells lose their cell-cell adhesion properties and gain a mesenchymal-like phenotype, which allows them to migrate through tissues and invade blood vessels (21). Thirdly, NOCA5 may also be involved in the regulation of the tumor microenvironment, which can play a critical role in promoting tumor growth and metastasis. For instance, NOCA5 could stimulate the production of cytokines and growth factors that promote angiogenesis and suppress immune surveillance

(22). Molecular parameters such as genetic mutations, gene expression profiles, and protein levels can provide valuable information on the biology of ovarian cancer and its response to therapy. The combination of molecular targeting treatment with classical medical imaging methods such as positron emission tomography/computed tomography (PET/CT) can potentially lead to the development of better early diagnosis models and will improve the management of patients with EOC (7, 23, 24). We suggest that NCOA5 gene may have potential value as a pathological diagnostic marker of ovarian cancer. NCOA5 was highly expressed in serous ovarian cancer and closely related to CA125 and HE4. NCOA5 may be a promising supplementary marker in serous ovarian cancer and help determine its management in the future. However, basic experiments are still needed to further confirm the role of NCOA5 in the development of EOC.

## Data availability statement

The original contributions presented in the study are included in the article/supplementary material. Further inquiries can be directed to the corresponding authors.

## Ethics statement

The studies involving human participants were reviewed and approved by Clinical ethical Committee of Changshu No.1 People's Hospital. The patients/participants provided their written informed consent to participate in this study.

## Author contributions

XS designed research. XS, DQ, PD, QL, and QX carried out research. DQ and KS analyzed data. XS, DQ, and KS drawn the figures and made the tables. XS, DQ, and PD wrote and revised the manuscript. All authors contributed to the article and approved the submitted version.

## Funding

Supported by Suzhou city's municipal youth Program in science and education, Jiangsu Province, China. [No.KJXW2018061].

## Conflict of interest

The authors declare that the research was conducted in the absence of any commercial or financial relationships that could be construed as a potential conflict of interest.

## Publisher's note



## References

1. Momenimovahed Z, Tiznobaik A, Taheri S, Salehiniya H. Ovarian cancer in the world: epidemiology and risk factors. *Int J Womens Health* (2019) 11:287–99. doi: 10.2147/IJWH.S197604

2. Torre LA, Trabert B, DeSantis CE, Miller KD, Samimi G, Runowicz CD, et al. Ovarian cancer statistics, 2018. *CA Cancer J Clin* (2018) 68(4):284–96. doi: 10.3322/caac.21456

3. Chen W, Sun K, Zheng R, Zeng H, Zhang S, Xia C, et al. Cancer incidence and mortality in China, 2014. *Chin J Cancer Res* (2018) 30(1):1–12. doi: 10.21147/j.issn.1000-9604.2018.01.01

4. Bowtell DD, Böhm S, Ahmed AA, Aspuria PJ, Bast RC Jr, Beral V, et al. Rethinking ovarian cancer II: reducing mortality from high-grade serous ovarian cancer. *Nat Rev Cancer* (2015) 15(11):668–79. doi: 10.1038/nrc4019

5. Coleman RL, Monk BJ, Sood AK, Herzog TJ. Latest research and treatment of advanced-stage epithelial ovarian cancer. *Nat Rev Clin Oncol* (2013) 10(4):211–24. doi: 10.1038/nrclinonc.2013.5

6. Oronsky B, Ray CM, Spira AI, Trepel JB, Carter CA, Cottrill HM. A brief review of the management of platinum-resistant-platinum-refractory ovarian cancer. *Med Oncol* (2017) 34(6):103. doi: 10.1007/s12032-017-0960-z

7. Delgado Bolton RC, Aide N, Colletti PM, Ferrero A, Paez D, Skanjeti A, et al. EANM guideline on the role of 2-[18F]FDG PET/CT in diagnosis, staging, prognostic value, therapy assessment and restaging of ovarian cancer, endorsed by the American college of nuclear medicine (ACNM), the society of nuclear medicine and molecular imaging (SNMMI) and the international atomic energy agency (IAEA). *Eur J Nucl Med Mol Imaging* (2021) 48(10):3286–302. doi: 10.1007/s00259-021-05450-9

8. Sarachana T, Hu VW. Differential recruitment of coregulators to the RORA promoter adds another layer of complexity to gene (dys) regulation by sex hormones in autism. *Mol Autism* (2013) 4(1):39. doi: 10.1186/2040-2392-4-39

9. Gao S, Li A, Liu F, Chen F, Williams M, Zhang C, et al. NCOA5 haploinsufficiency results in glucose intolerance and subsequent hepatocellular carcinoma. *Cancer Cell* (2013) 24(6):725–37. doi: 10.1016/j.ccr.2013.11.005

10. Dhar D, Seki E, Karin M. NCOA5, IL-6, type 2 diabetes, and HCC: the deadly quartet. *Cell Metab* (2014) 19(1):6–7. doi: 10.1016/j.cmet.2013.12.010

11. Chen GQ, Tian H, Yue WM, Li L, Li SH, Qi L, et al. NCOA5 low expression correlates with survival in esophageal squamous cell carcinoma. *Med Oncol* (2014) 31 (12):376. doi: 10.1007/s12032-014-0376-y

12. Ye XH, Huang DP, Luo RC. NCOA5 is correlated with progression and prognosis in luminal breast cancer. *Biochem Biophys Res Commun* (2017) 482 (2):253–6. doi: 10.1016/j.bbrc.2016.11.051

13. Sun K, Wang S, He J, Xie Y, He Y, Wang Z, et al. NCOA5 promotes proliferation, migration and invasion of colorectal cancer cells via activation of PI3K/AKT pathway. *Oncotarget* (2017) 8(64):107932–46. doi: 10.18632/oncotarget.22429

14. Edge SB, Compton CC. The American joint committee on cancer: the 7th edition of the AJCC cancer staging manual and the future of TNM. *Ann Surg Oncol* (2010) 17(6):1471–4. doi: 10.1245/s10434-010-0985-4

15. Li SH, Tian H, Yue WM, Li L, Li WJ, Chen ZT, et al. Overexpression of metastasis-associated protein 1 is significantly correlated with tumor angiogenesis and poor survival in patients with early-stage non-small cell lung cancer. *Ann Surg Oncol* (2011) 18(7):2048–56. doi: 10.1245/s10434-010-1510-5

16. Zheng ZC, Wang QX, Zhang W, Zhang XH, Huang DP. A novel tumor suppressor gene NCOA5 is correlated with progression in papillary thyroid carcinoma. *Onco Targets Ther* (2018) 11:307–11. doi: 10.2147/OTT.S154158

17. Liang Y, Zhang T, Shi M, Zhang S, Guo Y, Gao J, et al. Low expression of NCOA5 predicts poor prognosis in human cervical cancer and promotes proliferation, migration, and invasion of cervical cancer cell lines by regulating notch3 signaling pathway. *J Cell Biochem* (2019) 120(4):6237–49. doi: 10.1002/jcb.27911

18. Chudecka-Glaz AM. ROMA, an algorithm for ovarian cancer. *Clin Chim Acta* (2015) 440:143–51. doi: 10.1016/j.cca.2014.11.015

19. Tan Y, Liu F, Xu P. Knockdown of NCOA5 suppresses viability, migration and epithelial-mesenchymal transition, and induces adhesion of breast cancer cells. *Oncol Lett* (2021) 22(4):694. doi: 10.3892/ol.2021.12955

20. Zhang X, Liu G, Kang Y, Dong Z, Qian Q, Ma X. N-cadherin expression is associated with acquisition of EMT phenotype and with enhanced invasion in erlotinib-resistant lung cancer cell lines. *PloS One* (2013) 8(3):e57692. doi: 10.1371/journal.pone.0057692

21. He J, Zhang W, Li A, Chen F, Luo R. Knockout of NCOA5 impairs proliferation and migration of hepatocellular carcinoma cells by suppressing epithelial-to-mesenchymal transition. *Biochem Biophys Res Commun* (2018) 500(2):177–83. doi: 10.1016/j.bbrc.2018.04.017

22. Williams M, Liu X, Zhang Y, Reske J, Bahal D, Gohl TG, et al. NCOA5 deficiency promotes a unique liver protumorigenic microenvironment through p21WAF1/CIP1 overexpression, which is reversed by metformin. *Oncogene* (2020) 39(19):3821–36. doi: 10.1038/s41388-020-1256-x

23. Delgado Bolton RC, Calapaquí Terán AK, Pellet O, Ferrero A, Giammarile F. The search for new 2-18F-FDG PET/CT imaging biomarkers in advanced ovarian cancer patients: focus on peritoneal staging for guiding precision medicine and management decisions. *Clin Nucl Med* (2021) 46(11):906–7. doi: 10.1097/RLU.0000000000003784

24. Perelli F, Mattei A, Scambia G, Cavaliere AF. Editorial: methods in gynecological oncology. *Front Oncol* (2023) 13:1167088. doi: 10.3389/fonc.2023.1167088

frontiers | Frontiers in Oncology

TYPE Original Research
PUBLISHED 15 May 2023
DOI 10.3389/fonc.2023.1156973



OPEN ACCESS

EDITED BY
Carmine De Angelis,
University of Naples Federico II, Italy

REVIEWED BY
Pengpeng Qu,
Tianjin Central Hospital for Gynecology and Obstetrics, China
Anna Fialová,
SOTIO a.s., Czechia

*CORRESPONDENCE
Jung-Yun Lee
jungyunlee@yuhs.ac

RECEIVED 02 February 2023
ACCEPTED 21 April 2023
PUBLISHED 15 May 2023

CITATION
Kim Y-N, Lee K, Park E, Park J, Lee YJ, Nam EJ, Kim SW, Kim S, Kim YT and Lee J-Y (2023) Comprehensive genomic and immunohistochemical profiles and outcomes of immunotherapy in patients with recurrent or advanced cervical cancer. *Front. Oncol.* 13:1156973. doi: 10.3389/fonc.2023.1156973



# Comprehensive genomic and immunohistochemical profiles and outcomes of immunotherapy in patients with recurrent or advanced cervical cancer

Yoo-Na Kim[1], Kyunglim Lee[1], Eunhyang Park[2], Junsik Park[1], Yong Jae Lee[1], Eun Ji Nam[1], Sang Wun Kim[1], Sunghoon Kim[1], Young Tae Kim[1] and Jung-Yun Lee[1]*

[1]Department of Obstetrics and Gynecology, Institute of Women's Life Medical Science, Yonsei University College of Medicine, Seoul, Republic of Korea, [2]Department of Pathology, Institute of Women's Life Medical Science, Yonsei University College of Medicine, Seoul, Republic of Korea

**Purpose:** This study aimed to investigate genomic and immunohistochemical (IHC) profiles and immunotherapy outcomes in patients with cervical cancer.

**Methods:** Patients with recurrent cervical cancer who underwent tumor next-generation sequencing (NGS) with the TruSight Oncology 500 panel at Yonsei Cancer Center between June 2019 and February 2022, were identified. Patients who received treatment with checkpoint inhibitors during the same period were also identified. Clinical information, including histology, stage, human papillomavirus (HPV) genotype, IHCs profile, and therapy outcome, was reviewed.

**Results:** We identified 115 patients treated for recurrent cervical cancer, including 74 patients who underwent tumor NGS. Most of these 74 patients were initially diagnosed with advanced stage (63.6%) and had squamous cell histology (52.7%), and high-risk HPV (76.9%). Based on IHC analysis, the programmed death-ligand 1 combined positive score (PD-L1 CPS) was higher in patients with squamous cell carcinoma (SCC) than in those with adeno or mucinous types (P=0.020). HER2 receptor expression of 2+ and 3+ were identified in 5 and 1 patients, respectively, and significantly varied based on histology (p=0.002). Among the 74 patients, single nucleotide variants (SNVs) and copy number variations (CNVs) were identified in 60 (81.1%) and 13 patients (17.6%), respectively. The most common SNVs were PIK3CA, TP53, STK11, FAT1, and FBXW7 mutations. Mutations in PIK3CA, with two hotspot mutations, were frequently observed in patients with SCC histology, whereas mutations in TP53 were frequently observed in patients with non-SCC histology. Additionally, variations in FAT1 were exclusively identified in patients with SCC histology. Mutations in homologous recombination repair-associated genes were identified in 18 patients (24.3%). The most frequent CNV alteration was CCNE1

amplification. Moreover, among the 36 patients who underwent NGS and received immunotherapy, the tumor mutational burden and microsatellite instability were significantly correlated with immunotherapy duration. During this timeframe, 73 patients received pembrolizumab monotherapy, among whom a small portion showed a durable response.

**Conclusion:** Comprehensive genomic and IHC profiling may help identify potential candidates for targeted immunotherapy in patients with cervical cancer.

KEYWORDS

NGS, immunohistochemistry, immunotherapy, cervical cancer, personalized medicine

# 1 Introduction

Cervical cancer, frequently caused by infections with the human papillomavirus (HPV), is the fourth most common cancer among women globally, with an estimated 604,000 cases and 342,000 deaths reported in 2020 (1). Owing to vaccination against HP, early screening, and early intervention with conization, early-stage cervical cancer is effectively treated and controlled. However, the prognosis of advanced-stage cervical cancer remains poor, with a 5-year survival rate of 39%, 24%,15%, and less than 5% for stage III, stage Iva, stage IVb, and recurrent cancer, respectively (2, 3). Despite various preventive and early intervention strategies, the mortality rate of cervical cancer has not improved, suggesting that the standard treatment with platinum-based chemotherapy is insufficient for advanced-stage cervical cancer.

Various non-chemotherapeutic options, such as immune checkpoint inhibitors (ICI) and targeted agents, have been investigated to improve survival outcomes in cervical cancer (4–8). Of these, pembrolizumab, a programmed death-1 (PD-1) receptor inhibitor, is widely investigated and has received US Food and Drug Administration approval for patients with persistent, recurrent, or metastatic cervical cancer with a PD-L1 combined positive score (CPS) of ≥1 based on Keynote-158 (9). Previously reported predictive biomarkers for ICI include PD-L1 immunohistochemistry (IHC) and genomic assays, such as tumor mutational burden (TMB) or microsatellite instability (MSI) (10). Owing to the increased clinical use of next-generation sequencing (NGS), mutational profiling may help in further personalizing therapy for cervical cancer. Moreover, previous studies on the genomic landscape of cervical cancer have identified frequent alterations in genes, such as PIK3CA, EP300, FBXW7, and APOBEC signatures, associated with the process of carcinogenesis of virus-associated diseases (11, 12).

This study aimed to present a comprehensive profile of IHC and genomic biomarkers in patients with cervical cancer and the outcomes of immunotherapy from a single institution. We identified patients with cervical cancer who underwent tumor NGS with the TruSight Oncology 500 panel and collected clinical parameters such as histology, HPV genotyping, tumor markers, and IHC results for PD-L1 and human epidermal growth factor receptor 2 (HER2) receptor status. Furthermore, we investigated all patients with cervical cancer who received pembrolizumab monotherapy within the same timeframe to provide real-world data on immunotherapy outcomes.

# 2 Materials and methods

## 2.1 Patient recruitment and sample acquisition

Patients who were diagnosed with cervical cancer between June 2019 and February 2022 at Yonsei Cancer Hospital and underwent NGS with TruSight Oncology 500 were retrospectively identified. During the same period, all patients with cervical cancer who received pembrolizumab monotherapy were also identified. This study was approved by the hospital's institutional review board (IRB No # 4-2022-1399). The need for informed consent was waived because of the retrospective nature of the study.

## 2.2 NGS of tumor samples

Tumor samples were prepared from formalin-fixed paraffin-embedded (FFPE) tissues. An expert pathologist reviewed the hematoxylin and eosin-stained slides to ensure adequate tumor content. For DNA extraction, 2–5 slides of resected specimens with a thickness of 5 μm were used. FFPE samples with high tumor cellularity (>10%) were subjected to NGS analysis. Genomic DNA was extracted using a Maxwell CSC DNA FFPE Kit (Promega, Madison, WI, USA), according to the manufacturer's instructions. The products were sequenced using the NextSeq 550 System (Illumina Inc., San Diego, CA, USA). Mutational and copy number analyses were performed using a TruSight Oncology 500 panel (Illumina). For mutational analysis, FASTQ files were

uploaded to the Illumina BaseSpace software (Illumina) for variant interpretation. Only variants in coding regions, promoter regions, or splice variants were retained. In addition, we only retained variants present in 3% of the reads, with a minimum read depth of 250. All retained variants were reviewed against reference websites (Catalogue of Somatic Mutations in Cancer [http://evs.gs.washington.edu/EVS/], Precision Oncology Knowledge Base [http://oncokb.org], and dbSNP [https://www.ncbi.nlm.nih.gov/snp]). Only pathogenic variants were selected for further analysis. In the copy number analysis, only genes with more than a two-fold change relative to the average level were considered for amplification. TMB and MSI scores were obtained for patients who underwent NGS using the TruSight Oncology 500 panel.

## 2.3 IHC

FFPE tissue specimens were used for IHC analysis. After deparaffinization with xylene and rehydration with an alcohol-graded solution, IHC was performed using a Ventana Discovery XT Automated Slide Stainer (Ventana Medical System, Oro Valley, AZ, USA). Cell conditioning 1 buffer (citrate buffer, pH 6.0; Ventana Medical System) was used for antigen retrieval. Sections were incubated with primary antibodies against PD-L1 (1:50; clone 22C3; DAKO, Agilent Technologies, Santa Clara, CA, USA) and HER2 (1:1500; polyclonal; DAKO). For PD-L1 expression, CPS (1:50; clone 22C3; DAKO) was calculated as previously described (13). HER2 IHC was assessed according to the American Society of Clinical Oncology/College of American Pathologists guidelines based on the grading system, ranging from 0 to 3+ (14).

## 2.4 Collection of information on clinical variables, treatment received, and outcomes

Basic clinical information, such as age at diagnosis, histology, serum tumor markers, and FIGO stage at diagnosis, was obtained. We also assessed whether the patients received ICI or targeted therapy, and the name of the therapeutic agent, treatment duration, and date of disease progression were recorded.

## 2.5 Statistical analysis

Statistical analysis was performed using R version 4.0.3 (R Foundation for Statistical Computing, Vienna, Austria). Variant calling file from the aforementioned NGS pipeline was used for analysis and visualization using the "maftools" package in R.

Significance was calculated using Fisher's exact test or chi-square test for categorical variables and Student's *t*-test for continuous variables, where applicable. The Kaplan–Meier method was used to analyze treatment response and overall survival. For all analyses, significance was set at $P < 0.05$.

# 3 Results

A total of 115 patients with cervical cancer who either underwent NGS or received pembrolizumab were identified. Among these patients, the clinical characteristics and IHC profiles of 74 patients with NGS data were analyzed (Supplementary Table 1). These patients had advanced-stage cervical cancer (63.6%), squamous cell histology (52.7%), and high-risk HPV genotype (76.9%), and 61 patients (82.4%) harbored either single nucleotide variant (SNV) or gene copy number variant (CNV) alterations (Figure S1). The overall landscape of the pathogenic SNV alterations is shown in Figure S1. The most common alterations were observed in PIK3CA and TP53. PIK3CA showed two hotspot mutations, E542K and E545K, in 19 of the 23 (82.6%) patients with PIK3CA mutations. The most frequently highlighted pathways were PI3K, TP53, and Notch (Figure S1). Based on the somatic interaction plot, ERBB2, STK11, PIK3R1, PTEN, ARID1A, and CREEBP mutations were found to co-occur (Figure S1).

Pathogenic SNV alterations stratified by histology are shown in Figure 1A. Mutations in PIK3CA were relatively more common in patients with squamous cell histology, whereas mutations in TP53 were relatively more common in those with non-squamous histology. Mutations in FAT1 were exclusively identified in patients with squamous cell histology. The most common CNVs were CCNE1 amplification in five patients and ERBB2/3 amplification in two patients. CNV alterations based on histology are shown in Figure 1B. Pathogenic mutations in homologous repair (HRR)-associated genes were identified in 18 of 74 (24.3%) patients. Mutations in HRR-associated genes based on histology are shown in Figure 1C.

Clinical variables such as HPV genotype, serum tumor markers, and IHC were differentially distributed based on histology (Supplementary Table 2). Patients with squamous cell histology frequently harbored HPV 16 (46.2%) and high-risk genotype other than HPV 16 or 18 (26.9%), whereas patients with non-squamous frequently harbored HPV 18 (36.8% of patients with adeno or mucinous histology; 42.9% with other histology). Among the 45 patients who were investigated, the PD-L1 CPS score was higher in patients with squamous cell histology (median 15, range 0.5–90) than in those with adeno or mucinous histology (median 5, range 0–5) ($P = 0.013$; Figure 2). Moreover, among 39 patients tested for HER2 expression, most patients (90.9%) with squamous cell histology lacked HER2 expression (Supplementary Table 2). HER2 expression of 2+ or 3+ was relatively more common in patients with non-squamous histology ($P = 0.002$). Moreover, based on HER2 receptor status, two patients received HER2 receptor targeting agent, trastuzumab deruxtecan (T-DXd), based on enrollment in clinical trials. One patient had stage 3 disease (squamous cell histology, PD-L1 CPS 5, TMB 11 mut/Mb, and HER2 2+) and was initially treated with CCRTx but showed disease progression in the pelvis, lung, and supraclavicular lymph nodes after treatment with second-line chemotherapy. This patient received T-DXd for 1 year and is still undergoing treatment. The other patient had stage 4 disease with ovarian metastasis (adenocarcinoma histology, PD-L1 CPS 5, TMB 6.3 mut/Mb,

10.3389/fonc.2023.1156973

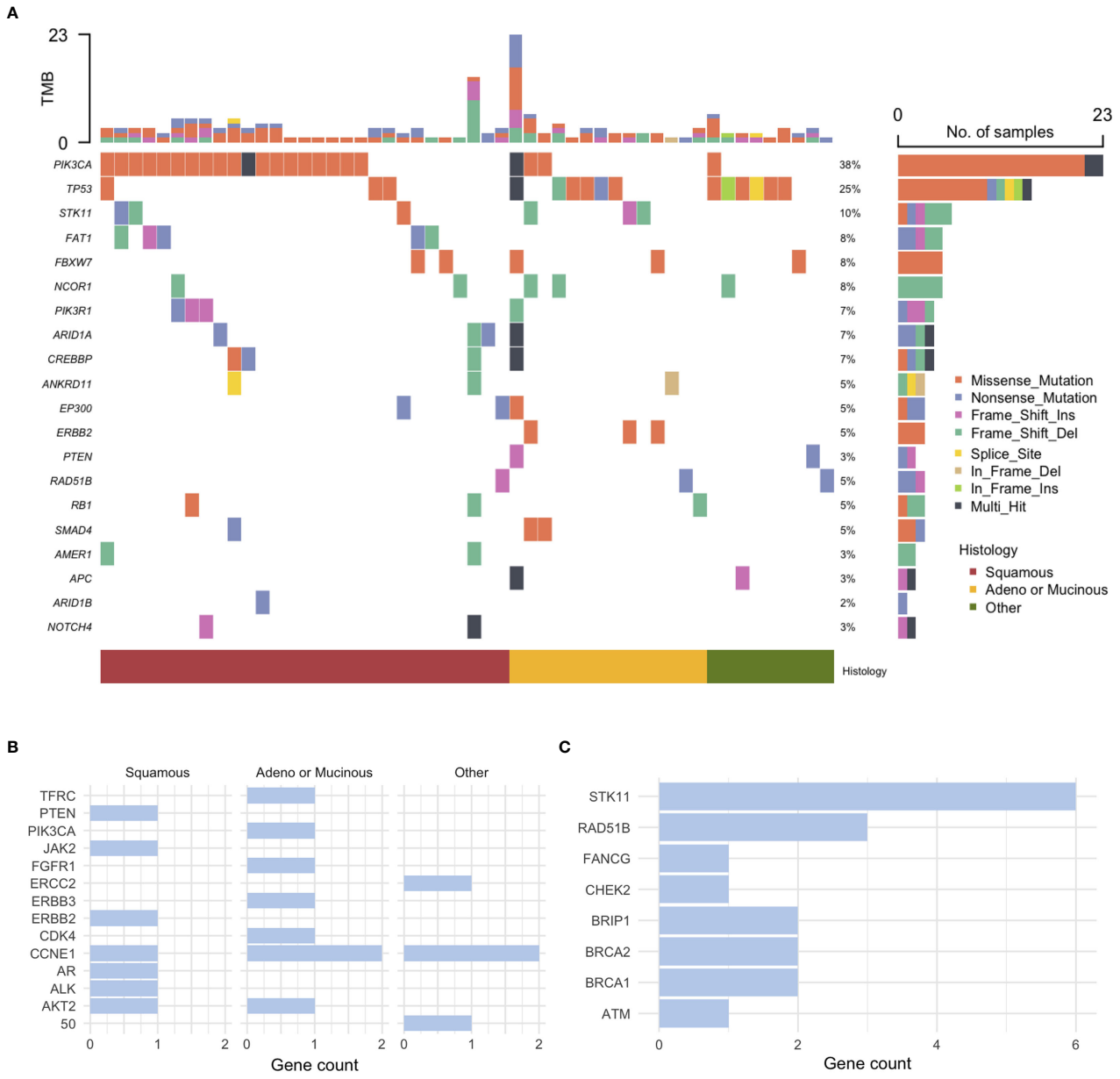


FIGURE 1
Genomic profiling of cervical cancer. **(A)** Pathogenic single nucleotide variant (SNV) alterations, **(B)** Copy number variation (CNV) alterations stratified by histology, and **(C)** mutations in homologous recombination repair-associated genes.

TP53 mutation, CCNE1 and ERBB2 amplification, and HER3 3+). After treatment with paclitaxel, carboplatin, and bevacizumab, this patient experienced recurrence in the vaginal vault and lung and received T-DXd as second-line therapy for 19 months, and is still undergoing treatment.

A total of 81 patients with cervical cancer underwent immunotherapy; monotherapy agents were: pembrolizumab (n = 73), tislelizumab (n = 4), nivolumab (n = 3), and atezolimumab (n = 1) (Figure 3A). Among the patients who underwent NGS, the median TMB was 6.3 mut/Mb (range 0.3–78.9) and the median MSI was 2.5% unstable sites (range 0–43.6). The progression-free survival (PFS) rate based on the type of immunotherapy with TMB and MSI values in these patients is shown in Figure 3A. Both TMB and MSI were significantly correlated with the duration of immunotherapy (Figures 3B, C). One patient with exceptionally high TMB and MSI in the scatter plots showed a durable response to pembrolizumab monotherapy; this patient had stage III adenocarcinoma and was negative for HPV. The presence of statistical significance in the correlation plots was dependent on the inclusion of this patient; if the patient was excluded, the significance was not observed (Figure S2).

For patients who received pembrolizumab monotherapy, a swimmer plot based on histology, PD-L1 CPS, and HPV status is shown in Figure 3D. The median age of patients receiving

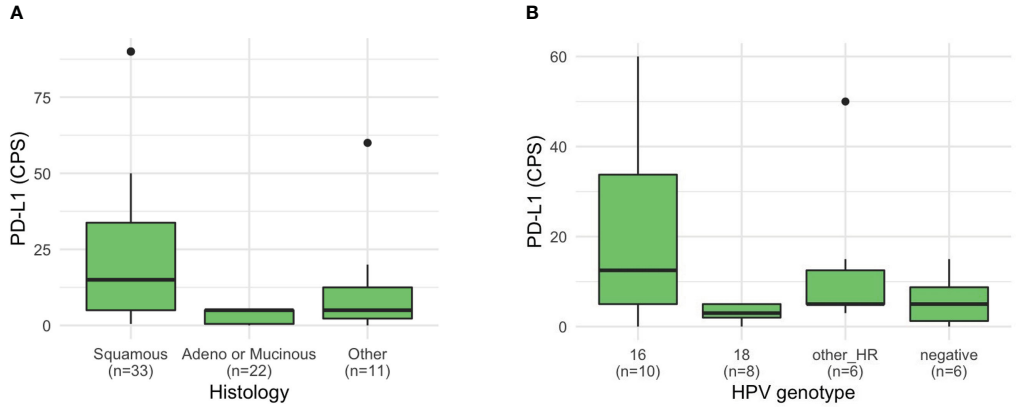


FIGURE 2
PD-L1 CPS of patients with cervical cancer. PD-L1 CPS based on **(A)** histology and **(B)** HPV genotype.

pembrolizumab was 48 (range: 32–80). In terms of ECOG status, 34.4% and 37.9% of the patients had ECOG statuses of 0 and 1, respectively; those with ECOG statuses 2 and 3 (17.2% and 10.3%, respectively) were also included in this retrospective study. In terms of prior lines of therapy, a majority (71.3%) had received one or two prior lines of treatment, but a sizable portion had also received three (17.2%) or four (10.3%). Most patients (23.3%) received pembrolizumab for one cycle as palliative care; five patients (6.8%) received pembrolizumab for ≥12 months, with two patients still undergoing treatment; and eight patients (11.0%) received pembrolizumab for 6–12 months, with two patients still undergoing treatment. The two patients with an exceptional response (≥12 months) to pembrolizumab monotherapy and who are still undergoing treatment both had advanced disease with lung metastasis, with or without brain metastasis. One patient who did not undergo NGS had exceptionally high PD-L1 SP263 (80%). Another patient showed a high mutational burden involving pathogenic SNV alteration of 15 genes and exhibited TMB of 78.9 mut/Mb and MSI 43.6% unstable MSI sites; PD-L1 was not tested.

## 4 Discussion

Cervical cancer diagnosed at an advanced-stage or in a recurrent disease setting is difficult to manage. Currently, many clinical trials on various immunotherapy agents and other targeted therapies, such as HER2 antibody–drug conjugates, are still ongoing to identify effective treatments for advanced or recurrent cervical cancer. Moreover, the identification of potential biomarkers using IHC and genomic assays is also important for personalized treatment for patients with advanced cervical cancer. The present study is a sizable study on patients with cervical cancer undergoing NGS with a well-described commercial panel. Most patients underwent TruSight Oncology 500 testing, which also provided the TMB and MSI values. We also included all patients with cervical cancer who underwent immunotherapy during the same period. This study provides real-world findings that encompass clinical, genomic, and treatment data, as well as outcomes of immunotherapy.

Previous studies have focused on either genomic alterations or therapeutic outcomes in cervical cancer. The landmark studies by the Cancer Genome Atlas (TCGA) (11, 15) have reported that the most frequent mutations in cervical cancer are PIK3CA (26%), EP300 (11%), FBXW7 (11%), and PTEN (8%) (11). In our study, PIK3CA mutations were identified in 23 of the 74 (31.1%) patients who underwent NGS; this rate is similar to or slightly higher than that in TCGA data, which are mostly based on Caucasian populations. In terms of prevalent mutations other than PIK3CA, our study revealed frequent mutations in TP53 (15 patients, 20.3%) and STK11 (6 patients, 8.1%), which is inconsistent with TCGA study. This difference may partially be attributed to the differences in histological subtypes, as approximately 75% of the cases were squamous cell histology in TCGA study, whereas only 52.8% of the patients had squamous cell histology in our cohort. Similar to our results, a previous study from China reported TP53 and STK11 mutations in 16% and 7% of the patients, respectively, suggesting ethnicity-related differences (16).

In the present study, we revealed that the genomic differences in SNVs and CNVs were partially associated with histology, as previously reported (15). We further investigated whether the HPV genotype may be associated with histology and found that among the most common subtypes, HPV 16 and HPV 18 may be associated with squamous cell type and adeno or mucinous type, respectively. Moreover, patients negative for HPV showed a similar distribution of histological subtypes to patients with HPV 16, suggesting the possibility of a false-negative HPV genotype in these patients. However, recent literature has suggested that HPV-independent cervical cancers may have different biology, bearing implications in carcinogenesis and treatment response (17). Additionally, owing to the advent of HPV vaccines, cervical cancers that originate from genotypes that are not covered by HPV vaccines or are HPV-independent may become more important in the future. Further studies on HPV based on NGS-based tests may help in further investigations (18).

The present study also highlights the potential use of IHC-based biomarkers for directing therapeutic options in cervical cancer. The PD-L1 CPS was particularly high in patients with squamous cell

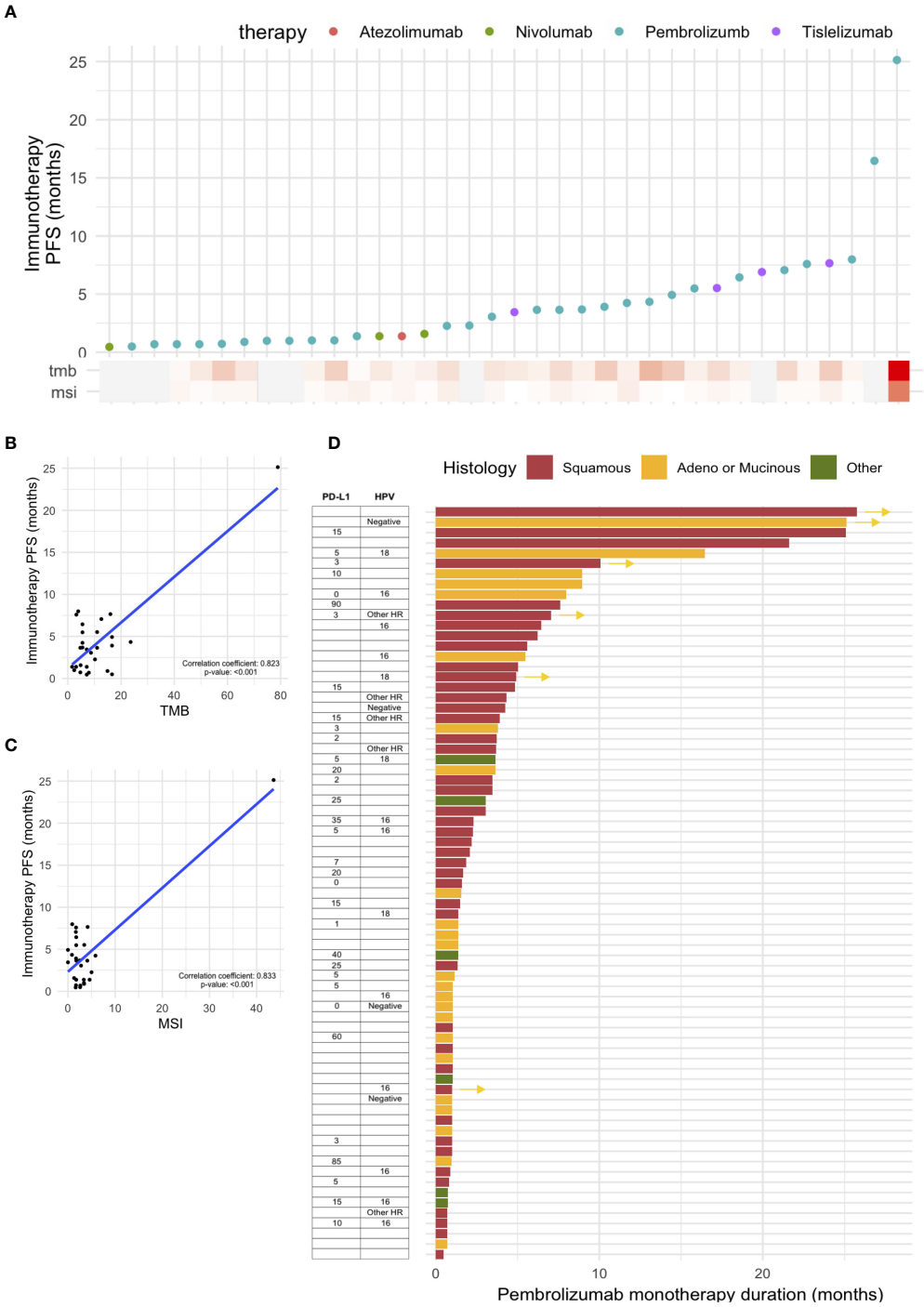


FIGURE 3
Outcomes of immunotherapy in cervical cancer. **(A)** Progression-free survival (PFS) based on various immunotherapy agents. PFS based on **(B)** tumor mutational burden (TMB) and **(C)** microsatellite instability (MSI). **(D)** Swimmer plot showing PFS based on pembrolizumab monotherapy, with PD-L1 CPS score and histology.

histology, with a median of 15. Patients with HPV 16 also showed a trend of high PD-L1 CPS, despite the lack of statistical significance owing to the limited number of patients with HPV genotype data. These findings suggest that patients with a high PD-L1 CPS may be candidates for immunotherapy, as suggested by previous clinical trials such as Keynote 158 and Checkmate 358 (6, 8, 9). Furthermore, our study showed that HER2 was not expressed in patients with squamous cell histology, whereas HER2 2+ and 3+ were identified in patients with non-squamous histology. Previous studies have indicated that a small, yet meaningful, proportion of patients with cervical cancer overexpress the HER2 receptor (19, 20). In our study, two patients overexpressing HER2 received T-DXd and showed a good response considering the treatment setting. The ongoing study, DESTINY-PanTumor02

(NCT04482309), will help to further investigate the effectiveness of T-DXd in the treatment of cervical cancer.

For immunotherapy outcomes, we found that the significant correlation between TMB and MSI with the duration of immunotherapy was largely driven by one patient with exceptionally high TMB and MSI showing a durable response. The calculation of the TMB and MSI using a panel-based sequencing approach may differ from the gold standard method of whole-exome sequencing-based testing and PCR-based testing of 5 MSI sites (21, 22). Although previous studies have suggested a high concordance between panel-based testing and the gold-standard methods (23), harmonizing data and establishing cutoffs across different panel designs remain challenging (24, 25).

In addition, the cohort characteristics are another, and perhaps more potent, confounder of immunotherapy outcomes. In the present study, our cohort represents real-world data based on the use of immunotherapy to treat cervical cancer. We revealed that the proportion of patients with a durable response is significantly lower than that observed in controlled clinical trial settings. A summary table comparing the present study with previous trials on mono-immunotherapy is given as Supplementary Table 3 (6, 9, 26). Unlike prospective clinical trial settings where only patients with good performance scores (ECOG 0 or 1) are included, our retrospective cohort included heavily pre-treated patients, approximately 40% of whom showed poor performance scores. Furthermore, about one-fourth of the patients received only one cycle of pembrolizumab for palliative purposes, and for most of these patients, it was the last therapy attempted before death. These cohort characteristics, including the use of palliative treatment and limited testing for PD-L1 CPS, pose difficulty in interpreting biomarkers in our study, such as TMB, MRI, or PD-L1 CPS. Despite these limitations, we still observed that few patients showed a durable response, and these patients had high PD-L1 SP263 or high TMB/MSI, which could be predicted based on the known biomarkers for immunotherapy.

This study had some limitations. First, this study is a retrospective study; although we collected clinical variables, IHC, and NGS data, these data were selectively tested based on the clinicians' discretion and may have caused potential selection bias. In addition, the choice of therapy was not based on systemic evaluation of a specific biomarker and was heterogeneous. As this was a single-center design, the practice patterns for IHC testing and immunotherapy use may differ in other centers. Moreover, the analysis was limited by the number of patients, especially because certain patients were not tested for certain biomarkers.

In conclusion, despite these limitations, our study represents a sizable cohort of patients with cervical cancer who underwent NGS with TruSight Oncology 500 or TruSight Tumor 170 panels, which are frequently used worldwide. To our knowledge, our study is the first to cover clinical variables, IHC results, genomic data, and immunotherapy outcomes. We found a considerable discrepancy between expected outcomes based on clinical trials and actual therapy outcomes in an unselected setting. These findings will help discuss therapeutic options with patients and identify new biomarkers or therapeutic agents for cervical cancer.

## Data availability statement

The raw data supporting the conclusions of this article will be made available by the authors, without undue reservation.

## Ethics statement

The studies involving human participants were reviewed and approved by Severance Hospital Institutional Review Board (IRB No # 4-2022-1399). Written informed consent for participation was not required for this study in accordance with the national legislation and the institutional requirements.

## Author contributions

Conceptualization: Y-NK and J-YL. Data curation: Y-NK and KL. Formal analysis: Y-NK and J-YL. Investigation: Y-NK, KL, EP, and J-YL. Methodology: Y-NK, EP, and J-YL. Supervision: JP, YL, J-YL, EN, SaK, SuK, and YK. Validation: EN, SaK, SuK, and YK. Visualization: Y-NK and J-YL. Writing – original draft: Y-NK. Writing – review and & editing: Y-NK, KL, EP, JP, YL, J-YL, EN, SaK, SuK, and YK. All authors contributed to the article and approved the submitted version.

## Conflict of interest

The authors declare that the research was conducted in the absence of any commercial or financial relationships that could be construed as a potential conflict of interest.

## Publisher's note



## Supplementary material

The Supplementary Material for this article can be found online at: https://www.frontiersin.org/articles/10.3389/fonc.2023.1156973/full#supplementary-material

# References


1. Sung H, Ferlay J, Siegel RL, Laversanne M, Soerjomataram I, Jemal A, et al. Global cancer statistics 2020: GLOBOCAN estimates of incidence and mortality worldwide for 36 cancers in 185 countries. *CA Cancer J Clin* (2021) 71(3):209–49. doi: 10.3322/caac.21660

2. Wright JD, Matsuo K, Huang Y, Tergas AI, Hou JY, Khoury-Collado F, et al. Prognostic performance of the 2018 international federation of gynecology and obstetrics cervical cancer staging guidelines. *Obstet Gynecol* (2019) 134(1):49–57. doi: 10.1097/AOG.0000000000003311

3. Pfaendler KS, Tewari KS. Changing paradigms in the systemic treatment of advanced cervical cancer. *Am J Obstet Gynecol* (2016) 214(1):22–30. doi: 10.1016/j.ajog.2015.07.022

4. Oaknin A, Friedman CF, Roman LD, D'Souza A, Brana I, Bidard FC, et al. Neratinib in patients with HER2-mutant, metastatic cervical cancer: findings from the phase 2 SUMMIT basket trial. *Gynecol Oncol* (2020) 159(1):150–6. doi: 10.1016/j.ygyno.2020.07.025

5. Monk BJ, Mas Lopez L, Zarba JJ, Oaknin A, Tarpin C, Termrungruanglert W, et al. Open-label study of pazopanib or lapatinib monotherapy compared with pazopanib plus lapatinib combination therapy in patients with advanced and recurrent cervical cancer. *J Clin Oncol* (2010) 28(22):3562–9. doi: 10.1200/JCO.2009.26.9571

6. Naumann RW, Hollebecque A, Meyer T, Devlin MJ, Oaknin A, Kerger J, et al. Safety and efficacy of nivolumab monotherapy in recurrent or metastatic cervical, vaginal, or vulvar carcinoma: results from the phase I/II CheckMate 358 trial. *J Clin Oncol* (2019) 37(31):2825–34. doi: 10.1200/JCO.19.00739

7. O'Malley DM, Neffa M, Monk BJ, Melkadze T, Huang M, Kryzhanivska A, et al. Dual PD-1 and CTLA-4 checkpoint blockade using balstilimab and zalifrelimab combination as second-line treatment for advanced cervical cancer: an open-label phase II study. *J Clin Oncol* (2022) 40(7):762–71. doi: 10.1200/JCO.21.02067

8. Xu Q, Wang J, Sun Y, Lin Y, Liu J, Zhuo Y, et al. Efficacy and safety of sintilimab plus anlotinib for PD-L1-Positive recurrent or metastatic cervical cancer: a multicenter, single-arm, prospective phase II trial. *J Clin Oncol* (2022) 40(16):1795–805. doi: 10.1200/JCO.21.02091

9. Chung HC, Ros W, Delord JP, Perets R, Italiano A, Shapira-Frommer R, et al. Efficacy and safety of pembrolizumab in previously treated advanced cervical cancer: results from the phase II KEYNOTE-158 study. *J Clin Oncol* (2019) 37(17):1470–8. doi: 10.1200/JCO.18.01265

10. Strickler JH, Hanks BA, Khasraw M. Tumor mutational burden as a predictor of immunotherapy response: is more always better? *Clin Cancer Res* (2021) 27(5):1236–41. doi: 10.1158/1078-0432.CCR-20-3054

11. Cancer Genome Atlas Research N, Albert Einstein College of M, Analytical Biological S, Barretos Cancer H, Baylor College of M and Beckman Research Institute of City of H, et al. Integrated genomic and molecular characterization of cervical cancer. *Nature* (2017) 543(7645):378–84. doi: 10.1038/nature21386

12. Alexandrov LB, Nik-Zainal S, Wedge DC, Aparicio SA, Behjati S, Biankin AV, et al. Signatures of mutational processes in human cancer. *Nature* (2013) 500(7463):415–21. doi: 10.1038/nature12477

13. Cha YJ, Kim D, Bae SJ, Ahn SG, Jeong J, Lee HS, et al. PD-L1 expression evaluated by 22C3 antibody is a better prognostic marker than SP142/SP263 antibodies in breast cancer patients after resection. *Sci Rep* (2021) 11(1):19555. doi: 10.1038/s41598-021-97250-2

14. Wolff AC, Hammond ME, Schwartz JN, Hagerty KL, Allred DC, Cote RJ, et al. American Society of clinical Oncology/College of American pathologists guideline recommendations for human epidermal growth factor receptor 2 testing in breast cancer. *Arch Pathol Lab Med* (2007) 131(1):18–43. doi: 10.5858/2007-131-18-ASOCCO

15. Ojesina AI, Lichtenstein L, Freeman SS, Pedamallu CS, Imaz-Rosshandler I, Pugh TJ, et al. Landscape of genomic alterations in cervical carcinomas. *Nature* (2014) 506(7488):371–5. doi: 10.1038/nature12881

16. Wen H, Guo QH, Zhou XL, Wu XH, Li J. Genomic profiling of Chinese cervical cancer patients reveals prevalence of DNA damage repair gene alterations and related hypoxia feature. *Front Oncol* (2021) 11:792003. doi: 10.3389/fonc.2021.792003

17. Fernandes A, Viveros-Carreno D, Hoegl J, Avila M, Pareja R. Human papillomavirus-independent cervical cancer. *Int J Gynecol Cancer* (2022) 32(1):1–7. doi: 10.1136/ijgc-2021-003014

18. Sastre-Garau X, Diop M, Martin F, Dolivet G, Marchal F, Charra-Brunaud C, et al. A NGS-based blood test for the diagnosis of invasive HPV-associated carcinomas with extensive viral genomic characterization. *Clin Cancer Res* (2021) 27(19):5307–16. doi: 10.1158/1078-0432.CCR-21-0293

19. Itkin B, Garcia A, Straminsky S, Adelchanow ED, Pereyra M, Haab GA, et al. Prevalence of HER2 overexpression and amplification in cervical cancer: a systematic review and meta-analysis. *PloS One* (2021) 16(9):e0257976. doi: 10.1371/journal.pone.0257976

20. Oh DY, Kim S, Choi YL, Cho YJ, Oh E, Choi JJ, et al. HER2 as a novel therapeutic target for cervical cancer. *Oncotarget* (2015) 6(34):36219–30. doi: 10.18632/oncotarget.5283

21. Meléndez B, Van Campenhout C, Rorive S, Remmelink M, Salmon I, D'Haene N. Methods of measurement for tumor mutational burden in tumor tissue. *Transl Lung Cancer Res* (2018) 7(6):661–7. doi: 10.21037/tlcr.2018.08.02

22. Boland CR, Thibodeau SN, Hamilton SR, Sidransky D, Eshleman JR, Burt RW, et al. A national cancer institute workshop on microsatellite instability for cancer detection and familial predisposition: development of international criteria for the determination of microsatellite instability in colorectal cancer. *Cancer Res* (1998) 58(22):5248–57.

23. Shimozaki K, Hayashi H, Tanishima S, Horie S, Chida A, Tsugaru K, et al. Concordance analysis of microsatellite instability status between polymerase chain reaction based testing and next generation sequencing for solid tumors. *Sci Rep* (2021) 11(1):20003. doi: 10.1038/s41598-021-99364-z

24. Fancello L, Gandini S, Pelicci PG, Mazzarella L. Tumor mutational burden quantification from targeted gene panels: major advancements and challenges. *J Immunother Cancer* (2019) 7(1):183. doi: 10.1186/s40425-019-0647-4

25. Siemanowski J, Schömig-Markiefka B, Buhl T, Haak A, Siebolts U, Dietmaier W, et al. Managing difficulties of microsatellite instability testing in endometrial cancer-limitations and advantages of four different PCR-based approaches. *Cancers (Basel)* (2021) 13(6). doi: 10.3390/cancers13061268

26. Frenel JS, Le Tourneau C, O'Neil B, Ott PA, Piha-Paul SA, Gomez-Roca C, et al. Safety and efficacy of pembrolizumab in advanced, programmed death ligand 1-positive cervical cancer: results from the phase ib KEYNOTE-028 trial. *J Clin Oncol* (2017) 35(36):4035–41. doi: 10.1200/JCO.2017.74.5471

frontiers | Frontiers in Oncology

TYPE Original Research
PUBLISHED 05 June 2023
DOI 10.3389/fonc.2023.1152991



OPEN ACCESS

EDITED BY
Umberto Malapelle,
University of Naples Federico II, Italy

REVIEWED BY
Neveen Said,
Wake Forest Baptist Medical Center, United States
Roberto C. Delgado Bolton,
Hospital San Pedro, Spain
Komsun Suwannarurk,
Thammasat University, Thailand

*CORRESPONDENCE
Jae Won Yun
jwyunmd@gmail.com
Eun-Suk Kang
eskang@skku.edu

†These authors have contributed equally to this work

RECEIVED 28 January 2023
ACCEPTED 09 May 2023
PUBLISHED 05 June 2023

CITATION
Haque R, Lee J, Chung J-Y, Shin H-Y, Kim H, Kim J-H, Yun JW and Kang E-S (2023) VGLL3 expression is associated with macrophage infiltration and predicts poor prognosis in epithelial ovarian cancer. *Front. Oncol.* 13:1152991. doi: 10.3389/fonc.2023.1152991



# VGLL3 expression is associated with macrophage infiltration and predicts poor prognosis in epithelial ovarian cancer

Razaul Haque [1,2†], Jaebon Lee [3†], Joon-Yong Chung [4], Ha-Yeon Shin [5], Hyosun Kim [5], Jae-Hoon Kim [5], Jae Won Yun [6*] and Eun-Suk Kang [1,2,7*]

[1]Department of Laboratory Medicine and Genetics, Samsung Medical Center, Seoul, Republic of Korea, [2]School of Medicine, Sungkyunkwan University, Suwon, Republic of Korea, [3]School of Medicine, Sungkyunkwan University, Seoul, Republic of Korea, [4]Molecular Imaging Branch, Center for Cancer Research, National Cancer Institute, National Institutes of Health, Bethesda, MD, United States, [5]Department of Obstetrics and Gynaecology, Gangnam Severance Hospital, Yonsei University College of Medicine, Seoul, Republic of Korea, [6]Veterans Medical Research Institute, Veterans Health Service Medical Center, Seoul, Republic of Korea, [7]Cell and Gene Therapy Institute, Research Institute for Future Medicine, Samsung Medical Center, Seoul, Republic of Korea

**Background/objective:** High-grade serous ovarian carcinoma (HGSOC) is the most common histologic type of epithelial ovarian cancer (EOC). Due to its poor survival outcomes, it is essential to identify novel biomarkers and therapeutic targets. The hippo pathway is crucial in various cancers, including gynaecological cancers. Herein, we examined the expression of the key genes of the hippo pathway and their relationship with clinicopathological significance, immune cells infiltration and the prognosis of HGSOC.

**Methods:** The Cancer Genome Atlas (TCGA) and Gene Expression Omnibus (GEO) data were curated to analyse the mRNA expression as well as the clinicopathological association and correlation with immune cell infiltration in HGSOC. The protein levels of significant genes in the HGSOC tissue were analysed using Tissue Microarray (TMA)-based immunohistochemistry. Finally, DEGs pathway analysis was performed to find the signalling pathways associated with VGLL3.

**Results:** VGLL3 mRNA expression was significantly correlated with both advanced tumor stage and poor overall survival (OS) (p=0.046 and p=0.003, respectively). The result of IHC analysis also supported the association of VGLL3 protein with poor OS. Further, VGLL3 expression was significantly associated with tumor infiltrating macrophages. VGLL3 expression and macrophages infiltration were both found to be independent prognostic factors (p=0.003 and p=0.024, respectively) for HGSOC. VGLL3 was associated with four known

10.3389/fonc.2023.1152991

and three novel cancer-related signalling pathways, thus implying that VGLL3 is involved in the deregulation of many genes and pathways.

**Conclusion:** Our study revealed that VGLL3 may play a distinct role in clinical outcomes and immune cell infiltration in patients with HGSOC and that it could potentially be a prognostic marker of EOC.

KEYWORDS

high-grade serous ovarian carcinoma, hippo pathway, VGLL3, prognosis, macrophage

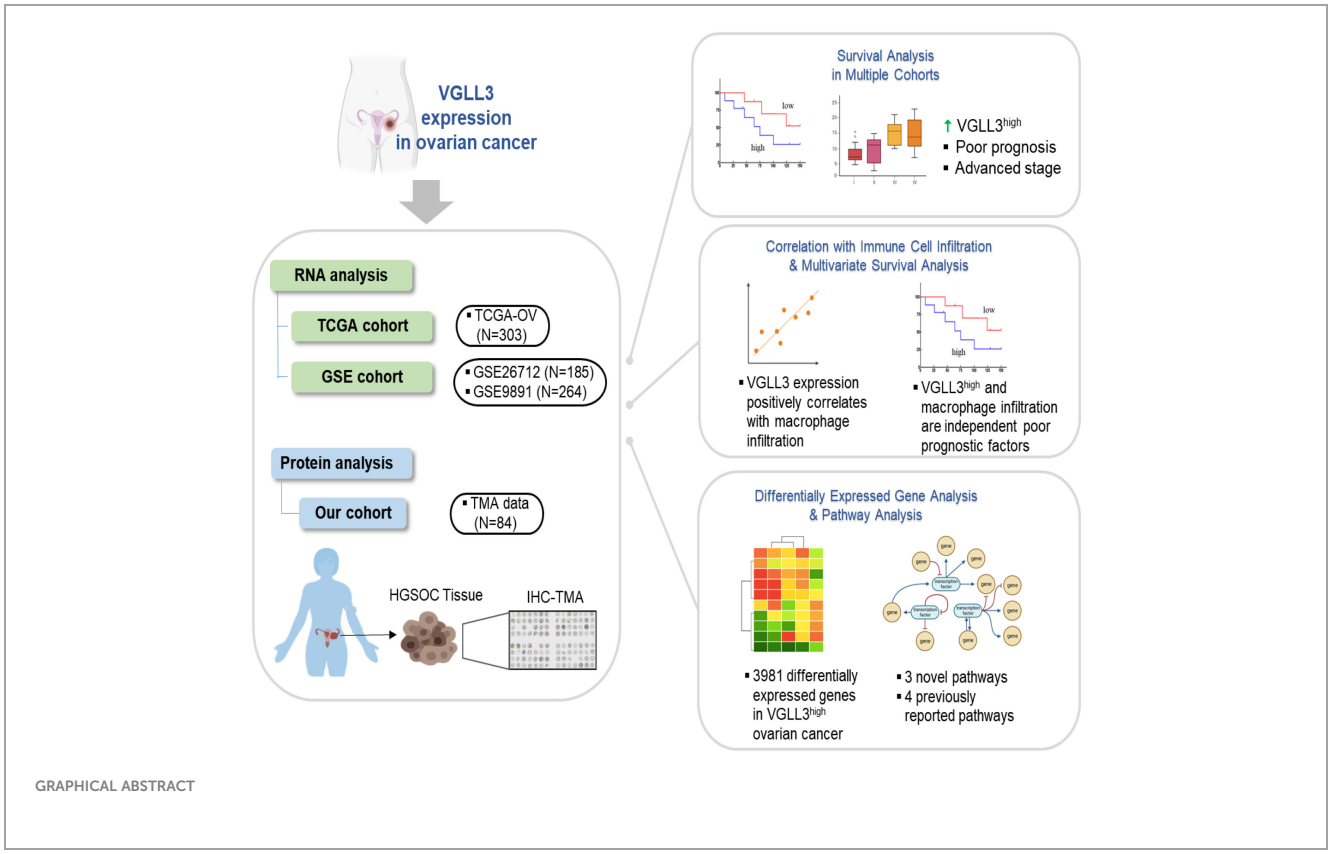


GRAPHICAL ABSTRACT

## Introduction

Epithelial ovarian cancer (EOC) is the most dominant form of ovarian cancer, which accounts for the highest rates of mortality and morbidity among the female sex (1). Despite the immense advancements in treatment strategy, the 5-year overall survival rate of EOC is still under 45% (2). Such poor prognosis may result from the complex and obscure pathogenesis of EOC, late diagnosis, a lack of predictive biomarkers, and ineffective target identification (3). Tumors in human ovary can be categorized into *surface epithelial-stromal* tumors, *sex cord-stromal* tumors, and *germ cell* tumors (4). Surface epithelial-stromal carcinoma can be further sub-grouped into serous (HGSOC and low-grade serous ovarian carcinoma), mucinous carcinoma, endometrioid carcinoma, clear cell carcinoma, and transitional cell carcinoma (or Brenner type (4). HGSOC considered as the most lethal EOC diagnosed at advanced stages, and results even higher percentage of mortality in ovarian cancer (5). However, characterization of HGSOC is very difficult, as they account for a very low number of mutations, and there is a scarcity of appropriate diagnosis markers. According to TCGA, the

**Abbreviations:** HGSOC, High-grade serous ovarian carcinoma; EOC, Epithelial ovarian cancer; OS, overall survival; TEADs, Transcriptional enhanced associate domains; YAP, Yes-associated protein; TAZ, Transcriptional co-activator with PDZ-binding motif; TIICs, Tumor-infiltrating immune cells; IHC, immunohistochemistry; TMA, Tissue Microarray; TCGA, The Cancer Genome Atlas; MSIT, Ministry of Science and ICT; FIGO, Federation of Gynaecology and Obstetrics; TIMER, Tumor Immune Estimation Resource; VEGFR2, Vascular endothelial growth factor receptor 2; PDGF, Platelet-derived growth factor gene; GEO, expression omnibus; RBDs, RNA Binding Proteins.

most common mutation found in Tp53 (96% cases), whereas mutations in other commonly mutated oncogenes such as *KRAS*, *BRAF*, *NRAS*, and *PIK3CA* are very rare in HGSOC (all less than 1%) (6, 7). Therefore, there is an urgent need to explore novel biomarkers to improve the diagnosis and early detection of HGSOC to improve treatment efficiency.

The hippo pathway is a critical regulator of morphogenesis, organ size determination, and tumorigenesis in many tissues, including the reproductive system (8, 9). Formation of the YAP/TAZ-TEADs complex serves as the key mechanism that stimulates the expression of target genes (e.g., connective tissue growth factor and cysteine-rich angiogenic inducer 61) that are essential for cell proliferation and survival (10). As a tumor suppressor pathway, dysregulation of the hippo pathway has been reported in various cancers (11). Yes-associated protein (YAP) and transcriptional coactivator with PDZ-binding motif (TAZ) plays an oncogenic role in EOC tumorigenesis by increasing cell proliferation and apoptotic resistance, reducing contact inhibition, and improving motility and anchorage-independent growth (12, 13). However, their clinicopathological outcomes in EOC are still debated.

Hippo pathway not only regulated by its core (YAP/TAZ) components, but also other regulatory and signalling molecules. Vestigial-like 3 (VGLL3) is a member of the VGLL family that also serves as a cofactor for transcriptional enhanced associate domains (TEADs) and participate in hippo signalling (14). TEAD1-4 recruits VGLL3 competitively to YAP/TAZ for their transcriptional activity (15). Despite the physiologic function is unknown, VGLL3 has recently been reported to be associated with the inhibition of adipocyte differentiation and the regulation of trigeminal nerve formation and cranial neural crest migration (16, 17). Now a day's multiple pieces of evidence suggest that VGLL3 is associated with different cancers (18–21). VGLL3 has previously been reported to play a tumor suppressive role in EOC by Gambaro et al. in 2013 (22). Since then, there have been no further reports elucidating the role of VGLL3 in EOC. Moreover, Gambaro et al. derived the hypothesis from a chromosome transfer experiment wherein the transfer of a chromosome fragment containing *VGLL3* gene suppressed tumor phenotypes in the ovarian tumor cell line OV90 (23, 24). However, *VGLL3* as a single-gene transfer did not generate stable VGLL3 expression and was unable to suppress the proliferation of OV90 cells (22). Therefore, it is essential to re-evaluate the role of VGLL3 in EOC.

There is increasing evidence suggesting that immune cell infiltration plays a crucial role in the prognosis of various tumors and affects OS. Infiltration of different immune cells, such as T cells, macrophages, mast cells, and natural killer cells, is known to be associated with either favourable or unfavourable prognosis (25). Zhang et al. recently showed that *VGLL3* serves as a novel unfavourable prognostic biomarker in stomach adenocarcinoma and correlates with immune evasion, particularly due to infiltration of macrophages and dendritic cells (21). However, the role of VGLL3 in the immune microenvironment of EOC remains to be elucidated

In this study, we performed a comprehensive analysis using public databases and web tools, as well as tissue microarray (TMA) to investigate the significance of key genes in hippo pathways, including *VGLL3*, *VGLL4*, *TEAD3*, *TEAD4*, *YAP*, and *TAZ*, on the clinicopathological characteristics and immune cell infiltration features of HGSOC. We also investigated the role of VGLL3 as a prognostic factor of HGSOC and its association with cancer-related signal transduction pathways.

# Materials and methods

## mRNA data sources and clinical information

The information on the mRNA expression and the clinical data of ovarian cancer were acquired from the Cancer Genome Atlas (TCGA) repository, Genome Data Analysis Centre (GDAC) (https://gdac.broadinstitute.org/), and the University of California Santa Cruz browser (https://xenabrowser.net/datapages/). For further analysis, 303 samples that had clinical and mRNA information available were selected (Table 1). The expression of genes was compared between normal ovarian (n=88) and tumor (n=426) tissues based on the GEPIA2 database (26) (http://gepia2.cancer-pku.cn/#index). For the validation of gene expression in HGSOC, we acquired data from the gene expression omnibus (GEO) in the form of GSE26712 (10 normal ovarian *vs*. 185 tumor tissue) and GSE9891 (264 HGSOC tissue samples).

## Cell culture

Four ovarian cancer cell lines, namely SKOV3, OVCAR3, OVCA429, OVCA433 and five primary EOC cell lines including YDOV-13 (originated from a malignant Brenner tumor), YDOV-139, YDOV-157, YDOV-161(originated from serous cystadenocarcinomas) and YDOV-151 (originated from a mucinous cystadenocarcinoma) were used in this study (27–30). The primary cell lines were established in Jae-Hoon Kim's lab and all cell lines were kindly provided by Jae-Hoon Kim (Gangnam Severance Hospital, Yonsei University). SKOV3 and OVCAR3 cell lines were maintained in RPMI-1640 media supplemented with 10% FBS and 1% with penicillin/streptomycin. The other cell lines were maintained in DMEM media containing 10% FBS and 1% penicillin/streptomycin. All the cell lines were cultured at 37°C in 5% $CO_2$.

## RNA isolation and real-time qPCR

At 70-80% of confluence, cells were washed with PBS, after which total RNA was extracted using TRIzol reagent (Ambion, Carlsbad, USA) according to the manufacturer's protocol. Total RNA (1 μg) from each sample was reverse-transcribed into cDNA using the Maxima First Strand cDNA Synthesis Kit (Thermo Scientific, Waltham, MA) according to the manufacturer's protocol. Real-time quantitative polymerase chain reaction (RT-

TABLE 1 Clinicopathological features of high-grade serous ovarian carcinoma patients from The Cancer Genome Atlas and TMA datasets.

| Clinical Factor | TCGA (n=302) | TMA (n=84) |
|---|---|---|
| Age (years, mean ± SD) | 59.10 ± 10.93 | 54.77 ± 10.41 |
| CTx response (n) (Sensitive/Resistant/unknown) | 200/40/62 | 67/15/2 |
| Death/Alive (n) | 183/119 | 50/34 |
| Overall survival (years, mean ± SD) | 3.04 ± 2.44 | 6.65 ± 5.03 |
| Pre-CA125 (n)<br>(Negative ≤35U/ml)/(Positive >35U/ml) | NA | 7/77 |
| Stage | | |
| Stage I (n) | 1 | 8 |
| Stage II (n) | 21 | 5 |
| Stage III (n) | 240 | 58 |
| Stage IV (n) | 38 | 13 |
| Unknown | 2 | – |
| Grade | | |
| G1 (n) | 1 | 2 |
| G2 (n) | 33 | 38 |
| G3 (n) | 260 | 44 |
| Others (GB, GX) (n) | 8 | – |

(n), Number of patients; CR, Complete response; PR, Partial response; SD, Stable disease; PD, Progressive disease; CTx, Chemotherapy; Others (GB, GX), GB, Grade borderline; GX, Grade cannot be assessed; NA, not available.

qPCR) was performed to quantify mRNA expression using SYBR Green PCR Master Mix (Enzynomics, Daejeon, Republic of Korea) and the QuantStudio 6 Flex real-time PCR system (Applied Biosystems, Foster City, CA). Relative mRNA expression was quantified using the comparative Ct (ΔCt) method and expressed as $2^{-\Delta\Delta Ct}$. The following primers were used for PCR: VGLL3: Forward 5'- CCAACTACAGTCACCTCTGCTAC-3' and Reverse 5'- ACCACGGTGATTCCTTACTCTTG-3', GPADH: Forward 5'- ATGGAAATCCCATCACCATCTT-3' and Reverse 5'- CGCCC CACTTGATTTTGG-3'.

## Protein extraction and western blotting

Total cell lysates were isolated using cell lysis buffer (RIPA buffer: Cell Signaling Technology #9806, Danvers, MA) containing protease inhibitor cocktail (Roche, Nutley, NJ). Protein concentrations were determined by BCA assay (Sigma-Aldrich, St. Louis, MO). Proteins were separated by SDS-PAGE and transferred from gels to 0.2 µm nitrocellulose membranes (Pall Corporation, Washington, NY). The nitrocellulose membrane was further incubated overnight at 4°C with rabbit anti-VGLL3 (1:1000, Novus Biologicals, NB100-56875, Centennial, USA) and rabbit anti-GAPDH (1:2000, Novus Biologicals, 4650S, Centennial, USA). After that membranes were incubated with HRP-conjugated anti-Rabbit IgG (1:1000, Cell Signaling Technology, 7074S, Danvers, MA) secondary antibody for 1 hour at RT, protein bands were visualised using western blotting luminol reagent (Santa Cruz Biotechology, Inc., Dallas, Texas).

## Patients' tissue samples and clinical information

The unstained slides from 84 HGSOC and 66 adjacent normal ovarian epithelial TMA blocks and their corresponding sets of clinical information were obtained from the Korea Gynaecologic Cancer Bank (KGCB) of Gangnam Severance Hospital, Yonsei University College of Medicine (No. HTB-P2021-5), funded by the Korean Government Ministry of Science and ICT (MSIT) (NRF-2017M3A9B8069610). All the patients were treated with first line chemotherapy. Tissue samples and medical records were obtained with the approval of the Institutional Review Board of Gangnam Severance Hospital (IRB#, HTB-P2021-5), Seoul, Republic of Korea. All procedures were conducted in accordance with the guidelines of the Declaration of Helsinki. Tumor staging was performed according to the classification established by the International Federation of Gynaecology and Obstetrics (FIGO). For all study participants, CA125 levels were measured at primary diagnosis up to 1 week preoperatively using Elecsys CA125 II ECLIA (Roche Diagnostics, Rotkreuz, Switzerland). The demographics and clinical characteristics of the individuals that participated in this study are listed in Table 1.

## Tumor infiltrating immune cell estimation

The estimated abundance of tumor-infiltrating immune cells (TIICs) was calculated using immunedeconv in R, which was downloaded from the Tumor Immune Estimation Resource (TIMER) 2.0 website (http://timer.cistrome.org/) (31). To elaborate, TIICs were inferred using three different tools, including EPIC (http://epic.gfellerlab.org/), TIMER (https://cistrome.shinyapps.io/timer/), and CIBERSORT (https://cibersort.stanford.edu). These three computational algorithms use deconvolution-based approaches that model gene expressions as the weighted sum of the expression profiles of the admixed cell types (32–34). The outlier of TIICs was eliminated using Tukey's method. Then, a correlation analysis between the abundance of TIICs and gene expressions was conducted using Pearson's method. A $p$-value < 0.05 and a correlation co-efficient R ≥ 0.30 were considered to represent a significant correlation.

## Immunohistochemical analysis

VGLL3 protein expressions were analysed by immunohistochemical guided TMA, which was described before (35). Briefly, deparaffinised and rehydrated sections were retrieved *via* microwave for 10 min in a pH 6.0 citrate buffer. Endogenous peroxidase was then inactivated using peroxidase blocking solution (Agilent, S2023, Dako, Glostrup, Denmark) for 20 minutes. Next, the tissue samples were incubated with the anti-VGLL3 primary antibody (1:200, Novus Biologicals, NBP2-31590, Centennial, USA) for 2 h at 25°C. The secondary antibody was applied for 1 h at 25°C, after which detection was performed using DAB Substrate-Chromogen solution (Agilent, K5007, Dako, Glostrup, Denmark). Lastly, the sections were counterstained using haematoxylin and mounted.

Stained TMA slides were digitized using the NanoZomer XR digital pathology (NDP) system (Hamamatsu, Hamamatsu City, Japan) at ×40 objective magnification with a single-focus layer. Digitized images were automatically analysed using Visiopharm software version 6.9.1 (Visiopharm, Hørsholm, Denmark). Regarding the expression value of VGLL3 nuclear staining, a brown nuclear staining intensity (0=negative, 1=weak, 2=moderate, and 3=strong) and a respective percentage were obtained. For VGLL3 cytoplasmic assessment, a brown cytoplasmic intensity (weak and strong) was obtained, and each proportion was analysed. Histoscores were calculated by multiplying the percentage of positive cells by their staining intensity.

## Differentially expressed gene analysis

VGLL3 mRNA raw read counts downloaded from GDAC were used to identify the association with differentially expressed genes (DEGs) using the DESeq2 package in R, and the cut-off value of FDR (offered as adjusted p-value) was 0.001 (p-value < 2.04e-4) (36). Using the identified DEGs correlated with VGLL3, pathway analysis was performed using ConsensusPathDB (http://cpdb.molgen.mpg.de/) (37). Next, among the identified pathways ($p$ value < 0.01, $q$ value < 0.2), cancer-related pathways were selected through a literature review and manual curation. We also conducted a heatmap analysis using complex heatmap package in R to identify the significant genes that were associated with selected pathways and high VGLL3 expression.

## Statistical analysis

Data were statistically analysed using R software version 4.0.2. (R 4.0.2, Auckland, New Zealand). All data values are expressed as mean ± standard error of the mean (S.E.M). To compare gene expression among groups with different clinical and pathological features, the DESeq2 package, Mann-Whitney test, and Kruskal-Wallis test were used. For survival analysis, Kaplan-Meier plot and log-rank test were conducted using the survival and survminer packages in R (38). To identify the independent prognostic factor, Cox regression analyses were performed and visualised using the forest plot package in R (39). $p$-values <0.05 were considered to be statistically significant.

# Results

HGSOC tumors samples from 302 TCGA and 84 TMA datasets were analysed according to stage and grade. TMA data was further analysed based on age, pre-CA125 level, and chemosensitivity after initial treatment. CA125 levels of >35 IU/mL (n=77) were considered to be positive, while levels of ≤35 IU/mL (n=7) were considered to be negative.

## Altered *VGLL3* mRNA expression had a prognostic significance in HGSOC

First, we analysed the expression levels of six key genes in the hippo pathway (*YAP1, TAZ, TEAD3, TEAD4, VGLL3*, and *VGLL4*) in HGSOC. We found that the expressions of *VGLL4*, *TEAD3*, *TEAD4*, and *YAP1* were all increased in HGSOC. By contrast, the expressions of *VGLL3* and *TAZ* were low in HGSOC (Figure 1A). The result was comparable to those obtained from the GSE9891 cohort (Supplementary Figure S1A). Interestingly, *VGLL3* expression was the lowest among all the genes in both the TCGA ($p$=<2e-16) and GSE9891 cohorts ($p$=<2e-16) (Figure 1A and Supplementary Figure S1A). When tumors were compared to normal ovarian samples, we found that *VGLL3* was significantly lower in tumor samples than it was in normal ovarian samples in both the TCGA and GSE26712 cohorts ($p$<0.05 and $p$=2.4e-07, respectively) (Supplementary Figures S1B, C). Whereas, *TEAD4* was significantly higher in tumor samples compared to normal ovarian samples in both the TCGA and GSE26712 cohorts ($p$<0.05 $p$=5.8e-07) (Supplementary Figures S1B, C). There were no significant differences observed regarding the expressions of *YAP1* and *VGLL4* between tumor and normal ovaries in either cohort. However, the expression of *TAZ* and *TEAD3* were discrepant between different datasets. Expression of *TAZ* in HGSOC was significantly lower in TCGA cohort (p<0.05), but higher in the GSE26712 cohort ($p$=2e-06) compared to normal ovary

10.3389/fonc.2023.1152991

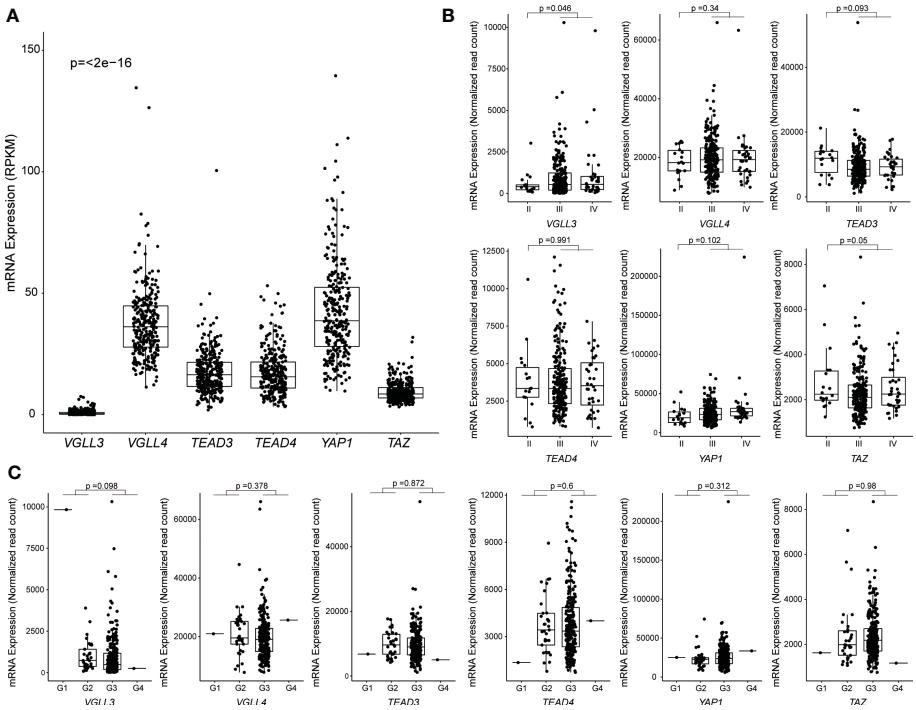


FIGURE 1
Correlation between mRNA expression and clinicopathological features in The Cancer Genome Atlas (TCGA) ovarian cancer data. Samples without RPKM and Raw read counts data were omitted. **(A)** Levels of mRNA expression among six genes. RPKM data from 296 samples were used, and the p-values were calculated using the Kruskal-Wallis test. **(B)** Levels of mRNA expression among different stages of HGSOC: Stage I (n = 0), Stage II (n = 18), Stage III (n = 239), Stage IV (n = 36). The *p*-value was calculated using the DESeq2 package. **(C)** Levels of mRNA expression among different grades of HGSOC: G1 (n = 1), G2 (n = 33), G3 (n = 254), G4 (n = 1). The *p*-value was calculated using the DESeq2 package. Each point represents an individual sample.

(Supplementary Figures S1B, C). No significant difference was observed in *TEAD3* expression between HGSOC *vs.* normal ovary in the TCGA cohort although it significantly increased in the GSE26712 cohort $p$=2.6e-05.

Finally, we checked the expression of VGLL3 both in mRNA and protein level in different OC cell lines. We observed different cell lines express different level of VGLL3 mRNA and protein (data not shown). Interestingly, we noticed that there was discrepancy of VGLL3 expression between mRNA and protein level in same cell line. The discrepancy was more prominent in SKOV3, YDOV13, and YDOV139 cell line (data not shown) and less prominent in OVCAR3 cell line, whereas, there was no observable discrepancy found in OVCA429, OVCA433, YDOV151, YDOV157 and YDOV161 cell lines in terms of VGLL3 expression at the mRNA and protein level.

Next, we explored the correlation of the above six hippo-related genes with the progression of HGSOC. *VGLL3* expression was found to be significantly increased in the advanced stages (stage III+IV) of HGSOC tumors ($p$=0.046) compared to in the early stage II (Figure 1B). However, *VGLL4, TEAD3, TEAD4, YAP*, and *TAZ* did not show any significant difference between stage II *vs.* stage III+IV in HGSOC (Figure 1B). When we checked the expressions of those six genes in different grades, we didn't observe significant differences in any genes between (G1+G2) *vs.* (G3+G4). However, for *VGLL3* expression, there was a decreasing trend observed in (G3+G4) relative to (G1+G2) ($p$=0.098) (Figure 1C).

Next, we checked the correlations of those six genes with the OS of patients with HGSOC. The mRNA expression of each gene was categorised into high and low groups (Supplementary Figure S2). The data showed that only *VGLL3* had a significant association with OS ($p$=0.003) (Figure 2), which was consistent in both the GSE26712 and GSE9891 ($p$=0.048, $p$=0.012, respectively) cohorts (Supplementary Figure S2B, C *right panel*). *VGLL3*high correlated with the lower OS in HGSOC, while *VGLL3*low was associated with better OS. However, the other five genes did not show any significant correlation with OS (Figure 2). Taken together, these findings suggest that the role of *VGLL3* mRNA is distinctive in HGSOC compared to the other five genes, which correlated with the characteristics of advanced tumor stages of HGSOC and poor survival outcomes.

## *VGLL3* mRNA expression was associated with macrophage infiltration and unfavourable prognosis

Then, we checked the correlation of six genes with immune cell infiltration and found that *VGLL3* was positively correlated with infiltration of macrophage, CD4+ T cell, and CD8+ T cell in HGSOC, while it was negatively correlated with B cells (Figures 3A–C). Interestingly, the correlation of *VGLL3* with macrophage infiltration was strongest among all other TIICs in

10.3389/fonc.2023.1152991

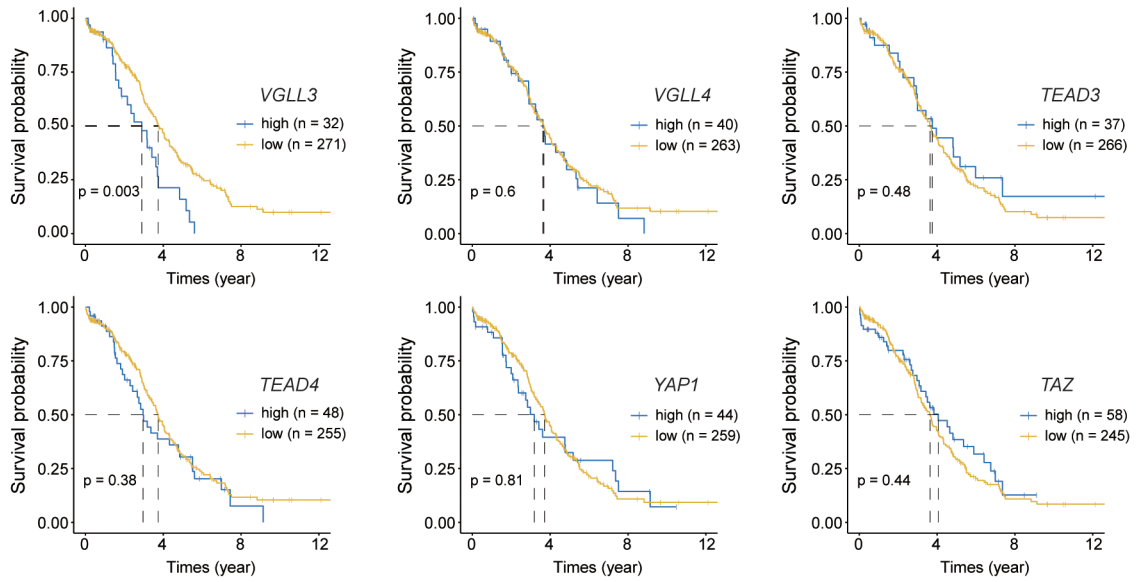


FIGURE 2
Kaplan–Meier curves for overall survival of six target genes. Normalised read counts data for 302 The Cancer Genome Atlas (TCGA) ovarian cancer samples were analysed for overall survival while comparing the high and low expression of each gene; Top: *from left to* right *VGLL3* ($p$=0.003), *VGLL4* ($p$=0.6), *TEAD3* ($p$=0.48); Bottom: *from left to right TEAD4* ($p$=0.38), *YAP1* ($p$=0.81), *TAZ* ($p$=0.44). High and low expression of each gene was selected based on the visual distinction described in Supplementary Figure S2. Statistical significance was evaluated using the log-rank test.

HGSOC. This finding was consistently revealed in all three computational tools (EPIC, R=0.38; $p$=1.8e-11, TIMER, R=0.44; $p$=2.7e-15, and CIBERSORT, R=0.44; $p$=7.2e-16). However, we could not find any significant correlation between the other five genes and HGSOC TIICs (Supplementary Figure S3). Then, we checked the correlation of *VGLL3* with two different subtypes of macrophage (M1 and M2 macrophage). We noted that, while there was no significant correlation found between *VGLL3* with M1 macrophage (Supplementary Figure S4A), *VGLL3* was found to be significantly correlated with M2 macrophage infiltration R=0.44; $p$=5.7e-16 (Supplementary Figure S4B), thus suggesting that the association of *VGLL3* with macrophage mainly comes from M2 macrophage.

Next, we investigated the association of macrophage infiltration with OS in HGSOC. Similar to VGLL3, high levels of macrophages were significantly correlated with poor overall survival ($p$=0.0057), whereas low levels of macrophage expression correlated with better OS (Figure 4A). Multivariate analysis further confirmed that *VGLL3* and macrophages were independent prognostic factors for HGSOC ($p$=0.003 and $p$=0.024, respectively) (Figure 4B and Supplementary Figure S5), thus suggesting that *VGLL3* serves as an independent unfavourable prognostic marker in HGSOC, possibly in association with macrophage infiltration.

## VGLL3 protein expression had similar effects on clinical outcomes as the *VGLL3* mRNA expression

Next, to investigate the significance of VGLL3 protein expression in HGSOC, immunohistochemistry-guided TMA score was analyzed at both nuclear and cytoplasmic level in our HGSOC cohort. Interestingly, VGLL3 protein expressions at both nuclear and cytoplasmic levels were significantly higher ($p$<0.001) in HGSOC tissues than it was in the normal adjacent tissues (Table 2 and Figures 5A, B). Then, we investigated the correlation of VGLL3 protein expression at both nuclear and cytoplasmic levels with different clinicopathological features of HGSOC (Table 3). There was no significant difference found regarding the expression of VGLL3 protein depending on age, FIGO stage, tumor grade, Pre-CA125 level, and chemo-sensitivity (Table 3).

To evaluate the prognostic role of VGLL3 protein in HGSOC, we applied Kaplan–Meier survival analysis by determining the $VGLL3^{high}$ and $VGLL3^{low}$ groups in a manner similar to that of the mRNA data. We found that high expressions of VGLL3 protein at nuclear levels was correlated with lower OS in patients with HGSOC, although it was not statistically significant (Figures 5C, D).

## DEGs and pathway analysis identified altered pathways associated with *VGLL3*

We investigated VGLL3-related pathways in cancer to explore the potential mechanism in HGSOC. The DEG analysis showed that around 3,981 genes were significantly associated with *VGLL3* expression. Pathway analysis using 3,981 DEGs revealed that the gene sets associated with *VGLL3* mRNA expression showed enhancements in extracellular matrix organization, focal adhesion, PI3K-Akt signalling pathway, and JAK-STAT signalling pathway (Figure 6A). The association of *VGLL3* with those pathways has been previously been reported in different cancers (21). Interestingly, along with previously reported

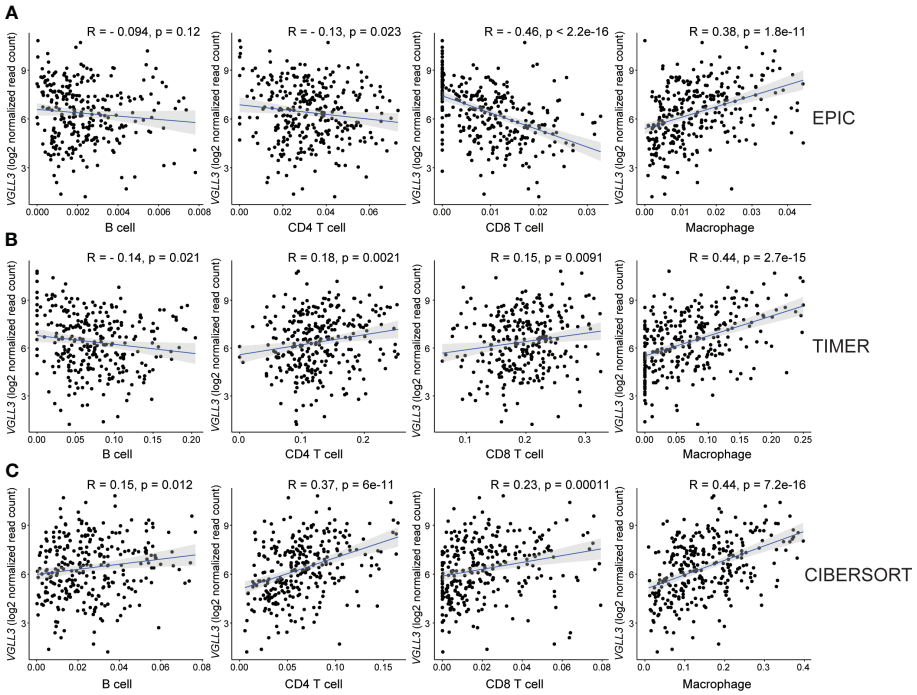


FIGURE 3
Correlation between *VGLL3* mRNA expression and immune cell infiltration. The levels of immune cell infiltrations were estimated using three databases: **(A)** EPIC, **(B)** TIMER, and **(C)** CIBERSORT abs mode. The three methods show that macrophage and *VGLL3* reached a consensus on a significantly positive correlation. The X-axis is the estimated values of three algorithms that represent immune cell fractions and the Y-axis represents the *VGLL3* mRNA expression. For CIBERSORT, cell fractions for each immune cell were considered as a summation of their subsets. After eliminating outliers of immune cell fractions using Tukey's method, Pearson's method was performed to determine the correlation between *VGLL3* gene and the immune cells (*from left to right*: B cell, CD4+ T cell, CD8+ T cell and macrophage), and the correlation coefficient was shown as R. For 303 The Cancer Genome Atlas (TCGA) ovarian cancer samples, the normalised read counts from TCGA Genome Data Analysis Center (GDAC) database and the immune cell infiltration levels from TIMER 2.0 website were downloaded and used to draw plots. A $p$ <0.05 and R ≥ 0.3 was considered as statistically significant.

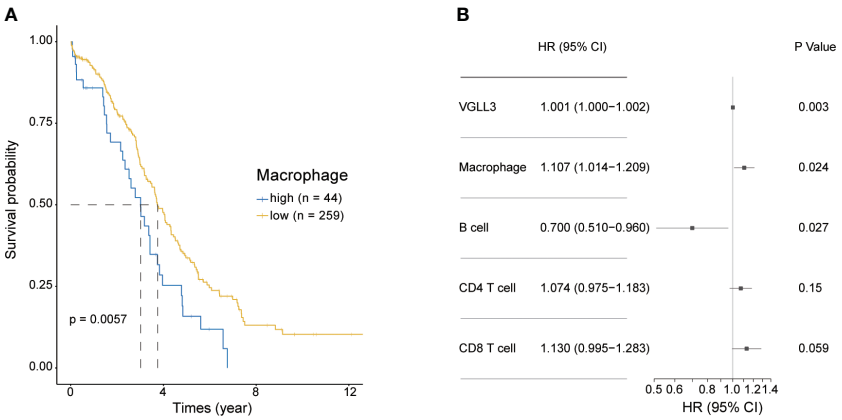


FIGURE 4
*VGLL3* and macrophages are unfavourable prognostic markers. Normalised read counts and infiltrated immune cell fractions estimated using EPIC for 303 HGSOC tissue samples were utilised. **(A)** Kaplan–Meier survival curves of OS comparing high (n=44) and low (n=259) macrophage infiltration in HGSOC, $p$=0.0057. **(B)** Forest plot visualizing the hazard ratio with a 95% confidence interval and $p$-value was calculated using multivariate Cox regression analysis. The levels of infiltrated immune cells estimated using EPIC were multiplied by 100 to transform them into percentile values. All variables were considered to be continuous variables.

TABLE 2 Comparison of VGLL3 protein expression in high-grade serous ovarian carcinoma and normal adjacent tissues.

| Variables | No | (%) | VgLL3_Nucleus | | VgLL3_Cytoplasm | |
|---|---|---|---|---|---|---|
| | | | Mean IHC score (95% CI) | *p*-value | Mean IHC score (95% CI) | *p*-value |
| Normal | 66 | 44.0 | 41.07 [27.69-54.45] | <0.0001 | 9.94 [2.61-17.28] | <0.0001 |
| HGSOC | 84 | 56.0 | 133.28 [121.42145.14] | | 48.07 [41.56-54.58] | |

A non-parametric Mann-Whitney U test was performed to compare each diagnosis parameter.

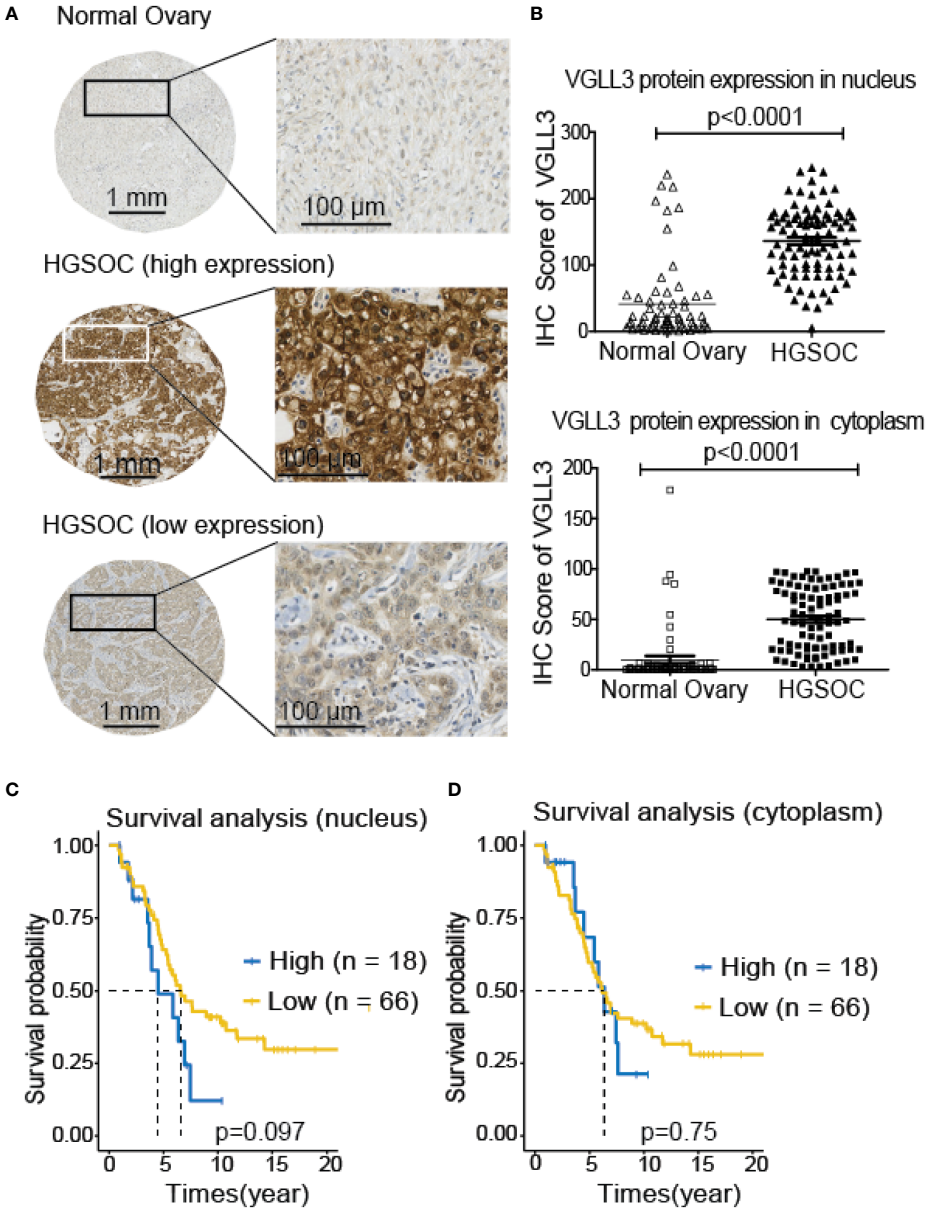


FIGURE 5
Expression of VGLL3 protein in normal ovary and HGSOC tissues and survival analysis depending on the expression levels of VGLL3 on nucleus and cytoplasm of cells. The unstained TMA blocks from 84 HGSOC and 66 adjacent normal ovarian tissues were immunohistochemically stained with anti-VGLL3 antibody, **(A)** Representative image of VGLL3 expression between HGSOC and adjacent normal ovary tissues. **(B)** IHC scores of VGLL3 in both nucleus and cytoplasm were calculated and compared between HGSOC and adjacent normal ovary, $p$ <0.0001. **(C, D)** Kaplan–Meier survival curves of OS comparing high (n=18) and low (n=66) expression of VGLL3 protein in HGSOC are shown both in nucleus ($p$=0.097) and cytoplasm ($p$=0.75). Each point represents an individual sample.

10.3389/fonc.2023.1152991

TABLE 3 VGLL3 protein expression in high-grade serous ovarian carcinoma according to the clinicopathological characteristics.

| Variables | No | (%) | VgLL3_Nucleus | | VgLL3_Cytoplasm | |
|---|---|---|---|---|---|---|
| | | | Mean IHC score (95% CI) | *p*-value | Mean IHC score (95% CI) | *p*-value |
| Age | | | | 0.336 | | 0.502 |
| ≤50 | 35 | 42.0 | 125.55 [108.31-142.79] | | 44.70 [34.29-55.12] | |
| >50 | 49 | 58.3 | 138.8 [124.23_153.37] | | 50.47 [41.67-59.27] | |
| FIGO stage | | | | 0.148 | | 0.063 |
| I/II | 13 | 15.5 | 153.65 [125.48-181.82] | | 62.56 [45.65-79.48] | |
| III/IV | 71 | 84.5 | 128.97 [116.83-141.11] | | 45.32 [38.03-52.61] | |
| Grade | | | | 0.250 | | 0.310 |
| G1+G2 | 40 | 47.6 | 126.92 [110.78-143.07] | | 44.55 [34.83-54.28] | |
| G3 | 44 | 52.4 | 139.05 [123.66-154.45] | | 51.27 [41.99-60.54] | |
| Pre CA-125 level | | | | 0.487 | | 0.331 |
| Negative (≤35U/ml) | 7 | 8.3 | 146.08 [107.32-184.83] | | 60.83 [37.63-84.02] | |
| Positive (>35U/ml) | 77 | 91.7 | 132.11 [120.43-143.80] | | 46.91 [39.92-53.91] | |
| Chemosensitivity | | | | 0.270 | | 0.331 |
| Sensitive | 67 | 79.8 | 137.60 [125.19-150.00] | | 50.88 [43.47-58.29] | |
| Resistant | 15 | 17.9 | 122.17 [95.95-148.38] | | 41.29 [25.63-56.96] | |

A non-parametric Mann-Whitney U test was performed to compare each diagnosis parameter.

pathways, we identified three novel pathways that were associated with *VGLL3*: Nonsense-Mediated Decay pathways (NMD), vascular endothelial growth factors A-vascular endothelial growth factor receptor 2 (VEGFA-VEGFR2) signalling pathway, and platelet-derived growth factor (PDGF) signalling pathway (Figure 6B). The heatmap of DEGs revealed a strong correlation with high *vs.* low *VGLL3* mRNA expressions (Supplementary Figure S6).

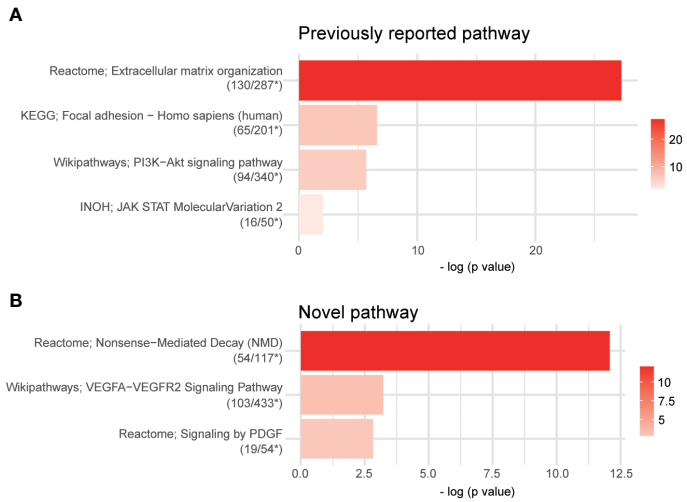


FIGURE 6
Pathway analysis using over-representation analysis from ConsensusPathDB (CPDB). Overall, 3,981 differentially expressed genes (DEGs) were identified after false discovery rate control (adjust *p*-value < 0.001, *p*-value < 2.04e-4). The cutoff p-value and *q*-value were 0.01 and 0.2 in overrepresentation analysis, respectively. **(A)** Four previously reported pathways and **(B)** three novel pathways were captured. Raw read counts for 296 samples from The Cancer Genome Atlas (TCGA) Genome Data Analysis Center (GDAC) database were used for DEGs analysis; *, The number of DEGs overlapped in the pathway/The total number of genes of the pathway.

## Discussion

In recent years, the role played by VGLL3 in cancers has attracted increasing research attention because of its dynamic behaviour in different cancers (18–22). In this study, we found that VGLL3 was an independent unfavourable prognostic factor of HGSOC, likely by affecting immune cells infiltration, particularly macrophages, and regulating or deregulating a significant number of oncogenic genes and pathways. The results suggest that VGLL3 is an important factor for HGSOC that correlates with tumor progression and immune evasion.

The malignancy of EOC largely depends on the constitutive activation/deactivation of different oncogenes, tumor suppressor genes, and transcription factors (40, 41). The correlation of VGLL3 in cancer proliferation, advanced tumor stage, grade, and poor prognosis has previously been reported in other cancers except for ovarian cancer (20–22). In line with previous reports, we found that VGLL3 expression in both mRNA and protein level was also correlated with advanced tumor stage and poor prognosis in HGSOC, suggesting that VGLL3 may promote the progression of HGSOC. Importantly, we may suggest a distinctive role of VGLL3 that conflicts with the previous report by Gambaro et al. where VGLL3 induction showed a tumor-suppressive phenotype in EOC (22). Given the ambivalent nature of genes with both oncogenic and tumor suppressor features, such as SMAD3 (42, 43), the association of VGLL3 with a significant number of genes in the DEG analysis suggests that the role of VGLL3 is too complex to be defined in a simple way. Therefore, a separate study using other OC cell lines is needed to reveal the mechanism of VGLL3 in EOC more precisely.

In contrast to the reduced expression of *VGLL3* mRNA in HGSOC, we found that VGLL3 protein expression was increased in HGSOC in comparison with adjacent normal ovarian tissue. A decent explanation for this discrepancy is currently unknown; one possible hypothesis might involve the effect of post-transcriptional modification. For example, mRNA regulatory elements and the affinity of RNA Binding Proteins (RBDs) increase RNA stability and translational efficiency of mRNA molecules, which leads to the aberrant expression of protein in tumor cells (44, 45). Therefore, we assume that post-transcriptional modifications, such as of *VGLL3* mRNA regulatory element and RBD, are more active in HGSOC than in the normal, which may increase VGLL3 mRNA stability as well as protein translation, and thereby increase its overexpression in protein level. Alternatively, the post-translation modification of VGLL3 protein might also play a role in stabilizing the VGLL3 protein, preventing their degradation, and thus increasing VGLL3 protein in HGSOC tumors. There is a need for an in-depth study to explore the post-transcriptional regulation of VGLL3 and its effect on VGLL3 mRNA stability and protein expression. Despite the fact that there is a discrepancy in VGLL3 mRNA and protein expression between tumor and normal tissues, we interestingly observed that higher levels of both VGLL3 mRNA and protein expression among tumor tissues were associated with the worse OS in HGSOC.

Tumor-infiltrating lymphocytes and the immune status of the tumor microenvironment have been reported to affect progression, therapeutic effects, and recurrence in many cancers (46). Tumor-associated macrophages (TAMs), which mainly belong to the M2 macrophage phenotype, are known to correlate with poor outcomes in solid cancers and play important roles in tumorigenesis (47). A high density of CD163+ M2-macrophages is predominantly associated with poor prognosis in ovarian cancer and known to be involved in tumor invasion, angiogenesis, metastasis, and early recurrence (48, 49). Moreover, the high M1/M2 ratio of tumor infiltrating macrophages correlates with prolonged survival time in EOC, while low M1/M2 ratio correlates with poor OS (50, 51). In this study, we also observed the association of *VGLL3* with macrophage infiltration in HGSOC, which likely contributed to the worsening of OS. Moreover, we found that M2 macrophage was more strongly correlated with *VGLL3* than M1 macrophage, suggesting that VGLL3 may be involved in the poor prognosis of HGSOC by association with macrophages, particularly M2 macrophage.

In addition to known clinical and molecular biomarkers such as *TP53*, *BRCA1/2*, and *MYC*, *VGLL3* regulates many key genes and pathways, and it is also related to clinical prognosis. High *VGLL3* expression has been found to activate several signalling pathways, such as MAPK, JAK-STAT, PI3K/Akt/mTOR, ECM, focal adhesion, and WNT pathways in many tumors (20, 21). In this report, we also discovered those pathways in HGSOC that correlated with high *VGLL3* expression. Further, we found three novel pathways (NMD, VEGFA-VEGFR2, PDGF) that were associated with high *VGLL3*, suggesting that *VGLL3* may regulate key genes in those pathways. Frequent activation of ECM, PI3K/Akt/mTOR, and VEGFA-VEGFR2 signalling pathways has been associated with higher invasive and migratory capacities in subpopulations of human OC (52–54). On the other hand, TAMs have reported to correlate with many signalling pathways including PI3K/AKT/mTOR signalling pathway, ECM, and focal adhesion molecules that modulate the tumor microenvironment (55–57). In this study, we connected *VGLL3* with macrophage infiltration and signalling pathways and demonstrated that VGLL3 may play a critical role in the poor prognosis of HGSOC. There is still a need for further research to show the direct interaction and functional interplay of VGLL3 with related molecules. It is important to identify new biomarkers to improve the management of ovarian cancer patients. In particular, focus should be given on non-invasive characterization of cancer to discover more efficient markers. Radiomics analysis using imaging techniques and implementations of new radiopharmaceuticals based on molecular features of tumor cells would be a good tool for non-invasive staging, prognosis and restaging of cancers. 2-[$^{18}$F] FDG PET/CT is considered the most popular and useful imaging technique for relapse detection in ovarian cancer patients, offering prognostic value. Ongoing research is conducting to explore new biomarkers in ovarian cancer patients by analysing imaging biomarkers in combination with clinical, pathological, and analytical data (58, 59).

Obviously, the limitation of our study is that it used public mRNA data not derived from our own patients and lacked evidence from *in vitro* and *in vivo* research. Nonetheless, the public DBs including TCGA contain decent numbers of curated data, and the findings were highly correlated with our immunohistochemistry-guided TMA in HGSOC tissue samples. Therefore, VGLL3 has been strongly suggested to have significance and a potential role in both mRNA and protein

levels, which represents the strength of this study. Currently, we are conducting research into investigating the molecular mechanism of VGLL3 in HGSOC as a continuation of this study.

## Conclusion

This study demonstrated that VGLL3 has potential prognostic value in HGSOC because its overexpression was shown to be associated with advanced tumor stage and poor prognosis. Moreover, VGLL3 was associated with TAM infiltration, which is frequently observed in the immunosuppressive microenvironment of cancer. Finally, the DEGs pathways and co-expressing genes identified in this study suggest the prospective molecular function of VGLL3 in cancer.

## Data availability statement

The original contributions presented in the study are included in the article/Supplementary Material. Further inquiries can be directed to the corresponding authors.

## Ethics statement

The studies involving human participants were reviewed and approved by Institutional Review Board of Samsung Medical Center (IRB#, SMC 2021-06-23), Seoul, Republic of Korea, and Institutional Review Board of Gangnam Severance Hospital (IRB#, HTB-P2021-5), Seoul, Republic of Korea. The patients/participants provided their written informed consent to participate in this study.

## Author contributions

Conception and design: RH, JY and E-SK. Curation of the data: RH, JL and JY. Analysis and interpretation of data: RH, JL, JY and E-SK. Collection of tissue sample and clinical information: H-YS, HK and J-HK. TMA guided immunohistochemistry perform and analysis: J-YC. Writing, review and revision of the manuscript: RH, JL, JY and E-SK. Supervision and fund acquisition: E-SK. All authors contributed to the article and approved the submitted version.

## Funding

This study was supported by the National Research Foundation of Korea (NRF-2019R1A2C2088715 and 2022R1F1A1075238), which is funded by the Korean government (The Ministry of Science and ICT), South Korea.

## Conflict of interest

The authors declare that the research was conducted in the absence of any commercial or financial relationships that could be construed as a potential conflict of interest.

## Publisher's note



## Supplementary material

The Supplementary Material for this article can be found online at: https://www.frontiersin.org/articles/10.3389/fonc.2023.1152991/full#supplementary-material

SUPPLEMENTARY FIGURE 1
mRNA expression levels of six target genes in HGSOC samples. **(A)** Expression of six target genes of 264 ovarian cancer tissues. *p* value was calculated using Kruskal-Wallis test. **(B)** Expression of six target genes analysed by GEPIA2 in ovarian cancer (n=426) specimen and compared to normal ovarian tissue (n=88). Red color means ovarian cancer tissues and blue color means normal ovarian tissues; *, $p<0.05$ **(C)** Expression of six target genes of 185 ovarian cancer tissues compared to those of 10 normal ovarian tissues. *p* value was calculated using Mann-Whitney U test.

SUPPLEMENTARY FIGURE 2
Expression of six target genes and Kaplan-Meier plot. **(A)** The distribution of each gene expression among 303 samples of The Cancer Genome Atlas (TCGA) ovarian cancer. Dashed line represents the cut-off for high and low expression. **(B)** *Left*: Set the cut-off for high *VGLL3* and low *VGLL3* expression in GSE26712 dataset, *Right:* Kaplan–Meier survival curves of OS comparing high (n=37) and low (n=148) expression of *VGLL3* in HGSOC, $p=0.048$. **(C)** *Left*: Set the cut-off for high *VGLL3* and low *VGLL3* expression in GSE9891 dataset, *Right:* Kaplan–Meier survival curves of OS comparing high (n=93) and low (n=171) expression of *VGLL3* in HGSOC, $p=0.012$. **(D)** Set the cut-off for high macrophage and low macrophage infiltrations in EPIC data. **(E)** Set the cut-off for high *VGLL3* and low *VGLL3* expression in TMA data.

SUPPLEMENTARY FIGURE 3
Correlation between five target genes (*VGLL4, TEAD3, TEAD4, YAP1*, and *TAZ*) and the level of infiltrated immune cells using **(A)** EPIC, **(B)** TIMER, and **(C)** CIBERSORT abs mode. The X-axis is the estimated values of three algorithms that represent immune cell fractions and the Y-axis represents the *VGLL3* mRNA. For CIBERSORT, cell fractions for each immune cell as a summation of their subsets were considered. After eliminating outliers using Tukey's method, Pearson's method was performed to find the correlation between *VGLL3* genes and the immune cells (from left to right: B cell, CD4+ T cell, CD8 + T cell and macrophage), and the correlation coefficient was shown as R. A $p<0.05$ was considered as statistically significant.

SUPPLEMENTARY FIGURE 4
Correlation of VGLL3 with the subsets of macrophages. After eliminating outliers of the level of infiltrated immune cells using Tukey's method, Pearson's method was performed to find the correlation between VGLL3 gene and **(A)** M1 macrophage and **(B)** M2 macrophage. Correlation

coefficient was shown as R. A p<0.05 and R≥ 0.30 was considered as statistically significant.

SUPPLEMENTARY FIGURE 5

Forest plot visualizing hazard ratios with 95% confidence interval and p-values calculated using multivariate Cox regression analysis. Levels of infiltrated immune cells were estimated using TIMER. All variables were considered continuous variables.

SUPPLEMENTARY FIGURE 6

Heatmap of DEGs between the *VGLL3*$^{high}$ and *VGLL3*$^{low}$ group. For the heatmap, the z score normalised value from the results of DESeq2 were used. The genes presented in the heatmap were selected genes that overlapped with the cancer gene list provided by Bushman laboratory (See Methods). Previously reported pathways had 128 overlapped genes in total, and novel pathways had 55 overlapped genes in total. * previously reported pathways; ** newly found pathways in this study.

# References

1. Fitzmaurice C, Dicker D, Pain A, Hamavid H, Moradi-Lakeh M, MacIntyre MF, et al. The global burden of cancer 2013. *JAMA Oncol* (2015) 1:505–27. doi: 10.1001/jamaoncol.2015.0735

2. Webb PM, Jordan SJ. Epidemiology of epithelial ovarian cancer. *Best Pract Res Clin Obstet Gynaecol* (2017) 41:3–14. doi: 10.1016/j.bpobgyn.2016.08.006

3. Au KK, Josahkian JA, Francis JA, Squire JA, Koti M. Current state of biomarkers in ovarian cancer prognosis. *Future Oncol* (2015) 11(23):3187–95. doi: 10.2217/fon.15.251

4. Chen VW, Ruiz B, Killeen JL, Coté TR, Wu XC, Correa CN, et al. Pathology and classification of ovarian tumors. *Cancer Suppl* (2003) 97:2631–42. doi: 10.1002/cncr.11345

5. Prat J, D'Angelo E, Espinosa I. Ovarian carcinomas: at least five different diseases with distinct histological features and molecular genetics. *Hum Pathol* (2018) 80:11–27. doi: 10.1016/j.humpath.2018.06.018

6. The Cancer Genome Atlas Research Network. Integrated genomic analyses of ovarian carcinoma. *Nature* (2011) 474:609–15. doi: 10.1038/nature10166

7. Liu J, Xu W, Li S, Sun R, Cheng W. Multi-omics analysis of tumor mutational burden combined with prognostic assessment in epithelial ovarian cancer based on TCGA database. *Int J Med Sci* (2020) 17(18):3200–13. doi: 10.7150/ijms.50491

8. Yu FX, Zhao B, Guan KL. Hippo pathway in organ size control, tissue homeostasis, and cancer. *Cell* (2015) 163(4):811–28. doi: 10.1016/j.cell.2015.10.044

9. Godin P, Tsoi M, Paquet M, Boerboom D. YAP and TAZ are required for the postnatal development and the maintenance of the structural integrity of the oviduct. *Reproduction* (2020) 160(2):307–18. doi: 10.1530/REP-20-0202

10. Hansen CG, Moroishi T, Guan KL. YAP and TAZ: a nexus for hippo signaling and beyond. *Trends Cell Biol* (2015) 25(9):499–513. doi: 10.1016/j.tcb.2015.05.002

11. Harvey KF, Zhang X, Thomas DM. The hippo pathway and human cancer. *Nat Rev Cancer* (2013) 13(4):246–57. doi: 10.1038/nrc3458

12. He C, Lv X, Hua G, Lele SM, Remmenga S, Dong J, et al. YAP forms autocrine loops with the ERBB pathway to regulate ovarian cancer initiation and progression. *Oncogene* (2015) 34:6040–54. doi: 10.1038/onc.2015.52

13. Jeong GO, Shin SH, Seo EJ, Kwon YW, Heo SC, Kim KH, et al. TAZ mediates lysophosphatidic acid-induced migration and proliferation of epithelial ovarian cancer cells. *Cell Physiol Biochem* (2013) 32:253–63. doi: 10.1159/000354434

14. Maeda T, Chapman DL, Stewart AF. Mammalian vestigial-like 2, a cofactor of TEF-1 and MEF2 transcription factors that promotes skeletal muscle differentiation. *J Biol Chem* (2002) 277:48889–98. doi: 10.1074/jbc.M206858200

15. Ma S, Tang T, Probst G, Konradi A, Jin C, Li F, et al. Transcriptional repression of estrogen receptor alpha by YAP reveals the hippo pathway as therapeutic target for ER+ breast cancer. *Nat Commun* (2022) 13(1):1061. doi: 10.1038/s41467-022-28691-0

16. Halperin DS, Pan C, Lusis AJ, Tontonoz P. Vestigial-like 3 is an inhibitor of adipocyte differentiation. *J Lipid Res* (2013) 54(2):473–81. doi: 10.1194/jlr.M032755

17. Simon E, Theze N, Fedou S, Thiebaud P, Faucheux C. Vestigial-like 3 is a novel Ets1 interacting partner and regulates trigeminal nerve formation and cranial neural crest migration. *Biol Open* (2017) 6:1528–40. doi: 10.1242/bio.026153

18. Hélias-Rodzewicz Z, Pérot G, Chibon F, Ferreira C, Lagarde P, Terrier P, et al. YAP1 and VGLL3, encoding two cofactors of TEAD transcription factors, are amplified and overexpressed in a subset of soft tissue sarcomas. *Genes Chromosomes Cancer* (2010) 49(12):1161–71. doi: 10.1002/gcc.20825

19. Hori N, Okada K, Takakura Y, Takano H, Yamaguchi N, Yamaguchi N. Vestigial-like family member 3 (VGLL3), a cofactor for TEAD transcription factors, promotes cancer cell proliferation by activating the hippo pathway. . *J Biol Chem* (2020) 295(26):8798–807. doi: 10.1074/jbc.RA120.012781

20. Zhang LH, Wang Z, Li LH, Liu YK, Jin LF, Qi XW, et al. Vestigial like family member 3 is a novel prognostic biomarker for gastric cancer. *World J Clin cases* (2019) 7(15):1954–63. doi: 10.12998/wjcc.v7.i15.1954

21. Zhang L, Li L, Mao Y, Hua D. VGLL3 is a prognostic biomarker and correlated with clinical pathologic features and immune infiltrates in stomach adenocarcinoma. *Sci Rep* (2020) 10:1355. doi: 10.1038/s41598-020-58493-7

22. Gambaro K, Quinn MCJ, Wojnarowicz PM, Arcand SL, de Ladurantaye M, Barrès V, et al. Vgll3 expression is associated with a tumor suppressor phenotype in epithelial ovarian cancer. *Mol Oncol* (2013) 7(3):513–30. doi: 10.1016/j.molonc.2012.12.006

23. Cody NA, Ouellet V, Manderson EN, Quinn MC, Filali-Mouhim A, Tellis P, et al. Transfer of chromosome 3 fragments suppresses tumorigenicity of an ovarian cancer cell line monoallelic for chromosome 3p. *Oncogene* (2007) 26(4):618–32. doi: 10.1038/sj.onc.1209821

24. Cody NA, Shen Z, Ripeau JS, Provencher DM, Mes-Masson AM, Chevrette M, et al. Characterization of the 3p12.3-pcen region associated with tumor suppression in a novel ovarian cancer cell line model genetically modified by chromosome 3 fragment transfer. *Mol Carcinog* (2009) 48:1077–92. doi: 10.1002/mc.20535

25. Shuguang Z, Min W, Shiqun W, Jie D, Jiwu W. Pan-cancer analysis of immune cell infiltration identifies a prognostic immune-cell characteristic score (ICCS) in lung adenocarcinoma. *Front Immunol* (2020) 11:1218. doi: 10.3389/fimmu.2020.01218

26. Tang Z, Kang B, Li C, Chen T, Zhang Z. GEPIA2: an enhanced web server for large-scale expression profiling and interactive analysis. *Nucleic Acids Res* (2019) 47 (W1):W556–60. doi: 10.1111/jcmm.16188

27. Cho H, Kim JH. Lipocalin2 expressions correlate significantly with tumor differentiation in epithelial ovarian cancer. *J Histochem Cytochem* (2009) 57:513–21. doi: 10.1369/jhc.2009.953257

28. Chay D, Cho H, Lim BJ, Kang ES, Oh YJ, Choi SM, et al. ER-60 (PDIA3) is highly expressed in a newly established serous ovarian cancer cell line, YDOV-139. *Int J Oncol* (2010) 37:399–412. doi: 10.3892/ijo_00000688

29. Cho H, Kang ES, Hong SW, Oh YJ, Choi SM, Kim SW, et al. Genomic and proteomic characterization of YDOV-157, a newly established human epithelial ovarian cancer cell line. *Mol Cell Biochem* (2008) 319(1-2):189–201. doi: 10.1007/s11010-008-9892-4

30. Cho H, Lim BJ, Kang ES, Choi JS, Kim JH. Molecular characterization of a new ovarian cancer cell line, YDOV-151, established from mucinous cystadenocarcinoma. *Tohoku J Exp Med* (2009) 218(2):129–39. doi: 10.1620/tjem.218.129

31. Sturm G, Finotello F, Petitprez F, Zhang JD, Baumbach J, Fridman WH, et al. Comprehensive evaluation of transcriptome-based cell-type quantification methods for immune-oncology. *Bioinformatics* (2019) 35(14):i436–45. doi: 10.1093/bioinformatics/btz363

32. Racle J, Gfeller D. EPIC: a tool to estimate the proportions of different cell types from bulk gene expression data. *Methods Mol Biol* (2020) 2120:233–48. doi: 10.1007/978-1-0716-0327-7_17

33. Li T, Fan J, Wang B, Traugh N, Chen Q, Liu JS, et al. TIMER: a web server for comprehensive analysis of tumor-infiltrating immune cells. *Cancer Res* (2017) 77(21): e108–10. doi: 10.1158/0008-5472.CAN-17-0307

34. Newman AM, Liu CL, Green MR, Gentles AJ, Feng W, Xu Y, et al. Robust enumeration of cell subsets from tissue expression profiles. *Nat Methods* (2015) 12 (5):453–7. doi: 10.1038/nmeth.3337

35. Choi CH, Kang TH, Song JS, Kim YS, Chung EJ, Ylaya K, et al. Elevated expression of pancreatic adenocarcinoma upregulated factor (PAUF) is associated with poor prognosis and chemoresistance in epithelial ovarian cancer. *Sci Rep* (2018) 8 (1):12161. doi: 10.1038/s41598-018-30582-8

36. Love MI, Huber W, Anders S. Moderated estimation of fold change and dispersion for RNA-seq data with DESeq2. *Genome Biol* (2014) 15:550. doi: 10.1186/s13059-014-0550-8

37. Kamburov A, Stelzl U, Lehrach H and Herwig R. The consensus path DB interaction database: 2013 update. *Nucleic Acids Res* (2013) 41(1):D793–800. doi: 10.1093/nar/gks1055

38. Therneau TM. Survival: a package for survival analysis in r. In: *R package version 3.1-12* (2020). Available at: https://CRAN.R-project.org/package=survival.

39. Gordon M. Forestplot: advanced forest plot using 'grid' graphics. In: *R package version 2.0.1* (2021). Available at: https://CRAN.R-project.org/package=forestplot.

40. Guo T, Dong X, Xie S, Zhang L, Zeng P, Zhang L. Cellular mechanism of gene mutations and potential therapeutic targets in ovarian cancer. *Cancer Manag Res* (2021) 13:3081–100. doi: 10.2147/CMAR.S292992

41. Nameki R, Chang H, Reddy J, Rosario I, Corona RI, Lawrenson K. Transcription factors in epithelial ovarian cancer: histotype-specific drivers and novel therapeutic targets. *Pharmacol Ther* (2021) 220:107722. doi: 10.1016/j.pharmthera.2020.107722

42. Millet C, Zhang YE. Roles of Smad3 in TGF-beta signaling during carcinogenesis. *Crit Rev Eukaryot Gene Expr* (2007) 17(4):281–93. doi: 10.1615/critreveukargeneexpr.v17.i4.30

43. Bae DS, Blazanin N, Licata M, Lee J, Glick AB. Tumor suppressor and oncogene actions of TGFbeta1 occur early in skin carcinogenesis and are mediated by Smad3. *Mol Carcinog* (2009) 48(5):441–53. doi: 10.1002/mc.20482

44. Audic Y, Hartley RS. Post-transcriptional regulation in cancer. *Biol Cell* (2004) 96:479–98. doi: 10.1016/j.biolcel.2004.05.002

45. Lin CY, Beattie A, Baradaran B, Dray E, Duijf PHG. Contradictory mRNA and protein misexpression of EEF1A1 in ductal breast carcinoma due to cell cycle regulation and cellular stress. *Sci Rep* (2018) 8:13904. doi: 10.1038/s41598-018-32272-x

46. Wang YQ, Chen YP, Zhang Y, Jiang W, Liu N, Yun JP, et al. Prognostic significance of tumor-infiltrating lymphocytes in nondisseminated nasopharyngeal carcinoma: a Large-scale cohort study. *Int J Cancer* (2018) 142(12):2558–66. doi: 10.1002/ijc.31279

47. Zhang WJ, Wang XH, Gao ST, Chen C, Xu XY, Sun Q, et al. Tumor-associated macrophages correlate with phenomenon of epithelial-mesenchymal transition and contribute to poor prognosis in triple-negative breast cancer patients. *J Surg Res* (2018) 222:93–101. doi: 10.1016/j.jss.2017.09.035

48. Yafei Z, Jun G, Guolan G. Correlation between macrophage infiltration and prognosis of ovarian cancer-a preliminary study. *BioMed Res* (2016) 27:305–12.

49. Yin M, Li X, Tan S, Zhou HJ, Ji W, Bellone S, et al. Tumor-associated macrophages drive spheroid formation during early transcoelomic metastasis of ovarian cancer. *J Clin Invest* (2016) 126(11):4157–73. doi: 10.1172/JCI87252

50. Zhang M, He Y, Sun X, Li Q, Wang W, Zhao A, et al. A high M1/M2 ratio of tumor-associated macrophages is associated with extended survival in ovarian cancer patients. *J Ovarian Res* (2014) 7:19. doi: 10.1186/1757-2215-7-19

51. Cheng H, Wang Z, Fu L, Xu T. Macrophage polarization in the development and progression of ovarian cancers: an overview. *Front Oncol* (2019) 9:421. doi: 10.3389/fonc.2019.00421

52. Cho A, Howell VM, Colvin EK. The extracellular matrix in epithelial ovarian cancer - a piece of a puzzle. *Front Oncol* (2015) 5:245. doi: 10.3389/fonc.2015.00245

53. Ediriweera MK, Tennekoon KH, Samarakoon SR. Role of the PI3K/AKT/mTOR signaling pathway in ovarian cancer: biological and therapeutic significance. *Semin Cancer Biol* (2019) 59:147–60. doi: 10.1016/j.semcancer.2019.05.012

54. Adham S, Sher I and Coomber B. Molecular blockade of VEGFR2 in human epithelial ovarian carcinoma cells. *Lab Invest* (2010) 90:709–23. doi: 10.1038/labinvest.2010.52

55. Qiu S, Deng L, Liao X, Nie L, Qi F, Jin K, et al. Tumor-associated macrophages promote bladder tumor growth through PI3K/AKT signal induced by collagen. *Cancer Sci* (2019) 110(7):2110–8. doi: 10.1111/cas.14078

56. Feng R, Yang S. Effects of combining erlotinib and RNA-interfered downregulation of focal adhesion kinase expression on gastric cancer. *J Int Med Res* (2016) 44:855–64. doi: 10.1177/0300060516647550

57. Pathria P, Louis TL, Varner JA. Targeting tumor-associated macrophages in cancer. *Trends Immunol* (2019) 40:310–27. doi: 10.1016/j.it.2019.02.003

58. Delgado Bolton RC, Aide N, Colletti PM, Ferrero A, Paez D, Skanjeti A, et al. EANM guideline on the role of 2-[18F] FDG PET/CT in diagnosis, staging, prognostic value, therapy assessment and restaging of ovarian cancer, endorsed by the American college of nuclear medicine (ACNM), the society of nuclear medicine and molecular imaging (SNMMI) and the international atomic energy agency (IAEA). *Eur J Nucl Med Mol Imaging* (2021) 10:3286–302. doi: 10.1007/s00259-021-05450-9

59. Delgado Bolton RC, Calapaquí Terán AK, Pellet O, Ferrero A, Giammarile F. The search for new 2-18F-FDG PET/CT imaging biomarkers in advanced ovarian cancer patients: focus on peritoneal staging for guiding precision medicine and management decisions. *Clin Nucl Med* (2021) 46(11):906–7. doi: 10.1097/RLU.0000000000003784

frontiers | Frontiers in Oncology

TYPE Review
PUBLISHED 29 June 2023
DOI 10.3389/fonc.2023.1147394



OPEN ACCESS

EDITED BY
Umberto Malapelle,
University of Naples Federico II, Italy

REVIEWED BY
Lorenzo Ceppi,
Niguarda Ca'Granda Hospital, Italy
Antonio Raffone,
Federico II University Hospital, Italy

*CORRESPONDENCE
Yuanjing Hu
julianna_hu@163.com

RECEIVED 18 January 2023
ACCEPTED 19 June 2023
PUBLISHED 29 June 2023

CITATION
Tang X and Hu Y (2023) The role of TCGA molecular classification in clear cell endometrial carcinoma. *Front. Oncol.* 13:1147394. doi: 10.3389/fonc.2023.1147394



# The role of TCGA molecular classification in clear cell endometrial carcinoma

Xinyue Tang[1] and Yuanjing Hu[2*]

[1]Graduate School, Tianjin Medical University, Tianjin, China, [2]Department of Gynecological Oncology, Tianjin Central Hospital of Obstetrics & Gynecology, Tianjin, China

Clear cell endometrial carcinoma (CCEC) represents a relatively rare and heterogeneous entity. Based on The Cancer Genome Atlas (TCGA) molecular classification, the risk stratification and management of endometrial cancer (EC) have been improved. Although the relationship of CCEC with the TCGA classification is less well understood, data has emerged to suggest that molecular classification plays an important role in the prognosis and management of CCEC. Most of patients with CCEC are characterized by p53abn or NSMP type and the prognosis of these patients is poor, whereas those with MMRd or POLEmut seem to have a favorable prognosis. Adjuvant therapy is recommended in CCEC with p53abn and NSMP. Advanced/recurrent CCEC with MMRd benefit much more from immune checkpoint inhibitors after the failure of platinum-based chemotherapy. In addition, bevacizumab plus chemotherapy upfront seems to improve outcomes of advanced/recurrent patients whose tumors harbored mutated TP53, including CCECs with p53abn. Further studies which exclusively recruit CCEC are urgently needed to better understand the role of molecular classification in CCEC. This review will provide an overview of our current understanding of TCGA classification in CCEC.

KEYWORDS

**clear cell endometrial carcinoma, TCGA, molecular classification, prognosis, adjuvant therapy**

## 1 Introduction

Clear cell endometrial cancer (CCEC) is an uncommon but aggressive histologic type that accounts for 1%-6% of endometrial cancer (EC), and characterized by poorer prognosis and chemotherapy resistance (1). A clear cell endometrial carcinoma usually features HNF1β positive, Napsin A positive, WT1 negative and estrogen receptor (ER)/progesterone receptor (PR) negative (2). Owing to the rarity of clear cell endometrial cancer, several features regarding CCEC are still unclear.

Traditionally, based on biological and clinical parameters, endometrioid endometrial cancer is considered as "type I" EC and accounts for 80% of EC, whereas non-endometrioid (i.e. serous and clear cell) histology tumors has been regarded as "type II" EC since it is not estrogen-related and has poor prognosis (3–5). However, CCEC overlaps with

endometrioid and serous carcinoma in many features: morphological, immunohistochemical, molecular and prognostic, so the new classifications are needed. In 2013, The Cancer Genome Atlas (TCGA) classified EC into 4 subtypes: POLE ultramutated (POLE), microsatellite instability hypermutated (MSI), copy-number low (CNL) and copy-number high (CNH) (6). As surrogate markers of the TCGA molecular subtypes, the Proactive Molecular Risk Classifier for Endometrial Cancer (ProMisE) subdivided different endometrial carcinomas into four prognostic molecular subgroups: POLE-mutated (POLEmut), mismatch-repair- deficient (MMRd), TP53-wild-type (NSMP) and TP53-abnormal (p53abn), and identified 4 molecular subtypes with distinct prognostic outcomes (7–9). Notably, clear cell endometrial carcinomas were not involved in the study. Unlike EC, the relationship between CCEC and TCGA classification has not been fully elucidated. In the present review, we tried to provide a comprehensive overview of the role of molecular classification in prognosis and management of CCEC.

## 2 The value of TCGA classifier in clear cell endometrial carcinoma

Since TCGA classification of EC was proposed, several groups have described the molecular classification of CCEC. CCEC was found within all four molecular subtypes and encompassed a wide range of clinical outcomes (4, 10, 11). Results are consistent across different reports, and demonstrated that the most prevalent subgroups were the p53abn and NSMP subgroups, while the MMRd and POLEmut subgroups were less common (9, 10, 12). A recently published meta-analysis suggested that POLEmut, MMRd, p53abn and NSMP accounted for about 3.5%, 11.4%, 35.1%, and 50% of patients with pure CCEC, respectively, while MMRd subgroup constituted the majority of mixed CCEC, accounting for about 50% of mixed CCECs (4). Women with p53abn and NSMP CCECs were older than women with MMRd and POLEmut subtypes. As a unique subgroup, the NSMP CCECs showed distinct clinical and pathological features, in particular older age, lower BMI, more aggressive clinical course and absent or minimal ER expression, compared to other NSMP ECs (10). In terms of prognosis, MMRd CCECs had a favorable prognosis with a 5-year OS >95%, while the prognosis of NSMP CCECs did not significantly differ from that of p53abn CCCs, with a 5-year OS <50% (4). In this review, none of the POLEmut patients died, which meant POLEmut CCCs conferred favorable prognosis. Other studies have also come to the conclusion consistent with this study, namely that patients with MMRd or POLEmut have better outcome than those with p53abn and NSMP (10, 11). Interestingly, some recent studies have analyzed the relationship between TCGA groups and classic prognostic factors (myometrial invasion, lymphovascular space invasion (LVSI)) in ECs (including CECCs) (13). LVSI was not associated with an increased risk of tumor recurrence or progression and death from disease in POLE-mt ECs, while it appeared as an independent predictor of poor outcome in the MSI group (14–16). Deep myometrial invasion did not appear as an independent prognostic factor for OS in EC patients; instead, it seemed to affect the risk of recurrence independently from the TCGA groups (17).

### 2.1 Adjuvant therapy

According to the NCCN guidelines, CCEC is considered a high-risk histologic type of EC and requires adjuvant therapy in most case. Even in early-stage CCEC, the risk of recurrence is still high and adjuvant chemotherapy mitigates the risk of distant metastases (18), however, in terms of decision-making regarding adjuvant treatment, the role of molecular classification is not still elaborated (19). Significantly, molecular classification has been incorporated into the ESGO/ESTRO/ESP guidelines as fundamental integrated information for prognostic risk group stratification and for tailoring adjuvant therapy in EC patients (3). Herein, we extracted CCEC-related descriptions from the updated risk stratification system (Table 1). According to ESGO/ESTRO/ESP guidelines, adjuvant treatment could be omitted for stage I/II CCEC patients with POLEmut of low-risk group, while chemotherapy +/− radiotherapy is recommended for stage I-IVA CCEC patients with p53abn and myometrial invasion of high-risk group. Due to the lack of randomized trials, the potential benefit of adjuvant therapy for CCEC patients of intermediate-risk group is unclear, consequently, the recommendation for adjuvant treatment or observation should be considered on a case-by-case basis following multidisciplinary discussion (3). Of note, CCECs with the molecular profile MMRd or NSMP are not allocated to the prognostic risk group in the ESGO/ESTO/ESP guidelines as only limited data were available for their prognostic relevance. Thus, for these patients, inclusion into prospective registries is recommended.

PORTEC-3 trial explored the benefit of combined adjuvant chemotherapy and EBRT(CTRT) versus EBRT alone in patients with high-risk EC (including CCEC) (20, 21). However, there is substantial interobserver variability in assessment of pathologic factors that define high-risk, so it remains a challenge to identify patients who will benefit from chemotherapy (22). In contrast, the

TABLE 1 Risk group related to clear cell endometrial carcinoma extracted from the ESGO/ESTRO/ESP guidelines.

| Risk group | Description related to CCEC[a] |
|---|---|
| Low risk | Stage I/II POLEmut CCEC; for stage III POLEmut cancers[b] |
| Intermediate risk | Stage IA and/or p53-abn CCEC without myometrial invasion and no or focal LVSI |
| High-intermediate risk | None |
| High risk | All stage CCEC with p53-abn and myometrial invasion |

CCEC, clear cell endometrial carcinoma; EC, endometrial cancer; LVSI, lymphovascular space invasion; p53-abn, p53-abnormal; POLEmut, polymerase epsilon-ultramutated.
[a]Stage III-IVA if completely resected without residual disease; table does not apply to stage III-IVA with residual disease or for stage IV.
[b]POLEmut stage III might be considered as low risk. Nevertheless, currently there are no data regarding safety of omitting adjuvant therapy.

molecular classification of EC is characterized by higher reproducibility. Following PORTEC-3 trial, León-Castillo, A., et al. used tissue samples from the PORTEC-3 clinical trial to investigate the prognostic relevance of the molecular classification and the relationship between the molecular subgroups and benefit from adjuvant CTRT in patients with high-risk EC (23). This study showed that patients with p53abn EC had a highly significant benefit from CTRT versus RT alone and patients with NSMP EC had a trend toward benefit from CTRT. Considering that p53abn and NSMP represent the majority of CCEC (4, 12), the above study is of great significance to guide the adjuvant treatment of CCEC. Although NSMP molecular subtype is not enrolled into the updated risk stratification system of ESGO/ESTO/ESP guidelines, it might be included in a high-risk category due to its aggressive features with the highest proportion of LVSI, deep myometrial invasion, node positive and advanced stage (III/IV) disease (10). The prognosis of NSMP CCECs seems not to significantly differ from p53abn CCECs, supporting a similar management for these two groups of patients.

It needs to be emphasized that patients with mixed endometrioid and clear cell carcinoma are characterized by MMRd (24). Similarly, Travaglino, A., et al. also pointed out that MMRd subgroups constituted the majority of mixed CCEC, accounting for about 50% of mixed CCECs (4). Therefore, it makes sense to explore adjuvant therapy strategies for CCEC with MMRd. However, only limited data are available for CCEC with MMRd. Molecular analysis of the PORTEC-3 trial suggested no, or limited benefit of adding chemotherapy in patients with MMRd EC (23). According to the recently published meta-analysis, for CCEC with MMRd, 5-year OS was 95.7 ± 4.3% in the main analysis and 90.9 ± 6.7% in the pure CCEC subgroup, and none of the MMRd patients died in the mixed CCEC group (4). The result supported that MMRd CCECs had a favorable prognosis, and MMRd CCECs might be included in a lower risk category. Therefore, further prospective data are needed to better define prognosis and role of adjuvant therapy in the MMRd group.

Significantly, the integration of molecular signature and clinicopathological factors would provide a more tailored management for ECs (25–27). An integrated clinicopathologic and molecular risk profile was established for EC with HIR features, separating them in favorable, intermediate and unfavorable groups, each with a clearly different prognosis (25). in this study it was shown that L1 cell adhesion molecule (L1CAM) overexpression was significant risk factors for both pelvic and distant recurrences, and within the NSMP group, β catenin (CTNNB1) was also found to be prognostic for distant recurrence. To evaluate the clinical role of this molecular-integrated risk profile in the determination of adjuvant treatment in patients with HIR EC, the PORTEC-4a study was initiated in 2016 (26, 28). Women with a favorable profile (POLE mutation, or NSMP without CTNNB1 mutations) were observed after surgery; women with an intermediate risk profile (mismatch repair-deficient (MMRd) or NSMP with CTNNB1 mutations) received adjuvant VBT; and women with any of the unfavorable risk factors (substantial LVSI, TP53 abnormal immunohistochemical staining or L1CAM overexpression) were treated with EBRT (26, 28). The primary endpoint of PORTEC-4a (NCT03469674) is vaginal recurrence, and the results are worth looking forward to. It is necessary to remark that these studies only included patients with endometrioid carcinoma, but it paves the way for future exploration of the integration of molecular signature and clinicopathological factors in CCEC population.

## 2.2 Treatment of recurrent/ advanced CCEC

Patients with recurrent/advanced disease are characterized by poor prognosis, with 5-year OS rates of 20%-25% (29). The treatment of patients with recurrent and progressive EC should be guided by several features, including the patient's condition, extent of the disease, prior therapies and molecular profile, and should always require a multidisciplinary approach which includes surgery, radiotherapy (RT), and chemotherapy (ChT). For advanced/recurrent disease not amenable to surgery and/or RT, the standard approach remains ChT or hormonal therapy. Currently, carboplatin AUC 5-6 plus paclitaxel 175 mg/m$^2$ every 21 days for six cycles should be considered the first-line therapy for recurrent or metastatic EC (3). In addition, some novel treatments are under constant exploration.

### 2.2.1 immune checkpoint inhibitors

NCCN and ESGO/ESTO/ESP guidelines have recommended several immune checkpoint inhibitors as a second-line treatment for recurrent/metastatic EC with MMRd (3, 19). Le, D.T., et al. have confirmed that the large proportion of mutant neoantigens in mismatch repair-deficient (MMRd) cancers made them sensitive to immune checkpoint blockade, regardless of the cancers' tissue of origin (30). In 2017, the Food and Drug Administration (FDA) approved pembrolizumab [anti-programmed cell death protein 1 (PD-1)] for treatment of advanced MSI-H or MMRd solid tumors. Given that 25%-30% of primary ECs are MMRd, indicating immune dysregulation, several immune checkpoint inhibitors have been approved for treatment of specific ECs. The KEYNOTE-158 clinical trial of pembrolizumab enrolling patients with MSI-H/dMMR advanced noncolorectal cancer who experienced failure with prior therapy confirmed the durable antitumor activity on EC population (including CCEC) (31, 32). Based on the KEYNOTE-158 trial, On March 21, 2022, FDA approved pembrolizumab, as a single agent, for patients with advanced endometrial carcinoma that is microsatellite instability-high (MSI-H) or mismatch repair deficient (MMRd), who have disease progression following prior systemic therapy in any setting and who are not candidates for curative surgery or radiation (33). The activity and safety of dostarlimab, an anti-PD-L1 (programmed death-ligand 1) agent, were analyzed in the GARNET trial (34). This ongoing phase Ib study has enrolled 104 patients with MMRd EC. Of these, 71 had measurable disease at baseline and 6 months follow-up and were included in the primary analysis. The confirmed ORR was 42.3% (a confirmed complete was seen in 12.7% patients; a partial response was seen in 29.6% patients) (34). In light of these results, FDA granted accelerated approval to dostarlimab-gxly for adult patients with MMRd recurrent or advanced endometrial cancer that has progressed on or

following a prior platinum-containing regimen (35). A phase III trial (KEYNOTE-775) including 827 EC patients (697 with pMMR disease and 130 with dMMR disease) with previously treated showed that pembrolizumab plus lenvatinib led to significantly longer OS (pMMR population: HR 0.68, 95%CI 0.56-0.84, P<0.001; overall: HR 0.62, 95% CI 0.51-0.75, P<0.001) and PFS (pMMR population: HR 0.60, 95%CI 0.50-0.72, P<0.001; overall: HR 0.56, 95% CI 0.47-0.66, P<0.001) than chemotherapy of the treating physician's choice (doxorubicin or paclitaxel) with advanced EC (36). Based on the results, FDA approved pembrolizumab in combination with lenvatinib for patients with advanced endometrial carcinoma that is not MSI-H/dMMR, who have disease progression following prior systemic therapy in any setting and are not candidates for curative surgery or radiation (37). However, only 47 CCECs were included in the KEYNOTE-775.Several ongoing trials are evaluating the activity of various checkpoint inhibitors in patients with recurrent/advanced CCEC. The information from the clinicaltrials.gov database is shown in Table 2.

In conclusion, the MMRd subtype plays an important role in the application of immunotherapy in advanced/recurrent CCEC. Similar to MMRd ECs, POLEmut ECs are also characterized by an extensive immune infiltrate, and their immunogenicity is thought to be the cause of their favorable prognosis (38, 39), however, few clinical trials that study the role of immune checkpoint inhibitors in POLEmut EC have been reported. Further evidence is needed to clarify the benefit of adding immunotherapy in patients with recurrent/progressive CCEC according to molecular classification.

### 2.2.2 targeted therapy

To some extent, molecular classification also plays a role in the targeted therapy of advanced/recurrent EC, including CCEC. According to NCCN guidelines, carboplatin/paclitaxel/bevacizumab could be considered as front-line systemic therapy for patients with advanced/recurrent EC. However, GOG86p trial, one of the first trials combining a targeted agent (either bevacizumab or temsirolimus) with standard chemotherapy for high risk or recurrent EC, showed no PFS benefit compared with historical controls, namely the carboplatin-paclitaxel arm of trial GOG209 (40, 41). Recently, based on molecular classification, Leslie, K.K., et al. performed an exploratory analysis to assess TP53 mutational status in patients from GOG86P and determined the implications on clinical outcomes (42). This exploratory study suggested that combining chemotherapy with bevacizumab, but not temsirolimus, might enhance PFS (HR 0.48;95%CI 0.31,0.75) and OS (HR 0.61;95% CI 0.38, 0.98) for patients whose tumors harbor mutant p53, whereas patients with P53wt did not have a markedly different PFS or OS on the bevacizumab arms compared to the temsirolimus arm. From a mechanistic perspective, the reason why p53 mutation is related to improvement in outcomes in response to bevacizumab may be the

TABLE 2 Ongoing trials of immune checkpoint inhibitors in clear cell endometrial carcinoma.

| ClinicalTrials.gov Identifier | Agent | Phase | Participants | Primary endpoint | Estimated completion date |
|---|---|---|---|---|---|
| NCT03603184 | Atezolizumab+ Paclitaxel/ Carboplatin | III | Patients with advanced/recurrent EC, including CCEC | Progression-free survival and overall survival | December, 2023 |
| NCT03914612 | Pembrolizumab + Carboplatin/ Paclitaxel | III | Patients with advanced/recurrent MMRd EC,including CCEC | Progression-free survival | June, 2023 |
| NCT05419817 | Pembrolizumab + Sitravatinib | II | Patients with recurrent EC and other solid tumors with MMRd,including CCEC | Objective response | December, 2026 |
| NCT05112601 | Nivolumab+ Ipilimumab | II | Patients with advanced/recurrent MMRd EC,including CCEC | Progression-free survival | April, 2026 |
| NCT04463771 | Retifanlimab+ Other therapies | II | Patients with advanced/metastatic EC, including CCEC | Objective response rate | June, 2025 |
| NCT03367741 | Nivolumab+ Cabozantinib | II | Patients with advanced,recurrent or metastatic EC,including CCEC | Progression-free survival | October, 2023 |
| NCT03241745 | Nivolumab | II | Patients with MMRd/hypermutated uterine cancer,including CCEC | Progression-free survival | August, 2023 |
| NCT02715284 | Dostarlimab | I | Patients with advanced solid tumors, including EC which includes CCEC | Number of treatment emergent AEs(TEAEs) | October, 2027 |
| NCT05092373 | Atezolizumab+ Cabozantinib/ Nab-paclitaxel | I | Patients with advanced solid tumors, including EC which includes CCEC | To assess the safety and tolerability of TTF, including the maximum tolerated dose (MTD) | September, 2026 |
| NCT04272034 | INCB099318 | I | Patients with advanced solid, including CCEC | Number of treatment emergent AEs(TEAEs) | June, 2024 |

MMRd, mismatch repair deficient; EC, endometrial cancer; CCEC, clear cell endometrial carcinoma; AEs, adverse events; TTF, tumor treating fields.

described link between the p53 protein and VEGF: wild type p53 protein inhibits transcription of angiogenic factors such as VEGF-A. It is reported that mutations in TP53 that negatively impact p53 wild type transcriptional activity may alleviate transcriptional repression of VEGF-A, resulting in higher expression of the direct target of bevacizumab (42, 43). To our knowledge, CCEC with p53abn accounts for 35% of all CCECs, and for those, bevacizumab combined with chemotherapy may be a good option. Limitedly, a chemotherapy-only reference arm was not included in the GOG-86P trial design, and sequencing was not performed on subjects from historical controls GOG-209 (42). Another potential limitation of this study is that only 16 CCEC patients were included in this study, and TP53 mutational analysis was available for only 7 of them. Future trials are needed to compare bevacizumab plus chemotherapy with chemotherapy alone in CCEC patients with p53abn.

Furthermore, since HER-2 overexpression has been described in the p53abn CCEC, it is possible that the subgroup may be sensitive to anti-HER-2 targeted therapy (27, 44). Additionally, a subset of p53abn ECs (including CCECs) shows high DNA damage and high PARP-1 expression, offering the possibility of using PARP-inhibitors to treat these cases (27, 45).

Of note, no data are available specifically for CCEC, either on immune checkpoint inhibitors or on targeted therapy. Successfully combining targeted agents and immunotherapy with molecular classification is an important future goal for recurrent/advanced CCEC therapy.

## 3 Conclusions

Herein, we summarize the role of molecular classification in the management and prognosis of clear cell endometrial cancer (CCEC) which represents an uncommon disease entity, with different characteristics from endometrioid and other non-endometrioid cancers. Theoretically, adjuvant therapy could be omitted in patients with stage I/II CCEC harboring POLE mutation, whereas adjuvant therapy is recommended in patients with NSMP and p53abn CCEC. With respect to MMRd CCEC, recommendations for adjuvant therapy are unclear. Immunotherapy seems to be the more promising treatment option for patients with advanced or recurrent CCEC characterized by MMRd. In terms of prognosis, CCECs with p53abn and NSMP account for a large majority of all CCECs and have poor clinical outcomes, while those with MMRd or POLEmut have very favorable outcomes. Clinical outcomes of CCEC are different from what has been reported previously, where review of EC in which molecular subtype classification had been applied revealed that POLE-mutated EC has a favorable prognosis, p53abn EC has a poor prognosis, and MMRd and NSMP EC have the intermediate prognosis. Thus, NSMP CCEC appear to be a distinct clinicopathological entity within the larger group of NSMP ECs. Moreover, the integration of molecular signature with pathological factors and genomic profiling would ensure a more tailored management of patients in accordance with the principles of the precision medicine. To date, the number of patients with CCEC is relatively small and few studies have focused exclusively on CCEC in the context of the TCGA classification, therefore, further studies that focus specially on CCEC are necessary, and future clinical trials which include molecular classification subgroups and specific targeted treatments in their design are also needed.

## Author contributions

YH conceived the project. All authors reviewed the literature and drafted the article. YH revised the manuscript. All authors contributed to the article and approved the submitted version.

## Conflict of interest

The authors declare that the research was conducted in the absence of any commercial or financial relationships that could be construed as a potential conflict of interest.

## Publisher's note



## References

1. Huang GS, Santin AD. Genetic landscape of clear cell endometrial cancer and the era of precision medicine. *Cancer*. (2017) 123(17):3216–8. doi: 10.1002/cncr.30743

2. Murali R, Davidson B, Fadare O, Carlson JA, Crum CP, Gilks CB, et al. High-grade endometrial carcinomas: morphologic and immunohistochemical features, diagnostic challenges and recommendations. *Int J gynecological Pathol Off J Int Soc Gynecological Pathologists* (2019) 38 Suppl 1(Iss 1 Suppl 1):S40–s63. doi: 10.1097/PGP.0000000000000491

3. Oaknin A, Bosse TJ, Creutzberg CL, Giornelli G, Harter P, Joly F, et al. Endometrial cancer: ESMO clinical practice guideline for diagnosis, treatment and follow-up. *Ann Oncol Off J Eur Soc Med Oncol* (2022) 33(9):860–77. doi: 10.1016/j.annonc.2022.05.009

4. Travaglino A, Raffone A, Santoro A, Raimondo D, Angelico G, Valente M, et al. Clear cell endometrial carcinomas with mismatch repair deficiency have a favorable prognosis: a systematic review and meta-analysis. *Gynecologic Oncol* (2021) 162(3):804–8. doi: 10.1016/j.ygyno.2021.07.007

5. Bae-Jump V. Unraveling the mystery of clear cell endometrial cancer. *Gynecologic Oncol* (2020) 158(1):1–2. doi: 10.1016/j.ygyno.2020.06.159

6. Kandoth C, Schultz N, Cherniack AD, Akbani R, Liu Y, Shen H, et al. Integrated genomic characterization of endometrial carcinoma. *Nature* (2013) 497(7447):67–73. doi: 10.1038/nature12113

7. Talhouk A, McConechy MK, Leung S, Yang W, Lum A, Senz J, et al. Confirmation of ProMisE: a simple, genomics-based clinical classifier for endometrial cancer. *Cancer* (2017) 123(5):802–13. doi: 10.1002/cncr.30496

8. Talhouk A, McConechy MK, Leung S, Li-Chang HH, Kwon JS, Melnyk N, et al. A clinically applicable molecular-based classification for endometrial cancers. *Br J cancer.* (2015) 113(2):299–310. doi: 10.1038/bjc.2015.190

9. Bogani G, Ray-Coquard I, Concin N, Ngoi NYL, Morice P, Enomoto T, et al. Clear cell carcinoma of the endometrium. *Gynecologic Oncol* (2022) 164(3):658–66. doi: 10.1016/j.ygyno.2022.01.012

10. Kim SR, Cloutier BT, Leung S, Cochrane D, Britton H, Pina A, et al. Molecular subtypes of clear cell carcinoma of the endometrium: opportunities for prognostic and predictive stratification. *Gynecologic Oncol* (2020) 158(1):3–11. doi: 10.1016/j.ygyno.2020.04.043

11. DeLair DF, Burke KA, Selenica P, Lim RS, Scott SN, Middha S, et al. The genetic landscape of endometrial clear cell carcinomas. *J pathology* (2017) 243(2):230–41. doi: 10.1002/path.4947

12. Travaglino A, Raffone A, Mascolo M, Guida M, Insabato L, Zannoni GF, et al. Clear cell endometrial carcinoma and the TCGA classification. *Histopathology* (2020) 76(2):336–8. doi: 10.1111/his.13976

13. Raffone A, Travaglino A, Raimondo D, Neola D, Maletta M, Santoro A, et al. Lymphovascular space invasion in endometrial carcinoma: a prognostic factor independent from molecular signature. *Gynecologic Oncol* (2022) 165(1):192–7. doi: 10.1016/j.ygyno.2022.01.013

14. He D, Wang H, Dong Y, Zhang Y, Zhao J, Lv C, et al. POLE mutation combined with microcystic, elongated and fragmented (MELF) pattern invasion in endometrial carcinomas might be associated with poor survival in Chinese women. *Gynecologic Oncol* (2020) 159(1):36–42. doi: 10.1016/j.ygyno.2020.07.102

15. McAlpine JN, Chiu DS, Nout RA, Church DN, Schmidt P, Lam S, et al. Evaluation of treatment effects in patients with endometrial cancer and POLE mutations: an individual patient data meta-analysis. *Cancer* (2021) 127(14):2409–22. doi: 10.1002/cncr.33516

16. Loukovaara M, Pasanen A, Bützow R. Mismatch repair protein and MLH1 methylation status as predictors of response to adjuvant therapy in endometrial cancer. *Cancer Med* (2021) 10(3):1034–42. doi: 10.1002/cam4.3691

17. Raffone A, Travaglino A, Raimondo D, Neola D, Renzulli F, Santoro A, et al. Prognostic value of myometrial invasion and TCGA groups of endometrial carcinoma. *Gynecologic Oncol* (2021) 162(2):401–6. doi: 10.1016/j.ygyno.2021.05.029

18. Crane E. Beyond serous: treatment options for rare endometrial cancers. *Curr Treat options Oncol* (2022) 23(11):1590–600. doi: 10.1007/s11864-022-01014-7

19. Abu-Rustum. NR, Yashar. CM, Bradley. K, Brooks. R, Campos SM. *NCCN Guidelines®Uterine Neoplasms.Version 1.2023* Available at: https://www.nccn.org/professionals/physician_gls/pdf/uterine.pdf.

20. de Boer SM, Powell ME, Mileshkin L, Katsaros D, Bessette P, Haie-Meder C, et al. Adjuvant chemoradiotherapy versus radiotherapy alone for women with high-risk endometrial cancer (PORTEC-3): final results of an international, open-label, multicentre, randomised, phase 3 trial. *Lancet Oncol* (2018) 19(3):295–309. doi: 10.1016/S1470-2045(18)30079-2

21. de Boer SM, Powell ME, Mileshkin L, Katsaros D, Bessette P, Haie-Meder C, et al. Adjuvant chemoradiotherapy versus radiotherapy alone in women with high-risk endometrial cancer (PORTEC-3): patterns of recurrence and post-hoc survival analysis of a randomised phase 3 trial. *Lancet Oncol* (2019) 20(9):1273–85. doi: 10.1016/S1470-2045(19)30395-X

22. Gilks CB, Oliva E, Soslow RA. Poor interobserver reproducibility in the diagnosis of high-grade endometrial carcinoma. *Am J Surg pathology* (2013) 37(6):874–81. doi: 10.1097/PAS.0b013e31827f576a

23. León-Castillo A, de Boer SM, Powell ME, Mileshkin LR, Mackay HJ, Leary A, et al. Molecular classification of the PORTEC-3 trial for high-risk endometrial cancer: impact on prognosis and benefit from adjuvant therapy. *J Clin Oncol Off J Am Soc Clin Oncol* (2020) 38(29):3388–97. doi: 10.1200/JCO.20.00549

24. Köbel M, Tessier-Cloutier B, Leo J, Hoang LN, Gilks CB, Soslow RA, et al. Frequent mismatch repair protein deficiency in mixed endometrioid and clear cell carcinoma of the endometrium. *Int J gynecological Pathol Off J Int Soc Gynecological Pathologists* (2017) 36(6):555–61. doi: 10.1097/PGP.0000000000000369

25. Stelloo E, Nout RA, Osse EM, Jürgenliemk-Schulz IJ, Jobsen JJ, Lutgens LC, et al. Improved risk assessment by integrating molecular and clinicopathological factors in early-stage endometrial cancer-combined analysis of the PORTEC cohorts. *Clin Cancer Res an Off J Am Assoc Cancer Res* (2016) 22(16):4215–24. doi: 10.1158/1078-0432.CCR-15-2878

26. Wortman BG, Bosse T, Nout RA, Lutgens L, van der Steen-Banasik EM, Westerveld H, et al. Molecular-integrated risk profile to determine adjuvant radiotherapy in endometrial cancer: evaluation of the pilot phase of the PORTEC-4a trial. *Gynecologic Oncol* (2018) 151(1):69–75. doi: 10.1016/j.ygyno.2018.07.020

27. Santoro A, Angelico G, Travaglino A, Inzani F, Arciuolo D, Valente M, et al. New pathological and clinical insights in endometrial cancer in view of the updated ESGO/ESTRO/ESP guidelines. *Cancers* (2021) 13(11):2623. doi: 10.3390/cancers13112623

28. van den Heerik A, Horeweg N, Nout RA, Lutgens L, van der Steen-Banasik EM, Westerveld GH, et al. PORTEC-4a: international randomized trial of molecular profile-based adjuvant treatment for women with high-intermediate risk endometrial cancer. *Int J gynecological Cancer Off J Int Gynecological Cancer Society* (2020) 30(12):2002–7. doi: 10.1136/ijgc-2020-001929

29. Creasman WT, Odicino F, Maisonneuve P, Quinn MA, Beller U, Benedet JL, et al. Carcinoma of the corpus uteri. FIGO 26th annual report on the results of treatment in gynecological cancer. *Int J gynaecology obstetrics: Off Organ Int Fed Gynaecology Obstetrics.* (2006) 95 Suppl 1:S105–43. doi: 10.1016/S0020-7292(06)60031-3

30. Le DT, Durham JN, Smith KN, Wang H, Bartlett BR, Aulakh LK, et al. Mismatch repair deficiency predicts response of solid tumors to PD-1 blockade. *Sci (New York NY).* (2017) 357(6349):409–13. doi: 10.1126/science.aan6733

31. Marabelle A, Le DT, Ascierto PA, Di Giacomo AM, De Jesus-Acosta A, Delord JP, et al. Efficacy of pembrolizumab in patients with noncolorectal high microsatellite Instability/Mismatch repair-deficient cancer: results from the phase II KEYNOTE-158 study. *J Clin Oncol Off J Am Soc Clin Oncol* (2020) 38(1):1–10. doi: 10.1200/JCO.19.02105

32. O'Malley DM, Bariani GM, Cassier PA, Marabelle A, Hansen AR, De Jesus Acosta A, et al. Pembrolizumab in patients with microsatellite instability-high advanced endometrial cancer: results from the KEYNOTE-158 study. *J Clin Oncol Off J Am Soc Clin Oncol* (2022) 40(7):752–61. doi: 10.1200/JCO.21.01874

33. *U.S.Food & drug administration* (2022). Available at: https://www.fda.gov/drugs/resources-information-approved-drugs/fda-approves-pembrolizumab-advanced-endometrial-carcinoma.

34. Oaknin A, Tinker AV, Gilbert L, Samouëlian V, Mathews C, Brown J, et al. Clinical activity and safety of the anti-programmed death 1 monoclonal antibody dostarlimab for patients with recurrent or advanced mismatch repair-deficient endometrial cancer: a nonrandomized phase 1 clinical trial. *JAMA Oncol* (2020) 6(11):1766–72. doi: 10.1001/jamaoncol.2020.4515

35. *U.S.Food & drug administration* (2021). Available at: https://www.fda.gov/drugs/resources-information-approved-drugs/fda-grants-accelerated-approval-dostarlimab-gxly-dmmr-endometrial-cancer.

36. Makker V, Colombo N, Casado Herráez A, Santin AD, Colomba E, Miller DS, et al. Lenvatinib plus pembrolizumab for advanced endometrial cancer. *New Engl J Med* (2022) 386(5):437–48. doi: 10.1056/NEJMoa2108330

37. *U.S.Food & drug administration* (2022). Available at: https://www.fda.gov/drugs/resources-information-approved-drugs/fda-grants-regular-approval-pembrolizumab-and-lenvatinib-advanced-endometrial-carcinoma.

38. van Gool IC, Eggink FA, Freeman-Mills L, Stelloo E, Marchi E, de Bruyn M, et al. POLE proofreading mutations elicit an antitumor immune response in endometrial cancer. *Clin Cancer Res an Off J Am Assoc Cancer Res* (2015) 21(14):3347–55. doi: 10.1158/1078-0432.CCR-15-0057

39. Gargiulo P, Della Pepa C, Berardi S, Califano D, Scala S, Buonaguro L, et al. Tumor genotype and immune microenvironment in POLE-ultramutated and MSI-hypermutated endometrial cancers: new candidates for checkpoint blockade immunotherapy? *Cancer Treat Rev* (2016) 48:61–8. doi: 10.1016/j.ctrv.2016.06.008

40. Aghajanian C, Filiaci V, Dizon DS, Carlson JW, Powell MA, Secord AA, et al. A phase II study of frontline paclitaxel/carboplatin/bevacizumab, paclitaxel/carboplatin/temsirolimus, or ixabepilone/carboplatin/bevacizumab in advanced/recurrent endometrial cancer. *Gynecologic Oncol* (2018) 150(2):274–81. doi: 10.1016/j.ygyno.2018.05.018

41. Miller D, Filiaci V, Fleming G, Mannel R, Cohn D, Matsumoto T, et al. Late-breaking abstract 1: randomized phase III noninferiority trial of first line chemotherapy for metastatic or recurrent endometrial carcinoma: a gynecologic oncology group study. *Gynecologic Oncol* (2012) 125(3):771. doi: 10.1016/j.ygyno.2012.03.034

42. Leslie KK, Filiaci VL, Mallen AR, Thiel KW, Devor EJ, Moxley K, et al. Mutated p53 portends improvement in outcomes when bevacizumab is combined with chemotherapy in advanced/recurrent endometrial cancer: an NRG oncology study. *Gynecologic Oncol* (2021) 161(1):113–21. doi: 10.1016/j.ygyno.2021.01.025

43. Farhang Ghahremani M, Goossens S, Haigh JJ. The p53 family and VEGF regulation: "It's complicated". *Cell Cycle (Georgetown Tex)* (2013) 12(9):1331–2. doi: 10.4161/cc.24579

44. Cagaanan A, Stelter B, Vu N, Rhode EN, Stewart T, Hui P, et al. HER2 expression in endometrial cancers diagnosed as clear cell carcinoma. *Int J gynecological Pathol Off J Int Soc Gynecological Pathologists* (2022) 41(2):132–41. doi: 10.1097/PGP.0000000000000783

45. Auguste A, Genestie C, De Bruyn M, Adam J, Le Formal A, Drusch F, et al. Refinement of high-risk endometrial cancer classification using DNA damage response biomarkers: a TransPORTEC initiative. *Modern Pathol an Off J United States Can Acad Pathology Inc* (2018) 31(12):1851–61. doi: 10.1038/s41379-018-0055-1

frontiers | Frontiers in Oncology

TYPE Original Research
PUBLISHED 03 July 2023
DOI 10.3389/fonc.2023.1142755



OPEN ACCESS

EDITED BY
Umberto Malapelle,
University of Naples Federico II, Italy

REVIEWED BY
Min Kyu Kim,
Sungkyunkwan University,
Republic of Korea
Pengpeng Qu,
Tianjin Central Hospital for Gynecology and Obstetrics, China
Tasaduq H. Wani,
University of Oxford, United Kingdom

*CORRESPONDENCE
Yanling Cai
caiyanling@hotmail.com
Jing Li
jingli1984@email.sdu.edu.cn

†These authors have contributed equally to this work

RECEIVED 12 January 2023
ACCEPTED 13 June 2023
PUBLISHED 03 July 2023

CITATION
Kong L, Xu F, Yao Y, Gao Z, Tian P, Zhuang S, Wu D, Li T, Cai Y and Li J (2023) Ascites-derived CDCP1+ extracellular vesicles subcluster as a novel biomarker and therapeutic target for ovarian cancer. *Front. Oncol.* 13:1142755. doi: 10.3389/fonc.2023.1142755



# Ascites-derived CDCP1+ extracellular vesicles subcluster as a novel biomarker and therapeutic target for ovarian cancer

Lingnan Kong[1,2], Famei Xu[2], Yukuan Yao[1,2], Zhihui Gao[2], Peng Tian[3], Shichao Zhuang[4], Di Wu[5,6], Tangyue Li[2], Yanling Cai[7*†] and Jing Li[2*†]

[1]Affiliated Hospital of Weifang Medical University, School of Clinical Medicine, Weifang Medical University, Weifang, China, [2]Department of Pathology, Zibo Central Hospital, Zibo, China, [3]Department of Ultrasonic, Zibo Central Hospital, Zibo, China, [4]Department of Gynecology, Zibo Central Hospital, Zibo, China, [5]Department of R&D, Shenzhen SecreTech Co., Ltd., Shenzhen, China, [6]Department of R&D, Vesicode AB, Solna, Sweden, [7]Guangdong Provincial Key Laboratory of Systems Biology and Synthetic Biology for Urogenital Tumors, The First Affiliated Hospital of Shenzhen University, Shenzhen Second People's Hospital, Shenzhen, China

**Introduction:** Ovarian cancer (OVCA) is one of the most prevalent malignant tumors of the female reproductive system, and its diagnosis is typically accompanied by the production of ascites. Although liquid biopsy has been widely implemented recently, the diagnosis or prognosis of OVCA based on liquid biopsy remains the primary emphasis.

**Methods:** In this study, using proximity barcoding assay, a technique for analyzing the surface proteins on single extracellular vesicles (EVs). For validation, serum and ascites samples from patients with epithelial ovarian cancer (EOC) were collected, and their levels of CDCP1 was determined by enzyme-linked immunosorbent assay. Tissue chips were prepared to analyze the relationship between different expression levels of CDCP1 and the prognosis of ovarian cancer patients.

**Results:** We discovered that the CUB domain-containing protein 1+ (CDCP1+) EVs subcluster was higher in the ascites of OVCA patients compared to benign ascites. At the same time, the level of CDCP1 was considerably elevated in the ascites of OVCA patients. The overall survival and disease-free survival of the group with high CDCP1 expression in EOC were significantly lower than those of the group with low expression. In addition, the receiver operating characteristic curve demonstrates that EVs-derived CDCP1 was a biomarker of early response in OVCA ascites.

**Discussion:** Our findings identified a CDCP1+ EVs subcluster in the ascites of OVCA patients as a possible biomarker for EOC prevention.

KEYWORDS

**extracellular vesicles, CDCP1, ovarian cancer, ascites, diagnose**

# 1 Introduction

Ovarian cancer (OVCA) is a prevalent kind of malignant tumor in the female reproductive system, and it has the highest mortality rate of all gynecological malignancies (1, 2). Epithelial ovarian cancer (EOC) accounts for approximately two-thirds of OVCA and is the most prevalent and fastest-progressing pathological subgroup (3, 4). OVCA is characterized by the development of ascites within the peritoneal cavity. Tumor cells of OVCA in ascites have the characteristics of epithelial-mesenchymal transitions that can be transformed into more invasive spindle cells. Therefore, it is completely reasonable to think that the production of malignant ascites should be closely relevant to high invasiveness of OVCA. It correlates with metastases and, hence, a dismal prognosis for OVCA (5).

Liquid biopsy (6), used for early screening, diagnosis, and prognosis, is an effective method for guiding treatment and reducing tumor mortality. Currently, serum tumor markers such as carbohydrate antigen 125 (CA125), carcinoembryonic antigen, α-Fetoprotein and human chorionic gonadotropin in conjunction with color doppler ultrasonography and computed tomography (7, 8), are frequently employed for OVCA diagnosis (9). However, the sensitivity and specificity of these tumor markers are inadequate for clinical applications, necessitating the search for new diagnostic or therapeutic targets.

Exosomes are extracellular vesicles (EVs) secreted by the majority of cells. It has been found that exosomes contain a variety of bioactive proteins, such as major histocompatibility complex I (MHC I) and major histocompatibility complex II (MHC II) involved in antigen presentation, as well as transmembrane proteins and annexins (10). Exosomes transport proteins, DNA and non-coding RNA from the host cells (11, 12). Cancer-derived exosomes have been demonstrated to facilitate cancer progression by stimulating angiogenesis, pre-conditioning of metastatic locations, suppressing immune systems and others (13). Exosomes have been demonstrated in the ascites of both OVCA patients (14) and non-cancerous patients with liver or kidney disorders. According to previous research, exosomes produced from ascites in OVCA patients have been demonstrated to correlate strongly with tumor burden, invasiveness, and poor prognosis. Meanwhile, ascites-derived exosomes can contribute to cancer growth by altering the tumor microenvironment, which alters cancer cells' biological characteristics and functions and various tumor cell behaviors (11). Therefore, the search for disease-specific exosome-associated markers has the potential to reveal the mechanism of peritoneum metastasis of OVCA and to propose diagnostic or therapeutic targets for OVCA (15). However, an important concern remains that diagnostic surface protein markers of exosomes may be too rare in abundance to be detected in the sample. Therefore, how to accurately analyze the composition of complex exosomes in ascites and obtain more effective information from ascites related exosomes for accurate diagnosis and treatment of diseases has become an urgent technical problem to be solved.

In this investigation, proximity barcoding assay (PBA) (16), a single-EVs analysis method developed by our collaborating group, was utilized to profile the expression of CDCP1 proteins at single EVs and followed by bioinformatic analysis for the identification of exosome subpopulation. Based on the results of PBA, the positive marker in ascites-derived EVs, CUB domain-containing protein 1 (CDCP1), was selected for further investigation.

CDCP1 (17) is a transmembrane protein that has been previously proven to be closely associated with the occurrence of colorectal cancer (18), lung cancer (19), breast cancer (20), prostate cancer (21) and other diseases (22, 23). The above studies have shown that CDCP1often is regard as an important hub for oncogenic signaling. It suggests that CDCP1 could be a promising and widely used biomarker for early diagnosis and prognosis. It was discovered that the proportion of CDCP1+ EVs in OVCA ascites was significantly elevated, indicating that EVs-derived CDCP1 can be considered a molecular biomarker for early surveillance and diagnosis of OVCA.

# 2 Materials and methods

## 2.1 Ethical approval, patient recruitment and sample collection

The study was approved by the Medical Ethics Committee of Zibo Center Hospital. Between Jan 2019 and Dec 2021, 8 patients with high-grade serous OVCA and 18 patients with non-cancer-disease-induced ascites were enrolled in our study at Zibo center Hospital, including patients with chronic kidney disease and heart failure. Non-cancer women were selected in the control group. Ensure that there is no history of ovarian cancer or other tumors, o abdominal or pelvic space occupation in imaging, and the expression of serological tumor markers is in the normal range. Only when these conditions are met at the same time can they be included in the control group. The ovarian cancer group selected patients who were diagnosed with EOC with ascites and did not receive radiotherapy or chemotherapy before surgery. After ascites samples were collected, they were centrifuged at 1,000 × g at 4°C for 15 min (R5810, Eppendorf, Germany) to remove cells and then at 10,000 × g at 4°C for 30 min (R5810, Eppendorf, Germany) to remove cell debris or aggregates.

Ultracentrifugation (Optima XPN100, Coulter Beckman with rotor SW45Ti) steps were performed at 100, 000 × g at 4°C for 70 min to precipitate EVs, followed by a washing step with phosphate buffered saline (PBS) and a second ultracentrifugation step at 100,000 × g at 4°C for 70 min. The pellets from 10 ml of ascites were resuspended in 100 μL PBS for further analysis. The size distribution and concentration of exosome suspension were analyzed via nanoparticle tracking analysis (NTA, nanosight NS300, Malvern Panalytical, UK). The EVs captured on analyzing surface were recorded via Scanning Electron microscopy (SEM, Zeiss, Germany).

## 2.2 Proximity barcoding assay and sequencing

To characterize the single EVs isolated from the ascites of OVCA and non-cancerous patients. We used proximity barcoding assay (PBA) to detect the expression of 113 proteins (Supplementary Table 1) on individual EVs. The majority of

proteins examined are known cancer biomarkers. The analysis was performed following the standard operating procedures defined by Vesicode (Solna, Sweden) and reported in our earlier paper (16). Briefly, antibodies labeled with designed DNA probes were utilized to identify exosomal proteins concurrently. The DNA probes comprise protein tags, molecular tags and universal binding sites to subsequent processes. With the assistance of EV barcoding templates, EV tags were attached to the 3' end of DNA probes to label the antibodies recognizing the same single EVs. Therefore, we generate DNA sequences comprising EV tag, protein tag and molecular tag. After library preparation, the sequencing was conducted using the Illumina NextSeq 500 platform with 75 cycles of single-end sequencing.

## 2.3 Exosomal proteome data analysis

The sequencing data were generated with high-throughput sequencing. The bcl2fastq software (version 2.20.0.42, Illumina Inc., USA) was used to convert raw data into fastq files of each sample. The fastQC technique was utilized to assess the read quality (24). The fastp technique controls read quality and adapter trimming (25). Reads with a quality score < 20 were eliminated. Sequencing reads comprising the EV tag, protein tag and molecular tag were evaluated to build a matrix of EV ID and protein expression data for each sample, which provides a high-dimensional protein abundance dataset at the single EV level for subsequent analysis.

The sum of protein counts from all single EVs in a sample was regarded as the raw protein expression data for assessing each protein's expression level in each sample. The raw protein expression values were normalized utilizing the trimmed mean of M-values (TMM) algorithm in the edgeR package (26).

The number of EVs with each pair of co-expressed proteins was counted as a protein combination dataset for analyzing the pattern of protein-protein combinations on individual EVs. The count per million (CPM) normalization procedure was applied prior to further examination of combination data. To examine the performance of EV proteins as a biomarker in the classification of patients and controls, we construct the receiver operating characteristic (ROC) curves and generate the area under the receiver operating characteristic curve (AUC) (27)values using the pROC package (v. 1.18.0). For EV subpopulation analysis, the unsupervised FlowSOM algorithm (28)was utilized to generate EV clusters. T-distributed stochastic neighbor embedding (t-SNE) was used for subpopulation visualization (29). The analyzes were conducted in R version 4.0.5.

## 2.4 Tissue chip, hematoxylin and eosin staining and immunohistochemical staining

Tissue chips of OVCA and control tissues were obtained from Shanghai Outdo Biotech Company (Shanghai, China; Cat # HOvaC154Su01). Before surgery, no treatment was given to patients pathologically diagnosed with OVCA. The antibody employed for IHC was Anti-WT-1 (dilution 1:100; cat. no. IR346; LBP, Guangzhou, China). Anti-CA125 (dilution 1:100; cat. # IM360; LBP, Guangzhou, China). Anti-ki67 (dilution 1:100; cat. # 790-4286; Roche, Basel, Switzerland). Tissues were cut into 2-3 μm slices for future usage, baked at 60°C for 30-60 minutes, and repaired at 92-95°C for half an hour. The first antibody and the second antibody were added after washing with PBS. The color was developed by diaminobenzidine at 37°C for 40 min. CDCP1 IHC was performed using an antibody against CDCP1 (Rabbit monoclonal to CDCP1-C-terminal; dilution 1:100; Abcam, ab252947; USA), as previously described.

Immunostaining was reviewed by two pathologists. However, clinical information was not visible to them. Scoring was performed by two experienced pathologists who were blinded to tissue identity using a grading system based on staining intensity (no staining, 0; weak, 1; moderate, 2; strong, 3) and percentage of positive-staining cells (1–25% positive, 1; 26–50%, 2; 51–75%, 3; 76–100%, 4) (30, 31). The final score was calculated as intensity score × percentage score. For survival analysis, the final score categorized CDCP1 expression in OVCA tissues as low (0–4) or high (5–12). Based on CDCP1 expression in tissue chips of 79 patients, Kaplan–Meier survival curves were constructed for high- and low-expression groups and assessed with a log-rank test ($p < 0.05$).

## 2.5 Bioinformatics analysis

The Cancer Genome Atlas (TCGA, https://cancergenome.nih.gov/) is a public project aimed at cataloging and discovering major carcinogenic genomic changes in the progression of human tumors by large-scale genome sequencing and thorough multidimensional analysis (32). The Gene Expression Profiling Interactive Analysis (http://gepia.cancer-pku.cn/index.html) is a recently developed bioinformatics platform that contains tissue expression data from 9736 tumors and 8587 normal samples. Making cancer genome data sets accessible to the public makes it possible to improve diagnostic methods, treatment criteria, and cancer prevention. In this study, "expression DIY" was used to compare CDCP1 in OVCA with control tissues in TCGA database, with $p < 0.05$ as the significant criterion for screening.

## 2.6 Enzyme-linked immunosorbent assay

Serum samples and ascites of patients with EOC were preserved at -80°C until use. Each sample was centrifuged for 20 min at 2,000 rpm and 4°C, and then the supernatant liquid was collected. CDCP1 was assessed with human-specific sandwich ELISA kits per the manufacturer's instruction (FMGBio, shanghai, China).

The final ELISA assay was performed as follows: washing buffer consists of 1.5 mM NaH2PO4, 8.5 mM Na2HPO4, 145 mM NaCl, 1 g/L Tween 20, deionized H2O, and pH 7.4. Then, 50 μL assay buffer was added to each well. First, 50 μL of either sample or control was added to each well. The calibrators are prepared by adding 50 μL assay buffer beforehand. Each well was then filled with 50 μL of biotinylated antigen solution. After incubation for 0.5 h at 37°C, the plates were washed five times with washing buffer before 50 μL of

horseradish peroxidase-avidin was added to each well. Incubate at 37°C for another 0.5 h. The plates were rinsed five times. Add 50 μL of chromogenic agent A and 50 μL of chromogenic agent B to each well, shake gently and mix well. Develop the color for ten minutes at 37°C, and add 50 μL of termination solution to each well to terminate the reaction. Each well's optical density (OD) was measured at 450 nm on the MultiSkan Ascent (Thermo Scientific, Odense, Denmark) by setting the blank wells to zero. The measurement must be conducted within 10 min of adding the termination solution. The regression equation of the standard curve is produced from the concentration and OD value, and then the results of samples and controls are read from this curve.

## 2.7 Statistical analysis

We applied the Shapiro-Wilk test to examine the normality of data distribution and the F-test to determine the variance homogeneity. The student's t-test was applied for differential expression analysis of groups with normal data distribution and homogenous variance. A non-parametric test was employed to compare protein expression between groups with unequal variance or abnormal distributions. The Mann-Whitney U test is applied if the data are not normally distributed. Welch's t-test is used for data having normal distribution but nonhomogeneous variance. We employed the Benjamini-Hochberg (BH) method to adjust the *p*-values. Other statistical analyzes were processed using SPSS 23.0 software (IBM Corporation, Armonk, NY, USA) and GraphPad Prism 5.0 (GraphPad Software, La Jolla, CA, USA). When $n \leq 5$ or the proportion of $n \leq 5$ is more than 20%, the Spelman rank correlation coefficient is used. $p < 0.05$ indicated that a statistically significant difference exists.

# 3 Results

## 3.1 Characterization of EVs derived from ascites samples

By creating cellular wax blocks of ascites from OVCA patients, it was discovered that tumor cells distinctively express CA125 and WT-1 (Figure 1A). Next, we performed NTA and SEM characterization prior to PBA profiling of single EV level proteins (Figure 1B). The obtained EVs from ascites samples of patients were analyzed using NTA. The median size is 100 nm, and there is a concentration of 5 particles per mL (Figure 1C). SEM images of the collected EVs reveal a diameter of approximately 100 nm (Figure 1D). During PBA analysis, EVs were immobilized on a surface by the interaction between CTB and GM1 groups in the lipid membrane of EVs. Figure 1E depicts the number of observed protein counts, EV counts, and resultant protein counts per exosome. There was no significant difference between OVCA and control groups. Following PBA analysis, we evaluated the total expression level of each protein. We discovered that among 13 significantly differentially expressed proteins, 12 were upregulated in the OVCA group, and 1 protein was down-regulated (Figure 1F). Among the Upregulated proteins includes CDCP1, epithelial cell adhesion molecule (EPCAM), integrinα6 (ITGA6), human tumor-associated calcium signal transducer 2 (TACSTD2), integrinα3 (ITGA3), integrinβ4 (ITGB4), CD151, CD9 and like other. CDCP1 levels were statistically significantly higher in the OVCA group compared to the control group (Figure 1G).

## 3.2 The CDCP1 + EVs cluster was enriched in the ascites of OVCA patients

We utilized FlowSOM, an unsupervised machine learning algorithm, to classify single EVs into clusters based on the similarity of their proteomic features. Twenty-eight clusters were obtained and are shown in the tSNE plot in Figure 2A. The Percentile of each subcluster and its representative protein are displayed in Figure 2B. To compare OVCA and control groups, we plotted the tSNE for each group (Figure 2C) and each sample (Figure 2D) and selected the subclusters with a significant difference. The plot of cluster 4 in Figure 2E depicts that the majority of the cluster of the EVs come from the OVCA group, i.e., 95.59%. The detection frequency of each protein in cluster 4 was plotted, and leading biomarkers include TACSTD2, EPCAM, erb-b2 receptor tyrosine kinase 2(ERBB2), ITGA3, lysosome associated membrane protein 1 (LAMP1), integrinβ1(ITGB1), epidermal growth factor receptor (EGFR), ITGA6, CD151, CDCP1 (Figure 2F).

## 3.3 The correlation between CDCP1 expression level and clinical prognosis of EOC patients

TCGA database analysis revealed that the CDCP1 expression level was positively correlated with OVCA (Figure 3A). According to previous research, CDCP1 is highly expressed in OVCA tissues. In addition, we collected ascites and serum samples from women with EOC and non-cancer and determined the expression level of CDCP1 by enzyme-linked immunosorbent assay (ELISA). The findings revealed that the expression of CDCP1 was elevated in the exosomes of OVCA patients with ascites [$n = 9$, $p < 0.05$, 95% confidence interval (CI) 65.74 to 385.1] while decreasing in their serum ($n = 8$, $p < 0.0001$, 95% CI -1675 to -829.0) (Figures 3B, C). A microarray of OVCA tissue was created, and clinical survival data for OVCA patients were evaluated to investigate the influence of varying levels of CDCP1+ expression on disease-free survival or overall survival in patients with OVCA. According to the intensity and proportion of CDCP1 positive expression in the cytoplasm of tumor cells, CDCP1 was categorized into high and low expression groups (Figure 3D). The results showed that the survival rate of patients with low expression of CDCP1 was significantly higher than that of patients with high expression of CDCP1 (Figure 3E). The expression level of ki67 was also favorably linked with overall survival ($n = 111$, $p < 0.05$) (Figure 3F). From the clinical follow-up data, it is showed that the longest disease-free survival time and overall survival time of patients with ovarian cancer can reach 109 months. The results demonstrated that both the overall survival time

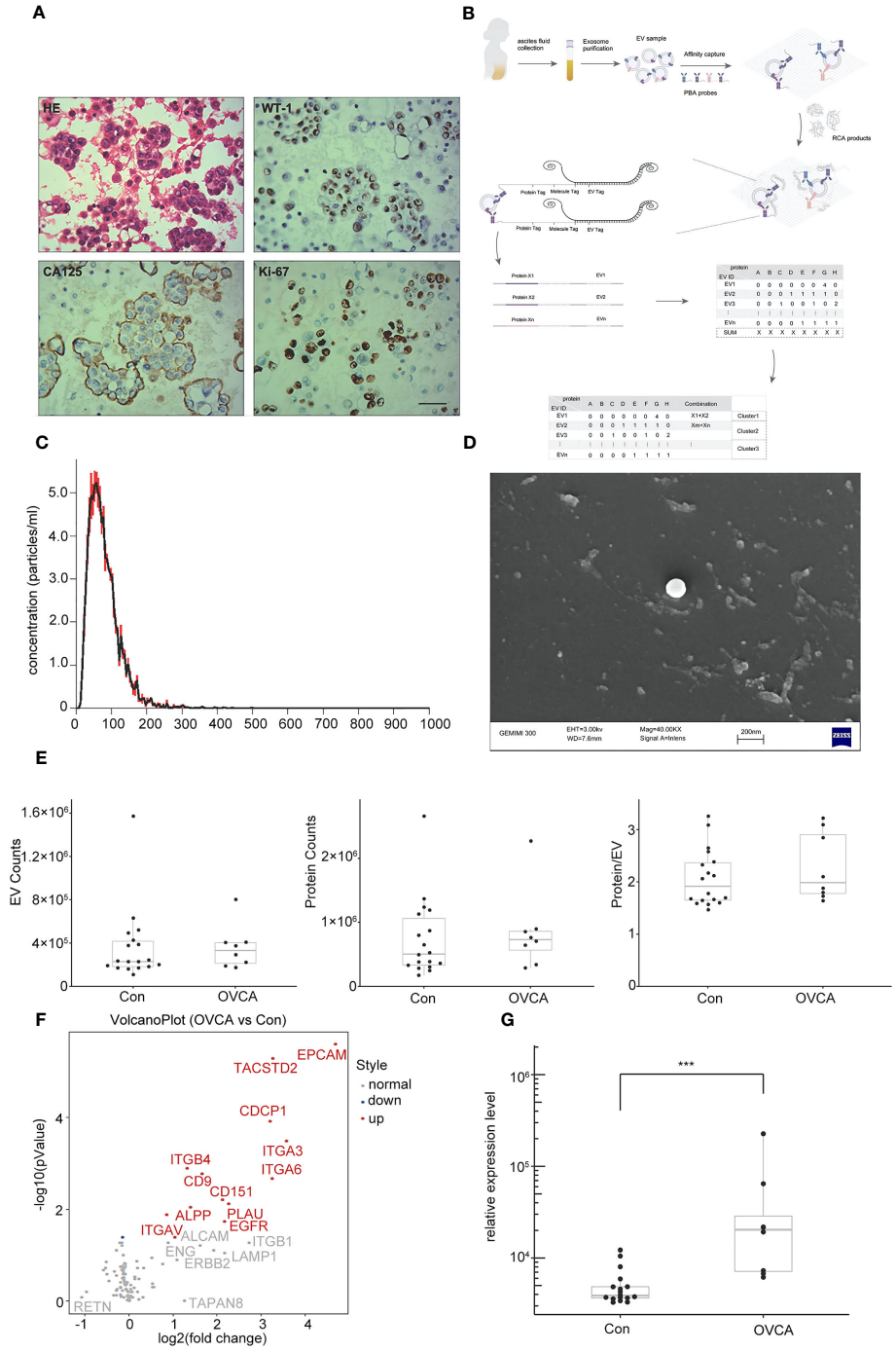


FIGURE 1
Extracellular vesicles (EVs) derived from ovarian cancer ascites samples. **(A)** Ovarian cancer (OVCA) tissue express WT-1, CA125 and ki67, scale bar 50 μm. **(B)** The protocol of Proximity Barcoding Assay (PBA) technology. **(C)** Exosomes were analyzed via nanoparticle tracking analysis. **(D)** Scanning Electron microscopy shows exosomes. **(E)** The count of EV and proteins. **(F)** Compared with the Con group, there were 12 upregulated, including CDCP1. **(G)** CDCP1 was shown higher expression in the OVCA group. ***p < 0.001.

(n = 78, $p < 0.05$) and the disease-free survival time (n = 76, $p < 0.05$) were significantly shorter in the high CDCP1 expression group than in the group with the low CDCP1 expression (Figures 3G, H). A comprehensive analysis of the expression level of CDCP1, clinicopathological grade and tumor TNM stage concluded that the expression level of CDCP1 varied significantly between different TNM stages (Table 1).

## 3.4 The diagnostic value of single EV protein biomarkers in OVCA

The protein combination pattern between the OVCA and Control groups differs significantly. OVCA group displays mostly highlighted protein combinations among the combinations we discovered (Figure 4A). CDCP1 protein tends to co-express with

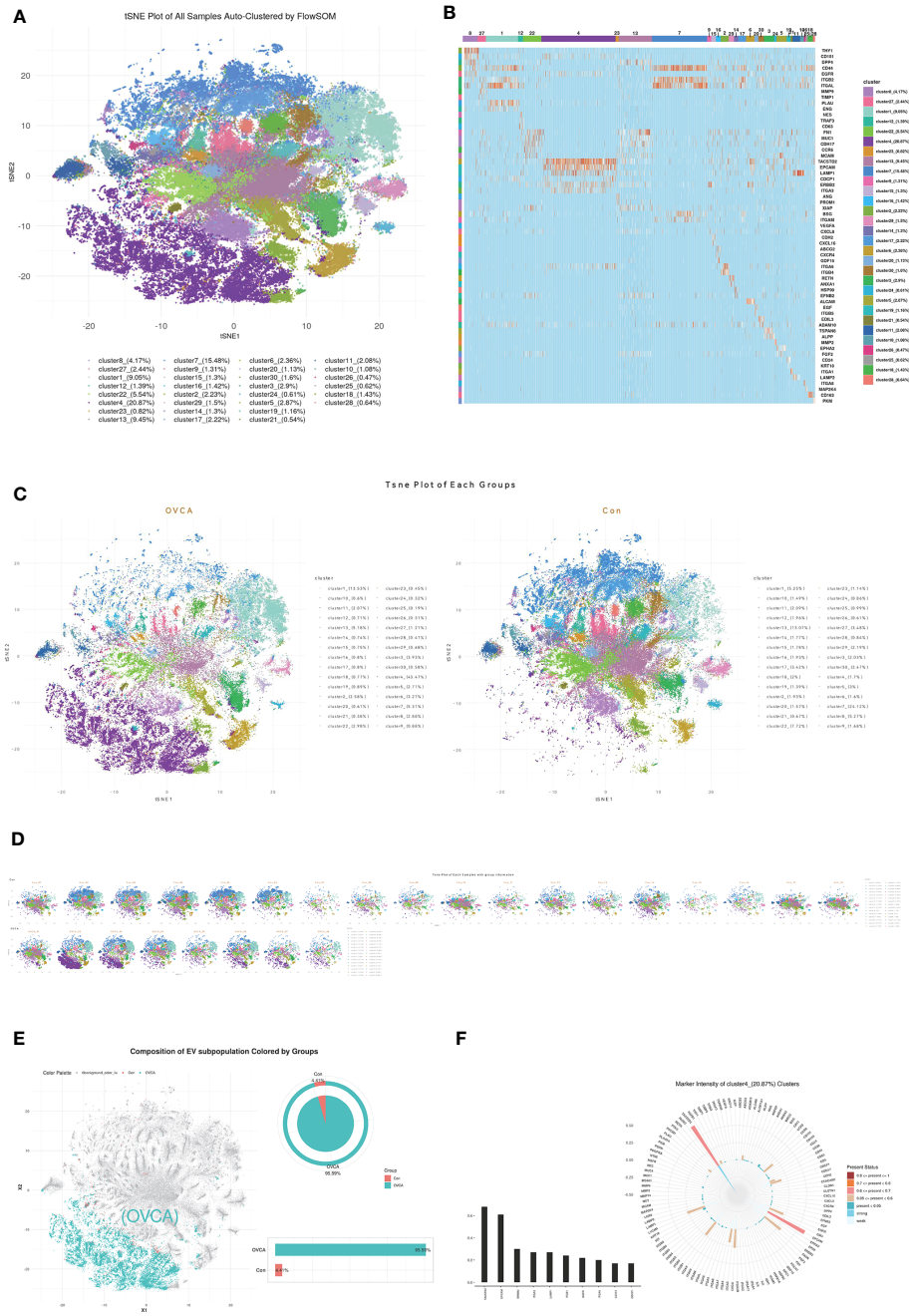


FIGURE 2
The CDCP1 + EVs cluster was enriched in the ascites of OVCA patients. **(A)** All samples were divided into twenty-eight clusters and demonstrated in the tSNE plot. **(B)** The Percentile of each subgroup and its characteristic protein. **(C)** EVs in ovarian cancer ascites and benign ascites. **(D)** tSNE of each sample with ovarian cancer and the control group. **(E)** OVCA ascites are mainly concentrated in cluster 4. **(F)** Major protein constituent of cluster 4.

ITGA6, ITGAL, ERBB2, and other proteins (Figure 4B). CDCP1 levels are significantly elevated. Using CDCP1 as a diagnostic biomarker, the AUC value in the ROC analysis is 0.9375 (Figure 4C). The combination of CDCP1 and ITGA6 proteins may differentiate between OVCA and non-cancer groups with a higher AUC value (0.9653) than CDCP1 alone (Figure 4D).

## 4 Discussion

CA125 is the main tumor marker for the diagnosis of EOC, but which is negative in some cases of EOC and affected by menstruation, pelvic inflammation, gynecological benign tumors and so on. As a new biomarker, human epididymis protein 4 has been used in the diagnosis

10.3389/fonc.2023.1142755

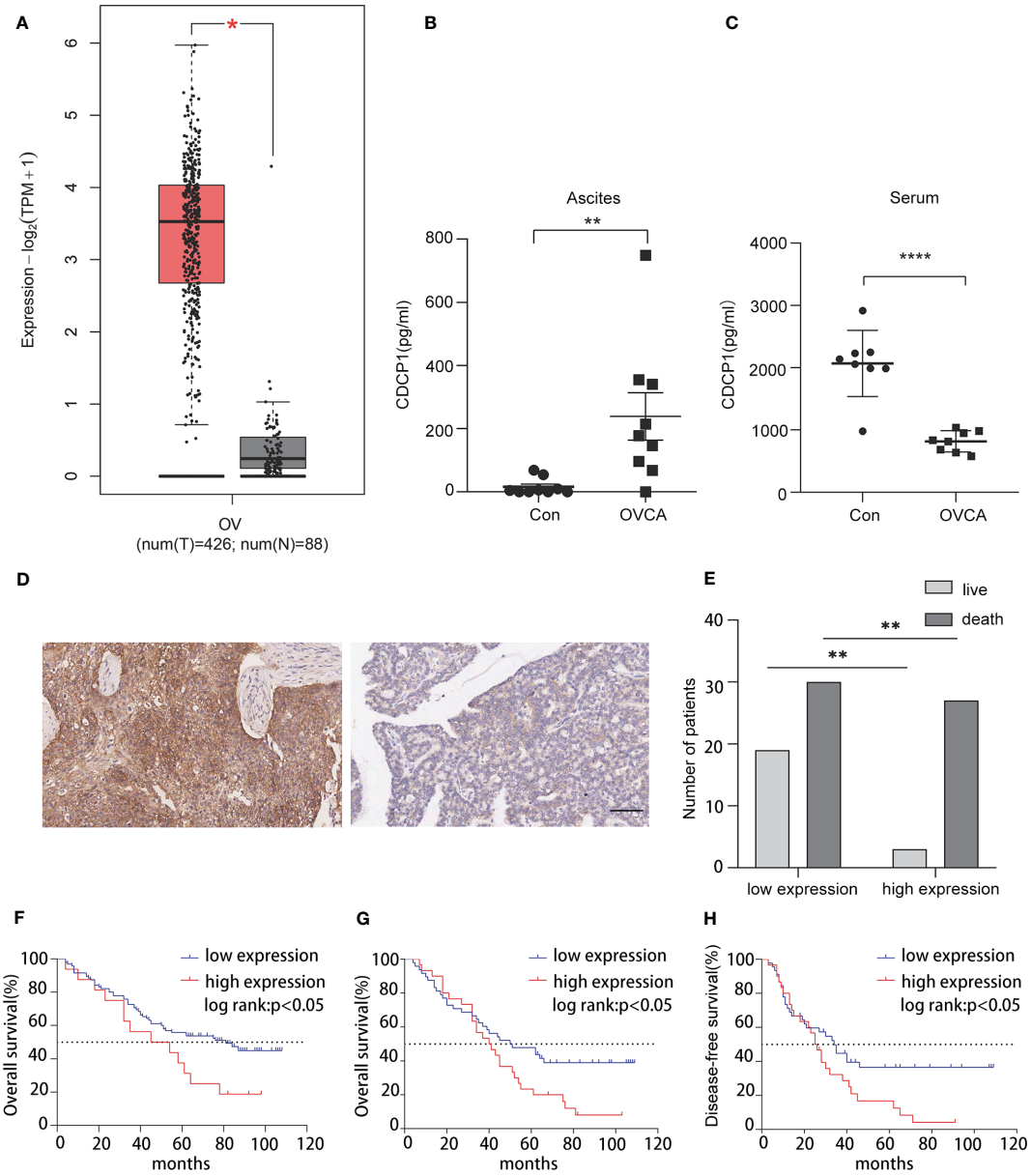


FIGURE 3
CDCP1 expression is associated with the prognosis of ovarian cancer patients. **(A)** CDCP1 expression level was positively linked with ovarian cancer in TCGA. **(B)** CDCP1 levels in the ascites were assessed using sandwich enzyme-linked immunosorbent assay ($p < 0.05$). **(C)** CDCP1 levels in the serum were assessed by the sandwich ELISA ($p < 0.0001$). **(D)** CDCP1 low and high expression as determined by IHC staining, scale bar 50 μm. **(E)** CDCP1 express level influenced survival. **(F)** Overall, greater ki-67 expression was associated with a shorter survival duration than low expression. **(G, H)** Overall and disease-free survival times of the group with high CDCP1 expression were significantly shorter than those with low CDCP1 expression. *$p < 0.05$, **$p < 0.01$, ****$p < 0.0001$.

of OVCA, but its expression varies greatly in different subtypes, so its clinical application is limited. The combined detection of multiple markers may improve the clinical application value of these markers (33), but more biomarkers does not mean more benefits (34). It is necessary to make a comprehensive judgment combined with clinical manifestations, imaging examination and so on.

Currently, the gold standard for diagnosing OVCA is a tissue biopsy, which is time-consuming, costly, and carries the danger of tumor spread; thus, a new molecular tool must be developed to enhance the detection rate of OVCA and the survival rate. As an early non-invasive diagnostic and therapeutic approach, liquid biopsy can detect tumor cells or tumor cell DNA fragments with high activity and immune evasion in peripheral body fluids such as blood, urine, and cerebrospinal fluid (35). In fact, circulating tumor cells (CTCs) is a kind of tumor cell that escapes from the primary tumor or metastasis to the peripheral blood circulation and survives, which is closely related to tumor metastasis and proliferation; ctDNA refers to the genetic material released by tumor cells after death or rupture, which mainly exists in the circulatory system of tumor patients too. It can also be used to

TABLE 1 The CDCP1 expression level varied between different stages.

| Characteristic | High | Low | Total | rs | p-value |
|---|---|---|---|---|---|
| Age(years) | | | | | |
| ≤50 | 9 | 21 | 30 | 0.117 | 0.306 |
| >50 | 20 | 28 | 48 | | |
| Null | | | 1 | | |
| Grades | | | | | |
| I | 3 | 10 | 13 | 0.179 | 0.125 |
| II | 0 | 1 | 1 | | |
| III | 27 | 34 | 61 | | |
| Null | | | 4 | | |
| T Stage | | | | | |
| T1 | 0 | 1 | 1 | 0.228 | 0.043* |
| T2 | 2 | 11 | 13 | | |
| T3 | 28 | 37 | 65 | | |
| N Stage | | | | | |
| N0 | 15 | 31 | 46 | 0.131 | 0.252 |
| N1 | 15 | 18 | 33 | | |
| M Stage | | | | | |
| M0 | 20 | 32 | 52 | -0.014 | 0.903 |
| M1 | 10 | 17 | 27 | | |
| TNM stage | | | | | |
| I | 0 | 1 | 1 | | |
| II | 2 | 11 | 13 | 0.098 | 0.389 |
| III | 18 | 20 | 38 | | |
| IV | 10 | 17 | 27 | | |

*$p < 0.05$.

monitor tumors in a real-time and dynamic manner. As expected, CTCs and circulating tumor DNA (ctDNA) have been extensively studied, and research has revealed that they are closely associated with the tumor burden but are insensitive to the early stage of cancer (36). However, viable tumor cells, apoptotic cells, and cell fragments can be found in peripheral blood, causing inaccuracies in CTC detection results.

Furthermore, ctDNA is fragmented, extremely low in concentration, and has a short half-life, necessitating great specificity and sensitivity in the detection technology (37). In recent years, there have been an increasing number of studies on exosomes, and the proteins carried on the surface of exosomes have the fingerprint characteristics of their mother cells, as the characteristics of the abnormal exosome subsets can be identified early through the analysis of proteins carried on the surface of exosomes (38). However, the existing technology makes it challenging to assess the fingerprint characteristics of a single exosome.

In the study, we used the PBA technique to evaluate the EVs derived from ascites and then categorized them based on the characteristics of proteins on the exosome membrane. PBA has the following advantages: (1) resolution of single exosome; (2) not limited by exosome size; (3) affinity capture of exosome without purification; (4) protein detection of single molecule sensitivity; (5) histological data of ultra-multi-factor simultaneous detection; (6) high-throughput detection of all single exosomes in samples. It was revealed that the sub-clusters of CDCP1+ EVs increased in the EVs derived from OVCA ascites. The experiment of the verification group confirms the significant expression of CDCP1 in OVCA ascites exosomes. It is hypothesized that it can be utilized as a marker for OVCA screening. The tissue microarray revealed that patients with elevated CDCP1 expression had a bad prognosis. Previous research has demonstrated that CDCP1 plays a vital role in tumor metastasis and invasion (39). However, this study has no statistically significant difference between distant metastases. We

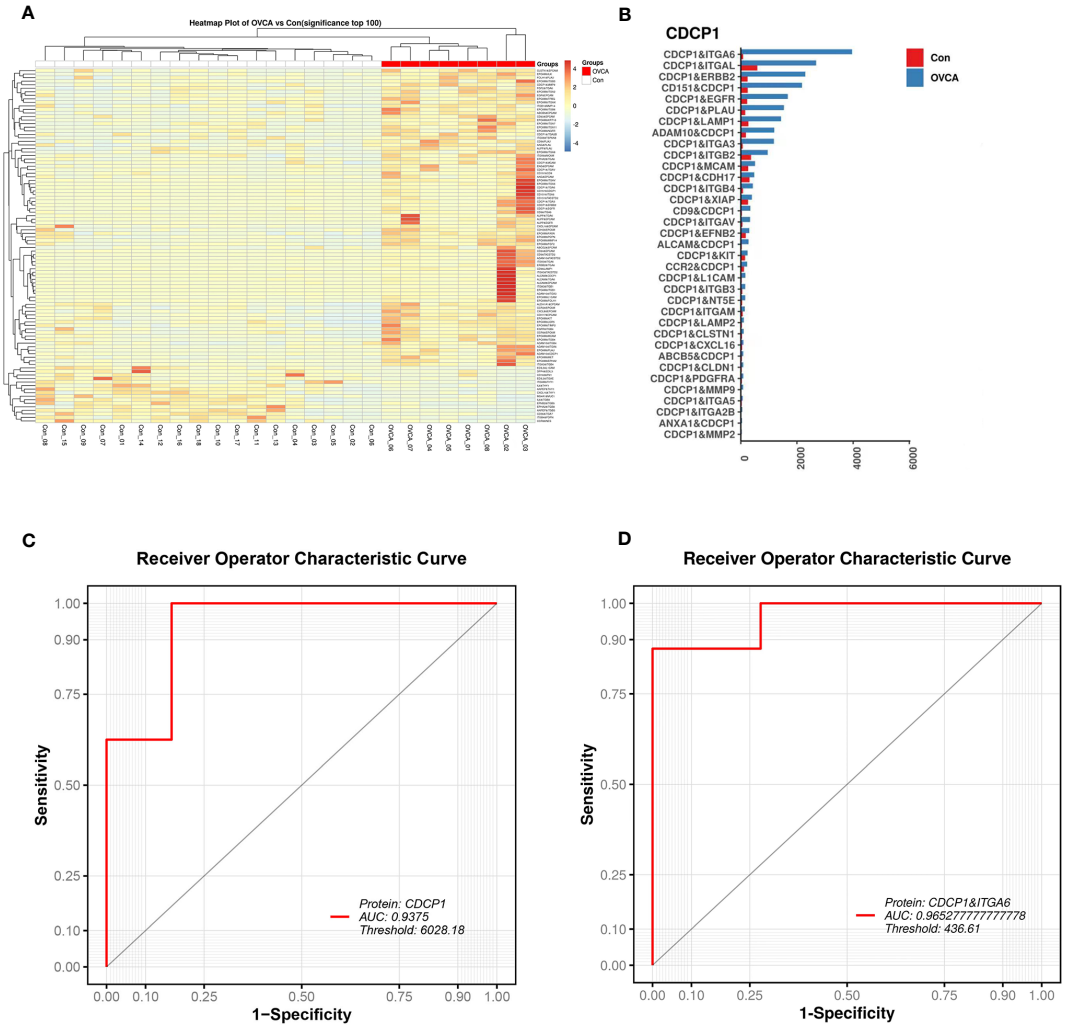


FIGURE 4
The diagnostic value of single EV protein biomarkers. **(A)** Multiple protein combinations are created in the OVCA group. **(B)** Characteristic protein combination constituted of CDCP1 in the OVCA group. **(C)** The receiver operating characteristic (ROC) curve for CDCP1. **(D)** The ROC curve for the combination of proteins CDCP1 and ITGA6.

suspect that the outcomes of this study may be attributable to the insufficient sample size. In addition, we have collected ascites and serum samples from women with OVCA and women without cancer, but the expression of CDCP1 is substantially different. Exosomes from OVCA cells are most abundant in ascites, whereas exosomes from other cell origins are somewhat depleted in serum, which may explain the analysis results. Currently, the precise mechanism of CDCP1 in the metastasis and invasion of OVCA is unclear, which is an issue worthy of investigation.

Shortly, our study identifies a novel screening marker and therapy target for early identification and treatment of OVCA, which will significantly increase the positive rate of an OVCA diagnosis. Exosomes can also be employed to treat metastatic or recurrent OVCA; however, this study is still in its infancy and requires additional clinical investigation.

## Data availability statement

The data presented in the study are deposited in the Figshare repository, accession address DOI: 10.6084/m9.figshare.23544642, found at - https://figshare.com/articles/dataset/_strong_Ascites-derived_CDCP1_extracellular_vesicles_subcluster_as_a_novel_biomarker_and_therapeutic_target_for_ovarian_cancer_strong_/23544642.

## Ethics statement

The studies involving human participants were reviewed and approved by Medical Ethics Expert Committee of Zibo Central Hospital. Written informed consent for participation was not

required for this study in accordance with the national legislation and the institutional requirements. The animal study was reviewed and approved by Medical Ethics Expert Committee of Zibo Central Hospital.

## Author contributions

JL, LK, and YC contributed to conception and design of the study. FX and SZ organized the database. ZG and DW performed the statistical analysis. LK wrote the first draft of the manuscript. YY, PT and TL wrote sections of the manuscript. All authors contributed to the article and approved the submitted version.

## Funding

This research was funded by Natural Science Foundation of Shandong Province, China, Grant Number ZR2022MH053; Zibo Key Research and Development Program, Grant Number 2019gy010006; Zibo Science and Academic Development Program, Grant Number 2018kj010078; Open Project of Zibo Gene Detection Technology Key Laboratory, Grant Number 2021WL01KF01.

## Acknowledgments

LK appreciates her supervisor JL for the guidance and help.

## Conflict of interest

DW is the inventor of proximity barcoding assay. He is the founder of Vesicode AB and Secretech Ltd.

The remaining authors declare that the research was conducted in the absence of any commercial or financial relationships that could be construed as a potential conflict of interest.

## Publisher's note



## Supplementary material

The Supplementary Material for this article can be found online at: https://www.frontiersin.org/articles/10.3389/fonc.2023.1142755/full#supplementary-material

SUPPLEMENTARY TABLE 1
The expression of 113 proteins in each sample.

## References

1. Jayson GC, Kohn EC, Kitchener HC, Ledermann JA. Ovarian cancer. *Lancet* (2014) 384(9951):1376–88. doi: 10.1016/S0140-6736(13)62146-7

2. Bray F, Ferlay J, Soerjomataram I, Siegel RL, Torre LA, Jemal A. Global cancer statistics 2018: globocan estimates of incidence and mortality worldwide for 36 cancers in 185 countries. *CA Cancer J Clin* (2018) 68(6):394–424. doi: 10.3322/caac.21492

3. Siegel RL, Miller KD, Fuchs HE, Jemal A. Cancer statistics, 2022. *CA Cancer J Clin* (2022) 72(1):7–33. doi: 10.3322/caac.21708

4. Kukla A, Piotrowska K, Misiek M, Chudecka-Glaz AM. Role of adipokines in ovarian cancer epidemiology and prognosis. *Ginekol Pol* (2022) 93(6):496–500. doi: 10.5603/GP.a2022.0035

5. Elias KM, Guo J, Bast RCJr. Early detection of ovarian cancer. *Hematol Oncol Clin North Am* (2018) 32(6):903–14. doi: 10.1016/j.hoc.2018.07.003

6. Poulet G, Massias J, Taly V. Liquid biopsy: general concepts. *Acta Cytol* (2019) 63 (6):449–55. doi: 10.1159/000499337

7. Barani M, Bilal M, Sabir F, Rahdar A, Kyzas GZ. Nanotechnology in ovarian cancer: diagnosis and treatment. *Life Sci* (2021) 266:118914. doi: 10.1016/j.lfs.2020.118914

8. Oaknin A, Guarch R, Barretina P, Hardisson D, Gonzalez-Martin A, Matias-Guiu X, et al. Recommendations for biomarker testing in epithelial ovarian cancer: a national consensus statement by the Spanish society of pathology and the Spanish society of medical oncology. *Clin Transl Oncol* (2018) 20(3):274–85. doi: 10.1007/s12094-017-1719-x

9. Bastani A, Asghary A, Heidari MH, Karimi-Busheri F. Evaluation of the sensitivity and specificity of serum level of prostasin, Ca125, ldh, afp, and Hcg+Beta in epithelial ovarian cancer patients. *Eur J Gynaecol Oncol* (2017) 38(3):418–24. doi: 10.12892/ejgo3695.2017

10. Lindenbergh MFS, Stoorvogel W. Antigen presentation by extracellular vesicles from professional antigen-presenting cells. *Annu Rev Immunol* (2018) 36:435–59. doi: 10.1146/annurev-immunol-041015-055700

11. Pakula M, Mikula-Pietrasik J, Witucka A, Kostka-Jeziorny K, Uruski P, Moszynski R, et al. The epithelial-mesenchymal transition initiated by malignant ascites underlies the transmesothelial invasion of ovarian cancer cells. *Int J Mol Sci* (2019) 20(1). doi: 10.3390/ijms20010137

12. Maas SLN, Breakefield XO, Weaver AM. Extracellular vesicles: unique intercellular delivery vehicles. *Trends Cell Biol* (2017) 27(3):172–88. doi: 10.1016/j.tcb.2016.11.003

13. Han L, Lam EW, Sun Y. Extracellular vesicles in the tumor microenvironment: old stories, but new tales. *Mol Cancer* (2019) 18(1):59. doi: 10.1186/s12943-019-0980-8

14. Cai J, Gong L, Li G, Guo J, Yi X, Wang Z. Exosomes in ovarian cancer ascites promote epithelial-mesenchymal transition of ovarian cancer cells by delivery of mir-6780b-5p. *Cell Death Dis* (2021) 12(2):210. doi: 10.1038/s41419-021-03490-5

15. Lee AH, Ghosh D, Quach N, Schroeder D, Dawson MR. Ovarian cancer exosomes trigger differential biophysical response in tumor-derived fibroblasts. *Sci Rep* (2020) 10(1):8686. doi: 10.1038/s41598-020-65628-3

16. Wu D, Yan J, Shen X, Sun Y, Thulin M, Cai Y, et al. Profiling surface proteins on individual exosomes using a proximity barcoding assay. *Nat Commun* (2019) 10 (1):3854. doi: 10.1038/s41467-019-11486-1

17. Casar B, He Y, Iconomou M, Hooper JD, Quigley JP, Deryugina EI. Blocking of Cdcp1 cleavage in vivo prevents akt-dependent survival and inhibits metastatic colonization through Parp1-mediated apoptosis of cancer cells. *Oncogene* (2012) 31 (35):3924–38. doi: 10.1038/onc.2011.555

18. He Y, Davies CM, Harrington BS, Hellmers L, Sheng Y, Broomfield A, et al. Cdcp1 enhances wnt signaling in colorectal cancer promoting nuclear localization of beta-catenin and e-cadherin. *Oncogene* (2020) 39(1):219–33. doi: 10.1038/s41388-019-0983-3

19. Dagnino S, Bodinier B, Guida F, Smith-Byrne K, Petrovic D, Whitaker MD, et al. Prospective identification of elevated circulating Cdcp1 in patients years before onset of lung cancer. *Cancer Res* (2021) 81(13):3738–48. doi: 10.1158/0008-5472.CAN-20-3454

20. Wright HJ, Hou J, Xu B, Cortez M, Potma EO, Tromberg BJ, et al. Cdcp1 drives triple-negative breast cancer metastasis through reduction of lipid-droplet abundance and stimulation of fatty acid oxidation. *Proc Natl Acad Sci U.S.A.* (2017) 114(32): E6556–E65. doi: 10.1073/pnas.1703791114

21. Ji D, Shang G, Wei E, Jia Y, Wang C, Zhang Q, et al. Targeting Cdcp1 gene transcription coactivated by Brd4 and Cbp/P300 in castration-resistant prostate cancer. *Oncogene* (2022) 41(23):3251–62. doi: 10.1038/s41388-022-02327-5

22. Khan T, Kryza T, Lyons NJ, He Y, Hooper JD. The Cdcp1 signaling hub: a target for cancer detection and therapeutic intervention. *Cancer Res* (2021) 81(9):2259–69. doi: 10.1158/0008-5472.CAN-20-2978

23. Heitmann JS, Hagelstein I, Hinterleitner C, Roerden M, Jung G, Salih HR, et al. Identification of Cd318 (Cdcp1) as novel prognostic marker in aml. *Ann Hematol* (2020) 99(3):477–86. doi: 10.1007/s00277-020-03907-9

24. Schmieder R, Edwards R. Quality control and preprocessing of metagenomic datasets. *Bioinformatics* (2011) 27(6):863–4. doi: 10.1093/bioinformatics/btr026

25. Chen S, Zhou Y, Chen Y, Gu J. Fastp: an ultra-fast all-in-One fastq preprocessor. *Bioinformatics* (2018) 34(17):i884–i90. doi: 10.1093/bioinformatics/bty560

26. Robinson MD, McCarthy DJ, Smyth GK. Edger: a bioconductor package for differential expression analysis of digital gene expression data. *Bioinformatics* (2010) 26 (1):139–40. doi: 10.1093/bioinformatics/btp616

27. Robin X, Turck N, Hainard A, Tiberti N, Lisacek F, Sanchez JC, et al. Proc: an open-source package for r and s+ to analyze and compare roc curves. *BMC Bioinf* (2011) 12:77. doi: 10.1186/1471-2105-12-77

28. Van Gassen S, Callebaut B, Van Helden MJ, Lambrecht BN, Demeester P, Dhaene T, et al. Flowsom: using self-organizing maps for visualization and interpretation of cytometry data. *Cytomet A* (2015) 87(7):636–45. doi: 10.1002/cyto.a.22625

29. Cieslak MC, Castelfranco AM, Roncalli V, Lenz PH, Hartline DK. T-Distributed stochastic neighbor embedding (T-sne): a tool for eco-physiological transcriptomic analysis. *Mar Genomics* (2020) 51:100723. doi: 10.1016/j.margen.2019.100723

30. Li N, Chen M, Cao Y, Li H, Zhao J, Zhai Z, et al. Bcl-2-Associated athanogene 3(Bag3) is associated with tumor cell proliferation, migration, invasion and chemoresistance in colorectal cancer. *BMC Cancer* (2018) 18(1):793. doi: 10.1186/s12885-018-4657-2

31. Li N, Mao D, Cao Y, Li H, Ren F, Li K. Downregulation of Sirt6 by mir-34c-5p is associated with poor prognosis and promotes colon cancer proliferation through inhibiting apoptosis Via the Jak2/Stat3 signaling pathway. *Int J Oncol* (2018) 52 (5):1515–27. doi: 10.3892/ijo.2018.4304

32. Tomczak K, Czerwinska P, Wiznerowicz M. The cancer genome atlas (Tcga): an immeasurable source of knowledge. *Contemp Oncol (Pozn)* (2015) 19(1A):A68–77. doi: 10.5114/wo.2014.47136

33. Dochez V, Caillon H, Vaucel E, Dimet J, Winer N, Ducarme G. Biomarkers and algorithms for diagnosis of ovarian cancer: Ca125, He4, rmi and Roma, a review. *J Ovarian Res* (2019) 12(1):28. doi: 10.1186/s13048-019-0503-7

34. Jacob F, Meier M, Caduff R, Goldstein D, Pochechueva T, Hacker N, et al. No benefit from combining He4 and Ca125 as ovarian tumor markers in a clinical setting. *Gynecol Oncol* (2011) 121(3):487–91. doi: 10.1016/j.ygyno.2011.02.022

35. Kosaka N, Kogure A, Yamamoto T, Urabe F, Usuba W, Prieto-Vila M, et al. Exploiting the message from cancer: the diagnostic value of extracellular vesicles for clinical applications. *Exp Mol Med* (2019) 51(3):1–9. doi: 10.1038/s12276-019-0219-1

36. Alix-Panabieres C, Pantel K. Challenges in circulating tumour cell research. *Nat Rev Cancer* (2014) 14(9):623–31. doi: 10.1038/nrc3820

37. Elazezy M, Joosse SA. Techniques of using circulating tumor DNA as a liquid biopsy component in cancer management. *Comput Struct Biotechnol J* (2018) 16:370–8. doi: 10.1016/j.csbj.2018.10.002

38. Yang C, Kim HS, Song G, Lim W. The potential role of exosomes derived from ovarian cancer cells for diagnostic and therapeutic approaches. *J Cell Physiol* (2019) 234 (12):21493–503. doi: 10.1002/jcp.28905

39. Dong Y, He Y, de Boer L, Stack MS, Lumley JW, Clements JA, et al. The cell surface glycoprotein cub domain-containing protein 1 (Cdcp1) contributes to epidermal growth factor receptor-mediated cell migration. *J Biol Chem* (2012) 287 (13):9792–803. doi: 10.1074/jbc.M111.335448

frontiers | Frontiers in Oncology

TYPE Original Research
PUBLISHED 13 July 2023
DOI 10.3389/fonc.2023.1149599



OPEN ACCESS

EDITED BY
Umberto Malapelle,
University of Naples Federico II, Italy

REVIEWED BY
Federica Perelli,
Santa Maria Annunziata Hospital, Italy
Tasaduq H. Wani,
University of Oxford, United Kingdom

*CORRESPONDENCE
Weiwei Feng
fww12066@rjh.com.cn
Haojie Lu
luhaojie@fudan.edu.com

†These authors have contributed equally to this work

RECEIVED 22 January 2023
ACCEPTED 26 June 2023
PUBLISHED 13 July 2023

CITATION
Li J, Feng X, Zhu C, Jiang Y, Liu H, Feng W and Lu H (2023) Intact glycopeptides identified by LC-MS/MS as biomarkers for response to chemotherapy of locally advanced cervical cancer. *Front. Oncol.* 13:1149599. doi: 10.3389/fonc.2023.1149599



# Intact glycopeptides identified by LC-MS/MS as biomarkers for response to chemotherapy of locally advanced cervical cancer

Jing Li[1†], Xiaoxiao Feng[2†], Chongying Zhu[3], Yahui Jiang[1], Hua Liu[1], Weiwei Feng[1*] and Haojie Lu[2*]

[1]Department of Obstetrics and Gynecology, Ruijin Hospital, School of Medicine, Shanghai Jiaotong University, Shanghai, China, [2]Department of Chemistry and NHC Key Laboratory of Glycoconjugates Research, Institutes of Biomedical Sciences, Fudan University, Shanghai, China, [3]Department of Laboratory of Obstetrics and Gynecology, Ruijin Hospital, School of Medicine, Shanghai Jiaotong University, Shanghai, China

**Objective:** For locally advanced cervical cancer (LACC), patients who respond to chemotherapy have a potential survival advantage compared to nonresponsive patients. Thus, it is necessary to explore specific biological markers for the efficacy of chemotherapy, which is beneficial to personalized treatment.

**Methods:** In the present study, we performed a comprehensive screening of site-specific N-glycopeptides in serum glycoproteins to identify glycopeptide markers for predicting the efficacy of chemotherapy, which is beneficial to personalized treatment. In total, 20 serum samples before and after neoadjuvant chemotherapy (NACT) from 10 LACC patients (NACT response, n=6) and NACT nonresponse, n=4) cases) were analyzed using LC-MS/MS, and 20 sets of mass spectrometry (MS) data were collected using liquid chromatography coupled with high-energy collisional dissociation tandem MS (LC-HCD-MS/MS) for quantitative analysis on the novel software platform, Byos. We also identified differential glycopeptides before and after chemotherapy in chemo-sensitive and chemo-resistant patients.

**Results:** In the present study, a total of 148 glycoproteins, 496 glycosylation sites and 2279 complete glycopeptides were identified in serum samples of LACC patients. Before and after chemotherapy, there were 13 differentially expressed glycoproteins, 654 differentially expressed glycopeptides and 93 differentially expressed glycosites in the NACT responsive group, whereas there were 18 differentially expressed glycoproteins, 569 differentially expressed glycopeptides and 99 differentially expressed glycosites in the NACT nonresponsive group. After quantitative analysis, 6 of 570 glycopeptides were identified as biomarkers for predicting the sensitivity of neoadjuvant chemotherapy in LACC. The corresponding glycopeptides included MASP1, LUM, ATRN, CO8A, CO8B and CO6. The relative abundances of the six glycopeptides, including MASP1, LUM, ATRN, CO8A, CO8B and CO6, were significantly higher in the NACT-responsive

group and were significantly decreased after chemotherapy. High levels of these six glycopeptides may indicate that chemotherapy is effective. Thus, these glycopeptides are expected to serve as biomarkers for predicting the efficacy of neoadjuvant chemotherapy in locally advanced cervical cancer.

**Conclusion:** The present study revealed that the N-glycopeptide of MASP1, LUM, ATRN, CO8A, CO8B and CO6 may be potential biomarkers for predicting the efficacy of chemotherapy for cervical cancer.

KEYWORDS

**neoadjuvant chemotherapy (NACT), locally advanced cervical cancer (LACC), glycopeptides, LC-MS/MS, biomarker**

# 1 Introduction

Cervical cancer remains the second most common cause of both cancer incidence and mortality in developing countries (1–3). Data from the National Cancer Institute Surveillance, Epidemiology and End Results Program (NCI SEER) reported that cervical cancer with 14100 new cases in 2022 and a 5-year relative survival of 66.7%, and it is very necessary to tailor them the more appropriate therapeutic and surveillance program (4, 5). Currently, concurrent chemoradiation (CCRT) is considered a standard therapy for locally advanced cervical cancer patients. However, as the Cochrane meta-analysis reported, CCRT shows a stage-dependent advantage over radiotherapy with 5-year survival benefits of 10% for women with stage IB to IIA cervical cancer, 7% for women with stage IIB cervical cancer and 3% for women with stage III to IVA cancer. Therefore, there are limitations in using CCRT for LACC treatment (6, 7).

Recently, several phase II trials have revealed that neoadjuvant chemotherapy (NACT) followed by chemoradiation exerts favorable outcomes in LACC. A weekly regimen of NACT followed by CCRT may be superior to CCRT alone (7–9). The overall NACT response rate ranges from 52% to 95% in different studies (10). The usage of NACT before radiotherapy may potentially eradicate subclinical distant metastasis, reduce the tumor size and correct pelvic anatomy distortion, ultimately allowing better delivery of the following therapy.

Combined analysis has shown that a better clinical response and pathologic response to NACT are associated with favorable PFS and OS (11). Stable disease post-NACT has also been identified as a poor prognostic sign (12). If these patients do not benefit from NACT, alternative therapies may be offered at an earlier stage. To improve the quality of life of nonresponders and avoid inherent resistance to chemotherapy/radiotherapy and potential toxicity as well as reduce the time until radiotherapy and cost, it is necessary to identify biomarkers to predict the efficacy of NACT.

Currently, there are no Food and Drug Administration (FDA)-approved biomarkers that can be used to predict the effectiveness of chemotherapy. Glycosylation is the most common posttranslational modification of proteins, and the decoration of the protein with a variety of glycans leads to the diversity of protein structures (13). Recently, advanced technologies have been developed and applied to the analysis of glycosylation of proteins (14), which has led to an understanding of the diversity and differences in glycans in certain proteins, suggesting that site-specific glycosylation of proteins play important roles in physiological and pathological functions (15). Aberrant glycosylation of glycoproteins is one of the most frequent changes that occurs in the cancer biological system (16–19). The importance of this phenomenon is to provide better survival conditions for cancer cell invasion. Changes in glycans include lost or excessive expression of certain structures, incomplete/truncated structures, accumulation of precursors and/or altered glycan expression (20). Modified glycosylation patterns are associated with cancer invasiveness and metastatic potential (21). Most of the FDA-approved biomarkers for cancer diagnosis and monitoring are glycoproteins (22). Because glycoproteins are often present on the cell surface or secreted from cells, they are present in serum and can serve as biomarkers. Therefore, discovering specific glycoproteins as biomarkers for differentiating the effectiveness of chemotherapy in cervical cancer is crucial.

Based on a clinical trial we are conducting (ethical number N-2018-239), we collected pre- and postchemotherapy serum samples from patients who received NACT. We used MS-based glycoproteomics analysis for differential determination of glycosylation composition changes at individual glycosites in whole serum between patients with and without NACT response. This approach enabled the identification of a panel of N-glycopeptides as potential biomarker candidates for chemotherapy efficacy in locally advanced cervical cancer.

# 2 Methods

## 2.1 Materials and reagents

Ammonium bicarbonate (ABC), dithiothreitol (DTT), iodoacetamide (IAA) and trifluoroacetic acid (TFA) were

purchased from Sigma-Aldrich (MO, USA). ZIC-HILIC particles and HPLC-grade acetonitrile (ACN) were purchased from Merck (Darmstadt, Germany). Sep-Pak C18 Vac cartridges were purchased from Waters (MA, USA).

Sequencing-grade trypsin was purchased from Hualishi (Beijing, China). Distilled water was purified by a Milli-Q system (Milford, USA). All other chemicals and reagents of the best available grade were purchased from Sigma-Aldrich (MO, USA).

## 2.2 Sample collection

We collected serum samples from patients before and after neoadjuvant chemotherapy. Patients were eligible if they presented with histologically confirmed squamous carcinoma or adenocarcinoma of the cervix stage FIGO IIB to IIIC. Patients were assigned to NACT with weekly cisplatin and paclitaxel followed by CCRT from December 2018 to January 2020. NACT consisted of intravenous paclitaxel (60 mg/m$^2$) and cisplatin (40 mg/m$^2$) on Days 1, 8, 15 and 22. For American Joint Committee on Cancer staging, pelvic magnetic resonance imaging (MRI) and PET/CT were performed. The chemotherapeutic response was scored at 7-10 days after the last course according to the RECIST v1.1 criteria as follows: complete resolution of the tumor (CR); partial response (PR, >30% decrease in the longest diameter); stable disease (SD, <30% decrease or >20% increase in the longest diameter); and progressive disease (PD). To reduce the effect of measurement error on the study results, imaging data from all patients were measured by the same radiological physician. The study was approved by Shanghai Jiaotong University School of Medicine affiliated with Ruijin Hospital Ethics Committee (N-2018-239) (7). Signed informed consent was obtained from all patients.

## 2.3 Serum samples

Patients were grouped according to chemotherapeutic effectiveness by RECIST v1.1 criteria (23). We collected paired serum samples from 10 patients before and after neoadjuvant chemotherapy with 6 patients classified as NACT response (CR/PR) and 4 patients classified as NACT nonresponse (SD/PD). In the present study, patients who classified as NACT response were called Pre_R and Trm R when they were before and after neoadjuvant chemotherapy; patients who classified as NACT nonresponse were called Pre_SD and Trm_SD when they were before and after neoadjuvant chemotherapy. The clinical characteristics of the patients were summarized in Table 1.

TABLE 1 Clinical characteristics of the patients with NACT response and nonresponse.

| Clinical characteristics | Patients (N=10) | |
|---|---|---|
| | NACT response (n=6) | NACT nonresponse (n=4) |
| Age (y) | 55.5 (46-68) | 51 (35-63) |
| Histopathology | | |
| Squamous carcinoma | 5 | 4 |
| Adenocarcinoma | 1 | 0 |
| Tumor size (cm) | 4.45 (3.0-6.9) | 6.55 (6.1-9.1) |
| FIGO stage (2018) | | |
| IIB | 1 | 0 |
| IIIA | 1 | 0 |
| IIIC1 | 3 | 4 |
| IIIC2 | 1 | 0 |
| Lymphatic metastasis | | |
| Positive | 4 | 4 |
| Negative | 2 | 0 |
| Therapeutic evaluation (CR/PR/SD/PD) | 2/4/0/0 | 0/0/4/0 |

CR, complete response; PR, partial response; SD, stable disease; PR, progressive disease.

## 2.4 Preparation of serum peptides

Human serum was diluted with 25 mM ABC. DTT was added to a final concentration of 10 mM, and the mixture was heated at 56°C. IAA was added to a final concentration of 20 mM to alkylate free cysteines in the dark for 30 min. The protein mixture was digested by trypsin with an enzyme to protein ratio of 1:50 (w/w) at 37°C overnight. To quench the reaction, 10% (vol/vol) trifluoroacetic acid (TFA) was added to a final concentration of 0.1% followed by centrifugation at 14,000×g for 20 min. C18 Sep-Pak cartridges were then used to desalt the digested products. Subsequently, the peptides were dried by vacuum centrifugation for further enrichment.

## 2.5 Enrichment of N-glycopeptides

For glycopeptide enrichment, the ZIC-HILIC column was equilibrated with 80% ACN containing 1% TFA three times, and glycopeptides were then loaded into the column three times and washed three times with 80% ACN containing 1% TFA. Enriched N-glycopeptides were eluted three times with 0.1% TFA. Subsequently, the enriched N-glycopeptides were dried by vacuum centrifugation and stored at −80°C for further analysis.

## 2.6 LC-ESI-MS/MS analysis

Peptides were resuspended in 0.1% FA and subjected to LC-MS/MS analysis using an Orbitrap Exploris480 mass spectrometer (Thermo Fisher Scientific, MA, USA) coupled to an EASY-

NanoLC 1200 system (Thermo Fisher Scientific, MA, USA) with a 75 μm × 50-cm long column (2 μm id). For serum N-glycopeptides, the flow rate was 200 nL/min, and the gradient was 120 min in total (0-90 min, 2%-25% B; 90-115 min, 25-45% B; 115-116 min, 45%-95% B; and 116-126:50 min, 95% B). The MS parameters for N-glycopeptide analysis were set as follows: Orbitrap resolution = 60 k; scan range (m/z) = 400-2000; maximum injection time = 50 ms; normalized AGC target = 300,000; dynamic exclusion after n times, n = 1; dynamic exclusion duration = 15 s. The MS/MS parameters for N-glycopeptide analysis were set as follows: isolation window = 2.2; detector type = Orbitrap; resolution = 15 k; AGC target = 200,000; HCD collision energy = 30% (NCE); stepped collision mode on; and energy difference of ±10%.

## 2.7 Data analysis

Raw data files were searched using Byonic™ software (Protein Metrics, San Carlos, CA, USA), and the mass tolerance of precursor ions and fragment ions was set as 10 ppm and 20 ppm, respectively. Trypsin was selected as the enzyme with a maximum of two missed cleavages allowed. The fixed modification was carbamidomethyl (C), and the variable modifications included oxidation (M), deamidation (N, Q) and N-glycan modifications (N). A human N-glycan database (from the Byonic database) containing 57 human plasma N-glycans was employed. The results were filtered at a confidence threshold of Byonic score >150, Delta modification score >10, PEP2D < 0.05 and FDR2D < 0.01 in Byologic (Protein Metrics) software, which inputs both MS1 raw data and Byonic search results. The theoretical m/z of the oxonium ions from GlcNAc (m/z 138.05, m/z 168.05 and m/z 204.09), NeuAc (m/z 274.09 and 292.10), GlcNAc-Hex (m/z 366.14), HexHexNAcFuc (m/z 512.20) and HexNAcHexNeuAc (m/z 657.23) in glycopeptides from HCD-MS are known for glycan identification.

# 3 Results

## 3.1 Framework for intact glycopeptide analysis

To reduce the sample preparation steps and improve the accuracy of quantification, as shown in Figure 1, we developed a workflow for large-scale intact N-glycopeptide identification, which included high-abundance protein depletion, glycopeptide enrichment, offline peptide fractionation and LC-ESI-MS/MS for differential determination of glycosylation composition changes in LACC patient sera between NACT responsive and nonresponsive patients. Ten pairs of serum samples from 10 patients before and after NACT were included. To further investigate these glycopeptides, we performed a quantitative analysis. The detection of low-abundance glycopeptides in complex mixtures is difficult due to the suppression of glycopeptide mass spectral signals in the presence of nonglycopeptides. To overcome this issue, highly efficient depletion of high-abundance proteins and enrichment of glycopeptides are needed.

## 3.2 Glycopeptide distribution based on the byonic score

Raw spectra of complex samples obtained from the DDA mode were retrieved by Byonic software. The results were filtered at a confidence threshold of Byonic score >150, Delta modification score >10, PEP2D < 0.05 and FDR2D < 0.01. Base on retention time, the distribution of glycopeptide scores is shown in Figure 2A.

As the patient serum contains a large number of glycopeptides, the Byonic score was set greater than 150 to increase the credibility of the results. As shown in Figure 2B, the fractions ranging from 300 to 500 contained the largest number of glycopeptides. Under these conditions, data on the distribution of glycosylation types were also obtained, including the number of glycoproteins, glycosites, glycopeptides, percentage of fucosylated glycopeptides and percentage of sialylated glycopeptides.

## 3.3 Glyco-distribution in human serum from samples

In the present study, we first performed a qualitative analysis. The component Venn diagram of the NACT responsive and nonresponsive groups before and after NACT is shown in Figure 3. To overcome the inhibition of signals by nonglycopeptides to facilitate glycopeptide detection, we combined ZIC-HILIC-based glycopeptide extraction to improve the MS signal of the glycopeptides. HILIC is a well-recognized technique for effectively enriching glycans and glycopeptides (24). Because many of these glycopeptides were in low abundance, we used this method to enrich the glycopeptides to enhance the mass spectrometry signal.

In total, 148 glycoproteins were identified, including 138 in the NACT responsive group and 138 in the NACT nonresponsive group. There were 13 differentially expressed glycoproteins in the NACT responsive group and 18 in the NACT nonresponsive group before and after chemotherapy (Figure 3A). A total of 2,279 glycopeptides were identified, including 1,973 in the NACT responsive group and 1,880 in the NACT nonresponsive group. The number of differentially expressed glycopeptides before and after chemotherapy was 654 in the NACT-responsive group and 569 in the NACT-nonresponsive group (Figure 3C). These identifications also corresponded to 496 glycosites, including 434 in the NACT responsive group and 430 in the NACT nonresponsive group. The differential glycosites before and after chemotherapy were 93 in the NACT responsive group and 99 in the NACT nonresponsive group (Figure 3B).

## 3.4 Glycopeptides identified as potential biomarker candidates by LC-ESI-MS/MS

To discover the differential glycopeptides for therapeutic predictive markers between NACT responsive and nonresponsive patients, LC-ESI-MS/MS was performed for quantitative analysis among individual patients. In a total of 10 pairs of serum samples

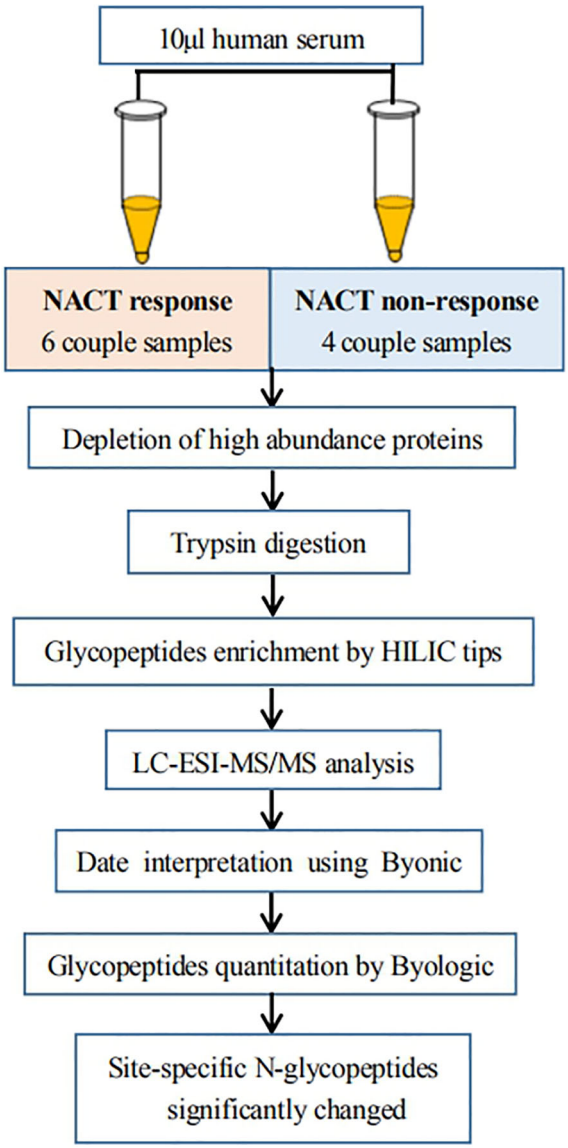


FIGURE 1
Workflow of quantitative LC-ESI-MS/MS analysis of intact N-glycopeptide derived from the sera between NACT response and NACT nonresponse patients.

(including 2 CR, 4 PR and 4 SD), we analyzed the results of quantified glycopeptides by Byologic software. These patient samples were classified into four types as follows: NACT response before treatment (n=6), NACT response after treatment (n=6), NACT nonresponse before treatment (n=4) and NACT nonresponse after treatment (n=4). The relative abundance of the glycopeptides was compared by *t test*.

In the present study, 20 glycopeptides had a significant difference between the NACT responsive and nonresponsive groups before treatment according to the LC-ESI-MS/MS results (Table 2). In total, 26 glycopeptides had a significant difference before and after treatment in the NACT responsive group (Table 3), and 10 glycopeptides had a significant difference before and after treatment in the NACT nonresponsive group (Table 4). After comparison, six differential glycopeptides (MASP1, LUM, ATRN, CO8A, CO8B and CO6) were screened out because they were differential in NACT responsive groups before and after treatment as well as in two groups before NACT (Table 5). There was no overlap with the glycopeptides that differed before and after chemotherapy in the NACT nonresponsive group.

Quantitative statistical analysis (*P values* were obtained by *t test*) was performed on the relative abundance of these six glycopeptides, and we found that the relative abundance of the six glycopeptides was significantly higher in the NACT responsive group than in the NACT nonresponsive group before treatment (Figure 4). In the NACT responsive group, the relative abundance of all six glycopeptides was significantly decreased after chemotherapy (Figure 5).

A

| Score Range | 150-300 | 300-400 | 400-500 | 500-600 | 600-700 | 700-800 | >800 |
|---|---|---|---|---|---|---|---|
| Pre_R | 142 | 354 | 359 | 289 | 230 | 185 | 131 |
| Pre_SD | 115 | 334 | 336 | 283 | 233 | 199 | 137 |
| Trm_R | 130 | 344 | 351 | 295 | 239 | 190 | 138 |
| Trm_SD | 114 | 319 | 310 | 257 | 228 | 191 | 135 |

B

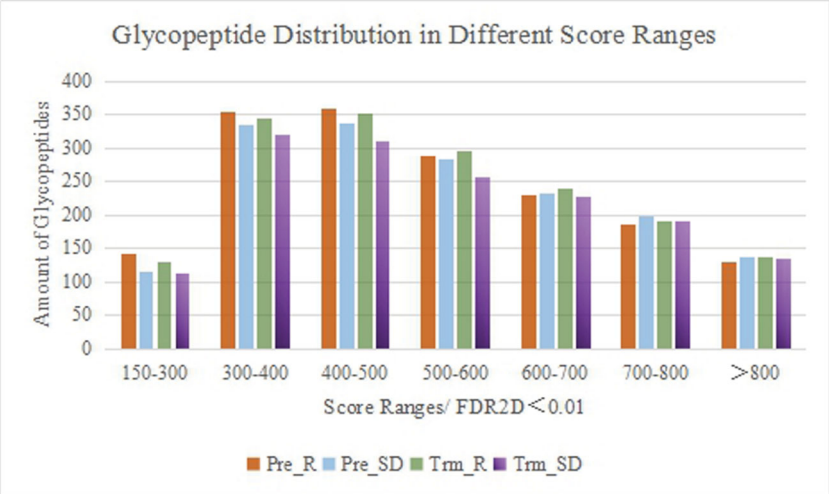


FIGURE 2
**(A)** Comparison of the distribution of glycopeptides in different score ranges among the samples between chemotherapy responsive and nonresponsive ones before and after NACT. **(B)** Column diagram shows the top 2 number of glycopeptides that are distributed between score 300-500.

## 3.5 Distribution of glycosylation types in the human serum samples

The site-specific glycosylation distribution of serum glycoproteins involves the number of glycopeptides, glycoproteins, glycosylation types and the proportion of glycosylated or sialylated glycopeptides. As shown in Figure 6, NeuAc was the dominant glycosylation type in LACC patient sera, and there was no significant difference in glycosylation sites and glycopeptide amounts of glycoproteins before and after NACT in the NACT response and NACT nonresponsive groups.

# 4 Discussion

Some studies have reported that LACC patients who respond to NACT benefit from NACT with improved OS and PFS compared to nonresponders. As a result, it is essential to identify which LACC patients may respond to chemotherapy and investigate common biomarkers to distinguish NACT responders.

In the present study, 26 glycopeptides were significantly different before and after treatment in the NACT-responsive group. Among these, six glycopeptides were screened out because they were differentially expressed not only in the NACT-responsive groups before and after treatment but also in the NACT responder and nonresponder groups before treatment. Thus, MASP-1, LUM, ATRN, CO8A, CO8B and CO6 may be used as promising glycopeptide biomarkers to distinguish NACT-responsive LACC patients who may benefit from NACT followed by CCRT. The relative abundances of the six glycopeptides, including MASP1, LUM, ATRN, CO8A, CO8B and CO6, were significantly higher in the NACT-responsive group and were significantly decreased after chemotherapy. High levels of these six glycopeptides may indicate that chemotherapy is effective. The innovation of the present study was the identification of soluble glycopeptides for LACC, which can be used to screen the efficacy of chemotherapy. Abnormal glycosylation is associated with tumor malignancy and disease progression. Glycosylation is one of the most extensive and important posttranslational modifications of proteins in organisms, accounting for 70% in the human body (25). Most glycans are abundant on the surface and cytoplasm of the cells. Glycan regulation has been confirmed to participate in various physiological processes. Glycans are composed of the galactose (Gal), N-acetylgalactosamine (GalNAc), glucose (Glc), fucose (Fuc) and mannose (Man) monosaccharides and their derivatives, including glucuronic acid (GlcA), xylose and sialic acids. The main classes of glycoproteins consist of at least five major types, namely, N-glycans, O-glycans, glycosaminoglycan, GPI-anchored proteins and O-linked GlcNAcylation (26). Site-specific glycosylation changes may become a promising predictive biomarker in clinical diagnosis and treatment. For instance, several studies have revealed site-specific glycosylation structural changes in serum glycoproteins as potential markers for early HCC, including ceruloplasmin, kininogen-1, α-1-antitrypsin and vitronectin (27). Recently,

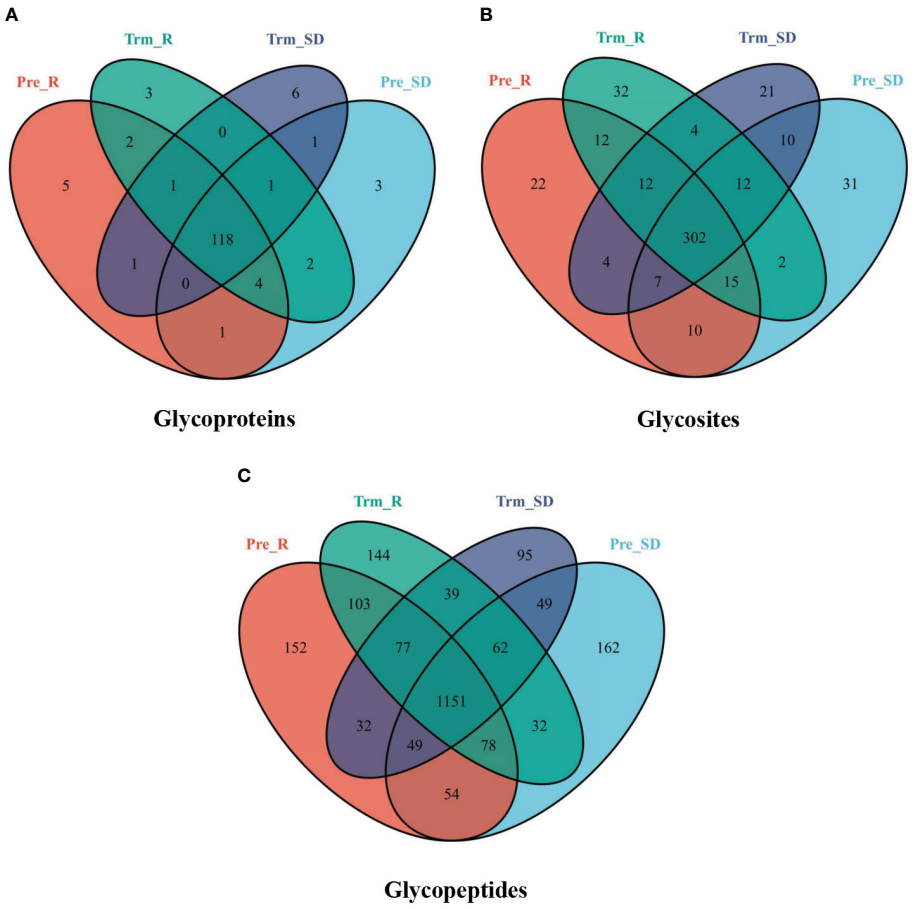


FIGURE 3
Venn diagram showing the number of **(A)** glycoproteins, **(B)** glycosites, and **(C)** glycopeptides from the NACT response (red), NACT nonresponse (blue) before treatment and NACT response (green), NACT nonresponse (purple) after treatment samples.

advances in mass spectrometry have enabled the discovery of site-specific glycopeptide markers for early cancer detection. The fucosylated and sialylated glycan structures of serum Hp have been shown to be significantly elevated in patients with HCC compared to patients with cirrhosis (28, 29).

In cervical cancer, glycosylation is also involved in cell metabolism, signal transduction, tumor cell division, tumor cell metastasis, immune regulation, cancer diagnosis and cancer management (30). It has been reported that the α2,6-terminal sialylation and fucosylation patterns of intracellular proteins exist in cervical cancer tissue rather than normal cervix tissue (31). In addition, elevated OGT and O-GlcNAcylation are associated with increased cell proliferation and reduced cellular senescence in HPV-induced cervical cancer (32). Glycosylation in cervical cancer also has significant implications for cancer treatment. For example, galectin-7 produces a CCRT response and acts as a significant predictor for cervical cancer patients treated with definitive radiation therapy (33).

Therefore, the present study aimed to investigate the glycosylation difference in the serum of NACT responders and nonresponders. In addition, we investigated potential glycopeptide biomarkers to distinguish LACC patients who will benefit from NACT followed by CCRT.

In the present study, we analyzed the site-specific N-glycosylation of serum in patients with locally advanced cervical cancer before and after chemotherapy. It was found that more than half of the glycosites were sialic acid followed by fucose. The relative abundance of glycopeptides was significantly higher in the NACT-responsive group before chemotherapy than in the NACT-nonresponsive group. Six potential glycopeptide biomarkers were quantified both in the chemosensitive group before and after chemotherapy as well as in the two groups before chemotherapy. The corresponding proteins included MASP-1, LUM, ATRN, CO8A, CO8B and CO6. Five of the six glycosites in these six differential glycopeptides contained sialic acid, and one glycosite contained fucose. The most significant cancer-associated changes in glycosylation are fucosylation, galactosylation, and sialylation (34). It is well known that sialic acid plays an important role in immune escape, virus infection, tumorigenesis and development (35). Also, compared with IgG glycans of non-response group, agalactosylated N-glycans increased while monosialylated N-glycans and digalactosylated N-glycans decreased in the response group of local advanced gastric cancer (LAGC) patients (34). According to a previous report, fucose is closely related to the proliferation, metastasis and immune response of tumor cells (36). The abnormal expression of glycosyltransferases (GTs) leading to aberrant

TABLE 2 List of the difference glycopeptides between NACT responsive and nonresponsive group before chemotherapy.

| No | Protein name | Sequence | Glycans | *P* value |
|---|---|---|---|---|
| 1 | ATRN_HUMAN | K.IDSTGnVTNELR.V | HexNAc(2)Hex(5) | 0.021 |
| 2 | IGJ_HUMAN | R.EnISDPTSPLR.T | HexNAc(4)Hex(5)Fuc(1)NeuAc(2) | 0.017 |
| 3 | A1AG1_HUMAN | R.NEEYnK.S | HexNAc(4)Hex(5)NeuAc(1) | 0.045 |
| 4 | A1AG1_HUMAN | R.NEEYnK.S | HexNAc(4)Hex(5)NeuAc(2) | 0.010 |
| 5 | C4BPA_HUMAN | R.FSLLGHASISCTVEnETIGVWR.P | HexNAc(4)Hex(5)NeuAc(2) | 0.048 |
| 6 | PROC_HUMAN | K.EVFVHPnYSK.S | HexNAc(4)Hex(5)NeuAc(2) | 0.021 |
| 7 | CO8A_HUMAN | R.GGSSGWSGGLAQnR.S | HexNAc(4)Hex(5)NeuAc(1) | 0.019 |
| 8 | CO8B_HUMAN | R.nVTEK.M | HexNAc(4)Hex(5)NeuAc(1) | 0.018 |
| 9 | CO6_HUMAN | K.VLnFTTK.A | HexNAc(4)Hex(5)NeuAc(1) | 0.035 |
| 10 | CO6_HUMAN | R.LSSnSTK.K | HexNAc(4)Hex(5)NeuAc(2) | 0.015 |
| 11 | PZP_HUMAN | K.VnITVCGEYTYGK.P | HexNAc(3)Hex(5)NeuAc(1) | 0.014 |
| 12 | C4BPB_HUMAN | K.TLFCnASK.E | HexNAc(4)Hex(5)NeuAc(2) | 0.015 |
| 13 | C4BPB_HUMAN | R.LGHCPDPVLVNGEFSSSGPVnVSDK.I | HexNAc(4)Hex(5)NeuAc(2) | 0.001 |
| 14 | CPN2_HUMAN | R.AFGSNPnLTK.V | HexNAc(4)Hex(5)NeuAc(1) | 0.007 |
| 15 | PEDF_HUMAN | K.VTQnLTLIEESLTSEFIHDIDR.E | HexNAc(4)Hex(5)NeuAc(2) | 0.014 |
| 16 | MASP1_HUMAN | R.NnLTTYK.S | HexNAc(4)Hex(5)NeuAc(2) | 0.001 |
| 17 | LUM_HUMAN | K.LHINHNnLTESVGPLPK.S | HexNAc(4)Hex(5)Fuc(1)NeuAc(1) | 0.010 |
| 18 | PHLD_HUMAN | K.LNVEAAnWTVR.G | HexNAc(4)Hex(5)NeuAc(1) | 0.013 |
| 19 | LG3BP_HUMAN | K.AAIPSALDTnSSK.S | HexNAc(5)Hex(6)NeuAc(2) | 0.030 |
| 20 | FCGBP_HUMAN | R.VITVQVAnFTLR.L | HexNAc(4)Hex(5)Fuc(1)NeuAc(1) | 0.006 |

TABLE 3 List of the difference glycopeptides before and after chemotherapy in NACT responsive group.

| No | Protein name | Sequence | Glycans | *P* value |
|---|---|---|---|---|
| 1 | ATRN_HUMAN | K.CEnLTTGK.H | HexNAc(4)Hex(5)NeuAc(1) | 0.047 |
| 2 | ATRN_HUMAN | K.IDSTGnVTNELR.V | HexNAc(2)Hex(5) | 0.041 |
| 3 | IGG1_HUMAN | R.EEQYnSTYR.V | HexNAc(4)Hex(4)Fuc(1) | 0.022 |
| 4 | C1R_HUMAN | K.EHEAQSnASLDVFLGHTNVEELMK.L | HexNAc(4)Hex(5)NeuAc(2) | 0.044 |
| 5 | C1R_HUMAN | R.CnYSIR.V | HexNAc(4)Hex(5)NeuAc(1) | 0.030 |
| 6 | CFAB_HUMAN | R.SPYYnVSDEISFHCYDGYTLR.G | HexNAc(4)Hex(5)NeuAc(1) | 0.027 |
| 7 | IGHA1_HUMAN | R.PALEDLLLGSEAnLTCTLTGLR.D | HexNAc(5)Hex(5)NeuAc(1) | 0.045 |
| 8 | C1QA_HUMAN | R.RNPPMGGNVVIFDTVITNQEEPYQnHSGR.F | HexNAc(4)Hex(5)Fuc(1)NeuAc(1) | 0.028 |
| 9 | FETUA_HUMAN | R.KVCQDCPLLAPLnDTR.V | HexNAc(4)Hex(5)NeuAc(2) | 0.048 |
| 10 | A1BG_HUMAN | R.EGDHEFLEVPEAQEDVEATFPVHQPGnYSCSYR.T | HexNAc(4)Hex(5)NeuAc(1) | 0.024 |
| 11 | CFAI_HUMAN | K.LISnCSK.F | HexNAc(4)Hex(5)NeuAc(2) | 0.043 |
| 12 | CFAI_HUMAN | K.LSDLSInSTECLHVHCR.G | HexNAc(4)Hex(5)NeuAc(2) | 0.020 |
| 13 | THBG_HUMAN | K.VTACHSSQPnATLYK.M | HexNAc(4)Hex(5)NeuAc(1) | 0.005 |
| 14 | CO2_HUMAN | K.QSVPAHFVALnGSK.L | HexNAc(2)Hex(5) | 0.043 |

*(Continued)*

TABLE 3 Continued

| No | Protein name | Sequence | Glycans | *P* value |
|---|---|---|---|---|
| 15 | CO8A_HUMAN | R.GGSSGWSGGLAQnR.S | HexNAc(4)Hex(5)NeuAc(1) | 0.001 |
| 16 | CO8B_HUMAN | R.nVTEK.M | HexNAc(4)Hex(5)NeuAc(1) | 0.019 |
| 17 | CFAH_HUMAN | K.IPCSQPPQIEHGTInSSR.S | HexNAc(4)Hex(5)NeuAc(2) | 0.022 |
| 18 | CO6_HUMAN | K.VLnFTTK.A | HexNAc(4)Hex(5)NeuAc(1) | 0.026 |
| 19 | CO6_HUMAN | R.LSSnSTK.K | HexNAc(4)Hex(5)NeuAc(2) | 0.028 |
| 20 | HGFL_HUMAN | R.AFHYnVSSHGCQLLPWTQHSPHTR.L | HexNAc(4)Hex(5)NeuAc(2) | 0.010 |
| 21 | PROP_HUMAN | K.YPPTVSMVEGQGEKnVTFWGR.P | HexNAc(4)Hex(5)Fuc(1)NeuAc(1) | 0.047 |
| 22 | MASP1_HUMAN | R.NnLTTYK.S | HexNAc(4)Hex(5)NeuAc(2) | 0.014 |
| 23 | LUM_HUMAN | K.KLHINHNnLTESVGPLPK.S | HexNAc(4)Hex(5)Fuc(1)NeuAc(1) | 0.000 |
| 24 | LUM_HUMAN | K.KLHINHNnLTESVGPLPK.S | HexNAc(4)Hex(5)Fuc(1)NeuAc(2) | 0.010 |
| 25 | LUM_HUMAN | K.LHINHNnLTESVGPLPK.S | HexNAc(4)Hex(5)Fuc(1)NeuAc(1) | 0.005 |
| 26 | LG3BP_HUMAN | K.AAIPSALDTnSSK.S | HexNAc(4)Hex(5)Fuc(1)NeuAc(1) | 0.011 |

glycosylation patterns are considered a marker of cancer. Recently, studies have found that GTs are involved in mediating multidrug resistance (MDR) in cancer cells through complex mechanisms and can influence therapeutic effect (37). Schultz et al. reported that ST6Gal I overexpression is a hallmark of ovarian cancer, and it is closely related to cisplatin-induced cell death. The overexpression of ST6Gal I reduced the activation of caspase 3, and it protected against cell death after cisplatin treatment. This indicates that

TABLE 4 List of the difference glycopeptides before and after chemotherapy in NACT nonresponsive group.

| No | Protein name | Sequence | Glycans | *P* value |
|---|---|---|---|---|
| 1 | IGG1_HUMAN | R.EEQYnSTYR.V | HexNAc(4)Hex(4)Fuc(1) | 0.031 |
| 2 | CO3_HUMAN | K.TVLTPATNHMGnVTFTIPANR.E | HexNAc(2)Hex(5) | 0.029 |
| 3 | IGHM_HUMAN | K.YKnNSDISSTR.G | HexNAc(4)Hex(5)Fuc(1)NeuAc(1) | 0.033 |
| 4 | FINC_HUMAN | R.DQCivDDITYNVnDTFHK.R | HexNAc(4)Hex(5)NeuAc(1) | 0.046 |
| 5 | CFAI_HUMAN | K.LISnCSK.F | HexNAc(4)Hex(5)NeuAc(2) | 0.003 |
| 6 | CO2_HUMAN | K.QSVPAHFVALnGSK.L | HexNAc(2)Hex(5) | 0.039 |
| 7 | CBG_HUMAN | R.AQLLQGLGFnLTER.S | HexNAc(4)Hex(5)NeuAc(1) | 0.045 |
| 8 | C4BPB_HUMAN | R.LGHCPDPVLVNGEFSSSGPVnVSDK.I | HexNAc(4)Hex(5)NeuAc(2) | 0.027 |
| 9 | ZA2G_HUMAN | R.FGCEIENnR.S | HexNAc(4)Hex(5)NeuAc(2) | 0.046 |
| 10 | ITIH3_HUMAN | K.TAFITnFTLTIDGVTYPGNVK.E | HexNAc(4)Hex(5)NeuAc(2) | 0.032 |

TABLE 5 List of the glycopeptides be different before and after chemotherapy in NACT responsive group, as well as in two groups before NACT.

| No | Protein name | Sequence | Glycans |
|---|---|---|---|
| 1 | ATRN_HUMAN | K.IDSTGnVTNELR.V | HexNAc(2)Hex(5) |
| 2 | CO8A_HUMAN | R.GGSSGWSGGLAQnR.S | HexNAc(4)Hex(5)NeuAc(1) |
| 3 | CO8B_HUMAN | R.nVTEK.M | HexNAc(4)Hex(5)NeuAc(1) |
| 4 | CO6_HUMAN | R.LSSnSTK.K | HexNAc(4)Hex(5)NeuAc(2) |
| 5 | MASP1_HUMAN | R.NnLTTYK.S | HexNAc(4)Hex(5)NeuAc(2) |
| 6 | LUM_HUMAN | K.LHINHNnLTESVGPLPK.S | HexNAc(4)Hex(5)Fuc(1)NeuAc(1) |

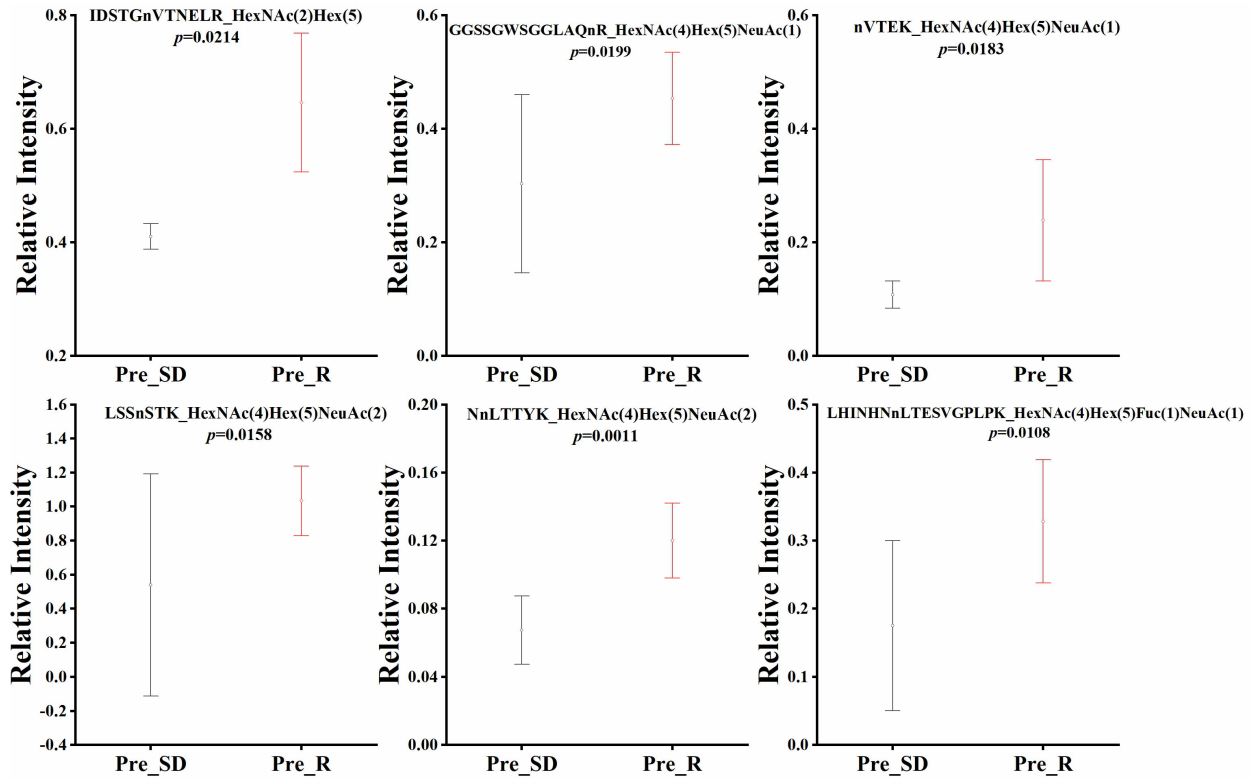


FIGURE 4
Box plot of relative abundance of N-glycopeptide in serum between NACT responsive (Pre_R) and nonresponsive (Pre_SD) patients before chemotherapy.

ST6Gal I may be a novel contributor to cisplatin resistance (38). Aloia et al. reported that increased expression of ST3Gal II in breast cancer could be predictive markers of poor prognosis (39). However, the biological mechanism for such a relationship between glycosylation and cancers has yet to be determined. In the future, we will strengthen cooperation with experts in the field of tumor resistance, and hope that we can further elucidate the mechanism.

The biological function of the six differential glycopeptides detected in the present study plays a key role in tumor occurrence and progression. Patients with higher serum MASP-1 levels may have exacerbated complement activation, which leads to basement membrane disorder and eventually to basement membrane injury or rupture, resulting in tumor invasion. A previous study has reported that the expression of MASP-1 is significantly increased in cervical cancer patients, HPV-positive patients and cervical secretory tissues with late FIGO stage (stage III - IV) (40). Similarly, the expression of MASP-1 in invasive cervical cancer is significantly higher than that in precancerous lesions, and higher serum levels of MASP-1 are associated with poor prognosis in cervical cancer (41). In the present study, the serum levels of MASP-1-related glycopeptides in the NACT-responsive group decreased significantly after chemotherapy, which was consistent with previous reports. The present results further illustrated the differences in glycopeptide sequences and the corresponding glycans. Recently, increasing experimental data have shown that LUM is expressed in various types of tumor tissues. LUM not only regulates extracellular water balance and collagen fiber formation but also impacts tumor growth, adhesion and migration (42). We found that after NACT, the relative abundance of LUM-related glycopeptides in the NACT-responsive group significantly decreased, indicating that the prognosis of LACC may be improved by inhibiting LUM-related glycopeptides. ATRN is involved in innate immune cell aggregation in the inflammatory response and may regulate the chemotactic activity of chemokines (43). ATRN is a predictive biomarker in prostate cancer because it distinguishes prostate cancer from benign prostatic hyperplasia (44). Complement C8 (CO8A and CO8B) and CO6 are members of the complement gene family; they are the main components of the membrane attack complex, and they are also part of the innate immune system. The complement of innate immunity exists in the tumor microenvironment, and the function of complement depends on the type of tumor and its heterogeneity, which may be antitumor or protumor (45). C8A is also used as a biomarker for predicting the benefit of trastuzumab in HER2-positive breast cancer patients (46). High C8A expression has a significant benefit in disease-free survival. Studies have shown that the expression level of C8B has a protective effect on the overall survival and recurrence-free survival of patients with HBV-related hepatocellular carcinoma (47). In the present research, we further illustrated the differences in glycopeptide sequences, including K.IDSTGnVTNELR.V, R.GGSSGWSGGLAQnR.S, R.nVTEK.M, R.LSSnSTK.K, R.NnLTTYK.S, K.LHINHNnLTESVGPLPK.S and the corresponding glycans. To our knowledge, this is the first study to demonstrate that serum intact N-glycosylation may be correlated with response to

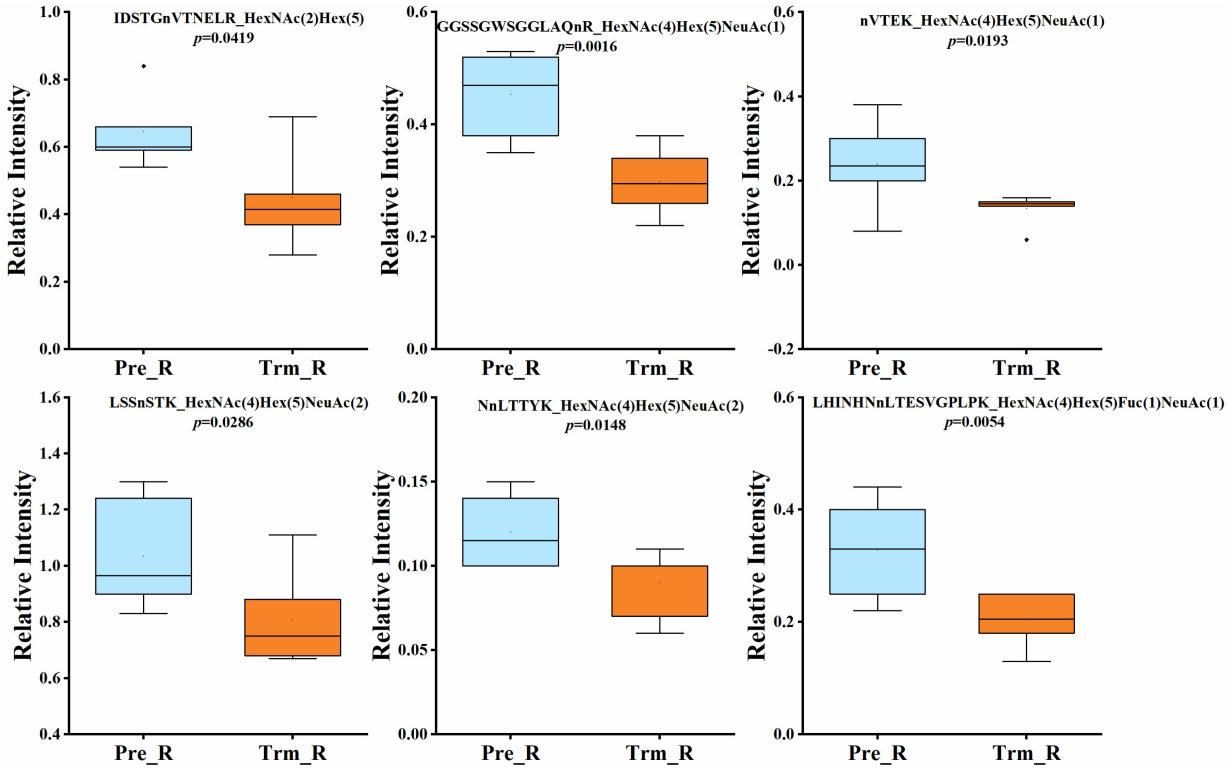


FIGURE 5
Box plot of relative abundance of N-glycopeptide in serum of NACT responsive patients before (Pre_R) and after chemotherapy (Trm_R).

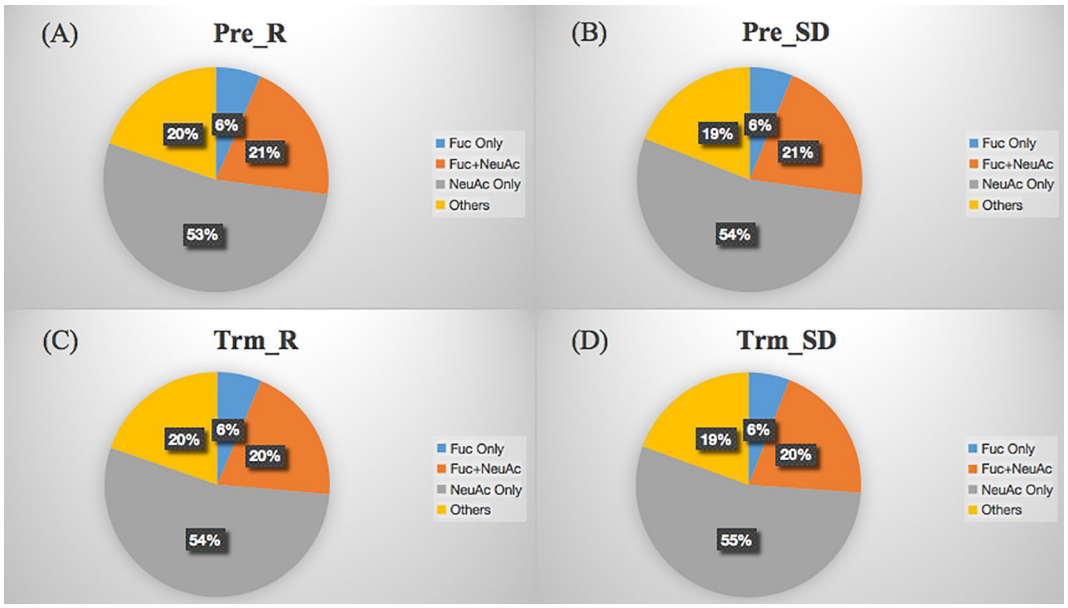


FIGURE 6
Distribution of glycosylation types of sera glycoproteins from NACT response (**A**, Pre_R), NACT nonresponse (**B**, Pre_SD) before treatment and NACT response (**C**, Trm_R), NACT nonresponse (**D**, Trm_SD) after treatment. The labels Fuc only, Fuc+NeuAc, NeuAc only and Others refer to the glycopeptides fucosylated only, fucosylated and sialylated, sialylated only and other glycosylated types, respectively.

NACT in LACC. Some of these altered N-glycopeptides have the potential to predict efficacy of NACT.

The present study highlighted the application of LC-MS/MS for the discovery of N-glycopeptides associated with LACC. After quantitative analysis, 6 of 570 glycopeptides were identified as biomarkers for predicting the sensitivity of neoadjuvant chemotherapy in LACC. The relative abundance of the six glycopeptides (corresponding proteins including MASP1, LUM, ATRN, CO8A, CO8B and CO6) was significantly higher in the NACT responsive group and was significantly decreased after chemotherapy. High levels of these six glycopeptides may indicate that chemotherapy is effective. In future studies, we will verify these glycopeptides by parallel reaction monitoring (RPM) to further improve the diagnostic efficacy. Additional biological mechanism studies should be performed to investigate how glycopeptides play a role in NACT responders.

## Data availability statement

The original contributions presented in the study are included in the article/supplementary material. Further inquiries can be directed to the corresponding authors.

## Ethics statement

The study was approved by Shanghai Jiaotong University School of Medicine affiliated with the Ruijin Hospital Ethics Committee (N-2018-239). The patients/participants provided their written informed consent to participate in this study.

## Author contributions

WF and HJL contributed to conception and design of the study. JL and XF organized the database and performed the statistical analysis. WF and HL assisted with provision and supervision of the study patients. CZ stored and processed the specimens. JL and XF wrote the first draft of the manuscript. WF, HJL, and YJ wrote sections of the manuscript. All authors contributed to manuscript revision, read, and approved the submitted version.

## Funding

The work was supported by Shanghai project (22DZ2291700) and the Greater Bay Area Institute of Precision Medicine (Guangzhou; no. IPM2021C005).

## Acknowledgments

The authors thank all the study participants for their great effort. Furthermore, the authors acknowledge the contributions of colleagues and institutions that aided the efforts of the authors.

## Conflict of interest

The authors declare that the research was conducted in the absence of any commercial or financial relationships that could be construed as a potential conflict of interest.

## Publisher's note



## References

1. Bray F, Ferlay J, Soerjomataram I, Siegel RL, Torre LA, Jemal A. Global cancer statistics 2018: GLOBOCAN estimates of incidence and mortality worldwide for 36 cancers in 185 countries. *CA Cancer J Clin* (2018) 68(6):394–424. doi: 10.3322/caac.21492

2. Bruni L, Serrano B, Roura E, Alemany L, Cowan M, Herrero R, et al. Cervical cancer screening programmes and age-specific coverage estimates for 202 countries and territories worldwide: a review and synthetic analysis. *Lancet Global Health* (2022) 10(8):e1115–27. doi: 10.1016/S2214-109X(22)00241-8

3. Zhou JY, Lei NJ, Tian WJ, Guo RX, Chen MY, Qiu LJ, et al. Recent progress of the tumor microenvironmental metabolism in cervical cancer radioresistance. *Front Oncol* (2022) 12:999643. doi: 10.3389/fonc.2022.999643

4. . Available at: https://seer.cancer.gov/statfacts/ (Accessed February 15th 2023).

5. Perelli F, Mattei A, Scambia G, Cavaliere AF. Editorial: methods in gynecological oncology. *Front Oncol* (2023) 13:1167088. doi: 10.3389/fonc.2023.1167088

6. Vale C, Tierney JF, Stewart LA, Brady M, Dinshaw K, Jakobsen A, et al. Reducing uncertainties about the effects of chemoradiotherapy for cervical cancer: a systematic review and meta-analysis of individual patient data from 18 randomized trials. *J Clin Oncol* (2008) 26(35):5802–12. doi: 10.1200/JCO.2008.16.4368

7. Li J, Liu H, Li Y, Li J, Shen LF, Long WQ, et al. Comparison of outcomes and side effects for neoadjuvant chemotherapy with weekly cisplatin and paclitaxel followed by chemoradiation vs. chemoradiation alone in stage IIB-IVA cervical cancer: study protocol for a randomized controlled trial. *Trials* (2022) 23(1):29. doi: 10.1186/s13063-021-05986-z

8. Singh RB, Chander S, Mohanti BK, Pathy S, Kumar S, Bhatla N, et al. Neoadjuvant chemotherapy with weekly paclitaxel and carboplatin followed by chemoradiation in locally advanced cervical carcinoma: a pilot study. *Gynecol Oncol* (2013) 129(1):124–8. doi: 10.1016/j.ygyno.2013.01.011

9. McCormack M, Kadalayil L, Hackshaw A, Hall-Craggs MA, Symonds RP, Warwick V, et al. A phase II study of weekly neoadjuvant chemotherapy followed by radical chemoradiation for locally advanced cervical cancer. *Br J Cancer* (2013) 108 (12):2464–9. doi: 10.1038/bjc.2013.230

10. Huang Y, Liu L, Cai J, Yang L, Sun S, Zhao J, et al. The efficacy and response predictors of platinum-based neoadjuvant chemotherapy in locally advanced cervical cancer. *Cancer Manag Res* (2020) 12(undefined):10469–77. doi: 10.2147/CMAR.S270258

11. Zhu Y, Yang J, Zhang X, Chen DX, Zhang SY. Acquired treatment response from neoadjuvant chemotherapy predicts a favorable prognosis for local advanced cervical cancer: a meta-analysis. *Med (Baltimore)* (2018) 97(17):e0530. doi: 10.1097/MD.0000000000010530

12. Park DC, Suh MJ, Yeo SG. Neoadjuvant paclitaxel and cisplatin in uterine cervical cancer: long-term results. *Int J Gynecol Cancer* (2009) 19(5):943–7. doi: 10.1111/IGC.0b013e3181a23c2e

13. Bangarh R, Khatana C, Kaur S, Sharma A, Kaushal A, Siwal SS, et al. Aberrant protein glycosylation: implications on diagnosis and immunotherapy. *Biotechnol Adv* (2023) 66:108149. doi: 10.1016/j.biotechadv.2023.108149

14. Li Q, Xie Y, Wong M, Barboza M, Lebrilla CB. Comprehensive structural glycomic characterization of the glycocalyxes of cells and tissues. *Nat Protoc* (2020) 15 (8):2668–704. doi: 10.1038/s41596-020-0350-4

15. Reily C, Stewart TJ, Renfrow MB, Novak J. Glycosylation in health and disease. *Nat Rev Nephrol* (2019) 15(6):346–66. doi: 10.1038/s41581-019-0129-4

16. Xu Z, Zhang Y, Ocansey DKW, Wang B, Mao F. Glycosylation in cervical cancer: new insights and clinical implications. *Front Oncol* (2021) 11:706862. doi: 10.3389/fonc.2021.706862

17. Kailemia MJ, Park D, Lebrilla CB. Glycans and glycoproteins as specific biomarkers for cancer. *Analytical Bioanalytical Chem* (2017) 409(2):395–410. doi: 10.1007/s00216-016-9880-6

18. Caval T, Alisson-Silva F, Schwarz F. Roles of glycosylation at the cancer cell surface: opportunities for large scale glycoproteomics. *Theranostics* (2023) 13:2605–15. doi: 10.7150/thno.81760

19. Sun KL, Feng ZY, Fan CY. A glycosylation signature for predicting the progression and immunotherapeutic response of prostate cancer. *J Gene Med* (2023) 25(6):3489–501. doi: 10.1002/jgm.3489

20. Varki. A. *Glycosylation changes in cancer*. Cold Spring Harbor (NY: Cold Spring Harbor Laboratory Press (2009).

21. Kobata A, Amano J. Altered glycosylation of proteins produced by malignant cells, and application for the diagnosis and immunotherapy of tumours. *Immunol Cell Biol* (2005) 83(4):429–39. doi: 10.1111/j.1440-1711.2005.01351.x

22. Pinho SS, Reis CA. Glycosylation in cancer: mechanisms and clinical implications. *Nat Rev Cancer* (2015) 15(9):540–55. doi: 10.1038/nrc3982

23. Eisenhauer EA, Therasse P, Bogaerts J, Schwartz LH, Sargent D, Ford R, et al. New response evaluation criteria in solid tumours: revised RECIST guideline (version 1.1). *Eur J Cancer* (2009) 45(2):228–47. doi: 10.1016/j.ejca.2008.10.026

24. Fang P, Ji Y, Silbern I, Doebele C, Ninov M, Lenz C, et al. A streamlined pipeline for multiplexed quantitative site-specific n-glycoproteomics. *Nat Commun* (2020) 11 (1):5268. doi: 10.1038/s41467-020-19052-w

25. Mechref Y, Muddiman DC. Recent advances in glycomics, glycoproteomics and allied topics. *Anal Bioanal Chem* (2017) 409(2):355–7. doi: 10.1007/s00216-016-0093-9

26. Ohtsubo K, Marth JD. Glycosylation in cellular mechanisms of health and disease. *Cell* (2006) 126(5):855–67. doi: 10.1016/j.cell.2006.08.019

27. Lin Y, Zhu J, Zhang J, Dai J, Liu S, Arroyo A, et al. Glycopeptides with sialyl Lewis antigen in serum haptoglobin as candidate biomarkers for nonalcoholic steatohepatitis hepatocellular carcinoma using a higher-energy collision-induced dissociation parallel reaction monitoring-mass spectrometry method. *ACS Omega* (2022) 7(26):22850–60. doi: 10.1021/acsomega.2c02600

28. Lin Y, Zhu J, Pan L, Zhang J, Tan Z, Olivares J, et al. A panel of glycopeptides as candidate biomarkers for early diagnosis of NASH hepatocellular carcinoma using a stepped HCD method and PRM evaluation. *J Proteome Res* (2021) 20(6):3278–89. doi: 10.1021/acs.jproteome.1c00175

29. Ang IL, Poon TC, Lai PB, Chan ATC, Ngai SM, Hui AY, et al. Study of serum haptoglobin and its glycoforms in the diagnosis of hepatocellular carcinoma: a glycoproteomic approach. *J Proteome Res* (2006) 5(10):2691–700. doi: 10.1021/pr060109r

30. Xu Z, Zhang Y, Ocansey DKW, Wang B, Mao F. Glycosylation in cervical cancer: new insights and clinical implications. *Front Oncol* (2021) 11:706862 (undefined). doi: 10.3389/fonc.2021.706862

31. Kim HJ, Kim SC, Ju W, Kim YH, Yin SY, Kim HJ. Aberrant sialylation and fucosylation of intracellular proteins in cervical tissue are critical markers of cervical carcinogenesis. *Oncol Rep* (2014) 31(3):1417–22. doi: 10.3892/or.2013.2938

32. Zeng Q, Zhao RX, Chen J, Li Y, Li XD, Liu XL, et al. O-Linked GlcNAcylation elevated by HPV E6 mediates viral oncogenesis. *Proc Natl Acad Sci U.S.A.* (2016) 113 (33):9333–8. doi: 10.1073/pnas.1606801113

33. Zhu H, Pei HP, Zeng S, Chen J, Shen LF, Zhong MZ, et al. Profiling protein markers associated with the sensitivity to concurrent chemoradiotherapy in human cervical carcinoma. *J Proteome Res* (2009) 8(8):3969–76. doi: 10.1021/pr900287a

34. Qin RH, Yang YP, Chen H, Qin WJ, Han J, Gu Y, et al. Prediction of neoadjuvant chemotherapeutic efficacy in patients with locally advanced gastric cancer by serum IgG glycomics profiling. *Clin Proteom* (2020) 17(1):4. doi: 10.1186/s12014-020-9267-8

35. Varki A. Sialic acids in human health and disease. *Trends Mol Med* (2008) 14 (8):351–60. doi: 10.1016/j.molmed.2008.06.002

36. Schultz MJ, Swindall AF, Wright JW, Sztul ES, Landen CN, Bellis SL, et al. ST6Gal-I sialyltransferase confers cisplatin resistance in ovarian tumor cells. *J Ovarian Res* (2013) 6:25. doi: 10.1186/1757-2215-6-25

37. Shan M, Yang D, Dou H, Zhang L. Fucosylation in cancer biology and its clinical applications. *Prog Mol Biol Transl Sci* (2019) 162(undefined):93–119. doi: 10.1016/bs.pmbts.2019.01.002

38. Wu YS, Chen XX, Wang SD, Wang SJ. Advances in the relationship between glycosyltransferases and multidrug resistance in cancer. *Clinica Chimica Acta* (2019) 495:417–21. doi: 10.1016/j.cca.2019.05.015

39. Aloia A, Petrova E, Tomiuk S, Bissels U, Déas O, Saini M, et al. The sialylglycolipid stage-specific embryonic antigen 4 marks a subpopulation of chemotherapy-resistant breast cancer cells with mesenchymal features. *Breast Cancer Res* (2015) 17:146. doi: 10.1186/s13058-015-0652-6

40. Kong L, Wang J, Cheng J, Zang C, Chen F, Wang W, et al. Comprehensive identification of the human secretome as potential indicators in treatment outcome of HPV-positive and -negative cervical cancer patients. *Gynecol Obstet Invest* (2020) 85 (5):405–15. doi: 10.1159/000510713

41. Maestri CA, Nisihara R, Mendes HW, Jensenius J, Thiel S, Messias R, et al. MASP-1 and MASP-2 serum levels are associated with worse prognostic in cervical cancer progression. *Front Immunol* (2018) 9:2742(undefined). doi: 10.3389/fimmu.2018.02742

42. Neill T, Schaefer L, Iozzo RV. Decoding the matrix: instructive roles of proteoglycan receptors. *Biochemistry* (2015) 54(30):4583–98. doi: 10.1021/acs.biochem.5b00653

43. Cima I, Schiess R, Wild P, Kaelin M, Schüffler P, Lange V, et al. Cancer genetics-guided discovery of serum biomarker signatures for diagnosis and prognosis of prostate cancer. *Proc Natl Acad Sci U.S.A.* (2011) 108(8):3342–7. doi: 10.1073/pnas.1013699108

44. Totten SM, Adusumilli R, Kullolli M, Tanimoto C, Brooks JD, Mallick P, et al. Multi-lectin affinity chromatography and quantitative proteomic analysis reveal differential glycoform levels between prostate cancer and benign prostatic hyperplasia sera. *Sci Rep* (2018) 8(1):6509. doi: 10.1038/s41598-018-24270-w

45. Li L, Yang W, Shen Y, Xu X, Li J. Fish complement C8 evolution, functional network analyses, and the theoretical interaction between C8 alpha chain and CD59. *Mol Immunol* (2020) 128(undefined):235–48. doi: 10.1016/j.molimm.2020.10.013

46. Willis S, Polydoropoulou V, Sun Y, Young B, Tsourti Z, Karlis D, et al. Exploratory analysis of single-gene predictive biomarkers in HERA DASL cohort reveals that C8A mRNA expression is prognostic of outcome and predictive of benefit of trastuzumab. *JCO Precis Oncol* (2018) 2(undefined), undefined. doi: 10.1200/PO.18.00016

47. Zhang Y, Chen X, Cao Y, Yang Z. C8B in complement and coagulation cascades signaling pathway is a predictor for survival in HBV-related hepatocellular carcinoma patients. *Cancer Manag Res* (2021) 13(undefined):3503–15. doi: 10.2147/CMAR.S302917

frontiers | Frontiers in Oncology

TYPE Original Research
PUBLISHED 18 October 2023
DOI 10.3389/fonc.2023.1131803



OPEN ACCESS

EDITED BY
Umberto Malapelle,
University of Naples Federico II, Italy

REVIEWED BY
Isabel Soto-Cruz,
National Autonomous University of Mexico, Mexico
Roberto C. Delgado Bolton,
Hospital San Pedro, Spain

*CORRESPONDENCE
Xiaomin Wang
wangxm_bthtm@163.com
Yun Wu
13847221258@163.com

RECEIVED 26 December 2022
ACCEPTED 05 September 2023
PUBLISHED 18 October 2023

CITATION
Ming C, Bai X, Zhao L, Yu D, Wang X and Wu Y (2023) RPL24 as a potential prognostic biomarker for cervical cancer treated by Cisplatin and concurrent chemoradiotherapy.
*Front. Oncol.* 13:1131803.
doi: 10.3389/fonc.2023.1131803



# RPL24 as a potential prognostic biomarker for cervical cancer treated by Cisplatin and concurrent chemoradiotherapy

Cheng Ming[1], Xuelian Bai[2], Lifeng Zhao[2], Dedong Yu[2], Xiaomin Wang[3]* and Yun Wu[2]*

[1]Department of Oncology, Baotou Central Hospital, Inner Mongolia Medical University, Baotou, China, [2]Department of Oncology, Baotou Central Hospital, Baotou, China, [3]Institute of Translational Medicine, Baotou Central Hospital, Baotou, China

Cervical carcinoma (CC) is the one of most common gynecologic cancers worldwide. The ribosomal proteins (RPs) are essential for ribosome assembly and function, and it has been verified that the abnormal expression of RPs was closely associated with tumorigenesis. In this study, we found that the RP large subunit 24 (RPL24) expression level was upregulated after the CC cell lines SiHa and HeLa were treated with Cisplatin (CDDP) *in vitro*. Simultaneously, a nude mouse xenograft model was used to examine the effect of RPL24 on tumor growth *in vivo*, which showed that overexpression of RPL24 can suppress tumor growth. Furthermore, we proved that RPL24 expression increased after CC patients were treated with concurrent chemoradiotherapy (CCRT), and the higher expression of RPL24 predicted a better prognosis using clinical data from 40 CC patients, verified via the Kaplan-Meier Plotter and LOGpc. These results revealed that RPL24 can be considered a potential biomarker to predict the prognosis of CC patients and assess CCRT efficacy.

KEYWORDS

**cervical cancer, RPL24, concurrent chemoradiotherapy, prognosis, biomarker**

## Introduction

Cervical cancer (CC) is one of the most common types of carcinomas among women globally, after only breast, colorectal, and lung cancer (1). Thus, identification of prognostic biomarkers or therapeutic targets for the management of CC is strongly warranted. The ribosomal proteins (RPs) are essential for ribosome assembly and function, including extra-ribosomal functions such as activation of p53-dependent or -independent pathways in response to large numbers of extracellular or intracellular stimuli and stress, resulting in cell cycle arrest, senescence, and apoptosis (2). Rpl24 encodes a highly basic protein of 157 amino acids. As a member of the RP family, Ribosomal protein L24 (RPL24) is a component of the 60S large ribosomal subunit and plays an essential role in ribosome biogenesis.

Large bodies of evidence have demonstrated that the abnormal expression of RPs, such as up- or down-regulation, is closely associated with tumorigenesis in different types of cancers, and high expression of RPs is a prognostic factor in some kinds of tumors (3). Abnormal RP expression has been verified in diverse cancer types in recent years using high-throughput techniques (4–7). To date, little is known about the role of RPL24 in CC. The extra-ribosomal functions of RPs are closely related to oncogenesis in different cancers. It has been reported that when RP is deleted or reduced, ribosome biogenesis is blocked, and ribosome biogenesis has recently emerged as an effective target for cancer therapy (8). Recently, with increased understanding of the RP-MDM2-p53 pathway, some RPs are known to block MDM2-mediated p53 ubiquitination and degradation by inhibiting MDM2 activation, thereby affecting cell cycle progression and apoptosis (9). Previous studies have shown that some RPs, including RPL5, RPL11, RPL23, RPL26, RPS2, RPS7, RPS14, RPS25, and RPS26, play critical roles in regulating p53 by interacting with MDM2 (10, 11).

The Belly Spot and Tail (Bst) mouse phenotype is caused by mutations of RPL24, resulting in defects of the eye, skeleton, and coat pigmentation (12, 13). The phenotype of these mice is largely caused by the aberrant upregulation of p53 protein expression during embryonic development. It has been proposed that RPL24 deficiency triggers the p53 response (14). *Rpl24*$^{Bst}$ mutant mouse also has been used to suppress protein translation and limit tumorigenesis in multiple mouse models of cancer (15). Adult hematopoietic stem cells (HSCs) self-renewal requires precise control of protein synthesis, an increase or decrease in which can impair HSCs function and may lead to leukemia or bone marrow (BM) failure (16). Ribosomal protein L24 mutation (Rpl24$^{Bst/+}$) is a ribosomal mutation that impairs ribosomal biogenesis, resulting in reduced Rpl24$^{Bst/+}$ HSCs protein synthesis and thus disrupts both fetal and adult HSCs self-renewal. Recent studies show that *Pten* deletion increased protein synthesis while *Rpl24Bst/+* blocked this effect, restoring HSC function and delaying leukaemogenesis in *Rpl24Bst/+* mice (17). RPL24 depletion suppresses tumorigenesis, proliferation and extends survival by promoting eEF2 phosphorylation via eEF2K in pre-clinical mouse model of colorectal cancer (CRC) with *Apc* deletion and *Kras* mutations (15). RPL24 recombinant protein has a significant tumor-suppressor effect in tumor-bearing mice and the human hepatocellular carcinoma HepG2 cell line (18). However, this corresponding mechanism study demonstrated that partial loss of RPL24 can inhibit the tumorigenesis mediated by the Akt or Myc-driven genes via translational inhibition of a subset of cap (eIF4E)-dependently translated mRNAs. Moreover, HDAC inhibitors used as conventional epigenetic drugs for tumor treatment, such as trichostatin-A (TSA), can inhibit the malignant proliferation of tumors through downregulation of RPL24 expression by inducing acetylation (19). In addition, RPL24 overexpression may confer some amycin resistance in the human hepatocellular carcinoma HepG2 cell line, according to the same research findings (20). Therefore, the role and significance of RPL24 in liver cancer appear contradictory. To date, little is known about the role of RPL24 in CC and the role of RPL24 in the effect appraisal of concurrent chemoradiotherapy (CCRT) of CC remains understudied. The research provides a solid basis for the elucidation of the RPL24's mechanism in CCRT of CC and a meaningful target for its treatment and prognosis.

# Materials and methods

## Bioinformatics

Based on The Cancer Genome Atlas (TCGA) database, the differential expression of RPL24 in CC tissues and paracancerous tissues was analyzed. The related genes that were positively and negatively related to the expression of CC were downloaded from TCGA database, and these genes were imported into Metascape bioinformatics analysis website tools (https://metascape.org/gp/index.html#/main/step1) for KEGG enrichment analysis to analyze the possible regulatory mechanism between RPL24 and cell cycle in CC. To detect the correlation between RPL24 level and recurrence-free survival (RFS), overall survival (OS), and progression-free survival (PFS) in CC patients, the K-M Plotter was adopted to perform a survival curve analysis with the Kaplan-Meier Plotter (https://kmplot.com/analysis/) and LOGpc (https://bioinfo.henu.edu.cn/DatabaseList.jsp).

## Cell culture and *in vitro* treatments

The human CC cell lines SiHa and HeLa were obtained from ATCC (Manassas, VA, USA) and cultured according to the manufacturer's instructions. These cell lines were plated into 6-well culture plates and were incubated at 37°C in a humidified atmosphere containing 95% air and 5% $CO_2$. After 24 h of culture, the cells adhered to the wall (approximately $3\times10^6$ cells) and treated with 20 uM CDDP (Catalog No.P4394-250MG, Sigma, USA), which was dissolved in normal saline before use. After being treated for 48 hours, the cultured cells were harvested.

## Flow cytometry assay

Flow cytometry is a valuable tool for determining the percentage of cells in each phase of the cell cycle (G0/G1, S, and G2/M) *in vitro* experiment, flow cytometry was used to detect changes in the cell cycles of HeLa and SiHa cells at different timepoints before and after treatment with CDDP(cisplatin). The cells were trypsinized and washed with PBS, followed by fixation at -20°Cwith 70% cold ethanol and permeabilization with 0.2% Triton-X100. After removing the supernatant, cells were stained with 500 µl propyl iodide staining solution to determine the DNA content of cells. The cells were incubated at 37°C for 20 minutes and the cell cycle was detected by flow cytometry. Flowjo software (Home | FlowJo, LLC) was used to simulate cell cycle distribution for correlation cycle fitting, and determine the proportion of cells in G0/G1, S, and G2/M phases.

## Western blotting

Western blotting was used to detect the expression levels of RPL24 protein in SiHa and HeLa before and after CDDP treatment. Equal amounts of protein samples were extracted from cells with RIPA lysis buffer. Then 50 μg of protein were loaded from each sample and separated using 10% SDS-PAGE before being electrophoretically transferred to PVDF membranes. 5% non-fat dry milk skimmed milk powder was dissolved in PBST(0.1% Tween 20) and blocked with PVDF membrane for 1 hour at room temperature.

Western blot with RPL24 antibody (Cat No: 17082-1-AP, Proteintech Co.,LTD, CN) at dilution of 1:500 incubated at room temperature for 1.5 hours. The membranes were washed with tris-buffered saline (TBS) and exposed to primary antibodies (RPL24 antibodies) at 4°C. Then the membranes were washed with TBST and incubated with appropriate a second antibody conjugated to horseradish peroxidase for 2 hours at room temperature. Eventually, the proteins expression of interest were visualized using an enhanced chemiluminescence reagent (Enlight Buffer from Engreen Co.,Ltd, CAT# No.29050, CN). The results of Western blotting were quantified using the semi-quantitative software ImageJ, the ratio of RPL24[at 1:600 dilution Wuhan sanying(Rabbit Polyclonal antibody)]/CCNB1[at 1:800 dilution AF6627(Rabbit Polyclonal antibody)]/p53[at 1:800 dilution AP062 (Murine monoclonal antibody)] to β-actin[at 1:1500 dilution AP2811 (Murine monoclonal antibody)] was subsequently calculated.

## Vector construction and transfection

To overexpress RPL24, we cloned full-length homo sapiens RPL24 sequences (NM_000986.4) into the vector pcDNA3.0. The RPL24 overexpression plasmid and empty plasmid were respectively transfected into SiHa cells using the Lipofectamine 2000 reagent (Invitrogen) according to the manufacturer's protocol. The positive clones, which were SiHa cells with a high expression of RPL24, were screened using a medium containing G418 (Calbiochem) and then the efficiency of transfection was examined using the western blot test. To obtain cell lines stably overexpressing RPL24, RPL24 was cloned into the lentivirus plasmid Pez-Lv105. Recombinant lentivirus infection and screening were performed according to the manufacturer's protocol (GeneCopoeia, Rockville, MD, USA).

## Construction of a nude mice subcutaneous transplantation model

All animal experiments in this study were agreed on by the Guide for the Care and Use of Laboratory Animals. Ten 6-week-old, female NOD/SCID mice (SHANGHAI SLAC, Shanghai) were purchased, housed in the animal facility at the Translational Medicine Central Laboratory, and randomly assigned to one of two groups. The mice were raised under standard conditions (12-hour light and dark cycle, 22 ± 0.5°C, and relative humidity of 40% to 70%, with ad libitum access to food and water).

Stable cell lines were obtained using screening with puromycin. These cell lines from the control and interference groups, which were transfected with RPL24, were formulated as a single-cell suspension of cells and injected into the subcutaneous skin of nude mice at 0.2 ml (about $3\times10^6$ cells per side). After a single subcutaneous injection of RPL24 cells into immunodeficient NOD/SCID mice, tumor formation and enlargement were observed 7-9 days later until the tumor size was significantly different, conforming to welfare ethical review of laboratory animal (tumor diameter should not be large, generally no larger than 15mm). The grafts appeared 21 days later. The tumor-bearing mice were sacrificed by dislocation, and the xenografts were dissected. Before the mice were sacrificed, they were euthanized with $CO_2$ inhalation to alleviate pain. No mice were treated with drugs while their general status and tumor volume were observed after tumorigenesis. We calculated the volume of subcutaneous tumors in nude mice regularly every 5 days and plotted the volume change curve of subcutaneous tumors. Tumor volume analyses were based on the following equation: Volume =(length ×width$^2$)×1/2. At the end of the study, tumor weight was measured.

## Patients and treatment

Data from 40 patients hospitalized with newly diagnosed CC from January 2017 to December 2019 in Baotou Central Hospital were collected and analyzed. The therapeutic methods were pelvic field ± para-aortic extended field radiotherapy, accompanied by concurrent platinum-based chemotherapy.

The inclusion criteria were histopathologic diagnosis of cervical squamous cell CC with complete clinical data, International Federation of Gynecology and Obstetrics (FIGO) stage IB1-IVA, KPS>70, agreement to receive CCRT, acceptance of a cervical puncture biopsy before and after CCRT, and signed voluntary informed consent. All 40 patients underwent the treatment as planned and were examined regularly. This study was approved by the Ethics Committee of Baotou Central Hospital.

## Immunohistochemical analysis

CC tissues were obtained, fixed in 10% formalin, embedded in 5μm- thick paraffin sections. Sections with well-preserved morphology were used for immunohistochemical staining. After dewaxing and hydration series, 17082-1-AP (RPL24 antibody, Proteintech Co.,LTD, CN) at dilution of 1:50 prepared in PBS buffer was incubated at room temperature for 2 hours, followed by immunohistochemistry kit [purchased from DAKO Co.,LTD, Denmark (Cat#:GK500705)] staining. The result was determined by the percentage of positive stained cells and cell staining intensity as follows: negative −, weak positive +, positive ++, and strongly positive +++. To eliminate scoring errors, two researchers independently reviewed each tissue section.

The results were analyzed to determine the pathological pattern and malignancy grade. Then the RPL24 expression of CC tissues after CCRT was detected, and the clinical stage, age, effect assessment of CCRT, apparent diffusion coefficient (ADC) value, and elated clinical factors were combined for evaluation.

## Statistical analysis

All experiments were independently performed at least three times. The influence of RPL24 expression on the survival outcome of patients with CC was analyzed using the Kaplan-Meier method using online public databases. Differences between groups were performed using unpaired t-tests, All the data were represented as mean ± standard deviation(SD) from three independent experiments. Fisher's exact probability test was used to process the count data. The correlation of RPL24 expression before and after CCRT was analyzed using the Spearman test. Statistical analysis was performed using SPSS version 26.0 software and GraphPad Prism v9.4.1. $P<0.05$ was considered as statistically significant.

# Results

## RPL24 expression was down-regulated in CC

TCGA database analysis showed that the expression level of RPL24 in CC tissues was reduced comparing with normal tissues (Figure 1A) (P<0.01). In addition, KEGG enrichment analysis revealed that the regulation of RPL24 was related to p53 in CC (Figure 1B).

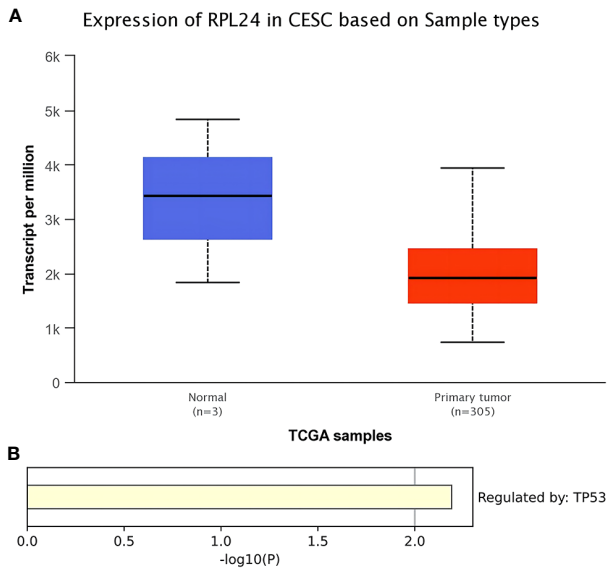


FIGURE 1
Bioinformatics analysis of RPL24 in CC. **(A)** Expression of RPL24 in CC tissues in TCGA database (r<0.05). **(B)** Enrichment analysis of RPL24 positively related genes in CC in Transcriptional Regulatory Relationships Unraveled by Sentence-based Text mining (TRRUST) database.

## High RPL24 expression predicts favorable prognosis in CC

The prognostic value of RPL24 in CC patients was tested using the K-M Plotter database and KaplanMeier Plotter Analysis of LOGpc. According to the Kaplan-Meier database, high expression of RPL24 was related to a favorable RFS in CC patients (HR=0.21; 95% CI, 0.06~0.69, $p$=0.0048) (Figure 2A) but was not correlated with OS ($P$>0.05) (Figure 2B). Meanwhile, an analysis based on the GSE14404 dataset in LOGpc showed that the high-RPL24 expression group had favorable OS (HR, 12.3115; 95%CI, 2.9025~52.221, $P$=7e-04; Figure 2C) for CC patients. In addition, an analysis of the GSE52904 dataset demonstrated that the increased-RPL24 expression group had favorable PFS (respectively, HR, 2.6231; 95%CI, 1.081~6.3651, $P$=0.033; HR, 2.6992; 95%CI, 1.1137~6.5421, $P$=0.0279; Figures 2D, E) for CC patients. These results indicate that the RPL24 expression level has prognostic significance in the GEO database and that CC patients with high RPL24 expression often have favorable prognoses. In conclusion, high RPL24 expression was significantly correlated with favorable RFS, OS, and PFS in CC patients.

## RPL24 expression increased by blocking cell cycle after CDDP treatment *in vitro*

Compared with negative control group, the proportion of G2/M phase cells was increased in HeLa and SiHa cells after CDDP treatment (Figure 3). The Western blotting analysis revealed, with β-actin as internal control, that RPL24, CCNB1 and p53 protein was overexpressed in SiHa and HeLa after CDDP treatment, but that it was expressed at a low level after saline treatment (Figure 4). CCNB1 is involved in mitotic regulation and is a marker of mitotic M-phase expression. The results of *in vitro* cell experiments showed that protein expression levels of RPL24 rose significantly in CC cell lines after CDDP treatment, accompanied by G2/M phase cells cycle arrest.

## Overexpression of RPL24 suppressed tumor growth *in vivo*

The aforementioned results demonstrated that RPL24 inhibited CC cell development *in vitro*. Therefore, to evaluate the role of RPL24 in tumorigenesis *in vivo*, a tumor xenograft nude mice model was constructed. The mice injected with RPL24-transfected SiHa cells showed markedly better general status with a reduced rate of tumor formation (Figures 5A, B). The volume and weight of tumors collected after the mice were sacrificed in the RPL24 group grew slower than those of the control group (Figures 5C, D). The stable cell lines was identified by immunoblots that RPL24 was highly expressed in SiHa cell lines (Figure 5E). We showed that RPL24 overexpression can reduce the growth and tumor formation rate of the mice, indicating that the low-RPL24 expression group had a poor prognosis.

10.3389/fonc.2023.1131803

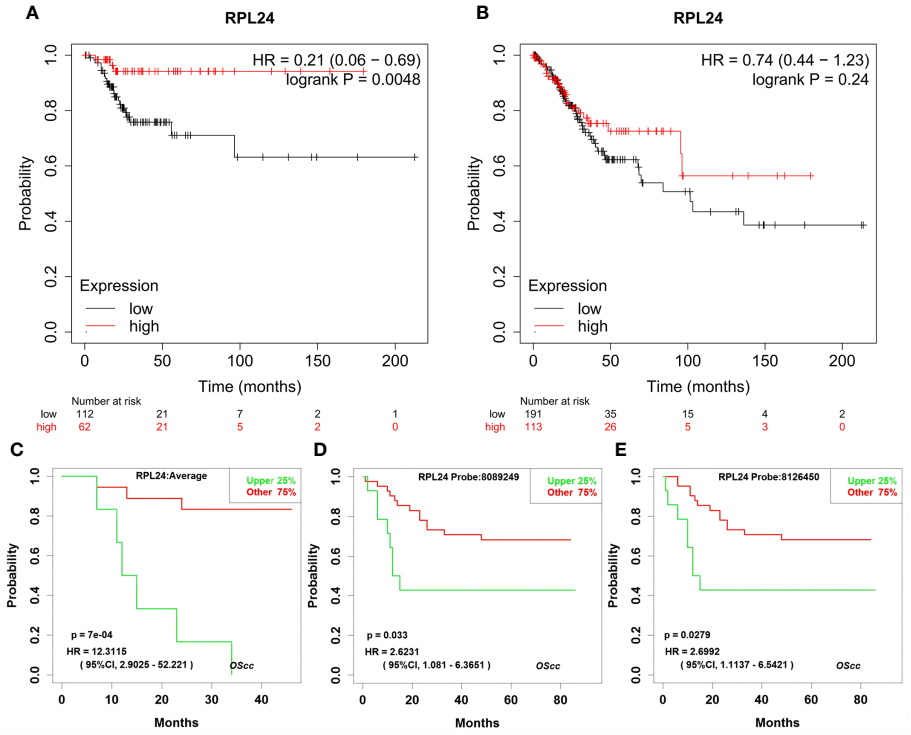


FIGURE 2
Effects of RPL24 on survival of patients with cervical cancer. The influence of overexpressed RPL24 on the survival of CC patients. **(A, B)** The RFS and OS of patients with cervical cancer related to RPL24 was acquired from the Kaplan online database. **(C)** Correlation between RPL24 expression and OS in GSE14404 dataset. **(D, E)** Correlation between RPL24 expression and PFS in GSE52904 dataset. CI, confidence interval; HR, hazard ratio; RPL24, ribosomal protein large subunit 24; OS, overall survival; PFS, progression- free survival; RFS, recurrence-free survival.

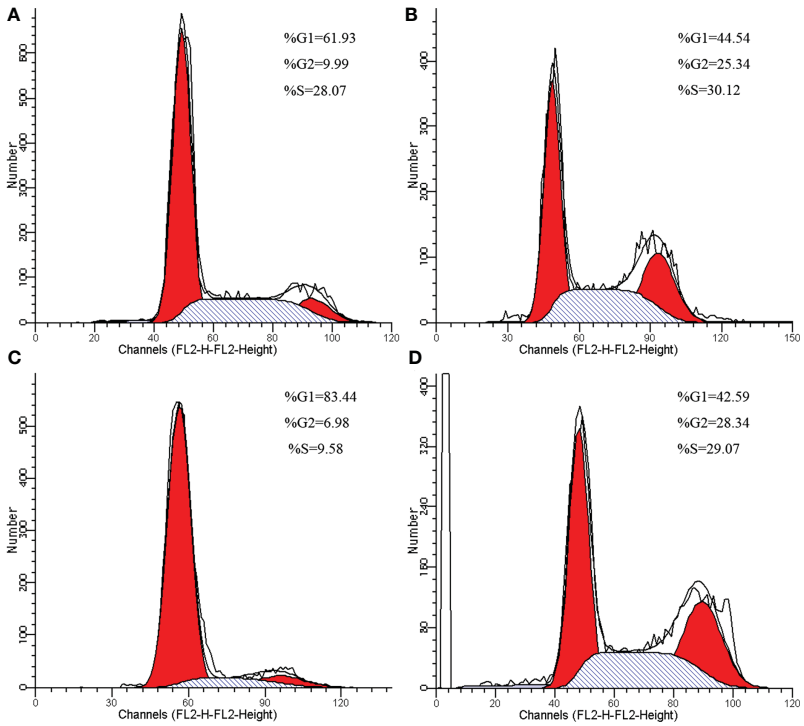


FIGURE 3
Cell cycle changes of HeLa and SiHa cells after CDDP treatment. **(A)** Cell cycle of HeLa cells in control group. **(B)** Effects of CDDP treatment on cell cycle of HeLa cells. **(C)** Cell cycle of SiHa cells in control group. **(D)** Effects of CDDP treatment on cell cycle of SiHa cells.

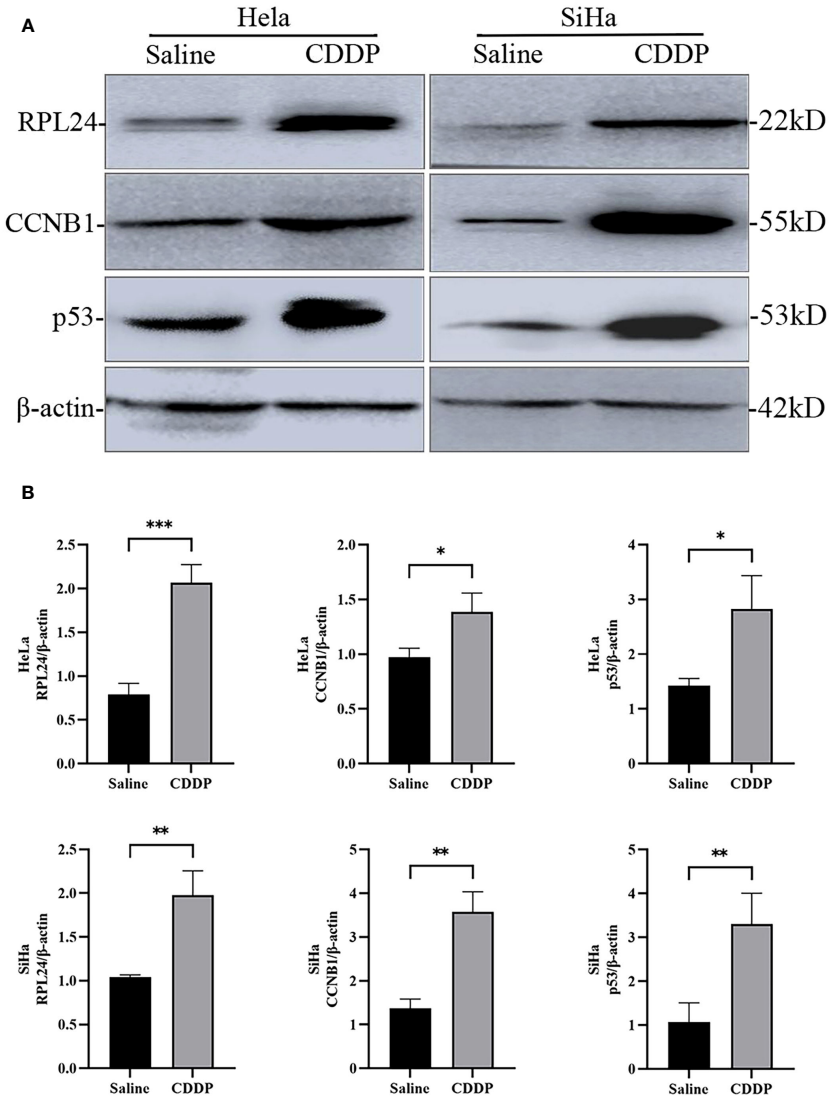


FIGURE 4
Difference in expression of RPL24/CCNB1/p53 and β-actin in SiHa and HeLa cells after saline or CDDP treatment. **(A)** Western blot analysis indicated that RPL24/CCNB1/p53 protein expression was higher in both HeLa and SiHa cells compared with before CDDP treatment. **(B)** Relative RPL24/CCNB1/p53 levels post CDDP treatment in both HeLa and SiHa cells (n=3, mean ± SD), statistical analysis was done by unpaired t-test corresponding p values shown. *r<0.05. **r<0.01. ***r<0.001.

## RPL24 expression increased after CCRT in most CC patients with the better prognosis

The characteristics of the 40 patients enrolled in the study are presented in Table 1 and representative immunohistochemical images of patients with stage IB1, IIB and IV CC before and after CCRT was shown in Figure 6. All patients were women with a mean age of 54.3 ± 10.0 years (range, 32 to 76). There were three cases (7.5%) of stage IB1, 34 cases (85%) of stage IIB, and 3 cases (7.5%) of stage IV CC. Twenty-six patients had a complete response (CR), 11 had a partial response (PR), and 3 had stable disease (SD). The correlation between RPL24 expression and therapeutic effect after CCRT are presented in Table 2. Analysis revealed that 26 CR patients and 11 PR patients highly expressed RPL24, 2 SD patients showed low expression of RPL24, and 1 SD patient showed high expression.

Twenty-six patients had CR, 11 patients had PR, and 1 patient had SD in all patients with high RPL24 expression, and only 2 patients with low RPL24 expression had SD (Table 2). RPL24 appeared to be a marker of a good prognosis. The association between RPL24 expression and patient curative effect was significant, and a positive association between RPL24 expression and patient curative effect was also observed (r =-0.575; p=0.004). In general, patients with high RPL24 expression after CCRT had a favorable prognosis.

# Discussion

The combination of bioinformatics and medicine is current main trend and plays a significant role in identifying and predicting cancer biomarkers. Also, a large number of candidate targets can be

10.3389/fonc.2023.1131803

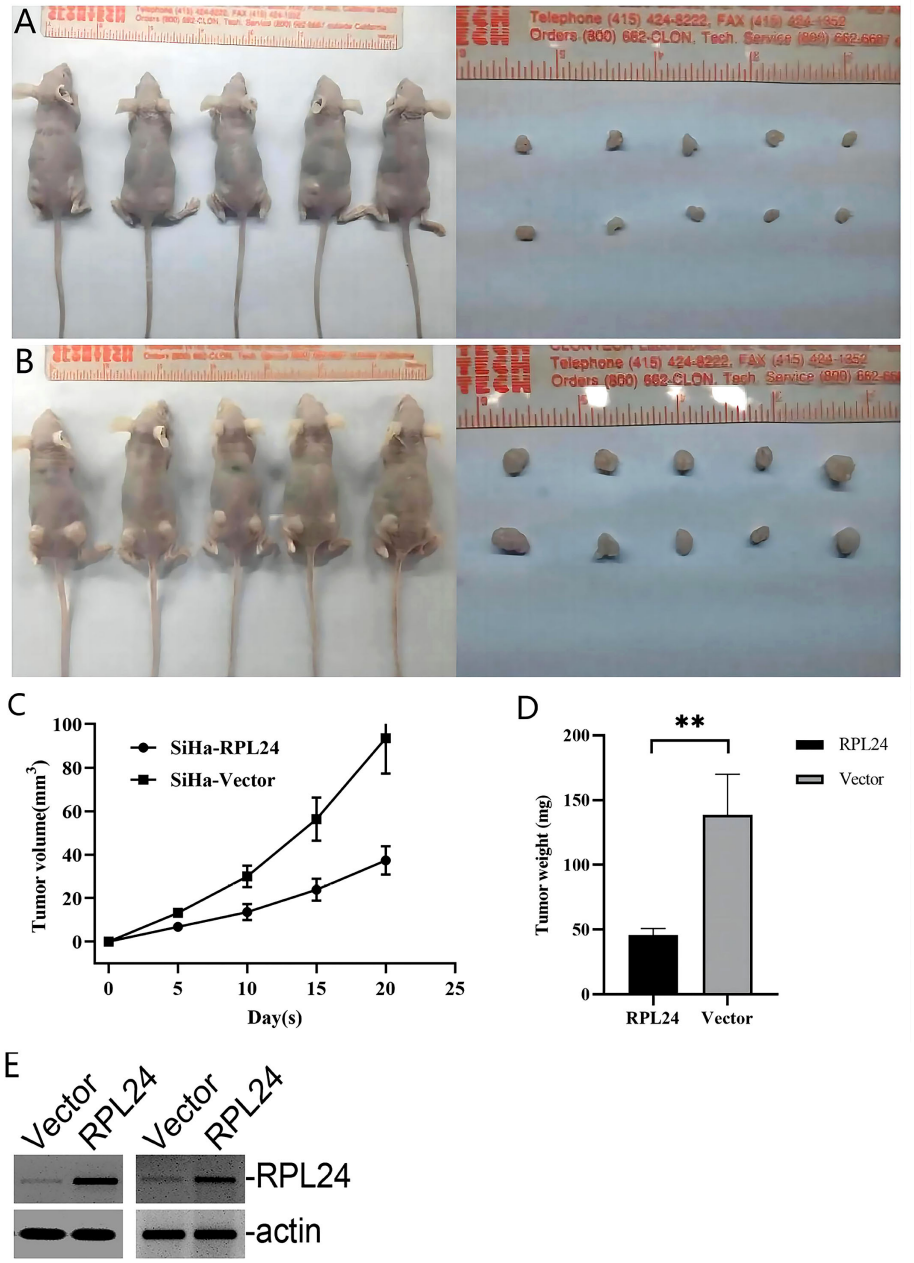


FIGURE 5
RPL24 overexpression suppresses SiHa cell proliferation *in vivo*. **(A)** Images of nude mice and xenograft tumors treated with RPL24 were captured at the end of the experiment. **(B)** Images of nude mice and xenograft tumors treated with Vector were captured at the end of the experiment. **(C)** Tumors volumes are shown as a function of days during the treatment (bars indicate the mean volume of all tumors ± SE). **(D)** Final tumor weights are shown following the treatment (bars indicate the mean weight of all tumors ± SE). **(E)** Representative immunoblots demonstrated overexpression of RPL24 in SiHa cell lines. **p<0.01.

provided for subsequent biological experimental verification, which will help promote the development of cancer precision medicine. Survival analysis is an important indicator for patients with carcinoma in assessing their prognosis. In our study, it was found that RPL24 expression was down-regulated in CC by TCGA database analysis, and based on the Kaplan-Meier plotter and LOGpc online database, a significant positive correlation between RPL24 expression status and RFS, OS, and PFS of CC patients was discovered, providing a theoretical basis for later clinical experiments, which indicated that RPL24 may play an important role in CC. To preliminarily verified the hypothesis, we used quantitative real-time PCR (qRT-PCR) and Western blotting to detect RPL24 expression in different CC cell lines, such as HCC94, C339, Hela and SiHa, and found that the expression level of RPL24 was the highest in highly differentiated CC cell line HCC94.

CDDP is well known as the first-line chemotherapy drug for CC, and it can block the cell cycle to G2/M, in which the CC cells are sensitive to the radiotherapy. The expression of p53 protein

10.3389/fonc.2023.1131803

TABLE 1 Detailed changes in therapeutic effect, ADC value, and RPL24 expression of 40 patients with cervical cancer before and after CCRT.

| S/N | Age | FIGO stage | clinical efficacy | ADC value (×10-6mm2/s) | | RPL24 staining | |
|---|---|---|---|---|---|---|---|
| | | | | Before | After | Before | After |
| 1 | 58 | IIb | PR | 626 | 1030 | + | ++ |
| 2 | 41 | IIb | PR | 904.2 | 1520.6 | + | ++ |
| 3 | 43 | IIb | CR | 689.3 | 1475.2 | - | +++ |
| 4 | 68 | IIb | CR | 650.4 | 1130 | - | ++ |
| 5 | 66 | IIb | SD | 775.6 | 1313 | - | - |
| 6 | 49 | IIb | PR | 621.6 | 1405 | + | + |
| 7 | 51 | IIb | CR | 673.2 | 1163.5 | + | ++ |
| 8 | 72 | IIb | PR | 736 | 1138.6 | + | + |
| 9 | 54 | IIb | CR | 553.7 | 980.3 | - | + |
| 10 | 62 | IIb | CR | 620.5 | 1034 | + | ++ |
| 11 | 58 | IIb | SD | 994 | 1060 | - | - |
| 12 | 70 | IIb | CR | 520.3 | 1034 | + | + |
| 13 | 62 | IIb | CR | 567.5 | 1290 | + | ++ |
| 14 | 55 | IB1 | CR | 754.4 | 1210 | - | ++ |
| 15 | 32 | IIb | CR | 702 | 1106 | - | ++ |
| 16 | 56 | IIb | CR | 634.4 | 1265.6 | + | + |
| 17 | 49 | IIb | PR | 657.1 | 1293.5 | + | + |
| 18 | 44 | IIb | PR | 855.1 | 1124 | - | + |
| 19 | 48 | IIb | CR | 670 | 1030 | + | ++ |
| 20 | 47 | IB1 | PR | 683.6 | 1311.5 | - | + |
| 21 | 62 | IIb | CR | 650 | 1090 | + | ++ |
| 22 | 54 | IV | CR | 659 | 1105 | - | ++ |
| 23 | 53 | IIb | CR | 704 | 1257 | - | + |
| 24 | 46 | IV | PR | 810 | 1200 | + | + |
| 25 | 76 | IIb | CR | 656.5 | 1101 | - | + |
| 26 | 48 | IIb | CR | 670.3 | 1069 | - | + |
| 27 | 50 | IIb | PR | 581.7 | 1028 | + | + |
| 28 | 49 | IIb | CR | 689 | 1202.9 | - | ++ |
| 29 | 45 | IIb | PR | 720.1 | 1310 | - | + |
| 30 | 51 | IB1 | CR | 663 | 1143 | - | ++ |
| 31 | 69 | IIb | CR | 695.43 | 1179.6 | + | ++ |
| 32 | 60 | IIb | CR | 557.2 | 865 | + | ++ |
| 33 | 63 | IIb | CR | 651 | 1097 | - | ++ |
| 34 | 42 | IIb | CR | 698 | 1098 | - | +++ |
| 35 | 39 | IIb | CR | 748 | 1203 | + | + |
| 36 | 47 | IIb | CR | 670 | 1205 | - | ++ |
| 37 | 71 | IV | PR | 669 | 1123 | - | + |

*(Continued)*

TABLE 1 Continued

| S/N | Age | FIGO stage | clinical efficacy | ADC value (×10-6mm2/s) | | RPL24 staining | |
|---|---|---|---|---|---|---|---|
| | | | | Before | After | Before | After |
| 38 | 52 | IIb | CR | 719 | 1266 | + | ++ |
| 39 | 49 | IIb | CR | 734 | 1209 | + | ++ |
| 40 | 62 | IIb | SD | 567.5 | 997.3 | - | - |

FIGO, International Federation of Gynecology and Obstetrics; CR, complete response; PR, partial response; SD, stable disease. The result was determined by the percentage of positive stained cells and cell staining intensity as follows: negative −, weak positive +, positive ++, and strongly, positive +++.

increased after treatment with CDDP, which induces p53-dependent apoptosis and p53-dependent pathways (21). RPs can interact with MDM2, inhibiting MDM2-mediated ubiquitination of p53 and regulating the transcriptional activity of p53. Importantly, RPs can enhance the ability of p53 to transcriptionally activate its target genes in response to DNA damage (22). Therefore, cells have the capability to induce G2/M cell cycle arrest.

After CDDP treatment, we found that hat protein expression levels of RPL24, CCNB1 and p53 rose significantly in CC cell lines, which was consistent with the results from KEGG enrichment analysis of coexpression gene set related to RPL24 in TCGA database, and it indicated that RPL24 may play a role in the control of CC cell cycle. It is possible that RPL24 is highly expressed in CDDP resistant cell, but we also found that CC patients with high RPL24 expression after CCRT had a favorable prognosis. By combining with the literature data, we speculated that RPL24 may be involved in the regulation of MDM2-p53 pathway and p53 monitoring system, and it played an important regulatory role in cervical carcinogenesis and development while its specific mechanisms remain to be investigated. Subsequently a mouse CC model was constructed showing that high RPL24 expression can//'/' inhibit tumor formation rate in mice, which suggested that RPL24 has a tumor-suppressive effect in CC.

To further analyze the clinical efficacy of RPL24 on CCRT, we performed clinical research, which revealed that the expression of RPL24 increased compared with that of pre-therapy. Most women reaped benefit in terms of CR and PR, but only three showed SD. Immunochemistry demonstrated that the expression of RPL24 protein was increased in stage IB1, IIB and IV CC tissues after CCRT compared with the control group before treatment. The results showed that overexpression of RPL24 was positively correlated with the therapeutic effect. Taken together, the correlation between RPL24 expression and the prognosis of CC patients was revealed. CC patients with RPL24 expression had better prognosis and longer survival. Thus, we suggest that RPL24 may serve as a prognostic marker for CC survival and also possess potential value for CC patients undergoing CCRT. In this regard, the integration of biologic biomarkers like RPL24 with other indicators, such as those derived from FDG PET/CT imaging in cervical cancer patients (23), may provide more powerful biomarkers. This could potentially enhance future patient management decisions. similar to the research on synergies currently being investigated in other tumors (24).

However, there was a more concrete enumeration of limitations. Firstly, we observed that the expression level of RPL24 is related to p53 and cell cycle, but the exact regulatory mechanism remains unclear, which can be elucidated by other methods such as co-immunoprecipitation in future. Secondly, There was no consistency among patients at different stages who may have received different types of chemotherapy or undergone various treatment protocols prior to CCRT. Additionally, no analysis was conducted on other drugs used during CCRT in this study. So in this clinical research, confounding factors were not sufficiently controlled, which maybe potentially cause the biases in the results. In addition, the different levels of the professional experiments among the radiologist and pathologist experience also affected the results. Thirdly, we were unable to study the correlation between RPL24 and radiotherapy because of the limitations resulted from the clinical factors. Fourthly, this study only included patients with cervical squamous cell CC, so the results should not be interpreted as an extension to all CC cases. Therefore, these limitations indicate the need for a more rigorous prospective study, which includes comprehensive patient logs and initiates a study that records patient conditions during CCRT. This may uncover differences that we did not identify and provide valuable insights for the treatment and management of CC. Meanwhile, the results still need to be further confirmed in multicenter and largescale clinical trials.

## Conclusion

Cervical cancer is one of the most common gynecological tumors in women. There is a lack of specific therapeutic and prognostic relevant markers compared with other malignant tumors. Our findings provide new insights indicating that RPL24 expression levels increased after CDDP treatment, which was confirmed in human CC lines and human cervical tumor tissues, and high RPL24 expression was associated with a better prognosis, which was further verified in an *in vivo* mouse model, human cervical tumor tissues, and online databases. Therefore, RPL24 might be a potential target in the treatment and prognostication of CC.

10.3389/fonc.2023.1131803

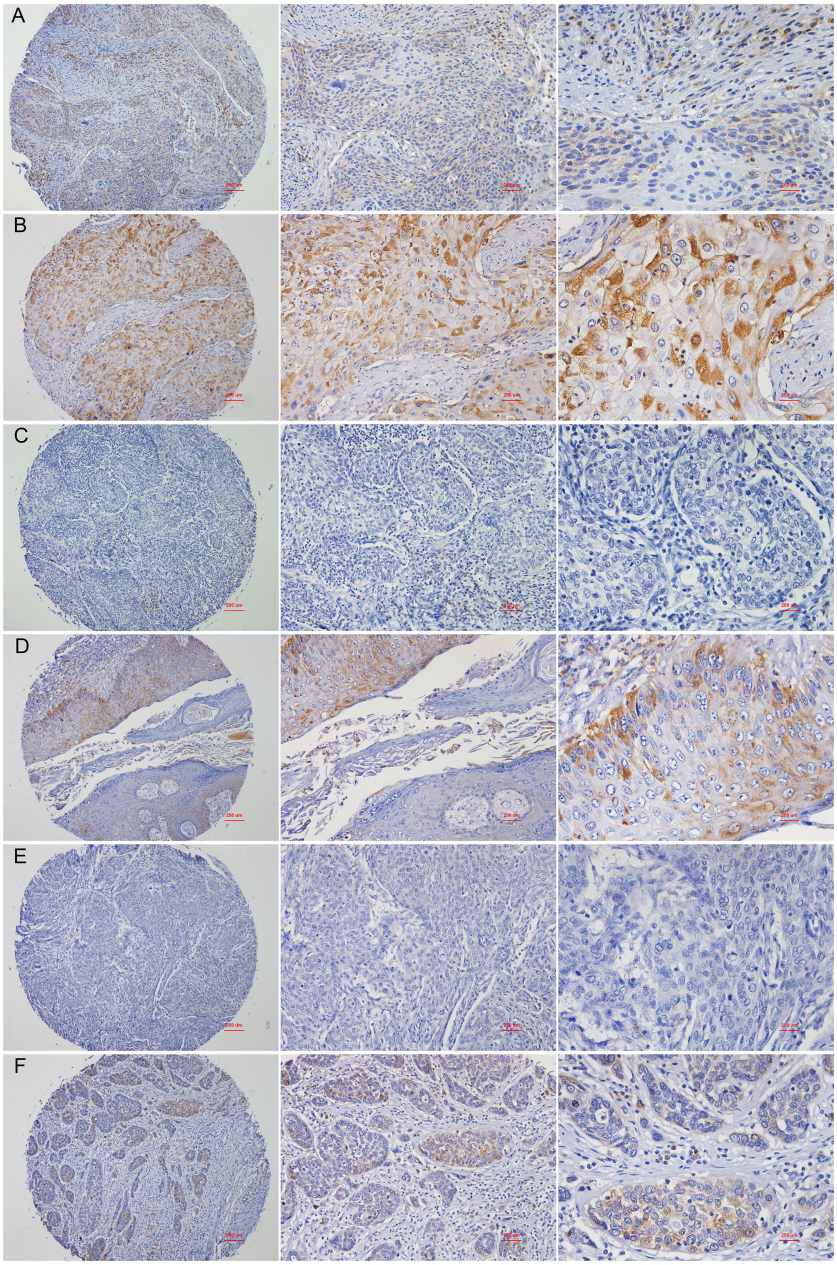


FIGURE 6
Representative images of immunohistochemical staining of RPL24. **(A)** Staining for RPL24 in CC tissues of stage of stage IB1 at ×40, ×100 and ×400 magnification respectively. **(B)** Staining for RPL24 in CC tissues of stage IB1 after CCRT at ×40, ×100 and ×400 magnification respectively. **(C)** Staining for RPL24 in CC tissues of stage IIB at ×40, ×100 and ×400 magnification respectively. **(D)** Staining for RPL24 in CC tissues of stage IIB after CCRT at ×40, ×100 and ×400 magnification respectively. **(E)** Staining for RPL24 in CC tissues of stage IV at ×40, ×100 and ×400 magnification respectively. **(F)** Staining for RPL24 in CC tissues of stage IV after CCRT at ×40, ×100 and ×400 magnification respectively.

TABLE 2 Correlation between therapeutic effect and RPL24 expression after CCRT in 40 patients with cervical cancer.

| Clinical treatment | | RPL24 staining after CCRT | | Sum |
|---|---|---|---|---|
| | | Low | High | |
| Clinical efficacy | CR | 0 | 26 | 26 |
| | PR | 0 | 11 | 11 |
| | SD | 2 | 1 | 3 |

Pearson's r=-0.575, p=0.004. *p<0.05.

## Data availability statement

The original contributions presented in the study are included in the article/supplementary material. Further inquiries can be directed to the corresponding authors.

## Ethics statement

The studies involving humans were approved by the Ethics Committee of Baotou Central Hospital. The studies were conducted in accordance with the local legislation and institutional requirements. The participants provided their written informed consent to participate in this study. The animal study was approved by the Ethics Committee of Baotou Central Hospital. The study was conducted in accordance with the local legislation and institutional requirements.

## Author contributions

YW contributed to conception and design of the study. XW organized the database and performed the statistical analysis. CM wrote the first draft of the manuscript. All authors contributed to the article and approved the submitted version.

## Funding

The current study was supported by the National Natural Science Foundation of China (Nos. 81860447 and 82160518) and the Natural Science Foundation of Inner Mongolia (Nos. 2020MS08004, 2020MS08053, and 2021MS08051).

## Conflict of interest

The authors declare that the research was conducted in the absence of any commercial or financial relationships that could be construed as a potential conflict of interest.

## Publisher's note



## References

1. Volkova LV, Pashov AI, Omelchuk NN. Cervical carcinoma: oncobiology and biomarkers. *Int J Mol Sci* (2021) 22(22):12571. doi: 10.3390/ijms222212571

2. Kang J, Brajanovski N, Chan KT, Xuan J, Pearson RB, Sanij E. Ribosomal proteins and human diseases: molecular mechanisms and targeted therapy. *Signal Transduct Target Ther* (2021) 6(1):323. doi: 10.1038/s41392-021-00728-8

3. Su XL, Hou YL, Yan XH, Ding X, Hou WR, Sun B, et al. Expression, purification, and evaluation for anticancer activity of ribosomal protein L31 gene (RPL31) from the giant panda (Ailuropoda melanoleuca). *Mol Biol Rep* (2012) 39(9):8945–54. doi: 10.1007/s11033-012-1763-0

4. Sun Z, Qiu Z, Wang Z, Chi H, Shan P. Silencing ribosomal protein L22 promotes proliferation and migration, and inhibits apoptosis of gastric cancer cells by regulating the murine double minute 2-protein 53 (MDM2-p53) signaling pathway. *Med Sci Monit* (2021) 27:e928375. doi: 10.12659/MSM.928375

5. Deisenroth C, Franklin DA, Zhang Y. The evolution of the ribosomal protein-MDM2-p53 pathway. *Cold Spring Harb Perspect Med* (2016) 6(12):a026138. doi: 10.1101/cshperspect.a026138

6. Dong Z, Jiang H, Liang S, Wang Y, Jiang W, Zhu C. Ribosomal protein L15 is involved in colon carcinogenesis. *Int J Med Sci* (2019) 16(8):1132–41. doi: 10.7150/ijms.34386

7. Xu L, Wang L, Jiang C, Zhu Q, Chen R, Wang J, et al. Biological effect of ribosomal protein L32 on human breast cancer cell behavior. *Mol Med Rep* (2020) 22(3):2478–86. doi: 10.3892/mmr.2020.11302

8. Lin Z, Peng R, Sun Y, Zhang L, Zhang Z. Identification of ribosomal protein family in triple-negative breast cancer by bioinformatics analysis. *Biosci Rep* (2021) 41 (1):BSR20200869. doi: 10.1042/BSR20200869

9. Cho J, Park J, Shin SC, Kim JH, Kim EE, Song EJ. Ribosomal protein S2 interplays with MDM2 to induce p53. *Biochem Biophys Res Commun* (2020) 523(2):542–7. doi: 10.1016/j.bbrc.2020.01.038

10. Li H, Zhang H, Huang G, Bing Z, Xu D, Liu J. Loss of RPS27a expression regulates the cell cycle, apoptosis, and proliferation via the RPL11-MDM2-p53 pathway in lung adenocarcinoma cells. *J Exp Clin Cancer Res* (2022) 41(1):33. doi: 10.1186/s13046-021-02230-z

11. Kim JH, Jung JH, Lee HJ, Sim DY, Im E, Park J, et al. UBE2M drives hepatocellular cancer progression as a p53 negative regulator by binding to MDM2 and ribosomal protein L11. *Cancers (Basel)* (2021) 13(19):4901. doi: 10.3390/cancers13194901

12. Oliver ER, Saunders TL, Tarlé SA, Glaser T. Ribosomal protein L24 defect in belly spot and tail (Bst), a mouse Minute. *Development* (2004) 131(16):3907–20. doi: 10.1242/dev.01268

13. Riazifar H, Sun G, Wang X, Rupp A, Vemaraju S, Ross-Cisneros FN, et al. Phenotypic and functional characterization of Bst+/- mouse retina. *Dis Model Mech* (2015) 8(8):969–76. doi: 10.1242/dmm.018176

14. Barkić M, Crnomarković S, Grabusić K, Bogetić I, Panić L, Tamarut S, et al. The p53 tumor suppressor causes congenital malformations in Rpl24-deficient mice and promotes their survival. *Mol Cell Biol* (2009) 29(10):2489–504. doi: 10.1128/MCB.01588-08

15. Knight JR, Vlahov N, Gay DM, Ridgway RA, Faller WJ, Proud C, et al. *Rpl24*$^{Bst}$ mutation suppresses colorectal cancer by promoting eEF2 phosphorylation via eEF2K. *Elife* (2021) 10:e69729. doi: 10.1101/2021.05.05.442715

16. Signer RA, Magee JA, Salic A, Morrison SJ. Haematopoietic stem cells require a highly regulated protein synthesis rate. *Nature* (2014) 509(7498):49–54. doi: 10.1038/nature13035

17. Magee JA, Signer RAJ. Developmental stage-specific changes in protein synthesis differentially sensitize hematopoietic stem cells and erythroid progenitors to impaired ribosome biogenesis. *Stem Cell Rep* (2021) 16(1):20–8. doi: 10.1016/j.stemcr.2020.11.017

18. Hou YL, Ding X, Hou W, Song B, Wang T, Wang F, et al. Overexpression, purification, and pharmacologic evaluation of anticancer activity of ribosomal protein L24 from the giant panda (Ailuropoda melanoleuca). *Genet Mol Res* (2013) 12(4):4735–50. doi: 10.4238/2013.October.18.11

19. Wilson-Edell KA, Kehasse A, Scott GK, Yau C, Rothschild DE, Schilling B, et al. RPL24: a potential therapeutic target whose depletion or acetylation inhibits polysome assembly and cancer cell growth. *Oncotarget* (2014) 5(13):5165–76. doi: 10.18632/oncotarget.2099

20. Guo YL, Kong QS, Liu HS, Tan WB. Drug resistance effects of ribosomal protein L24 overexpression in hepatocellular carcinoma HepG2 cells. *Asian Pac J Cancer Prev* (2014) 15(22):9853–7. doi: 10.7314/APJCP.2014.15.22.9853

21. Lee BJ, Chon KM, Kim YS, An WG, Roh HJ, Goh EK, et al. Effects of cisplatin, 5-fluorouracil, and radiation on cell cycle regulation and apoptosis in the hypopharyngeal carcinoma cell line. *Chemotherapy* (2005) 51(2-3):103–10. doi: 10.1159/000085769

22. Cui D, Li L, Lou H, Sun H, Ngai SM, Shao G, et al. The ribosomal protein S26 regulates p53 activity in response to DNA damage. *Oncogene* (2014) 33(17):2225–35. doi: 10.1038/onc.2013.170

23. Adam JA, Loft A, Chargari C, Delgado Bolton RC, Kidd E, Schöder H, et al. EANM/SNMMI practice guideline for [18F]FDG PET/CT external beam radiotherapy treatment planning in uterine cervical cancer v1.0. *Eur J Nucl Med Mol Imaging* (2021) 48(4):1188–99. doi: 10.1007/s00259-020-05112-2

24. Delgado Bolton RC, Calapaquí Terán AK, Fanti S, Giammarile F. The concept of strength through synergy applied to the search of powerful prognostic biomarkers in gastroesophageal cancer: an example based on combining clinicopathological parameters, imaging-derived sarcopenia measurements, and radiomic features. *Clin Nucl Med* (2023) 48(2):156–7. doi: 10.1097/RLU.0000000000004357

# Frontiers in Oncology

**Advances knowledge of carcinogenesis and tumor progression for better treatment and management**

The third most-cited oncology journal, which highlights research in carcinogenesis and tumor progression, bridging the gap between basic research and applications to imrpove diagnosis, therapeutics and management strategies.

---

## Discover the latest Research Topics

See more →


**Frontiers**

Avenue du Tribunal-Fédéral 34
1005 Lausanne, Switzerland
frontiersin.org

**Contact us**

+41 (0)21 510 17 00
frontiersin.org/about/contact